MODELING AND SIMULATION OF A SOLAR POWERED ADSORPTION REFRIGERATION SYSTEM

BY

SULEIMAN, Rekiyat Bgirl Omohu

DEPARTMENT OF MECHANICAL ENGINEERING
AHMADU BELLO UNIVERSITY, ZARIA
NIGERIA

JUNE 2011

MODELING AND SIMULATION OF A SOLAR POWERED ADSORPTION REFRIGERATION SYSTEM

BY

SULEIMAN, REKIYAT BGIRL OMOHU B.Eng, M.Sc (ABU)
Ph.D/Eng/32504/01-02

**A DISSERTATION SUBMITTED TO THE
POSTGRADUATE SCHOOL
AHMADU BELLO UNIVERSITY, ZARIA
NIGERIA**

**IN PARTIAL FULFILMENT FOR THE AWARD
OF DOCTOR OF PHILOSOPHY IN
MECHANICAL ENGINEERING**

**DEPARTMENT OF MECHANICAL ENGINEERING
AHMADU BELLO UNIVERSITY, ZARIA
NIGERIA**

JUNE 2011

DECLARATION

I declare that the work in the dissertation entitled 'Modeling and Simulation of a Solar Powered Adsorption Refrigeration System' has been performed by me in the Department of Mechanical Engineering under the supervision of Profs. C.O. Folayan, S.Y. Aku and E.J. Bala.

The information derived from the literature has been duly acknowledged in the text and a list of references provided. No part of this dissertation was previously presented for another degree or diploma at any university.

REKIYAT BGIRL OMOHU SULEIMAN _____ _____

CERTIFICATION

This thesis titled **MODELING AND SIMULATION OF A SOLAR POWERED ADSORPTION REFRIGERATION SYSTEM** meets the regulation governing the award of the degree of **Doctor of Philosophy** in the **Department of Mechanical Engineering** of **Ahmadu Bello University, Zaria**, and is approved for its contribution to knowledge and literary presentation.

Prof. C.O. Folayan _____ _____
Chairman, Supervisory Committee

Prof. S.Y. Aku _____ _____
Member, Supervisory Committee

Prof. E.J. Bala _____ _____
Member, Supervisory Committee

Dr. D.S. Yawas _____ _____
Head of Department

Prof. A.A. Joshua _____ _____
Dean, School of Postgraduate Studies

DEDICATION

To the memory of my wonderful mum, Hajia H.A. Moru and

To Khadija, Hauwa, Hussaini, Awwal and Shehu Idris, I say thank you for being there.

ACKNOWLEDGEMENTS

I would like to thank my major supervisor Prof. C.O. Folayan for his belief, continuous support, contributions and guidance throughout my period of study.

I also would like to thank my minor supervisors, Prof. S.Y. Aku and Prof. E.J. Bala, the entire members of academic staff, technical staff and secretarial staff of the Department of Mechanical Engineering, A.B.U., Zaria for their words of encouragement and support over the years.

Finally, I wish to express my gratitude to my entire family (immediate and in-laws) and my friends, your collective support has been wonderful.

ABSTRACT

The search for renewable, eco-friendly energy source other than fossil fuels which is ozone depleting and responsible for climate change to power refrigeration systems has led to the present research.

The modeling and simulation of a solar powered adsorption refrigeration system using three types of collectors (flat plate, evacuated tube, and parabolic trough collectors), with activated carbon/methanol as the adsorbent/adsorbate pair has been undertaken in this study.

A study of the adsorption bed was carried out to determine the effects of generation, evaporation and condensation temperatures on the performance of the cooling system. This was then used in the optimization of the solar thermal system in the sizing of the collector area and hot water storage tank. A transient simulation of the cooling system with an evaporator temperature of $0^{o}C$ and condenser temperature of $25^{o}C$ was subsequently carried out with the TRNSYS software over a period of a typical year.

The Flat plate collector system gave average values of refrigeration effect of 4814.83 kJ, solar coefficient of performance (COP_s) of 0.024, a cooling coefficient of performance (COP) of 0.608 and a heating efficiency of 0.46. The Evacuated tube collector powered system achieved average values of refrigeration effect of 5528.05 kJ, COP_s of 0.025, a COP of 0.612 and a heating efficiency of 0.61. The Parabolic trough collector powered system however gave average values of refrigeration effect of 5654.73 kJ, COP_s of 0.025, a COP of 0.613 and a heating efficiency of 0.76. The three systems were able to achieve a cold room temperature of about $1^{o}C$.

Some experimental results were used to validate the simulation results and they were determined to have a good level of agreement with a consistent overestimation of COP of 29.9%

TABLE OF CONTENTS

DECLARATION..... i

CERTIFICATION..... ii

DEDICATION..... iii

ACKNOWLEDGEMENTS..... iv

ABSTRACT..... v

TABLE OF CONTENTS..... vii

LIST OF FIGURES..... xi

LIST OF TABLES..... xxii

LIST OF APPENDICES..... xxiii

NOMENCLATURE..... xxiv

CHAPTERS

1. INTRODUCTION..... 1

1.1 Solar Powered Cooling Systems..... 2

1.1.1 Solar Cooling Cycles..... 3

1.1.2 Absorption Refrigeration Cycle..... 5

1.1.3 Adsorption and Chemical Reaction Refrigeration Cycle..... 9

1.1.4 Dessicant Refrigeration System..... 12

1.1.5 Ejector Refrigeration Cycle..... 15

1.1.6 Rankine Refrigeration Cycle..... 16

1.1.7 Stirling Refrigeration Cycle..... 17

1.1.8 Thermoelectric Refrigeration System..... 19

1.1.9 Vapor Compression Refrigeration Cycle..... 20

1.2 Adsorbent/Adsorbate Pairs for Refrigeration Systems..... 21
1.2.1 Silica gel..... 22
1.2.2 Zeolite..... 22
1.2.3 Activated alumina..... 23
1.2.4 Calcium chloride..... 23
1.2.5 Activated carbons..... 23
1.2.6 Metal oxides..... 23
1.2.7 Porous Metal hydrides (PMH)..... 24
1.2.8 Composite adsorbents..... 24
1.3 Definitions..... 25
1.3.1 System..... 25
1.3.2 Refrigeration Cycle..... 25
1.3.3 Cycle time..... 25
1.3.4 Coefficient of Performance..... 25
1.3.5 Specific Cooling Power (SCP)..... 26
1.3.6 Gross Solar Coefficient of Performance (COPs)..... 26
1.4 Statement of the Problem..... 26
1.5 The Present Research..... 28
1.6 Aim and Objectives of Research..... 28
1.7 Justification for the Research..... 29
2. LITERATURE REVIEW..... 31
3. THERMODYNAMICS OF ADSORPTION CYCLES..... 46
3.1 Basic Adsorption Refrigeration Cycle..... 46
3.2 Heat Recovery Adsorption Refrigeration Cycle..... 49

3.3 Heat and Mass Recovery Adsorption Refrigeration Cycle..... 50

3.4 Methodology..... 52

3.5 Simulation of a Simple Adsorption Refrigeration Cycle..... 53

4. SYSTEM DESCRIPTION AND MATHEMATICAL MODELING..... 58

4.1 System Description..... 58

4.2 Modeling of System Components..... 62

4.2.1 Solar Collector..... 62

4.2.2 Water Storage Tank and Adsorbent Bed..... 69

4.2.3 Condenser..... 75

4.2.4 Evaporator..... 78

4.3 Refrigeration Effect and System Efficiency..... 79

5. SOLAR THERMAL SYSTEM MODEL AND OPTIMIZATION..... 81

5.1 Thermal System Modeling..... 82

5.1.1 Solar Thermal Collectors..... 82

5.1.2 Storage Tank..... 85

5.1.3 Weather Data..... 85

5.2 System Optimization..... 87

5.2.1 Flat Plate Collector (FPC)..... 88

5.2.2 Parabolic Trough Collector (PTC)..... 94

5.2.3 Evacuated Tube Collector..... 99

6. ADSORPTION REFRIGERATION SYSTEM SIMULATION..... 104

6.1 Adsorption Refrigeration System with FPC..... 107

6.2 Adsorption Refrigeration System with ETC..... 121

6.3 Adsorption Refrigeration System with PTC..... 134

6.4 Calculations..... 149

6.5 Discussion of Results..... 155

6.6 Validation of Simulation with some Experimental Results…....…… 157

6.7 Relative Cost Comparison of Simulated systems……...…. 163

7. CONCLUSIONS AND RECOMMENDATIONS..... 165

7.1 CONCLUSIONS…….……...……. 165

7.2 RECOMMENDATIONS……...……..… 166

REFERENCES..... 166

LIST OF FIGURES

Figure 1.1 Solar Cooling Paths (Pridasawas, 2006)…….. 4

Figure 1.2 Simple Absorption Refrigeration System (Pridasawas and Nemariam, 2003).. 6

Figure 1.3 Pressure-Temperature Diagram of Absorption Refrigeration System (Pridasawas and Nemariam, 2003)..... 7

Figure 1.4 Solar Powered Platen-Munters Refrigeration System (Pridasawas and Nemariam, 2003)…..... 8

Figure 1.5 Adsorption Refrigeration Process……..….. 10

Figure 1.6 Adsorption Regeneration Process……..…….. 10

Figure 1.7 Dessicant Refrigeration System (Pridasawas and Nemariam, 2003).…..…… 13

Figure 1.8 Dessicant Cooling Process…….……. 14

Figure 1.9 Ejector Refrigeration Cycle (Pridasawas, 2006)……...……..... 15

Figure 1.10 Schematic of a Rankine Refrigeration System (Pridasawas and Nemariam, 2003)…….....… 16

Figure 1.11 Different Configurations of Stirling Refrigerators (Lundqvist, 1993)…..... 18

Figure 1.12 Thermodynamic Cycle of a Stirling Refrigeration System……...… 18

Figure 1.13 Peltier's Element……...…… 19

Figure 1.14 Schematic of a Vapor Compression Refrigeration System..... 20

Figure 1.15 Heat Balance for a Refrigeration Cycle……...……..… 25

Figure 2.1 Simplified view of El-Fadar et al Adsorption System……..……. 37

Figure 2.2 Test Setup for the Solar Hybrid Methanol/Silica gel Cooling System (Mande et al., 1996)..... 38

Figure 2.3 Solar Powered Adsorption Refrigeration System (Rahman et al, 2006)..... 39

Figure 2.4 Schematic of the Two-bed ACF-ethanol Adsorption chiller Cycle (Saha et al, 2007b)..... 41

Figure 2.5 Schematic of a Solid Adsorption Cooling System with Flat Tube Heat Exchangers as Adsorption Bed (Chang et al, 2007)..... 43

Figure 2.6 Experimental Layout of an Adsorption Refrigerator (Lemmini and Errougani, 2005)..... 44

Figure 2.7 Schematic Diagram of a Combined Adsorption Chiller (Habib et al, 2011)..... 45

Figure 3.1 Clapeyron Diagram of the Ideal Adsorption Cycle..... 47

Figure 3.2 P-T-x Diagram of Heat and Mass Recovery Cycle..... 51

Figure 3.3 Effect of Evaporation Temperature on Adsorption System COP (T_{cond} = 30^{o}C)..... 55

Figure 3.4 Effect of Condensing Temperature on Adsorption System COP (T_{ev} = 0^{o}C)..... 56

Figure 3.5 Effect of Generation Temperature on Adsorption System COP (T_{cond} = 25^{o}C)..... 57

Figure 4.1 Schematic View of the Proposed Solar Water Heating and Cooling System.....59

Figure 4.2 Clapeyron Diagram for the Hybrid Solar Heating and Cooling System with Heat Recovery..... 61

Figure 4.3 Cross-section of a Flat plate Solar Collector..... 63

Figure 4.4 Schematic View of a Parabolic Trough Solar Collector (solarpipe – scheme.svg)..... 66

Figure 4.5 Evacuated Tube Collector..... 68

Figure 4.6 View of a Glass-glass Evacuated Tube..... 68

Figure 4.7 Schematic of the Manifold Arrangement Adsorbent Bed..... 70

Figure 4.8 Cross-section of Co-axial Adsorbent Tube..... 70

Figure 4.9 Condenser Tube in Stagnant Pool of Water..... 75

Figure 5.1 Year Round Ambient Temperature for Kano, Nigeria..... 86

Figure 5.2 Year Round Solar Radiation Data for Kano, Nigeria..... 86

Figure 5.3 Flow Chart of Solar Thermal Optimization Process..... 87

Figure 5.4 Solar Thermal System Modeled in TRNSYS with a Flat plate Collector..... 88

Figure 5.5 FPC Useful Energy Gain vs Collector Slope ($A=1m^2$, $A=2m^2$)..... 89

Figure 5.6 FPC Useful Energy Gain vs Collector Slope ($A=5m^2$, $A=7m^2$)..... 89

Figure 5.7 FPC Useful Energy Gain vs Collector Slope ($A=10m^2$)..... 90

Figure 5.8 Effect of Collector Area on Storage Tank Temperature (FPC).....91

Figure 5.9 Effect of Storage Volume on FPC Useful Energy Gain and Tank Temperature (April)..... 92

Figure 5.10 Effect of Storage Volume on FPC Useful Energy Gain and Tank Temperature (August)..... 93

Figure 5.11 Effect of Storage Volume on FPC Useful Energy Gain and Tank Temperature (December)..... 94

Figure 5.12 Solar Thermal System Modeled in TRNSYS with a Parabolic Trough Collector..... 95

Figure 5.13 Effect of Collector Area on Storage Tank Temperature (PTC)..... 96

Figure 5.14 Effect of Storage Volume on PTC Useful Energy Gain and Tank Temperature (April)..... 97

Figure 5.15 Effect of Storage Volume on PTC Useful Energy Gain and Tank Temperature (August)..... 98
Figure 5.16 Effect of Storage Volume on PTC Useful Energy Gain and Tank Temperature (December)..... 98
Figure 5.17 Effect of Storage Volume on Tank Temperature (PTC)..... 99
Figure 5.18 Solar Thermal System Modeled in TRNSYS with an Evacuated Tube Collector..... 99
Figure 5.19 Effect of Collector Area on Storage Tank Temperature (ETC)..... 100
Figure 5.20 Effect of Storage Volume on ETC Useful Energy Gain and Tank Temperature (April)..... 101
Figure 5.21 Effect of Storage Volume on ETC Useful Energy Gain and Tank Temperature (August)..... 102
Figure 5.22 Effect of Storage Volume on ETC Useful Energy Gain and Tank Temperature (December)..... 102
Figure 6.1 Adsorption Refrigeration System Simulated with a Flat Plate Collector..... 108
Figure 6.2 Variation of Adsorption Bed Temperature and Desorbed Mass with Time (FPC Jan)..... 109
Figure 6.3 Effect of Adsorption Bed Temperature on Coefficient of Performance (FPC Jan)..... 109
Figure 6.4 Variation of Adsorption Bed Temperature and Desorbed Mass with Time (FPC Feb)..... 110
Figure 6.5 Effect of Adsorption Bed Temperature on Coefficient of Performance (FPC Feb)..... 110

Figure 6.6 Variation of Adsorption Bed Temperature and Desorbed Mass with Time (FPC Mar)..... 111

Figure 6.7 Effect of Adsorption Bed Temperature on Coefficient of Performance (FPC Mar)..... 111

Figure 6.8 Variation of Adsorption Bed Temperature and Desorbed Mass with Time (FPC Apr)..... 112

Figure 6.9 Effect of Adsorption Bed Temperature on Coefficient of Performance (FPC Apr)..... 112

Figure 6.10 Variation of Adsorption Bed Temperature and Desorbed Mass with Time (FPC May)..... 113

Figure 6.11 Effect of Adsorption Bed Temperature on Coefficient of Performance (FPC May)..... 113

Figure 6.12 Variation of Adsorption Bed Temperature and Desorbed Mass with Time (FPC Jun)..... 114

Figure 6.13 Effect of Adsorption Bed Temperature on Coefficient of Performance (FPC Jun)..... 114

Figure 6.14 Variation of Adsorption Bed Temperature and Desorbed Mass with Time (FPC Jul)..... 115

Figure 6.15 Effect of Adsorption Bed Temperature on Coefficient of Performance (FPC Jul)..... 115

Figure 6.16 Variation of Adsorption Bed Temperature and Desorbed Mass with Time (FPC Aug)..... 116

Figure 6.17 Effect of Adsorption Bed Temperature on Coefficient of Performance (FPC Aug)..... 116

Figure 6.18 Variation of Adsorption Bed Temperature and Desorbed Mass with Time (FPC Sep)..... 117

Figure 6.19 Effect of Adsorption Bed Temperature on Coefficient of Performance (FPC Sep)..... 117

Figure 6.20 Variation of Adsorption Bed Temperature and Desorbed Mass with Time (FPC Oct)..... 118

Figure 6.21 Effect of Adsorption Bed Temperature on Coefficient of Performance (FPC Oct)..... 118

Figure 6.22 Variation of Adsorption Bed Temperature and Desorbed Mass with Time (FPC Nov)..... 119

Figure 6.23 Effect of Adsorption Bed Temperature on Coefficient of Performance (FPC Nov)..... 119

Figure 6.24 Variation of Adsorption Bed Temperature and Desorbed Mass with Time (FPC Dec)..... 120

Figure 6.25 Effect of Adsorption Bed Temperature on Coefficient of Performance (FPC Dec)..... 120

Figure 6.26 Adsorption Refrigeration System Simulated with an Evacuated Tube Collector..... 121

Figure 6.27 Variation of Adsorption Bed Temperature and Desorbed Mass with Time (ETC Jan)..... 122

Figure 6.28 Effect of Adsorption Bed Temperature on Coefficient of Performance (ETC Jan)..... 122

Figure 6.29 Variation of Adsorption Bed Temperature and Desorbed Mass with Time (ETC Feb)..... 123

Figure 6.30 Effect of Adsorption Bed Temperature on Coefficient of Performance (ETC Feb)..... 123
Figure 6.31 Variation of Adsorption Bed Temperature and Desorbed Mass with Time (ETC Mar)..... 124
Figure 6.32 Effect of Adsorption Bed Temperature on Coefficient of Performance (ETC Mar)..... 124
Figure 6.33 Variation of Adsorption Bed Temperature and Desorbed Mass with Time (ETC Apr)..... 125
Figure 6.34 Effect of Adsorption Bed Temperature on Coefficient of Performance (ETC Apr)..... 125
Figure 6.35 Variation of Adsorption Bed Temperature and Desorbed Mass with Time (ETC May)..... 126
Figure 6.36 Effect of Adsorption Bed Temperature on Coefficient of Performance (ETC May)..... 126
Figure 6.37 Variation of Adsorption Bed Temperature and Desorbed Mass with Time (ETC Jun)..... 127
Figure 6.38 Effect of Adsorption Bed Temperature on Coefficient of Performance (ETC Jun)..... 127
Figure 6.39 Variation of Adsorption Bed Temperature and Desorbed Mass with Time (ETC Jul)..... 128
Figure 6.40 Effect of Adsorption Bed Temperature on Coefficient of Performance (ETC Jul)..... 128
Figure 6.41 Variation of Adsorption Bed Temperature and Desorbed Mass with Time (ETC Aug)..... 129

Figure 6.421 Effect of Adsorption Bed Temperature on Coefficient of Performance (ETC Aug)..... 129
Figure 6.43 Variation of Adsorption Bed Temperature and Desorbed Mass with Time (ETC Sep)..... 130
Figure 6.44 Effect of Adsorption Bed Temperature on Coefficient of Performance (ETC Sep)..... 130
Figure 6.45 Variation of Adsorption Bed Temperature and Desorbed Mass with Time (ETC Oct)..... 131
Figure 6.46 Effect of Adsorption Bed Temperature on Coefficient of Performance (ETC Oct)..... 131
Figure 6.47 Variation of Adsorption Bed Temperature and Desorbed Mass with Time (ETC Nov)..... 132
Figure 6.48 Effect of Adsorption Bed Temperature on Coefficient of Performance (ETC Nov)..... 132
Figure 6.49 Variation of Adsorption Bed Temperature and Desorbed Mass with Time (ETC Dec)..... 133
Figure 6.50 Effect of Adsorption Bed Temperature on Coefficient of Performance (ETC Dec)..... 133
Figure 6.51 Adsorption Refrigeration System Simulated with a Parabolic Trough Collector..... 134
Figure 6.52 Variation of Adsorption Bed Temperature and Desorbed Mass with Time (PTC Jan)..... 135
Figure 6.53 Effect of Adsorption Bed Temperature on Coefficient of Performance (PTC Jan)..... 135

Figure 6.54 Variation of Adsorption Bed Temperature and Desorbed Mass with Time (PTC Feb)..... 136
Figure 6.55 Effect of Adsorption Bed Temperature on Coefficient of Performance (PTC Feb)..... 136
Figure 6.56 Variation of Adsorption Bed Temperature and Desorbed Mass with Time (PTC Mar)..... 137
Figure 6.57 Effect of Adsorption Bed Temperature on Coefficient of Performance (PTC Mar)..... 137
Figure 6.58 Variation of Adsorption Bed Temperature and Desorbed Mass with Time (PTC Apr)..... 138
Figure 6.59 Effect of Adsorption Bed Temperature on Coefficient of Performance (PTC Apr)..... 138
Figure 6.60 Variation of Adsorption Bed Temperature and Desorbed Mass with Time (PTC May)..... 139
Figure 6.61 Effect of Adsorption Bed Temperature on Coefficient of Performance (PTC May)..... 139
Figure 6.62 Variation of Adsorption Bed Temperature and Desorbed Mass with Time (PTC Jun)..... 140
Figure 6.63 Effect of Adsorption Bed Temperature on Coefficient of Performance (PTC Jun)..... 140
Figure 6.64 Variation of Adsorption Bed Temperature and Desorbed Mass with Time (PTC Jul)..... 141
Figure 6.65 Effect of Adsorption Bed Temperature on Coefficient of Performance (PTC Jul)..... 141

Figure 6.66 Variation of Adsorption Bed Temperature and Desorbed Mass with Time (PTC Aug)..... 142

Figure 6.67 Effect of Adsorption Bed Temperature on Coefficient of Performance (PTC Aug)..... 142

Figure 6.68 Variation of Adsorption Bed Temperature and Desorbed Mass with Time (PTC Sep)..... 143

Figure 6.69 Effect of Adsorption Bed Temperature on Coefficient of Performance (PTC Sep)..... 143

Figure 6.70 Variation of Adsorption Bed Temperature and Desorbed Mass with Time (PTC Oct)..... 144

Figure 6.71 Effect of Adsorption Bed Temperature on Coefficient of Performance (PTC Oct)..... 144

Figure 6.72 Variation of Adsorption Bed Temperature and Desorbed Mass with Time (PTC Nov)..... 145

Figure 6.73 Effect of Adsorption Bed Temperature on Coefficient of Performance (PTC Nov)..... 145

Figure 6.74 Variation of Adsorption Bed Temperature and Desorbed Mass with Time (PTC Dec)..... 146

Figure 6.75 Effect of Adsorption Bed Temperature on Coefficient of Performance (PTC Dec)..... 146

Figure 6.76 Adsorbent Bed Temperature and Water Bath Temperature versus Cycle Time (Wang et al, 2002)……..……..... 159

Figure 6.77: Adsorbed Mass Variation during Isosteric Heating-Desorption Process for Adsorber 1 and Isosteric Cooling-Adsorption Process for Adsorber 2 (El Fadar, 2009b).161

Figure 6.78: Effect of the Heat Source Temperature on SCP and on COP_{cycle} (El Fadar et al, 2009b)..... 161

Figure 6.79: Comparison between El Fadar's Results and Present Study Simulated Values……..... 162

Figure 6.80: Isobaric Adsorption Properties of Activated Carbon (a) Methanol, (b) Ammonia (Wang, 2006)…...…….....….... 163

LIST OF TABLES

Table 1.1 Differences between Adsorption and Chemical Reaction Cycles..... 11

Table 2.1 Natural Energy Resources in Nigeria..... 28

Table 4.1 Configurations of Typical Solar Thermal Collectors..... 67

Table 5.1 Parameters for the Flat Plate Single glazing Collector..... 82

Table 5.2 Parameters for the Parabolic Trough Collector..... 83

Table 5.3 Parameters for the Evacuated Tube Solar Collector..... 84

Table 6.1 Parameters Used in Simulation of Adsorption Unit..... 105

Table 6.2 Recommended Average Days for Months and Values of n_1 (Day of the Year) by Months..... 107

Table 6.3 Simulated Parameters of the Adsorption Refrigeration System..... 147

Table 6.4 Simulated Performance Parameters of the Adsorption Refrigeration System..... 148

Table 6.5 Evaporator and Condenser Design Parameters..... 154

Table 6.6 Comparison of Wang's Experimental Results with Simulated values…..... 158

LIST OF APPENDICES

A: Matlab Code for Adsorption Cycle Simulation..... 175

B: TRNSYS Deck File for FPC Powered Adsorption Refrigeration System..... 177

C: TRNSYS Deck File for ETC Powered Adsorption Refrigeration System..... 187

D: TRNSYS Deck File for PTC Powered Adsorption Refrigeration System..... 197

E: Equations for Determining the Efficiencies of the FPC, ETC, and PTC Collectors..... 208

NOMENCLATURE

c_p	Specific heat capacity at constant pressure (kJ/kg K)
c_v	Specific heat capacity at constant volume (kJ/kg K)
d	diameter (m)
g	Acceleration due to gravity (m/s^2)
h_a	Heat of adsorption (kJ/kg K)
h_c	Convective heat transfer coefficient (W/m^2K)
h_d	Heat of desorption (kJ/kg K)
k	Thermal Conductivity (W/m K)
m	mass (kg)
$\dot{m}$	mass flow rate (kg/s)
r_{ev}	Inner radius of evaporator tube (m)
x	Mass of adsorbed adsorbate per kg of adsorbent
x_{max}	Maximum mass of adsorbed adsorbate per kg of adsorbent
x_{min}	Minimum mass of adsorbate left after desorption per kg of adsorbent
x_o	Adsorption capacity of adsorbent at saturation pressure
A	Slope of saturation curve for methanol
A_c	Area of Collector (m^2)
A_r	Area of Receiver (m^2)
C	Concentration ratio
F_R	Overall collector heat removal efficiency factor
ΔH	Average heat of sorption (kJ/kg)
I	Global (total) horizontal radiation (kJ/hr m^2)

I_T Global radiation incident on the tilted solar collector (kJ/hr m^2)

L Length (m)

L_e Latent heat of evaporation of methanol (kJ/kg)

Nu Nusselt number

P Pressure (bar)

Pr Prandtl number

Q Heat Transfer (kJ)

Qu Useful energy gain by collector (kJ/hr)

R Gas constant

Ra Rayleigh number

Re Reynolds number

R_{ev} Outer radius of evaporator tube (m)

T Temperature (K)

U_L Overall thermal loss coefficient of the collector per unit area (kJ/hr m^2 K)

V Volume (m^3)

W Width of collector aperture (m)

Greek Symbols

μ Dynamic viscosity (kg/m s)

η Thermal efficiency

ρ Density (kg/m^3)

ν Kinematic viscosity (m^2/s)

α Short-wave absorptance of the absorber

τ Short-wave transmittance of the collector cover

Subscripts

a	ambient
ac	activated carbon
ad	Adsorbent tube
c	Collector
co	Condenser
cr	Cold room
ev	Evaporator
g	generation
i	Inside
l	Liquid
m	Methanol
ml	Methanol liquid
mv	Methanol vapor
o	Outside
w	Water
wt	Water tank
v	vapor

Abbreviations

COP	Coefficient of Performance
COPs	Solar Coefficient of Performance
SCP	Specific Cooling Power
FPC	Flat Plate Collector

ETC Evacuated Tube Collector

PTC Parabolic Trough Collector

CHAPTER ONE

INTRODUCTION

Refrigeration is defined as the process of removing heat from an enclosed space or from a substance for the purpose of lowering the temperature (Encyclopedia Britannica). Energy supply to refrigeration and air conditioning systems constitutes a significant percentage of energy consumption in our world. The International Institute of Refrigeration (IIR) has estimated that approximately 15% of all electricity produced worldwide is used for refrigeration and air conditioning processes of various kinds (Lucas 1988). This value is on the increase because of increasing thermal comfort expectations and global warming. Refrigeration plays an important role in our world, primarily for the preservation of food, healthcare materials (storage of vaccines, blood and medicine), and human thermal comfort (air-conditioning and temperature regulation).

Cooling in industrialized countries depends heavily on grid electricity which is supplied continuously and reliably to every part of the country. In contrast, refrigeration is required in developing countries to boost agricultural production and commerce, in large areas without a reliable source of electricity supply; hence an alternative method of powering refrigeration is necessary.

Renewable energies supply 14% of the world's primary energy demand in 2002. These renewable energies include solar, wind, tidal, geothermal and wave energy with their utilization increasing (about 5.7% annually) faster than other primary energy sources (International Energy Agency(IEA), 2004). The primary source of all renewable energies except geothermal energy is solar radiation with 5.4×10^{24} J per year solar energy striking

the earth's surface (Demirocak, 2008). The use of solar energy as an alternative energy source has also generated a lot of interest in the last few years because of the environmental considerations that apply all over the world. Many applications for solar energy have been considered, including transportation and refrigeration systems among others. The advantages of using solar energy for powering thermal systems can be summarized as follows

- It reduces dependency on imported fuels
- It improves the diversity of energy supply
- It saves scarce natural resources
- It reduces greenhouse gas emissions at very low costs by reducing the use of fossil fuels which are responsible for their emission
- Curbs urban air pollution
- It is immediately available at the point of use
- Reduces heating/cooling energy bill
- It has been proven by many researches to be reliable
- It creates local jobs thereby stimulating the local economy
- Finally and most importantly, it is inexhaustible.

1.1 SOLAR POWERED COOLING SYSTEMS

Solar cooling is not a new idea as passive cooling of buildings dates back to ancient times (Florides et al, 2002). Passive cooling is defined as the attainment of evaporative cooling, thermal inertia of the building, ventilation and shading (Sayigh and McVeigh, 1992). Passive solar cooling is however not always enough to achieve thermal comfort and it is to this end that active solar cooling systems driven by cost effective heat sources are

introduced. An important way to develop a more efficient utilization of energy and launch technological transformation with energy saving as an integral part is the utilization of solar energy and industrial waste heat. These can serve as compensation for the complete heat transfer process from a low-temperature heat source to a high-temperature heat source. Solar powered refrigeration and air conditioning have become very attractive during the last few years, since the amount of solar radiation and cooling loads both reach maximum levels in the same season. Using available technologies, solar energy can be converted to electricity or heat to power refrigeration systems.

The solar powered cooling system generally consists of three main parts: (1) solar energy conversion equipment, (2) the refrigeration system and (3) the cooled object. The solar-driven refrigeration system can be classified into two main groups depending on the mode of energy supply - thermal/work driven systems and electricity (photovoltaic) driven systems. Each group can again be classified according to the type of refrigeration cycle. The appropriate cycle in each application depends on cooling demand, power and the temperature levels of the refrigerated object and the environment.

1.1.1 Solar Cooling Cycles

There are two main paths from the inflow of solar energy

- Solar thermal collectors to heat
- PV cells to electricity

(1) Thermal Driven Systems

- Absorption refrigeration cycle
- Adsorption refrigeration cycle

- Chemical Reaction refrigeration cycle
- Desiccant cooling cycle
- Ejector refrigeration cycle
- Rankine refrigeration cycle

(2) Electricity (photovoltaic) Driven Systems

- Stirling refrigeration cycle
- Thermo-electric (Peltier) refrigeration cycle
- Vapor compression refrigeration cycle

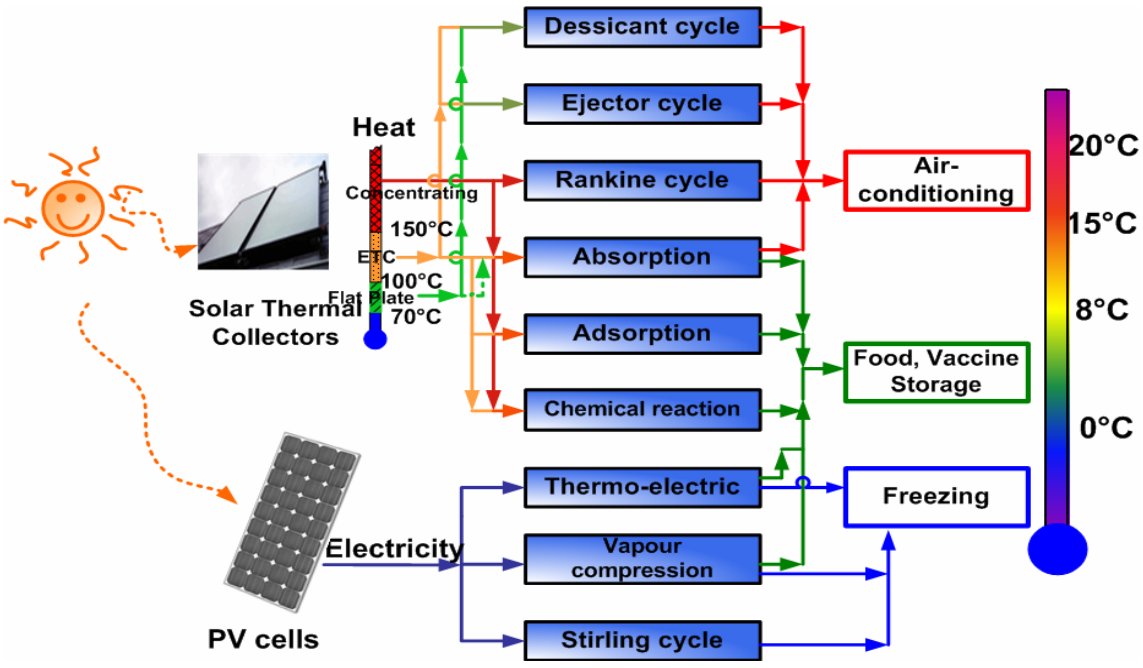


Figure 1.1: Solar Cooling Paths (Pridasawa, 2006)

Figure 1.1 shows a number of possible paths from solar energy to cooling services with different collector types giving different temperature levels. Solar thermal-driven air

conditioning cycles can be based on absorption cycles, adsorption cycles, duplex Rankine, desiccant cooling cycles or ejector refrigeration cycles. However, low temperature applications for food storage can be based on vapor compression cycle, thermoelectric cycle (Peltier), absorption cycle, adsorption cycle and chemical reaction cycle.

1.1.2 Absorption Refrigeration Cycle

It is the first type of solar refrigeration system to be introduced and it is available now in the market as small packaged systems. The absorption refrigeration cycle makes use of the ability of one liquid substance, the absorbent, to absorb relatively large volumes of the vapor of another liquid substance (the refrigerant). The absorbent has the ability to absorb large quantities of vapor when cold and gives it up when heated. The main components of the system are an absorber, a generator, a condenser an expansion valve, an evaporator, a heat exchanger and a pump as shown in Fig. 1.2. The pressure-temperature diagram for this system is shown in Fig. 1.3.

The cycle operates such that refrigerant vapor enters the condenser and is condensed. Liquid refrigerant thus flows to the evaporator through an expansion valve which reduces the pressure of the refrigerant to evaporator pressure. Cooling effect is achieved at the evaporator by the vaporization of the refrigerant at low pressure. The refrigerant vapor then

flows into the absorber where it dissolves in the weak refrigerant solution. The resultant "rich solution" is pumped to the generator where it is heated up and the refrigerant is given

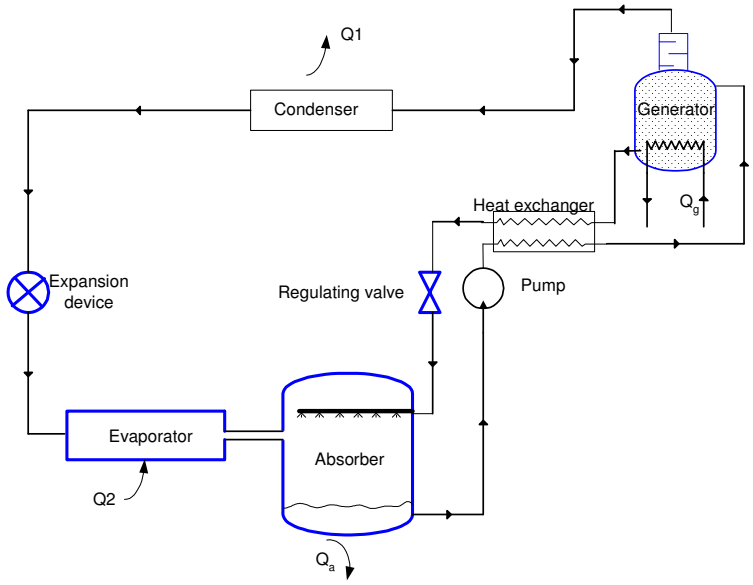


Fig 1.2: Simple Absorption Refrigeration System (Pridasawas & Nemariam, 2003)

up and it goes to the condenser. The weak solution from the generator is passed through a heat exchanger and returned to the absorber to absorb refrigerant vapor. The refrigeration and regeneration processes occur simultaneously producing a continuous cooling effect.

The absorption refrigeration cycle can be designed in different configurations viz- single effect cycle, multi effect cycle and the Platen Munters cycle. The single effect cycle can be operated continuously or intermittently with ammonia-water solution as the refrigerant/absorbent working pair in low temperature applications and water-lithium bromide pair for air-conditioning applications.

In multi effect absorption cycles, the coefficient of performance (COP) is improved by the addition of extra heat exchangers arranged in such a way that the heat can be used at different temperature levels.

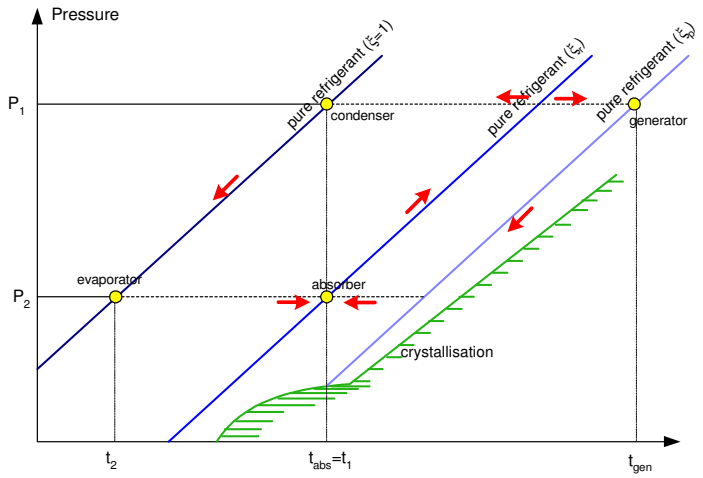


Fig1.3: Pressure-Temperature diagram of absorption refrigeration system (Pridasawas & Nemariam, 2003)

The Platen-Munters cycle system shown in Fig 1.4 is also referred to as the Electrolux refrigerator and principally was invented from the division of applied thermodynamics and refrigeration, KTH, Sweden. It is developed from the Carré absorption cycle but operating without pump. It has no moving parts and no auxiliary energy supply system. Its principle of operation is similar to that of the single effect absorption cycle, with ammonia as the refrigerant, water as the absorption media and hydrogen as the inert gas. Hydrogen is used to maintain a constant total pressure in the whole system by being circulated between the evaporator and the absorber thereby making up the pressure difference between the high and low pressure sides. Meanwhile ammonia vapor from the generator is cooled in the condenser before flowing as liquid ammonia to the evaporator. In the evaporator, the liquid ammonia is exposed to hydrogen. The liquid ammonia evaporates because of its low pressure causing the cooling effect. The ammonia-hydrogen mixture then enters the absorber from where the hydrogen is returned through the heat

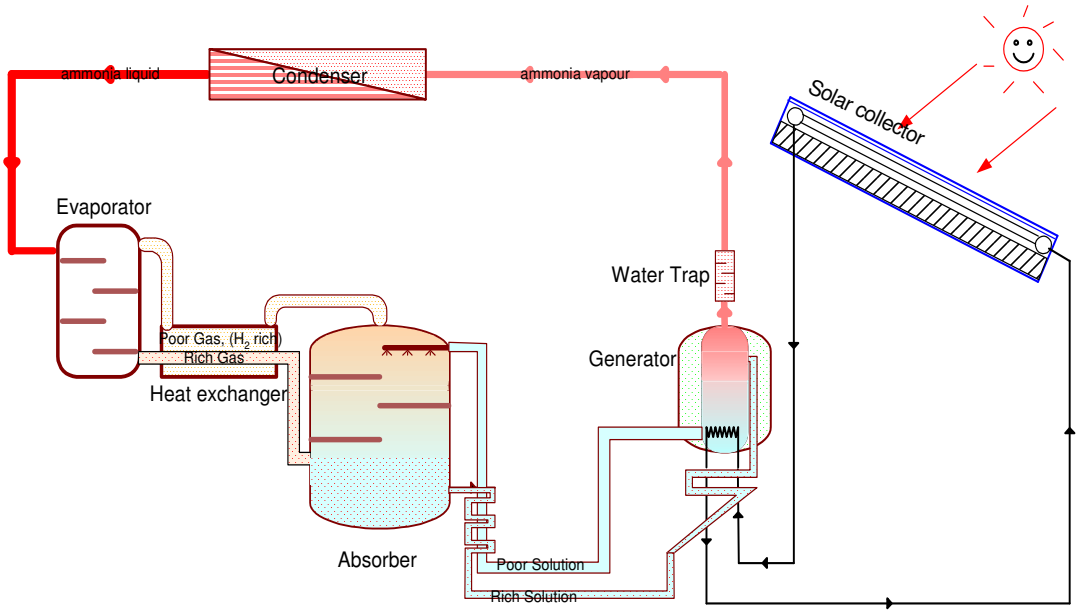


Fig 1.4: Solar powered Platen-Munters refrigeration system (Pridasawas, 2003)

exchanger to the evaporator, while the ammonia is absorbed in the water solution. The generator temperature usually lies in the range of 120°C to 180°C with natural gas, kerosene, or electricity as the heat source.

Working Media

Work media used with this refrigerating cycle over the years are: Ammonia/ Water, which need a rectifier (water separator) in the system, Water/ lithium Bromide, Water/ Lithium Chloride and Water/ Calcium chloride. For air conditioning systems however, Water/ Lithium Bromide is preferred for safety reasons and it needs no rectifier due to large pressure difference between the boiling points of water and lithium bromide. In the single-stage cycle a COP of 0.6 – 0.8 is obtainable (Gordon and Ng, 2000) and this can be increased to 1.35 for a double effect two-stage cycle.

1.1.3 Adsorption and Chemical Reaction Refrigeration Cycle

Adsorption and Chemical Reaction refrigeration cycles are similar to each other but for the processes which occur in the cycles. The force causing the adsorption process is a physical adsorption force while for the chemical reaction process it is a chemical adsorption force.

Adsorption is a reversible process by which a fluid molecule is fixed onto a porous material. When the molecule is fixed, it looses some energy - adsorption is exothermic. An adsorption cycle does not use mechanical energy but only heat energy. The cycle consists of an adsorber, a condenser, and an evaporator and it can either be an intermittent or continuous cycle. Solid adsorption refrigeration has attracted more and more attention in recent years because of its advantages in energy saving and environmental friendliness.

The one bed or intermittent system is advantageous in its simple structure and low initial cost. The adsorber is heated leading to high temperature and pressure of the adsorbent which induces desorption of refrigerant vapor. The desorbed vapor liquefies in the condenser. The liquefied refrigerant is then passed to the evaporator through an expansion valve which lowers the pressure of the condensate. These processes are depicted in Figs 1.5 and 1.6. At the end of the day, the adsorber releases heat thereby decreasing the temperature of the adsorbent with an attendant decrease in pressure. This induces adsorption of refrigerant vapor; the liquefied refrigerant is vaporized in the evaporator achieving the cooling effect. It can be used in applications where continuous cooling or higher cooling capacity is not required, such as cooling drinks, storage of vaccines etc. The intermittent system has the disadvantage however of a lower system performance in terms of Coefficient of Performance (COP) and Specific Cooling Power (SCP). The numbers of adsorbers can be increased to enhance efficiency and the process can also be adapted to be continuous by staggering the several adsorbers in a multi-bed system. In a typical two-bed

cycle, one bed is heated during the desorption period and the other bed is cooled during the adsorption period. The time for the completion of a full cycle of adsorption and desorption is known as cycle time. The heating and cooling steps are reversed when the beds reach desired upper and lower temperature limits of the adsorption cycle. These temperatures will vary depending upon the selection of the refrigerant (adsorbate) and the adsorbent.

Working Media

For the adsorption cycle, typical and commercial adsorbents are made from silica gel,

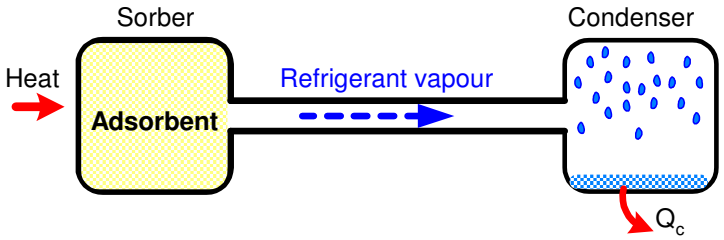


Fig 1.5: Adsorption Refrigeration Process

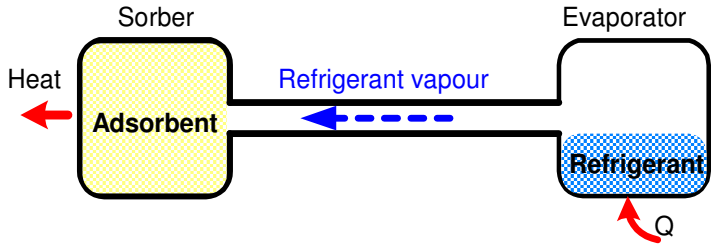


Fig 1.6: Adsorption Regeneration Process

zeolite and activated carbons. The adsorbates (refrigerant fluid) could be water, ammonia or methanol. Water as a refrigerant is used for temperatures $\geq 0^{o}C$ while ammonia and methanol are used for temperatures $\leq 0^{o}C$. The working media for the chemical adsorption cycles are ammonia salts with alkaline compounds e.g. Barium Chloride ($BaCl_2$), Manganese Chloride ($MnCl_2$), Strontium Chloride ($SrCl_2$) etcetera and Hydrogen and

Methyl hydrides with low-hysteresis intermetallic or meshed metal compounds e,g Lanthanum-Nickel alloys like $LaNi_5$, $LaNi_{4.5}$ $M_{0.5}$ where M can be Iron (Fe), Cobalt (Co), Manganese (Mn), Copper (Cu), Chromium (Cr), Silicon (Si). (Pridasawas, 2006).

The physical adsorption process is a reversible process with heat of adsorption not usually exceeding 80kJ $mole^{-1}$, the chemical adsorption process is however difficult to reverse with heat of adsorption up to 800kJ $mole^{-1}$(Webb and Na, 2003).

Table 1.1: Differences between Adsorption and Chemical reaction cycles

	Adsorption Cycle	Chemical reaction Cycle
Physical Process	The physical adsorption process on the surface of the adsorbent does not result in its macroscopic structure change.	Macroscopic structure changes occur after chemical reaction.
Thermodynamic operation of the cycle.	It is a bivalent process, heat supply to adsorber is that required to raise its temperature from its minimum value to the maximum adsorption temperature.	This is a monovalent process with more heat supply required for the adsorption cycle to achieve high kinetics of reaction.
Adsorbate/ Adsorbent pair	Ammonia/ Activated carbon, Methanol/ activated carbon, water/ silica gel etc.	Ammonia salts with alkaline compounds ($BaCl_2$, $MnCl_2$, $SrCl_2$, etc). Methyl hydrides with low-hysteresis intermetallic compounds ($LaNi_5$, $LaNi_{4.5}M_{0.5}$, etc)

Number of Sorbers	The number of sorbers depends on the cycle with one sorber being adequate for a basic cycle. More sorbers are however used to enhance system efficiency.	Hydrogen does not change phase in methyl hydride pairs, so two sorbers are needed to show the temperature lift.

1.1.4 Desiccant Refrigeration System

The desiccant cooling process is a combination of the dehumidification and evaporative cooling process. Evaporative cooling is based on the phenomenon where evaporation of a liquid absorbs heat from the substances in contact with it. The heat absorbed during evaporation is a function of the latent heat of evaporation of the liquid. The amount of evaporative cooling achieved depends on the difference between the wet and dry bulb temperature, the larger the difference, the greater the potential for evaporative cooling. Desiccants by definition are natural or synthetic substances capable of absorbing or adsorbing water vapor due to the difference of water vapor pressure between surrounding air and the desiccant surface (Daou et al, 2006).

There are three major components operating under atmospheric pressure – a dehumidifier, an evaporative cooler and a regenerator. Heat exchangers are also used to increase system efficiency. A typical desiccant refrigeration system is shown in Fig 1.7. Outdoor air is dehumidified with a solid or liquid desiccant where some of the moisture is removed, resulting in rising of the air temperature and decreasing of the humidity (1-2). The air is then cooled by exchanging sensible heat to the returned air in the heat exchanger (2-3). The

temperature of the supply air is further lowered and humidified to the desired humidity by the humidifier or the evaporative cooler before entering the cooling space (3-4).

The returned air from the cooling space is returned to the evaporative humidifier (5-6). It is humidified to a lower temperature at the same enthalpy but with a higher humidity. The cooled air enters the energy recovery unit where it acts as the cooling medium for the supply air (6-7). The air temperature is increased after passing the heat recovery (heat

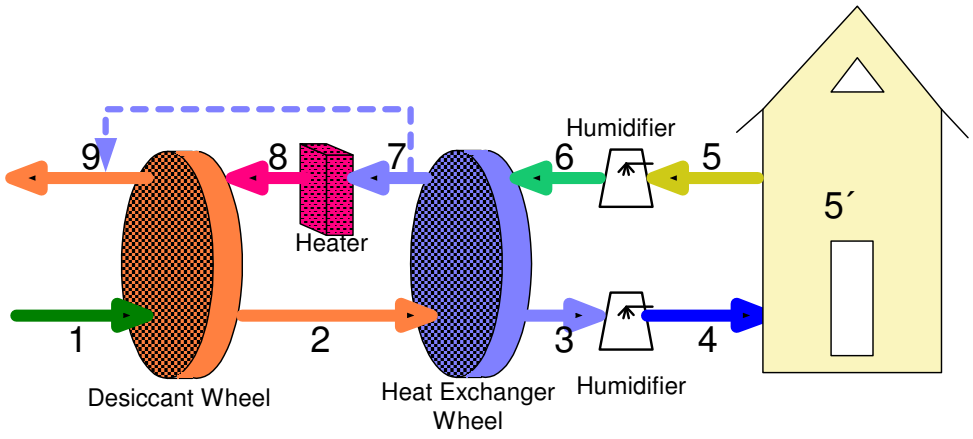


Fig 1.7: Desiccant Refrigeration system (Pridaswas, 2003)

exchanger wheel). It is then passed through a heater, where it is further heated (7-8), and then enters the reactivation sector of the desiccant rotor to reactivate the desiccant (8-9). The wet air leaves the rotor as the exhaust air. This process is shown in the Mollier's diagram in Fig 1.8. The energy supply to the heater depends on the temperature of the return air entering the desiccant wheel at stage 8. The humidity of the entering air and the effectiveness of the desiccant affect the amount of energy supply. Low-temperature heat can be supplied to the heater such as solar energy from flat plate solar collector, waste heat

from industry or geothermal energy. A small amount of electricity is however required for rotating the wheels.

Working Media

The desiccant materials for a solid-desiccant system are usually silica gel, activated alumina, Zeolite or other molecular sieve materials. For a liquid desiccant system, the desiccant dehumidifier's hygroscopic aqueous solution can be triethylene glycol (TEG), $CaCl_2$-H_2O, LiBr-H_2O, LiCl-H_2O and etc. In this system, the dehumidifier is designed

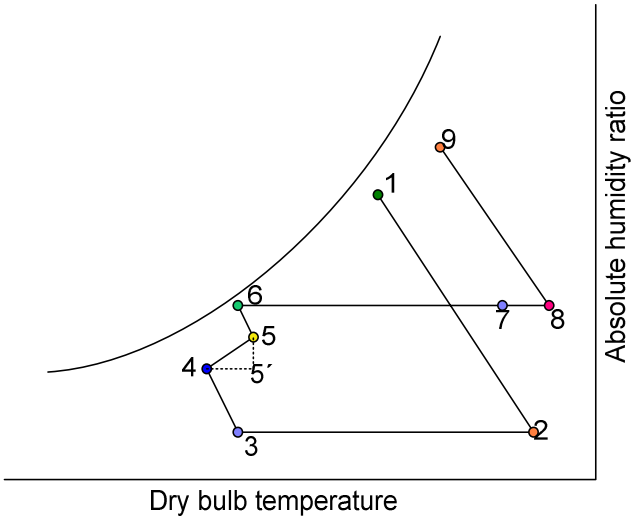


Fig 1.8: Desiccant cooling process

to converge the process air and the sorbent solution in order to absorb the humidity directly from the air. The regenerator is used to regenerate the sorbent by heating.

1.1.5 Ejector Refrigeration Cycle

An ejector refrigeration system is a system that can be driven by low temperature heat supply. Solar energy and waste heat from heat-operated processes can be integrated with an ejector refrigeration system.

The major components of the solar-driven refrigeration system are an ejector, a condenser, a generator, an evaporator, an expansion device and a pump. The compressor of the conventional vapor compression cycle is replaced with the generator, ejector and pump.

The vapor from the low temperature evaporator is sucked into the high velocity vapor stream in the ejector. The suction is achieved by the high velocity vapor stream passing

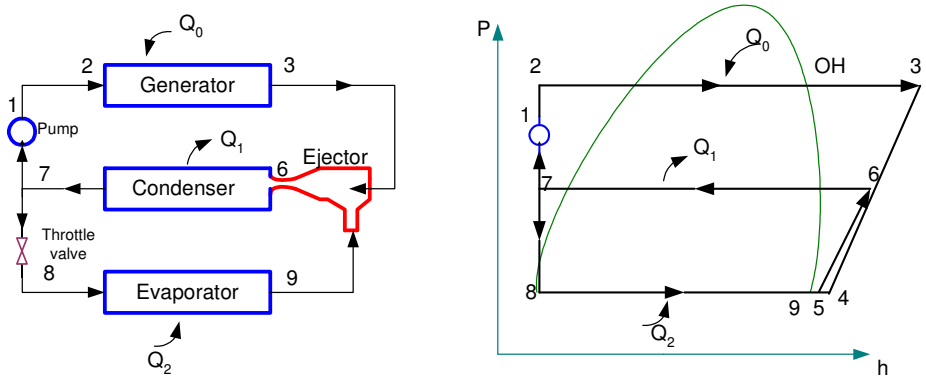


Fig 1.9: Ejector Refrigeration Cycle (Pridasawas, 2006)

through the convergent-divergent nozzle in the ejector since the pressure is low in its narrowest section. The stream from the evaporator thus reaches subsonic velocity and mixing occurs in a mixing zone at the end of the converging section. After mixing, the combined stream becomes a transient supersonic stream whose velocity is high enough to increase its pressure after deceleration in the diffuser to a suitable condensing pressure. The stream from the ejector then enters the condenser where it is condensed and heat rejected to the environment. A part of the fluid is pumped to the generator from the condenser while

the rest go to the evaporator reaching the evaporator pressure by passing through the expansion device.

Working Media

Refrigerants used with the ejector refrigeration system include water, R113, R114, R141b, R134a, R11 and R12.

1.1.6 Rankine Refrigeration Cycle

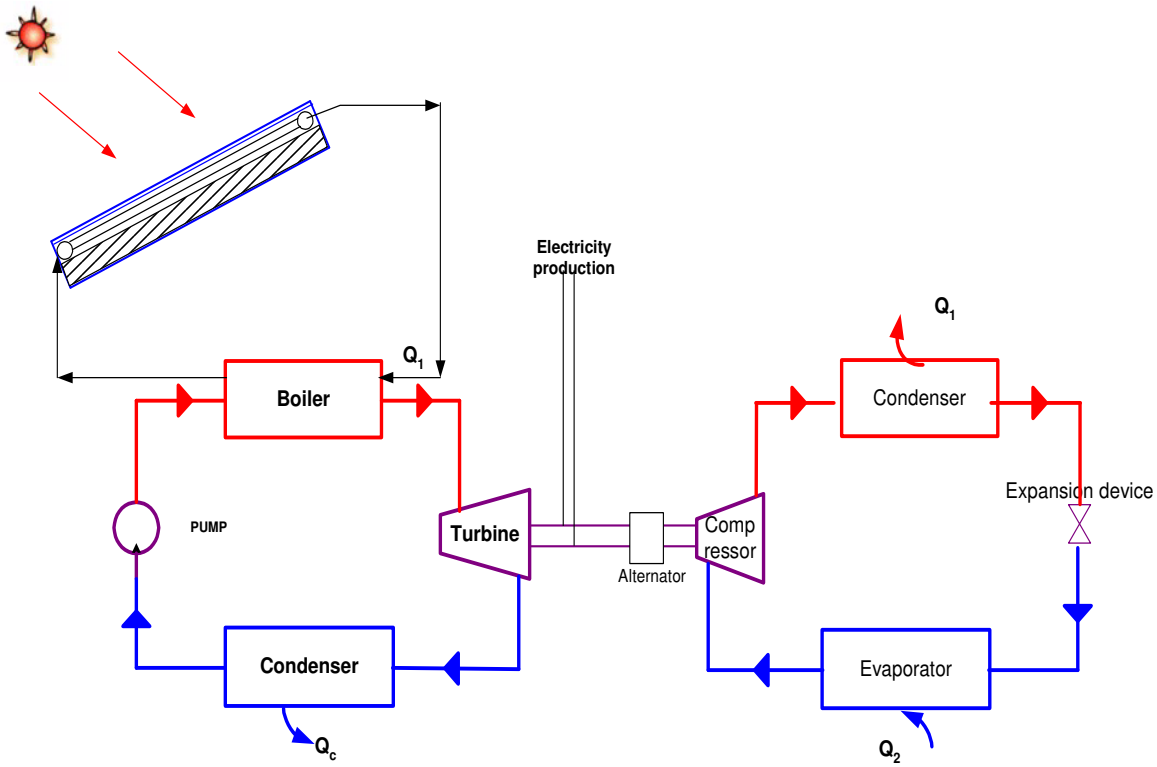


Fig 1.10: Schematic of a Rankine refrigeration system (Pridasawas, 2003)

The Rankine refrigeration cycle is a combination of the Rankine power cycle and the vapor compression refrigeration cycle. In this configuration, the compressor of the vapor

compression cycle is driven by the turbine work output of the Rankine cycle. A schematic view of the Rankine refrigeration system is shown in Fig 1.10.

The solar-operated Rankine cycle using water as the working fluid, is very similar to the conventional power plant. Superheating and an extraction process are needed to prevent erosion of the turbine blades and increase efficiency. The working fluid in the Rankine power cycle and the refrigeration cycle can be different but the choice of refrigerant for the solar loop should be such that moisture is avoided in the turbine. For the solar operated cycle, superheating might be difficult, depending on the working fluid adopted, because of the high temperatures required from the solar collector.

Working Media

R114 is the preferred refrigerant, since the outlet temperature from the turbine is appreciatively higher than the condensation temperature giving the advantage of preheating the refrigerant before it enters the boiler (Pridasawas, 2003). R114 is however not environmentally friendly as it is an ozone depleting chemical.

1.1.7 Stirling Refrigeration Cycle

The principle of this refrigeration cycle is based on the change of pressure and temperature of a gas when heated or cooled at constant volume.

The Stirling refrigeration system consists of a hermetically sealed capsule with two moving parts – a piston and a displacer as illustrated in Fig 1.11 below. The displacer contains the working medium (refrigerant). When the gas is compressed by the piston, the temperature inside the cylinder rises and heat is rejected to the hot side. On the other hand, if the gas is expanded, the temperature inside the cylinder drops and heat is absorbed at the cold side.

The ideal Stirling cycle consists of four thermodynamic processes – two isothermal reversible processes and two constant-volume reversible processes, shown in Fig 1.12. A regenerator is added for inputting and rejecting heat from the refrigerant, it also stores heat during the cycle's change of phase. The operating temperature of the Stirling cycle is wide when compared with other refrigeration cycles. This is because gas is used as the refrigerant and as such there is no phase change from liquid to vapor.

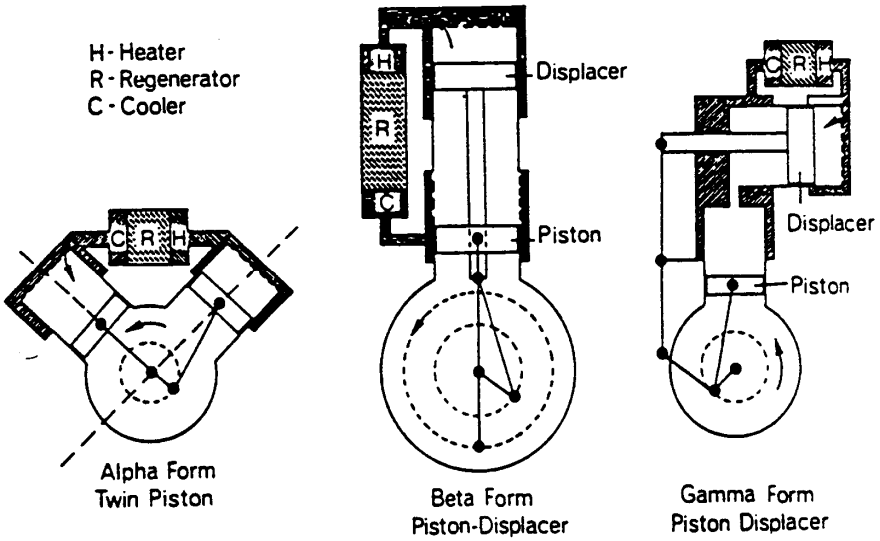


Fig 1.11: Different configurations of Stirling Refrigerators (Lundqvist, 1993)

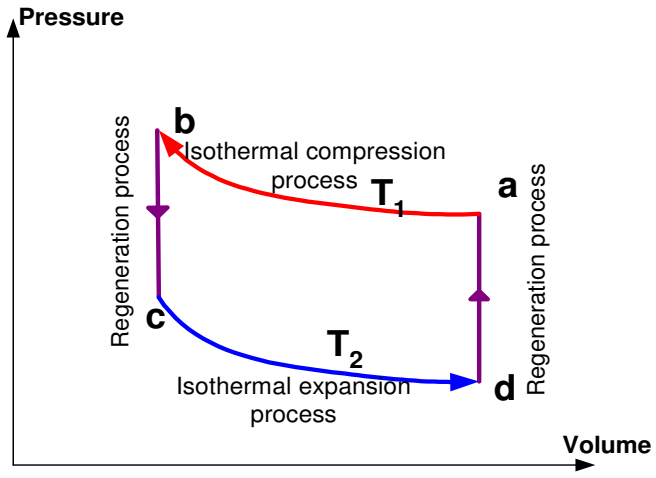


Fig 1.12: Thermodynamic cycle of a Stirling refrigeration system

Working Media

Only a few gases can be used as the refrigerant in this system – helium, nitrogen and air.

1.1.8 Thermoelectric Refrigeration System

The thermoelectric refrigeration system is also known as the Peltier refrigerator. Electric potential difference can be measured from two different metal junctions when these junctions have different temperatures. This is because electric current moves from a higher potential to a lower potential. This is known as the Seebeck effect (thermocouple). The reverse of this was developed by Peltier in 1834 (Pridasawas, 2003). If electric current is forced through an electric circuit with different metal junctions, the difference in temperatures between the ends of these metals can be measured; this phenomenon is called the Peltier effect. Here, the different temperatures and heat absorbed are proportional to the electric potential difference.

Fig 1.13 shows a Peltier's element composed of N and P type semiconductor materials, the electric conductors are made of copper. The upper electric conductor represents the cold side and lower electric conductor represents the hot side.

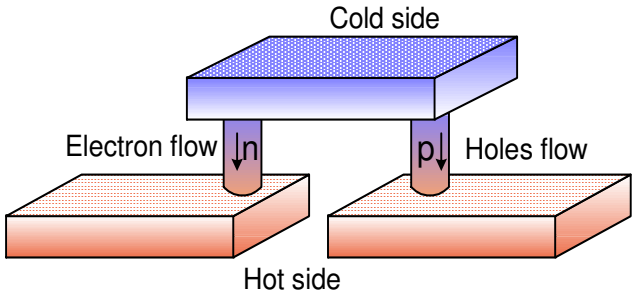


Fig 1.13: Peltier's element

1.1.9 Vapor Compression refrigeration Cycle

Vapor compression systems are the most widely used technology for air-conditioning and refrigeration today because of their high efficiency and reliability (Demirocak, 2008). Electricity is the main energy source for this type of system. This energy can be supplied with solar energy by integrating the vapor compression system with a photovoltaic cell or solar thermal collectors with Rankine engines.

The system consists of a compressor, a condenser, an expansion device and an evaporator as seen in Fig 1.14. The refrigerant vapor in the compressor undergoes isentropic compression to a high temperature and pressure. The high-pressure vapor is then condensed through an isobaric process in the condenser with heat being rejected to the surrounding. The refrigerant vapor thus becomes liquid refrigerant. The liquid refrigerant is then passed on to the evaporator through the expansion device which throttles the refrigerant to

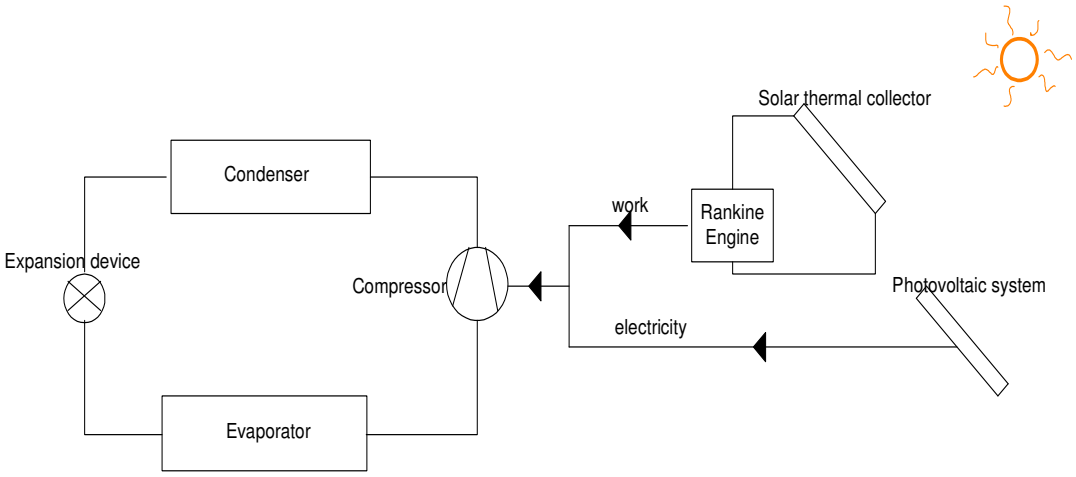


Fig 1.14: Schematic of a Vapor compression refrigeration system

evaporator pressure. In the evaporator, the refrigerant undergoes a constant pressure heat absorption process resulting in the cooling effect.

1.2 ADSORBENT/ ADSORBATE PAIRS FOR REFRIGERATION SYSTEMS

The discovery of the ozone depleting properties of Chlorofluorocarbons (CFCs) and Hydrofluorocarbons (HFCs) refrigerants and their attendant global warming problems led to the Montreal Protocol which called for their ban. This protocol scheduled 1996 as the end of the production of CFCs while the production of Hydro-chlorofluorocarbons (HCFCs) is to end by 2030 (Waszkiewicz et al, 2001). Alternatives to hydrofluorocarbons as refrigerants are naturally occurring substances like ammonia, carbon dioxide, methanol, water and air. These can be used in sorption processes to produce refrigeration and have been studied for the last twenty years as a technological alternative to vapor compression systems. Sorption cooling systems have the advantage of being environmentally friendly as they employ safe and non polluting refrigerants.

Adsorption is a surface phenomenon occurring at the interface of two phases, in which cohesive forces act between the molecules of all substances irrespective of their state of aggregation. The solid and the fluid adsorbed in the solid surface are referred to as the adsorbent and the adsorbate respectively. Adsorption however may be due to a physical process (physisorption) or a chemical process (chemisorption) with the heat of adsorption small in physisorption and large in chemisorption. Adsorbent substances are usually restored to their original state by a desorption process involving the application of heat though some chemisorption process maybe irreversible.

Adsorbent with affinity for polar substances like water are termed hydrophilic. Examples of these include silica gel, zeolite and active alumina. Non-polar adsorbents (hydrophobic) have more affinity for gases and oils than for water; these include substances like activated carbons, polymer adsorbents and silicates.

Some commercially available solid adsorbents are listed below.

1.2.1 Silica gel

It is made from pure silica and retains about 5% chemically traces of water and is generally not used for applications over 200^{o}C. Silica gel is available in various pore sizes though the smaller the pore size, the greater the area per unit mass with a typical pore size of 650m^2g^{-1}. Silica gel has a large capacity for adsorbing water at high pressures making it very useful as a desiccant in dehumidification processes but it is also used for the separation of liquids and gases. The heat of adsorption of water vapor on silica gel is however largely due to the heat of condensation of water (Srivastava and Eames, 1998).

1.2.2 Zeolite

They are naturally occurring alumino-silicate minerals also referred to as molecular sieves. Many types of synthetic zeolites have been developed for special applications over the years e.g. types 4A, 5A, 10X and 13X developed by the Linde Co., USA. These types have typical cavity volumes ranging from 0.05 to 0.30cm^3g^{-1}. They can be heated up to 500^{o}C without damage to their adsorption and regeneration properties and have been used for applications like drying and separation of hydrocarbon mixtures (type 4A), separation of paraffins and some cyclic hydrocarbons (type 5A), and the adsorption of a wide range of adsorbates (type 10X and 13X).

1.2.3 Activated alumina

It is an aluminum oxide in a porous form prepared by the dehydration of aluminum hydrates (e.g. $Al_2O_3.3H_2O$) to about 6% moisture level (Srivastava and Eames, 1998). It has a surface area ranging between 150-500m2g-1 and is generally used as a drying agent and as an adsorbent for polar organic substances.

1.2.4 Calcium chloride

Calcium chloride has good potential use as a solid chemical adsorbent for methanol and ethanol vapors and also as a low temperature liquid desiccant. Calcium chloride remains solid until saturated after which it dissolves in water.

1.2.5 Activated carbons

These are made by pyrolizing and carbonizing source materials like coal, lignite, wood, nut shells and synthetic polymers at high temperatures between 700-800^{o}C. Activated carbons are available as powders, granules, molecular sieves and carbon fibers. Activated carbon powder is used for the adsorption of liquids, the granules for air purification and gas separation, molecular sieves (micro-porous form) for separation of nitrogen and oxygen in air. Activated carbon fibers are however made by carbonizing synthetic fibers and are available in forms of mats, cloth and fiber chips used for air and water purification.

1.2.6 Metal oxides

These include titanium oxide, zirconium oxide and magnesium oxide and are used as adsorbents in chemisorption processes e.g. cerium oxide is used for the adsorption of fluoride in waste water.

1.2.7 Porous Metal hydrides (PMH)

Specially developed PMH containing Ni, Fe, La, Al, H, have very high rates of sorption and heat of adsorption with hydrogen as adsorbate. They have promising uses in the development of metal hydride refrigeration systems.

1.2.8 Composite adsorbents

They are made from metallic frames, zeolites and natural graphite. Composite adsorbents have been proposed to improve the heat transfer rates in adsorbent beds thereby increasing the performance of adsorption refrigeration systems.

In adsorption refrigeration systems, the choice of the working fluid (adsorbate) depends largely on the evaporation temperature required. The adsorbate must also have a high latent heat of evaporation and small molecular dimension to allow for easy adsorption.

Water as an adsorbate has the disadvantage of not being usable for evaporator temperatures lower than 0^{o}C. The first disadvantage of using ammonia as the adsorbate in refrigeration is its toxicity. Copper can not be used as the adsorber material due to the corrosion of copper by ammonia, adsorber material for ammonia is usually steel which cannot be cooled with water to prevent corrosion.

Methanol is however environmentally friendly, non-toxic and has the added advantage of a freezing point temperature of -97.68^{o}C (Methanex Corporation), this allows very low evaporator temperatures to be obtained in refrigeration systems using methanol as adsorbate. It also has the added advantage of boiling at 64.6^{o}C (Methanex Corporation) which makes it easy to drive the system with low temperature heat source. Methanol, however, like most alcohols tend to dissociate at temperatures above 200^{o}C.

1.3 DEFINITIONS

Some of the terms used in this research are defined below:

1.3.1 System

It typically refers here to the combination of refrigeration cycles, a solar energy converter subsystem and a cooling load subsystem as is used for all energy conversion processes that can be enclosed by a system boundary.

1.3.2 Refrigeration Cycle

This describes the thermodynamic cycle in which heat is absorbed at one temperature level and lifted to a higher temperature level where it is rejected.

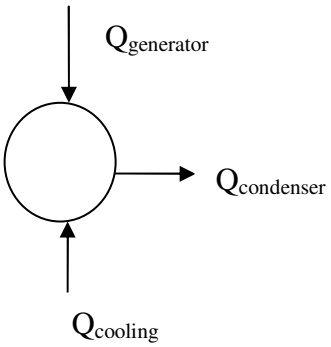


Fig1.15: Heat balance for a refrigeration cycle

1.3.3 Cycle time

This is the time taken for the completion of a full cycle of adsorption and desorption.

1.3.4 Coefficient of Performance (COP)

The efficiency in cooling is called the “coefficient of performance’. It is generally the ratio of the cooling effect to the heat input. i.e. how much energy that can be removed from a cold space (Q_e) for each unit of energy expended (Q_g).

$$COP = \frac{Q_e}{Q_g} \quad \text{.....1.1}$$

1.3.5 Specific Cooling Power (SCP)

This is another efficiency indicator defined as the ratio between the cooling production and the cycle time per unit of adsorbent mass. The SCP reflects the size of the system, for a nominal cooling load, higher SCP values indicated compactness of the system.

$$SCP = \frac{Q_e}{t_{cycle}.m_{ad}} \quad \text{.....1.2}$$

1.3.6 Gross Solar Coefficient of Performance (COP_s)

COP_s is defined as the ratio between the cooling production and the incident solar energy on the surface of solar collector during the whole day.

$$COP_s = \frac{Q_e}{\int A_c\, I(t) \partial t} \quad \text{.....1.3}$$

1.4 STATEMENT OF THE PROBLEM

The world appears to be emerging from the worst economic crises in decades and many countries have made pledges under Copenhagen Accord (UN Conference on Climate change) to reduce greenhouse-gas emissions (IEA, 2010).

Renewable energy sources will have to play a central role in moving the world onto a more secure, reliable and sustainable energy path. The potential of renewable energy is unquestionably large, but the rate at which their contribution to world's energy needs grows, depends critically on government support to make renewable energy cost-

competitive with other energy sources and also stimulate technological advances in the field.

Nigeria is blessed with an array of conventional energy-resources, prominent among which are crude oil, tar sands, natural gas and coal. In addition, there are substantive potentials for renewable energy-resources such as hydro, solar, wind, biomass, wave and tidal, and some geothermal as shown in Table 1.2 below. Despite these resources Nigeria is currently in a precarious situation due to the inability to satisfy the energy needs of its people. In the year 2005, the name-plate capacity for electricity generation in Nigeria was put at 6500 MW against an electricity demand of about 10,000 MW. Of this 6500 MW, only 3959 MW is available for distribution, due to the ageing of power plants and poor maintenance (Ibitoye and Adenikinju, 2007). It is therefore a daily struggle to make the needed equilibrium between supply and demand of its electric power in the utility grid; this is in addition to the call for a reduction in the consumption of energy generated by fossil fuels to reduce global warming. Renewable energy resources are however expected to become increasingly competitive as fossil-fuel prices rise and renewable technologies mature, the latter can only be achieved with government support. Government support for this energy source can, in principle, be justified by the long term economic, energy-security and environmental benefits they will eventually bring.

Despite rising energy use across the world, many poor households in developing countries still have no access to modern energy services, as at the year 2003, less than 45% of the Nigerian population had access to electric power. However, Nigeria being a tropical nation, the demand for cold storage (refrigeration) can hardly be overemphasized. Now more than ever, the challenges of finding alternative sources of energy to power some of the nation's energy requirements become more apparent daily, hence the need to research into fields

where the abundant solar energy (Table 1.2) available could be efficiently harnessed and applied for powering some systems. Prioritization of access to modern energy services can help accelerate social and economic development.

Table 1.2: Natural energy resources in Nigeria

Energy type	Resource estimate
Crude oil	36 billion barrels
Natural gas	185 trillion cubic feet
Hydro power	14,750 MW
Coal	2.75 billion metric tons
Solar radiation	3.5-7.0 kWh/m2-day
Wind energy	2.0-4.0 m/s
Biomass	144 million tons/yr
Wave and tidal energy	150,000 TJ/yr

Source: Ibitoye and Adenikinju (2007)

1.5 THE PRESENT RESEARCH

The present research is to model a solar powered refrigeration system powered by three different collectors with Kano, Nigeria as its location of operation. The optimized system will then be simulated and its performance studied.

1.6 AIM AND OBJECTIVES OF RESEARCH

The aim of this research is to obtain the best system performance of a solar powered adsorption refrigeration system. This is achieved by the following specific objectives

(i) Studying some parameters that affect the performance of the system viz:

- ✓ Condensation Temperature
- ✓ Evaporation Temperature
- ✓ Generation Temperature
- ✓ Area of Collector
- ✓ Collector slope
- ✓ Volume of Storage Tank
- ✓ Mass of adsorbent

(ii) Optimizing these parameters for best system performance.

(iii) Validation of the simulation results.

1.7 JUSTIFICATION FOR THE RESEARCH

From the literature review, various combinations of adsorbate/adsorbent pairs and configurations have been reported as designed, constructed and tested. Some simulations using TRNSYS, Engineering equation solver (EES), and Matlab have been done.

- At the moment absorption refrigeration cycles are most promising technologies, however, the adsorption cycles have the distinct advantage over the other heat driven refrigeration cycles in their ability to be driven by heat of relatively low temperature.
- For food storage and freezing the adsorption system still remains the most viable for solar powered refrigeration though the COP theoretically possible (0.3-0.8) is yet to be achieved in systems so far developed.

- Two adsorbent/adsorbate pairs are for now predominant in refrigeration systems – Zeolite/water and activated carbon/methanol. Zeolite/water is usually used for cooling systems while activated carbon/methanol is used in ice making systems.

However none of these efforts have attempted to optimize each subunit of the adsorption system either for air cooling or refrigeration in this part of the world with abundant solar energy resources.

This work presents an efficient solar adsorption refrigeration system using the activated carbon-methanol pair with an attempt to optimize the heating and cooling subsystems for the given environmental data, so that construction maybe attempted later on the basis of expected optimum performance.

CHAPTER TWO

LITERATURE REVIEW

Solar cooling is not a new idea as passive cooling of buildings dates back to ancient times (Florides et al, 2002). Passive cooling is attaining comfort by evaporative cooling, thermal inertia of the building, ventilation and shading (Sayigh and McVeigh, 1992).Passive solar cooling is however not always enough to achieve thermal comfort and it is to this end that active solar cooling systems driven by cost effective heat sources are introduced.

A number of researchers have over the years worked on absorption refrigeration systems. Ezeilo (1978) compared flat plate collectors and solar concentrators for supplying heat for generation in an adapted kerosene-fired domestic Electrolux refrigerator. The flat plate collector was of a single glass cover type with blackened corrugated copper plate to which were soldered copper pipes; the concentrator was wooden parabola with small strips of reflecting mirrors glued onto the inner surface. The flat plate collector was found to be more effective giving temperatures drop of 14^{o}C below ambient as against 6^{o}C obtained with the parabolic concentrator.

Onochie (1987) designed and constructed a vapor absorption refrigerator with a flat plate single glaze collector design made of copper. The working media was methanol-lithium bromide and zinc bromide solution. Methanol was the refrigerant while the mixture of lithium bromide and zinc bromide (ratio 2:1) was the absorbent. The design achieved a minimum evaporator temperature of -8^{o}C.

Awoniyi (1980) designed and constructed a solar-powered vapor absorption refrigeration system but could not carry out performance tests due to fabrication errors- inability to get a leak proof set-up.

Erhard et al (1998) conducted the testing and simulation of a solar powered sorption cooling machine with no moving parts. The absorber/desorber was mounted inside a concentrating solar collector. The working consists of ammonia as refrigerant and strontium chloride as the absorbing medium. A numerical simulation program for this machine was developed and tested.

Florides et al (2002) modeled and simulated an absorption solar cooling system using the TRNSYS simulation program and a typical meteorological year file for Nicosia, Cyprus. System optimization was carried out in terms of type of collector, size of storage tank, collector slope and area. The optimized system consists of a $15m^2$compound parabolic collector tilted $30^o$from the horizontal and a 600liters hot water storage tank.

Valizadeh (1996) proposed a Platen-Munters system using ammonia-water and hydrogen with an evacuated solar collector and thermal storage. The design evaporator temperature is -19^oC with a solar collector temperature of 200^oC.

Bula et al (2000) carried out a thermodynamic simulation of a solar absorption refrigeration cycle with an ammonia-water binary mixture. It was found that the heat exchanger efficiency determines the maximum temperature that can be used at the generator in order to obtain maximum COP out of the system.

Mittal (2006) however modeled and simulated a solar absorption cooling system for India. The study showed that the hot water inlet temperature affects the surface area of some of the system components, increasing this temperature decreases the absorber and solution heat-exchanger surface area and increases the system COP.

Ileoje (1983) designed, constructed and tested a solar powered adsorption refrigerator consisting of a flat plate double cover collector made of steel sheets. The working media employed was ammonia-calcium chloride, with ammonia as the refrigerant and calcium chloride the absorbent. The design achieved an ice production of 0.41 kg/m^2/day.

Enibe and Ileoje (1997) designed solar collectors from aluminum and steel, filled with the adsorbent. The results showed that with the developed steel collector, the COP of the system could be improved by at least 30%, though the COP in the tested condition was found to be 0.08. This COP could be improved upon by enhancing the cooling of the collector during re-adsorption and upgrading the heat transfer characteristics of the evaporator.

Anyanwu et al (2001) simulated a solid adsorption solar refrigerator using activated carbon/methanol adsorbent/refrigerant pair. The peak plate and tube surface temperatures and methanol generation were predicted to within 3%, 25% and 4% respectively. The peak times and time for commencement of generation were however accurately predicted.

Anyanwu and Ezekwe (2003) carried the design, construction and test run of a solid adsorption solar refrigerator using activated carbon/methanol pair. The flat plate collector had an effective exposed area of 1.2m^2. Ambient temperature during generation and adsorption varied from 18.5-34^oC. The refrigerator yielded evaporator temperatures ranging from 1.0-8.5^oC for water initially at 24-28^oC.

Anyanwu (2005) carried out a thermodynamic design procedure for a solid adsorption solar refrigerator. This procedure was applied to systems with activated carbon/methanol, activated carbon/ammonia and zeolite/water as adsorbent/adsorbate pairs. The results gave a maximum possible solar COP as 0.3, 0.19 and 0.16 for zeolite/water, activated

carbon/ammonia and activated carbon/methanol respectively when a conventional flat plate solar collector was used.

A recent study by Anyanwu and Ogueke (2005), suggests that zeolite/water is the best pair for air conditioning applications, while activated carbon/ ammonia is better for low temperature applications e.g. food preservation and freezing. The study also showed that the most important parameters for operation are adsorption and condensation temperatures. Evaporator temperature has little effect on system performance. The maximum possible net solar COP was found to be 0.3, 0.19 and 0.16 for zeolite/water, activated/ammonia and activated carbon/methanol respectively when a conventional flat plate solar collector is used.

The effect of different collector design parameters on the performance of solar powered solid adsorption refrigerator using activated carbon-methanol pair was studied by Ogueke and Anyanwu (2008). The study showed that the optimized collector plate absorptivity/emissivity combination yield a 175% improvement in COP and 92% improvement in condensate yield. The optimal choice of parameters was found to be 0.133m for tube spacing and 476 kg/m^3 for adsorbent packing density.

Researches have also been carried out around the world; Boubakri et al (1992b), from experimental study concluded that for solar powered adsorptive ice-makers, nocturnal temperature appeared to be an important factor. Cold nights (10^{o}C) largely increased production with an average daily production of ice at 4 kg/m^2. This had an increase of 1 kg of ice with a nocturnal cooling system.

Headley et al (1994) experimented with charcoal-methanol adsorption refrigerator powered by a compound parabolic concentrating solar collector (CPC) of concentration ratio 3.9 and aperture area 2.0m^2. The copper tube receiver of the CPC was packed with 2.5 kg of

adsorbent 207E3. 1 kg of ice at an evaporator temperature of -6^{o}C was produced, the net solar COP being of the order of 0.02. Maximum receiver/adsorbent temperature was 154^{o}C on a day when the insolation was 26.8 MJ/m^2. However, temperatures in excess of 150^{o}C were found to be undesirable as it favored the conversion of methanol to dimethyl ether, a non condensable gas which inhibits both condensation and adsorption. The major advantage of the system is its ability to produce ice even on overcast days with insolation of $\leq$ 10MJ/m^2.

Oertal and Fischer (1998) built a continuous adsorption cooling system for solid storage using silica gel/ methanol pair. Flat plate solar collectors were used to supply heat to the sorption reactor. A refrigeration temperature of -2^{o}C was found to be achievable with a reaction temperature of 80-90^{o}C.

Li and Sumathy (1999) worked on a solar powered ice maker with solid adsorption pair of activated carbon and methanol. Domestic type charcoal was used as the adsorbent and a simple flat plate collector with an exposed area of 0.92m^2 employed to produce ice of about 4-5 kg/day at an evaporator temperature of about -6^{o}C. Coefficient of performance (COP) of the system ranged between 0.1-0.12.

Hildbrand et al (2004) built an adsorptive solar refrigerator in Yverdon-les-Bain, Switzerland. Silica gel and water adsorption pair was used with cylindrical tubes functioning as both the adsorber system and the solar collector. The collector is of flat plate, double glazed design 2m^2 in area. The condenser is air-cooled while the evaporator holds 40 litres of water that can freeze. The COP_{SR} obtained ranged from 0.10 - 0.25 with a mean value of 0.16.

Li and Wang (2002) studied the effect of design parameters and ambient conditions on the performance of a solar powered solid adsorption refrigerator. The results showed that the

significant parameter which affects the system is the number of collectors and the heat transfer between the metallic plate and adsorbent. The study showed that ambient conditions also strongly affect the performance of the solar refrigerator.

Zhang and Wang (2002) proposed a continuous adsorption system for heating and cooling. During the daytime, the system works on the heating mode, producing 30kg of hot water at about 48^{o}C with the $COP_{heating}$ of 0.34. At night however, the cooling mode switches on with a cooling capacity of 0.13MJ/m^2 of the heat collecting area but with a $COP_{cooling}$ of 0.18.

Eduardo and Sagredo (2004) designed and constructed a solar energy refrigeration system using vacuum concentric tubes with adsorption. Activated charcoal and methanol was employed as the working fluid, though the system is still in its early stages of development.

Wu et al (2009) carried out a mathematical simulation and experimental study of a modified zeolite 13X-water adsorption refrigeration module. The calculated values were then validated with experimental data and a good correlation obtained.

El Fadar (2009a) studied an adsorption refrigeration system powered by a parabolic trough collector and coupled with a heat pipe illustrated in Fig 2.1. The study showed that for each aperture width value of the collector, there is an optimum external radius of adsorbent bed. The COP is 0.18 for an evaporator, condenser, adsorption temperatures of 0^{o}C, 28^{o}C, 24^{o}C respectively.

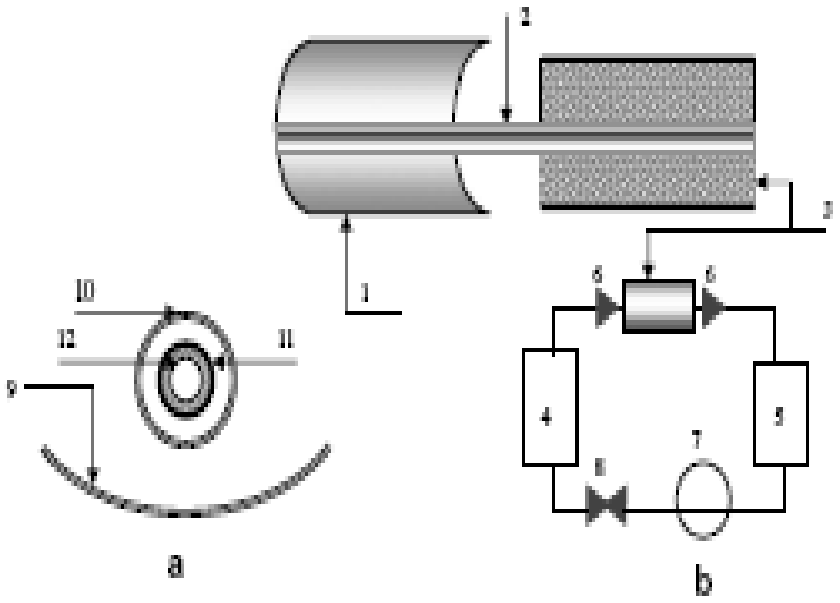


Fig 2.1: Simplified view of the El Fadar et al system: 1.PTC; 2. heat pipe; 3. adsorber; 4. evaporator; 5. condenser; 6. valves; 7. tank; 8. expansion valve; 9. reflective surface; 10. glazing; 11. absorber; 12.wick.

The above study was repeated by El Fadar (2009b) without the heat pipe. Under climatic conditions of daily solar radiation of 17.5MJ/m^2, operating conditions – evaporator and condenser temperature of 0^{o}C and 30^{o}C respectively with a heat source temperature of 100^{o}C, the results indicated a system SCP of 104W/kg, refrigeration cycle COP of 0.43 and a useful cooling of 2515kJ per 0.8m^2 of collector area.

A solar hybrid methanol/silica gel based on the adsorption cooling system was designed and tested by Mande et al (1996) for the storage of agricultural products in India. The test setup is as shown in Fig 2.2 below. The 10kW_{th} capacity cooling unit offered cooling with a COP of 0.3 to maintain a cold storage at 1 to 3^{o}C and cooling density of 100W/kg of silica gel at an evaporator temperature of 0^{o}C.

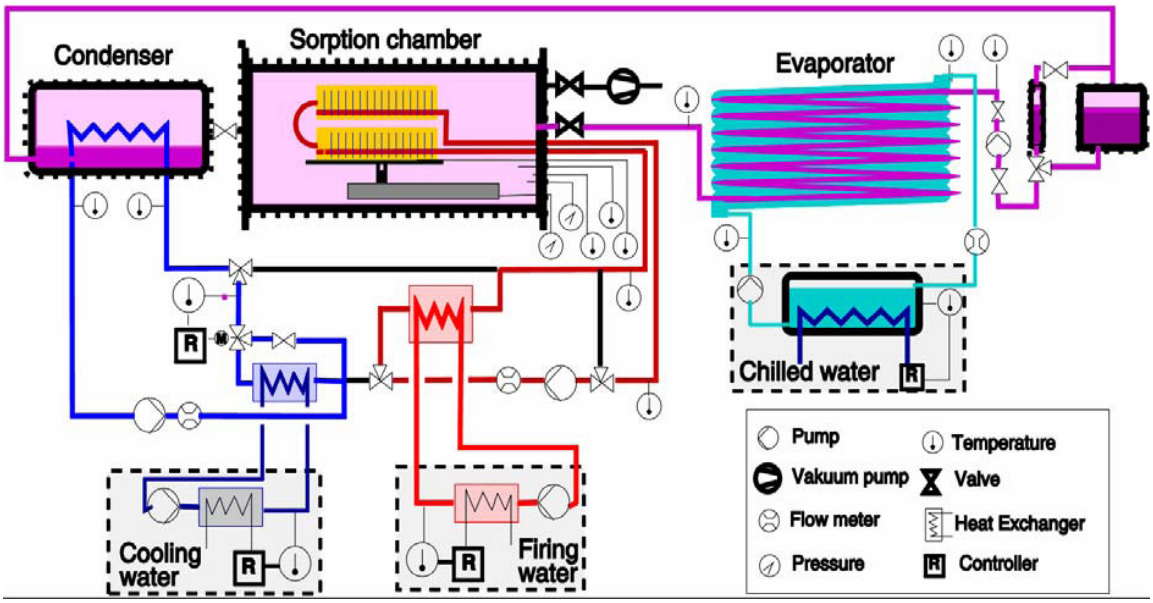


Fig 2.2: Test setup for the Solar Hybrid methanol/silica gel cooling system (Mande, 1996)

The performance of two adsorption ice making test units using activated carbon and a carbon composite as adsorbents was investigated by Wang et al (2006). The physical adsorption icemaker that employed consolidated activated carbon-methanol as working pair had an optimum coefficient of refrigeration performance (COP), specific volume cooling power density (SCP_v) and specific cooling power per kg of adsorbent (SCP) of 0.125, 9.25kW/m^3 and 32.6W/kg, respectively. The composite adsorption system that employed the consolidated composite adsorbent had a maximum COP, SCP_v and SCP of 0.35, 52.68kW/m^3 and 493.2 W/kg, respectively for ice making mode.

Khattab (2004) developed a novel solar powered adsorption refrigeration module and tested with four types of bed techniques and four reflector arrangements. The module gave an optimum daily ice production of 6.9 and 9.4kg/m^2 and net solar COP of 0.136 and 0.159 for cold and hot climates respectively.

An experimental evaluation of an adsorptive solar-powered refrigerator applied to ice production using activated carbon-methanol pair was made by Leite et al (2004). The

machine produced 6kg of ice per day, which correspond to a solar coefficient of performance (COP_s) of 0.085.

Rahman et al (2006) designed and fabricated a solar powered adsorption refrigeration system at the Islamic University of Technology, Bangladesh as illustrated in Fig 2.3. The system was tested with activated charcoal/methanol and refrigerant R-11 pairs. A domestic type of charcoal was chosen as the adsorbent and a simple flat plate collector with an exposed area of $0.4m^2$ was employed to produce cooling. Readings were taken on hourly basis for both activated charcoal-methanol and activated charcoal-refrigerant R-11. For the activated charcoal-methanol pair, the water in the tank was heated to a maximum temperature of 82^oC and minimum temperature obtained was 17^oC was obtained in the evaporator, while the for the pair of activated charcoal-refrigerant R-11, the water in the a

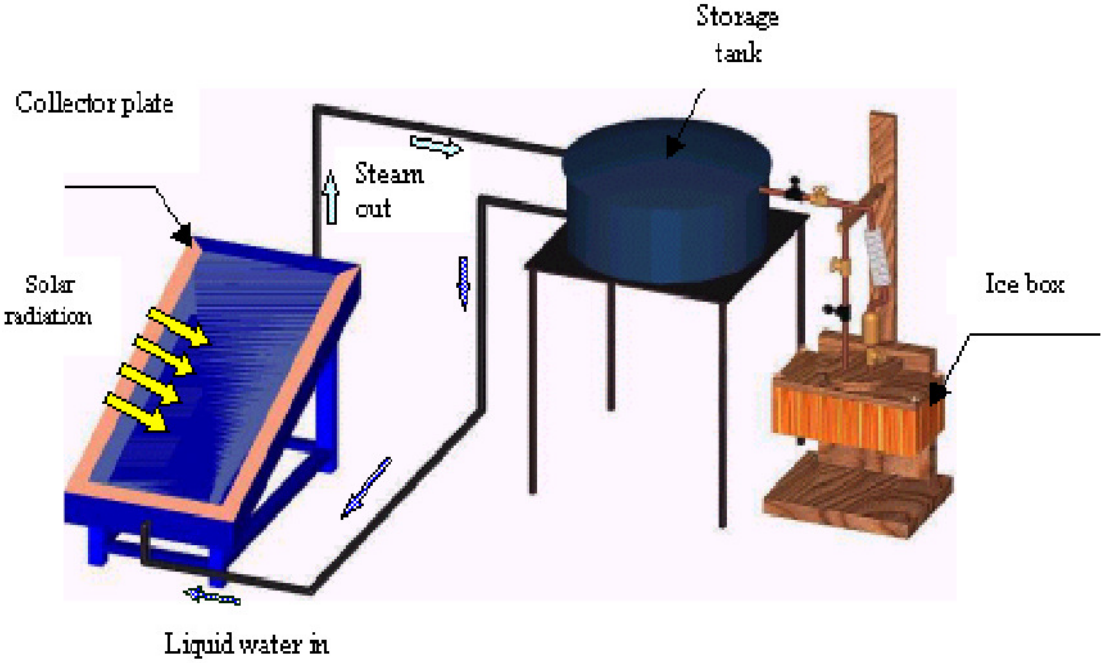


Fig 2.3: Rahman Solar powered adsorption refrigeration system (Rahman, 2006)

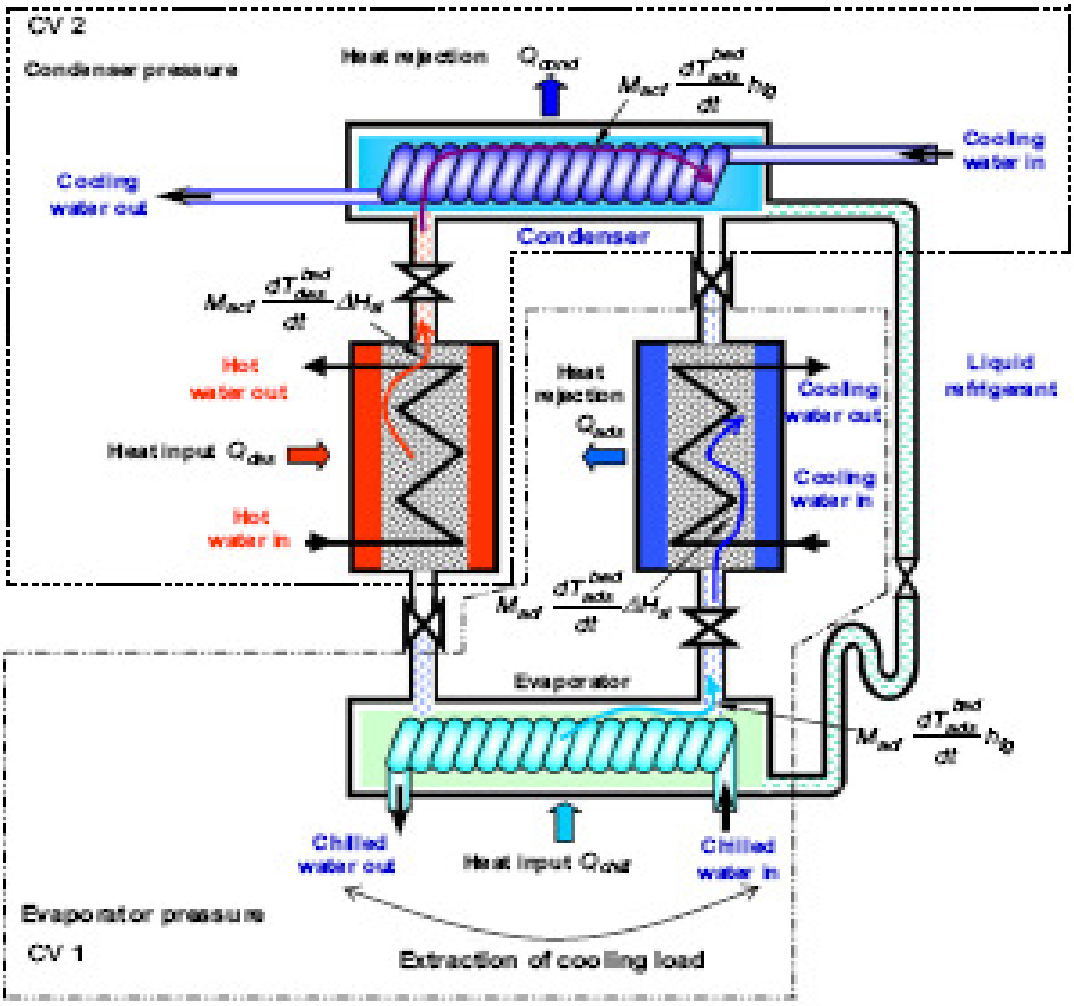
maximum temperature of 90^{o}C with a minimum temperature of 16^{o}C achieved in the evaporator.

Waszkiewicz et al (2001) analyzed an adsorption refrigeration system using zeolite and methanol. A thermal model based on Dubnin-Astakhov equation and its thermodynamic analysis was presented. The effective specific heat dQ/dT was found to depend on the thermal properties of zeolite, heat of adsorption and the amount of fluid adsorbent per unit temperature change. Computer simulation to determine the effects of operating conditions find typical estimates of COP as 0.535 for a single bed cycle and about 0.925 for a twin bed cycle.

The TRNSYS 16 and EES simulation tools were used to model and analyze the performance of a solar-driven ejector refrigeration system by Pridasawas (2007). The whole system was modeled under the TRNSYS environment, with the model of the ejector refrigeration subsystem developed in the Engineering Equation Solver (EES) program. The results from the simulation indicated an average yearly system thermal ratio (STR) of about 0.22, cooling subsystem COP of 0.48 and solar collector efficiency of 0.47 at an evaporator temperature of 15^{o}C and condenser temperature of 5^{o}C above ambient temperature. The system has an evacuated collector area of 50m^{2} and hot water storage tank volume of 2m^{3}.

Saha et al (2007) presented the transient modeling for a two bed, activated carbon fiber (ACF)-ethanol adsorption chiller shown in Fig 2.4. The adsorption-evaporation process is shown in CV1 wile the desorption-condensation process is shown in CV2. This innovative adsorption chiller employs pitch based ACF of type A-20 as adsorbent which is a fibrous adsorbent having the advantages of fast adsorption rate, high porosity and ease of handling when compared with granular adsorbents and powdered adsorbents. Ethanol is used as refrigerant as it presents no harm to the environment; it is non-toxic and has comparatively

higher vapor pressure even at low temperature. This system utilizes effectively low-temperature waste heat sources of temperature between 60 and 95°C along with a coolant at 30°C. Regardless of initial mass distribution, the ACF-adsorption chiller is able to achieve the same cyclic-steady-state within three cycles of 1890 secs.



Hamamoto et al (2006) investigated the system performance of an adsorption cycle. The cycle utilizes activated carbon fiber (ACF)/methanol as adsorbent/refrigerant pair. In this work, specific cooling effect (SCE) and COP of the system are numerically operated from

the adsorption equilibrium theory with different hot, cooling and chilled fluid inlet temperatures. It was shown that there is an optimum condition for COP to reach a maximum and the system shows better performance with lower chilled fluid inlet temperature between -20 and 20^{o}C.

Hamdih and Al-Muhtaseb (2009) presented the design of a prototype of a solar adsorption refrigeration unit suitable for use as an air-conditioning and refrigeration unit in remote areas. The device uses the activated carbon/methanol pair. A minimum refrigerator temperature of 9^{o}C was obtained for an ambient temperature of 26^{o}C. The gross cycle coefficient of performance of 0.688 was obtained.

Chang (2007) studied experimentally a solid adsorption cooling system with silica gel as the adsorbent and water as the adsorbate. To reduce manufacturing costs and simplify the construction of the adsorption chiller, a vacuum tank was designed to house the adsorption bed and evaporator/condenser. Flat-tube type heat exchangers were used for the adsorption beds in order to increase the heat transfer area and improve the heat transfer ability between the adsorbent and heat exchanger fins as shown in Fig 2.5. Under the standard test conditions of 80^{o}C hot water, 30^{o}C cooling water, and 14^{o} C chilled water inlet temperatures, a cooling power of 4.3kW and a coefficient of performance (COP) for cooling of 0.45 were obtained. It provided a specific cooling of 176W/kg of adsorbent. At lower hot water flow rates however, a higher COP of 0.53 can be achieved.

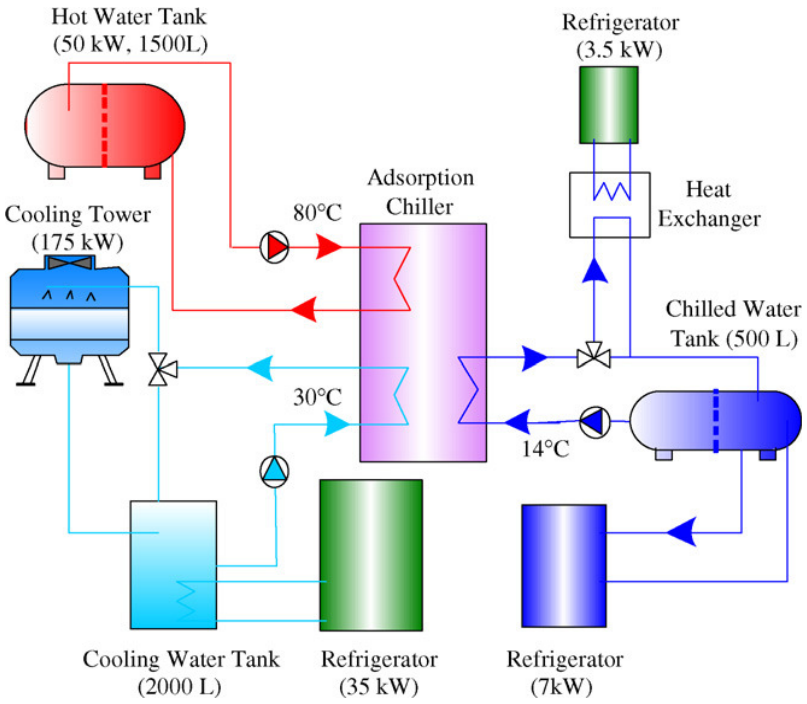


Fig 2.5: Schematic of solid adsorption cooling system with flat tube heat exchangers as adsorption bed (Chang, 2007).

Lemmini and Errougani (2005) built and tested a solar-powered adsorption refrigerator using AC35-methanol pair in Rabat, Morocco. The system consists of a flat-plate collector, a condenser and an evaporator (Fig 2.6). Experimental results showed that the unit can produce cold air even for rainy and cloudy days and solar COP ranges between 0.05 and 0.08 for an irradiation between 12,000 and 27,000kJ/m^2, a daily mean ambient temperature between 14 and 18^{o}C and temperature achieved by the evaporator ranging from -5 and 8^{o}C.

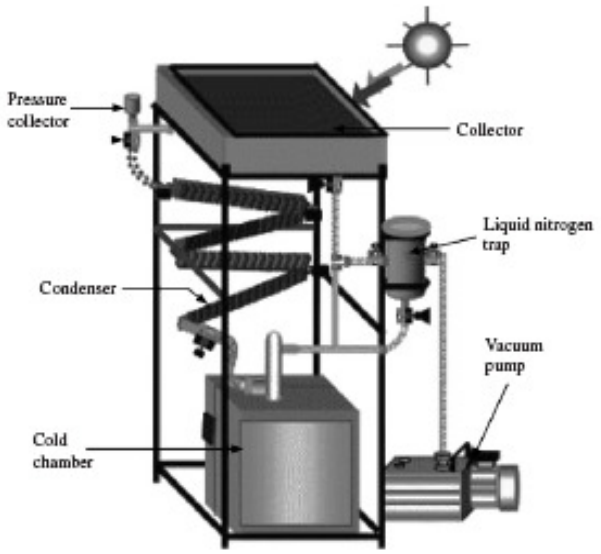


Fig 2.6: Experimental layout of Lemmini (2005) adsorption refrigerator

Yeung and Sumathy (2003), presented the description and operation of a solar-powered hybrid adsorption ice-maker with activated carbon fiber and methanol as the working pair. The analysis indicated that by adapting more adsorbers instead of the conventional single adsorber, the system performance could be improved. Employing an evacuated vacuum tube collector with an exposed area of $2m^2$ a COP of 0.56 and 6kg of ice per day were achieved.

Habib et al (2011) carried out an investigation on the performance of a combined adsorption refrigeration cycle. This novel combined cycle has the activated carbon (AC)-R507a as the bottom cycle and AC-R134a cycle as the top cycle with the bottom cycle delivering refrigeration load at as low as -10^oC as presented in Fig 2.7. The cycle simulation is based on the experimentally confirmed adsorption isotherms, kinetics and isosteric heat of adsorption data for R134a and R507A on highly porous based activated carbon of type Maxsorb III. The optimum cooling capacity, coefficient of performance (COP) and chiller efficiency are calculated in terms of cycle time, switching time,

regeneration and brine inlet temperatures. Results show that the combined adsorption cycles are feasible even when low-temperature heat source is available.

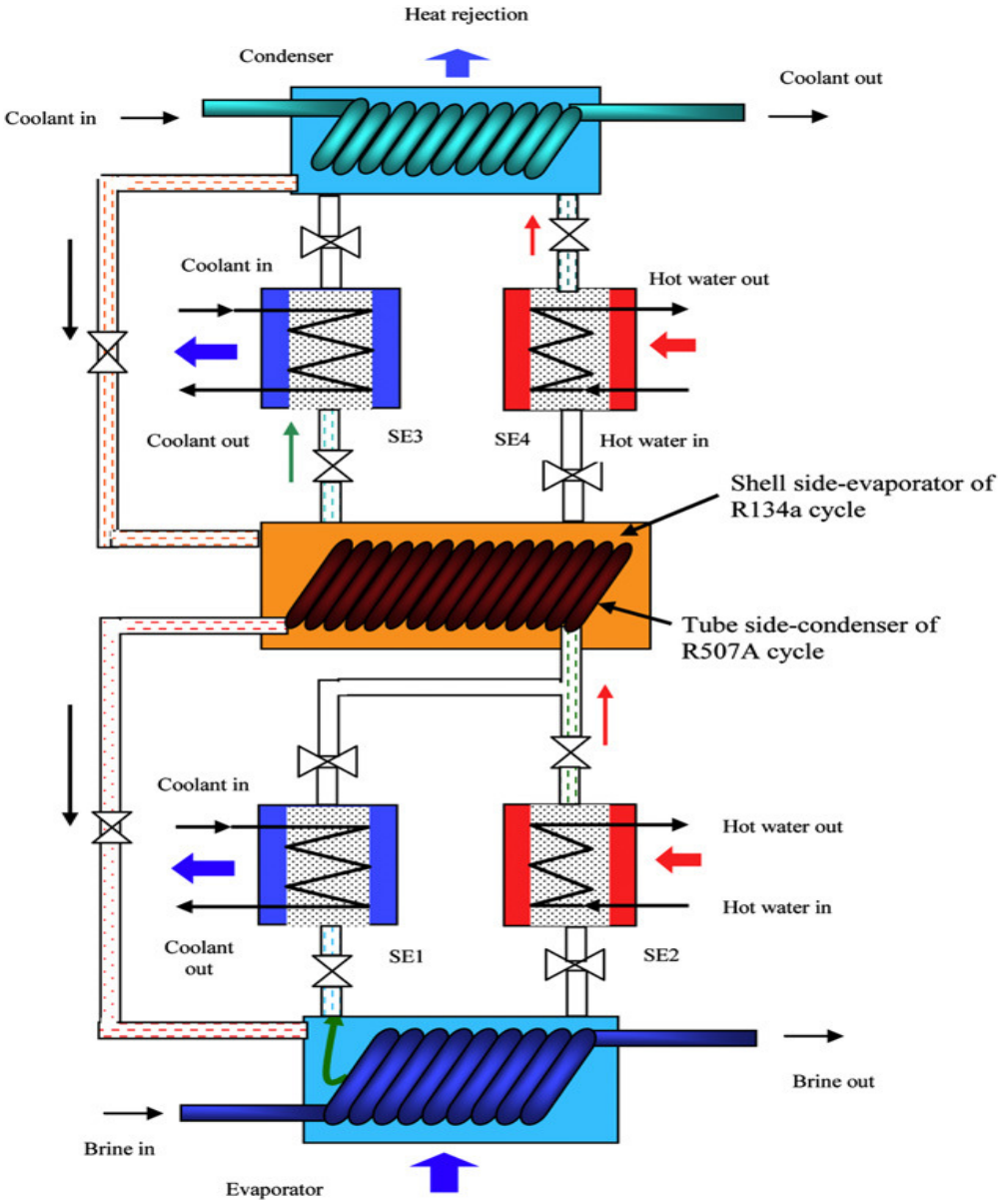


Fig 2.7: Schematic diagram of a combined adsorption chiller (Habib et al, 2011)

CHAPTER THREE

THERMODYNAMICS OF ADSORPTION CYCLES

The thermodynamic design procedure for the adsorption refrigeration cycle using the activated carbon-methanol pair as adsorbent/adsorbate is presented. Adsorption refrigeration has been studied extensively and typical adsorption refrigeration cycles have been developed. These cycles include intermittent (basic) cycle, heat recovery cycle and the heat and mass recovery cycle.

3.1 BASIC ADSORPTION REFRIGERATION CYCLE

A basic adsorption refrigeration cycle consists of four thermodynamic processes as explained in Chapter 1. These processes are as represented on the Clapeyron diagram Fig. 3.1. The idealized cycle begins at point A where the adsorbent is at a low temperature T_A and low-pressure P_e (evaporator pressure). A – B represents the isosteric heating (constant concentration) of the adsorbent with the adsorbate. The continued heating of the adsorbent from B to D causes some adsorbate to be desorbed and its vapor is condensed at point C. Desorption takes place at constant pressure (isobaric) and the heat required is the heat of desorption plus sensible heating of the adsorbent bed. When the adsorbent reaches its maximum temperature $T_{D,}$ desorption stops with the transfer of liquid adsorbate from the condenser to the evaporator (C – E). The adsorbent bed is then subjected to isosteric cooling decreasing the temperature from T_D to T_F and a corresponding decrease of pressure from P_c to P_e. The adsorbent bed

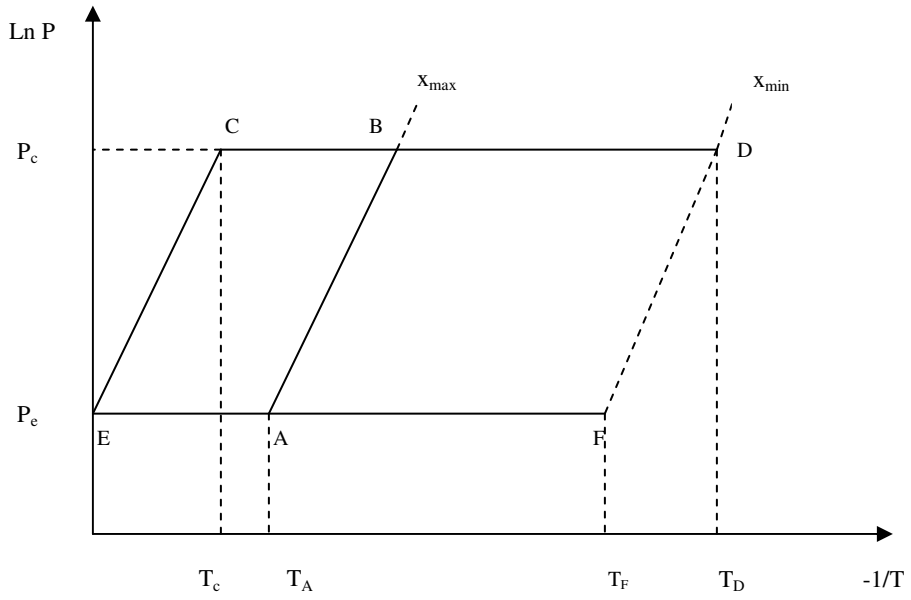


Fig. 3.1: Clapeyron diagram of the ideal adsorption cycle

adsorbs the adsorbate from the evaporator when its pressure reaches the evaporator pressure $P_{e,}$ the temperature of the adsorbent bed thereby drops from T_F to T_A. This process is an isobaric process with the heat given off being the heat of adsorption plus that of sensible cooling.

The heat input to the system and the refrigeration effect needs to be evaluated if the COP of the cycle is to be determined. From fig 3.1, for the processes A – B (isosteric heating) and B – D (isobaric desorption), heat is added to the adsorbent bed.

The heat input to the adsorbent bed for isosteric heating (A – B) can be evaluated as

$$Q_{ih} = m_{ac}\left(c_{p_{ac}} + c_{v_m} x_{\max}\right)\left(T_B - T_A\right) \quad \text{.....3.1}$$

where m_{ac} is the mass of activated carbon in kg, c_{pac} is the specific heat of activated carbon in kJ/kg.K, c_{vm} is the specific heat of methanol in adsorbed in kJ/kg.K and x_{max} is the maximum mass of adsorbed adsorbate per kg of adsorbent.

The heat required for the desorption process (B – D) has two components-

$$Q_{id} = Q_{des} + Q_{sh} \quad \text{……..3.2}$$

where Q_{des} is the heat of desorption given by

$$Q_{des} = m_{ac} \int_{x_{\max}}^{x_{\min}} \Delta H \, dx \quad \text{……..3.3}$$

ΔH is the average heat of sorption for the adsorbent/adsorbate pair in kJ/kg evaluated at condenser pressure.

Q_{sh} is the sensible heat of adsorbent plus its adsorbate content evaluated as

$$Q_{sh} = m_{ac} c_{p_{ac}} \left(T_D - T_B\right) + m_{ac} c_{p_m} \int_{T_B}^{T_D} x(T)\, dT \quad \text{……..3.4}$$

The useful refrigeration effect which is the energy that must be supplied to the evaporator, Q_{ev}, is evaluated as the difference between the latent heat of evaporation of the cycled adsorbate and the sensible heat of the adsorbate entering the evaporator at condensation temperature.

$$Q_{ev} = m_{ac}\left(x_{\max} - x_{\min}\right)\left[L_e\left(T_e\right) - \int_{T_e}^{T_c} c_{p_{ml}}\left(T\right) dT \right] \quad \text{……3.5}$$

C_{pml} is the specific heat of methanol in liquid phase and L_e is the heat of evaporation of methanol in kJ/kg and x is the mass of adsorbed adsorbate per kg of adsorbent.

The coefficient of performance (COP) for the operation is thus given as

$$COP = \frac{Q_{ev}}{Q_{ih} + Q_{id}} \quad \text{……...3.6}$$

3.2 HEAT RECOVERY ADSORPTION REFRIGERATION CYCLE

This cycle is a quasi continuous cycle usually operated with two adsorbent beds out of phase. One adsorbent bed is heated while the other is cooled. The bed to be cooled transfers its heat to the adsorber bed that is to be heated, this heat comprises of the sensible heat and the heat of adsorption thus increasing the COP of the system. The operation of the heat recovery cycle is however more complicated than the intermittent cycle since this cycle includes several valves, pumps, auxiliary heaters/cooler and control unit.

In evaluating the COP of the heat recovery adsorption cycle, the recovered heat (Q_{reg}) has to be determined. Q_{reg} is however dependent on the heats released during isosteric cooling of the adsorber bed and during the isobaric adsorption phase.

The heat released by the adsorbent bed in isosteric cooling (D – F) in fig 3.1, is the sensible heat only and is evaluated as

$$Q_{ic} = m_{ac}\left(c_{p_{ac}} + c_{v_m} x_{\min}\right)\left(T_D - T_F\right) \quad \text{.....3.7}$$

For the isobaric adsorption phase (F – A), the total heat released (Q_{ia}) is the sum of the heat of adsorption (Q_{ads}) and the sensible heat (Q_{sa}) generated from cooling the adsorbent and adsorbate from temperature T_F to T_A, minus the energy needed to heat up the vapor from evaporation to adsorption temperature (Q_{vea}).

$$Q_{ia} = Q_{ads} + Q_{sa} - Q_{vea} \quad \text{.....3.8}$$

where

$$Q_{ads} = -m_{ac}\int_{x_{\min}}^{x_{\max}} \Delta H \, dx \quad \text{.....3.9}$$

The heat of sorption H is evaluated for equation (3.9) at the evaporator pressure. Q_{sa}, the sensible heat released by cooling the adsorbent and its adsorbate content is

$$Q_{sa} = m_{ac} c_{p_{ac}} \left(T_F - T_A\right) + m_{ac} c_{p_m} \int_{T_A}^{T_F} x(T) dT \quad \text{.....3.10}$$

And

$$Q_{vea} = m_{ac} \sum_{i}^{n} \left(x_i - x_{i-1}\right) c_{p_m} \left(T_e\right) \left(\overline{T}_s - T_e\right) \quad \text{.....3.11}$$

$\overline{T}_s$ is the average saturation temperature evaluated between i and (i – 1), and

$$n = \frac{x_{\max} - x_{\min}}{k} \quad \text{.....3.12}$$

k << 1 is a constant related to the accuracy of the model (Demirocak, 2008).

3.3 HEAT AND MASS RECOVERY ADSORPTION REFRIGERATION CYCLE

Mass recovery has been proven to be very effective in raising the cooling capacity of heat recovery adsorption heat pumps. In this system, at the end of each half cycle, one adsorber is cold while the other is hot. The cold adsorber which is at a low pressure requires pressurization to the condenser pressure, while the high pressure (hot) adsorber needs to be depressurized to the evaporator pressure. This pressurization and depressurization process is achieved by transferring vapor from the hot adsorber to the cold adsorber. This process which is also referred to as the internal heat recovery process has been reported to increase COP by more than 10% (Sumathy et al, 2003).

The P-T-x diagram of an ideal heat and mass recovery cycle is shown in fig 3.2. The mass recovery cycle ($a_2 – a_3 – g_1^1 - g_1 – g3 – a_1^1 - a_1 – a_2$) is an extended form of a two bed basic or heat recovery cycle ($a_2 – g_1 – g_2 – a_1 – a_2$).

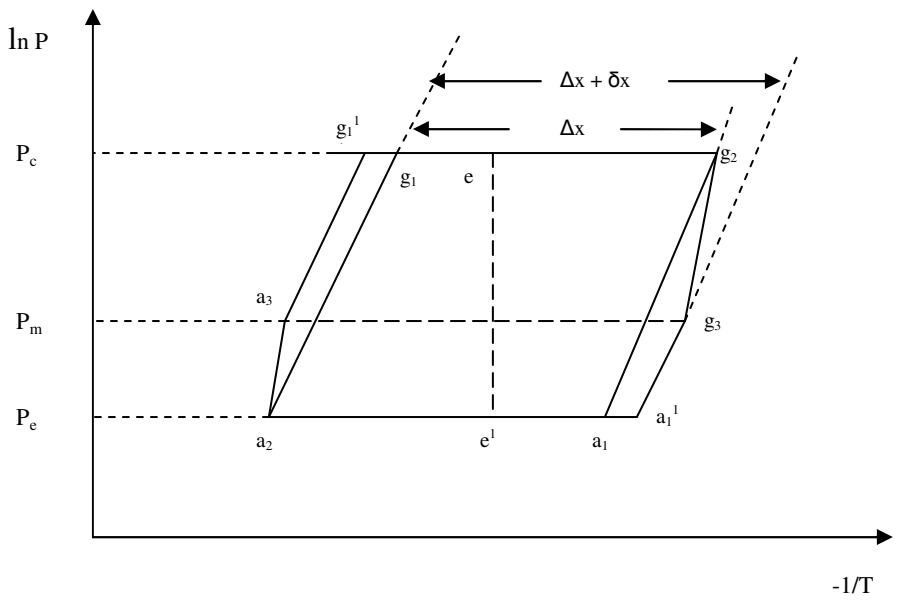


Fig. 3.2: P-T-x diagram of heat and mass recovery cycle

The cycled mass increases from Δx to (Δx + δx), which results in an increase in refrigeration effect. The cycle starts with the mass recovery process ($g_2 - g_3$ and $a_2 - a_3$). After this pressure equalization, the final pressures of the two adsorbers are equal.

$$P_{a_3} = P_{g_3} = P_m \qquad \text{……..3.13}$$

The heat recovery process then starts with heat being transferred from the hot adsorber to the cold adsorber ($g_3 - e^1$), to achieve this, the hot adsorber is first depressurized ($g_3 - a_1^1$), then it adsorbs vapor from the evaporator ($a_1^1 - e^1$). On the other hand, the cold adsorber is initially pressurized ($a_3 - g_1^1$) and vapor subsequently desorbed (g_1^1 - e). Theoretically, it is assumed that the heat recovery process continues until the adsorbers are at the same temperature (i.e. $T_e = T_e^1$), but in practice, there exists a small difference in temperatures T_e and T_e^1 at the end of the heat recovery process. The adsorbers are finally connected to the heat source and sink (to close each half cycle) respectively ($e - g_2$ and e^1 - a_2). The second half cycle follows the same process except that the roles of the adsorbers are reversed. In

simulating this model, it is usually assumed that the entire vapor desorbed from the hot adsorbent bed is adsorbed by the cold adsorbent bed.

$$\Delta x_{g_2-g_3} = \Delta x_{a_2-a_3} \quad \text{.....3.14}$$

The mass recovery process is also assumed to occur under adiabatic conditions where the temperature variation is dependent on the adsorption or desorption in the individual bed.

$$\int_{T_{a_3}}^{T_{a_2}} \left(c_{p_{ac}} + x c_{p_m} \right) dT = \int_{T_{a_3}}^{T_{a_2}} H \, dx \quad \text{.....3.15}$$

And

$$\int_{T_{g2}}^{T_{g_3}} \left(c_{p_{ac}} + x c_{p_m} \right) dT = \int_{T_{g2}}^{T_{g_3}} H \, dx \quad \text{.....3.16}$$

Where dx, the change in the adsorbed mass of adsorbate is evaluated between the temperatures shown.

3.4 METHODOLOGY

The following methodology is to be employed in achieving the objectives listed above.

(i) First a thermodynamic design of the adsorption cooling system will be undertaken.

(ii) Modeling of the adsorbent-refrigerant pair used in the adsorption cycle will be carried out using Matlab to determine the effect of condensation, evaporation and generation temperatures on system performance and to obtain optimum values of these temperatures for the adsorbent-refrigerant pair chosen.

(iii) A solar thermal system will then be constructed using the Transient System Simulation software (TRNSYS) integrating three types of collectors namely; flat plate, evacuated tube and the parabolic trough solar collectors.

(iv) The performance of the solar thermal system with the integrated collectors will be studied to determine the optimum values of parameters such as the collector area, slope and storage tank volume.

(v) The optimized solar thermal system will then be linked to the adsorption cycle to produce a solar powered adsorption refrigeration system which operates on the temperatures obtained above.

(vi) Steady and seasonal transient simulations will then be carried out on the solar powered adsorption refrigeration system constructed in TRNSYS to evaluate its year round performance after which the simulation results will be validated.

3.5 SIMULATION OF A SIMPLE ADSORPTION REFRIGERATION CYCLE

The simulation of the basic adsorption refrigeration cycle is undertaken with the simulation model developed with Matlab as shown in Appendix A. This simulation allows the COP of the system as a function of the regeneration temperature to be determined for different evaporator and condenser temperatures. In order to calculate the COP for the basic refrigeration cycle, some assumptions are made –

(i) The specific heat of dry activated carbon is assumed to be constant with a value of 711 J/kgK.

(ii) Specific heat of methanol in the bulk liquid phase has a value of 2534 J/kgK. The specific heat of methanol vapor at constant pressure is taken as 1820 J/kgK, while the specific heat of methanol vapor at constant volume is 1560 J/kgK (Hassan et al, 2011).

(iii) The heat of sorption for activated carbon-methanol pair is calculated from the Clausius-Clapeyron equation (Wang, 2001) as

$$H = R\,A\frac{T}{T_s} \quad \text{……..3.17}$$

where R is the gas constant for methanol with a value of 260 J/kgK, T is the sample temperature K, T_s is the saturation temperature corresponding to the gas pressure P. A is a constant corresponding to the slope of the saturation curve on a plot of lnP vs. ($-1/T_s$), for methanol A = 4666 (Khattab, 2006).

(iv) The saturation pressure of methanol is related to its temperature by the Antoine equation (Khattab, 2006)

$$\log_{10} P = a - \frac{b}{T + c} \quad \text{…….3.18}$$

with P in mmHg, T in K and a = 18.587, b = 3626.55, c = -34.29.

(v) The adsorption equilibrium equation used in the simulation is the Dubnin-Astakhov equation

$$x = x_o \exp\left[-k\left(\frac{T}{T_s} - 1\right)^n\right] \quad \text{…….3.19}$$

where x is adsorbed mass of adsorbate per unit of adsorbent mass in kg/kg evaluated at the temperature (T) and pressure (P) of the adsorbent bed. x_o is the adsorption capacity at temperature $T = T_s$ and pressure $P = P_s$. T_s is the saturation temperature at saturation pressure P_s, while T is the adsorbent bed temperature. k and n are characteristic parameters of the refrigeration pair.

Adsorption properties of activated carbon-methanol were tested by Li (2003) and the coefficients of the D-A equation (equation 3.19) are given as: $x_o = 0.45$, k = 13.38 and n = 1.5 for evaporator temperatures ranging from -20 to 35^{o}C.

The results of the simulation generated by the developed MATLAB code (Appendix A) are presented in the figures 3.3 and 3.4.

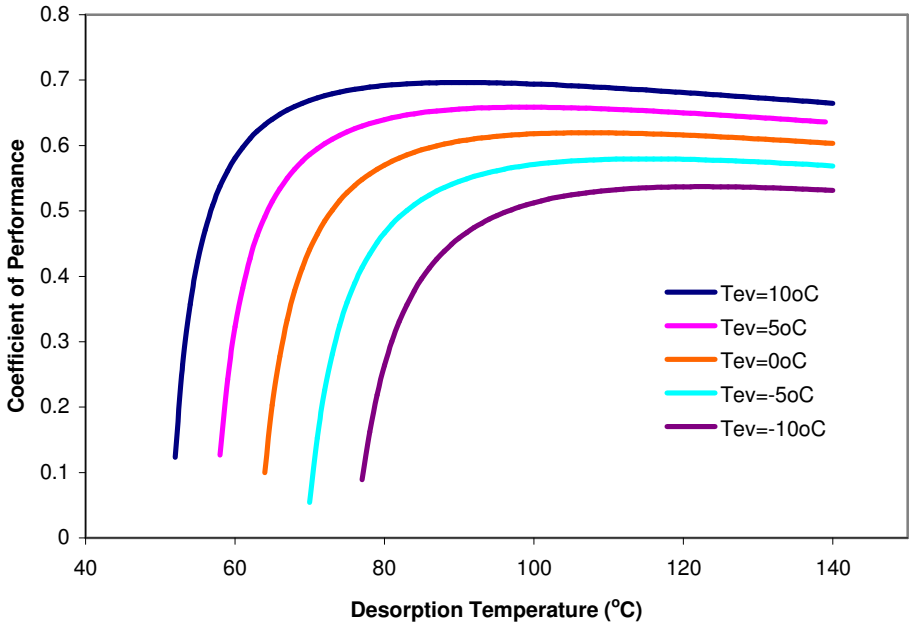


Fig.3.3: Effect of Evaporation Temperature on system COP (T_{cond}=30°C)

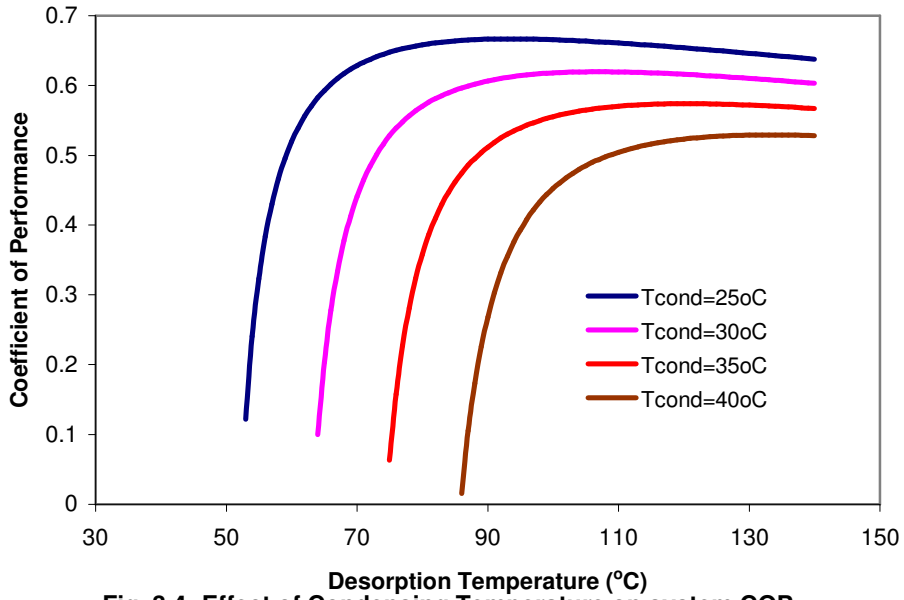


Fig. 3.4: Effect of Condensing Temperature on system COP (T_{ev}=0°C)

From the simulation results presented in Fig.3.3, for the activated carbon-methanol pair, as the evaporator temperature reduces, for a given condenser temperature, the COP reduces for a given regeneration temperature i.e. a higher regeneration temperature is required for the same value of COP. This is because the energy required to raise the temperature from T_{ev} to T_{cond} increases as reflected in the higher desorption temperatures.

Fig. 3.4 shows the variation in COP as the condenser temperature changes for a given evaporator temperature. The higher the condenser temperature, for a given evaporator temperature, the higher the regeneration temperature required.

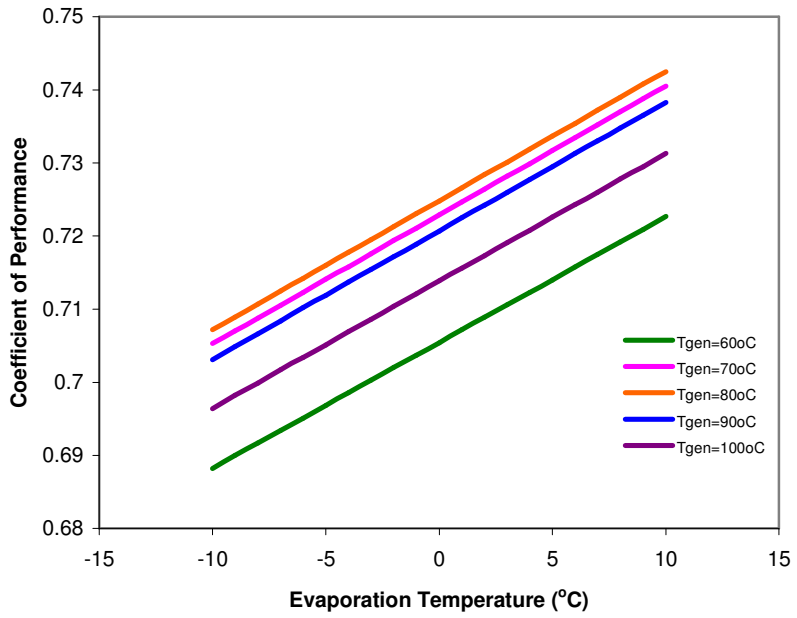


Fig. 3.5: Effect of Generation Temperature on system COP(Tcond=25°C)

The effect of generation temperature on the system COP for varying evaporation temperatures is shown in Fig.3.5 above. It shows that for a given system, there is an optimum generation temperature beyond which the system COP reduces. This is because heating beyond the optimum generation temperature does not result in commensurate desorption of refrigerant, rather it increases the sensible heat gained by the adsorbent bed. This results in longer cooling time required at the end of desorption.

CHAPTER FOUR

SYSTEM DESCRIPTION AND MATHEMATICAL MODELING

The solar powered adsorption refrigeration system is being designed for improved efficiency. First a system description is presented after a mathematical model of the system is subsequently developed and finally a simulation of the design would be carried out to optimize the design parameters using the Engineering Equation Solver (EES), Matlab and Transient Systems Simulation software (TRNSYS).

4.1 SYSTEM DESCRIPTION

The solar powered adsorption system proposed is a hybrid system capable of heating and cooling to achieve higher efficiency and better usefulness in practice. The system is to operate on an activated carbon-methanol adsorption pair.

The system consisting of the following components as shown schematically in Figure 4.1 below: solar collector, water tank, adsorbers, hot water storage tank, condenser, an evaporator and valves for control of flow can be grouped into two subsystems – the solar collector subsystem (heating) and the refrigeration subsystem.

In the solar heating subsystem, solar energy gained through the solar collector during daylight hours is transferred to the water in the pipes below it and accumulated in the water tank. As the solar irradiance increases, the temperature of the water tank rises, and consequently the temperature of the adsorbent bed which is immersed in the water tank also rise with an attendant rise in pressure from the evaporator. The temperature of the

adsorbent bed is assumed to reach a level very close to the water temperature in the tank (an ideal process).

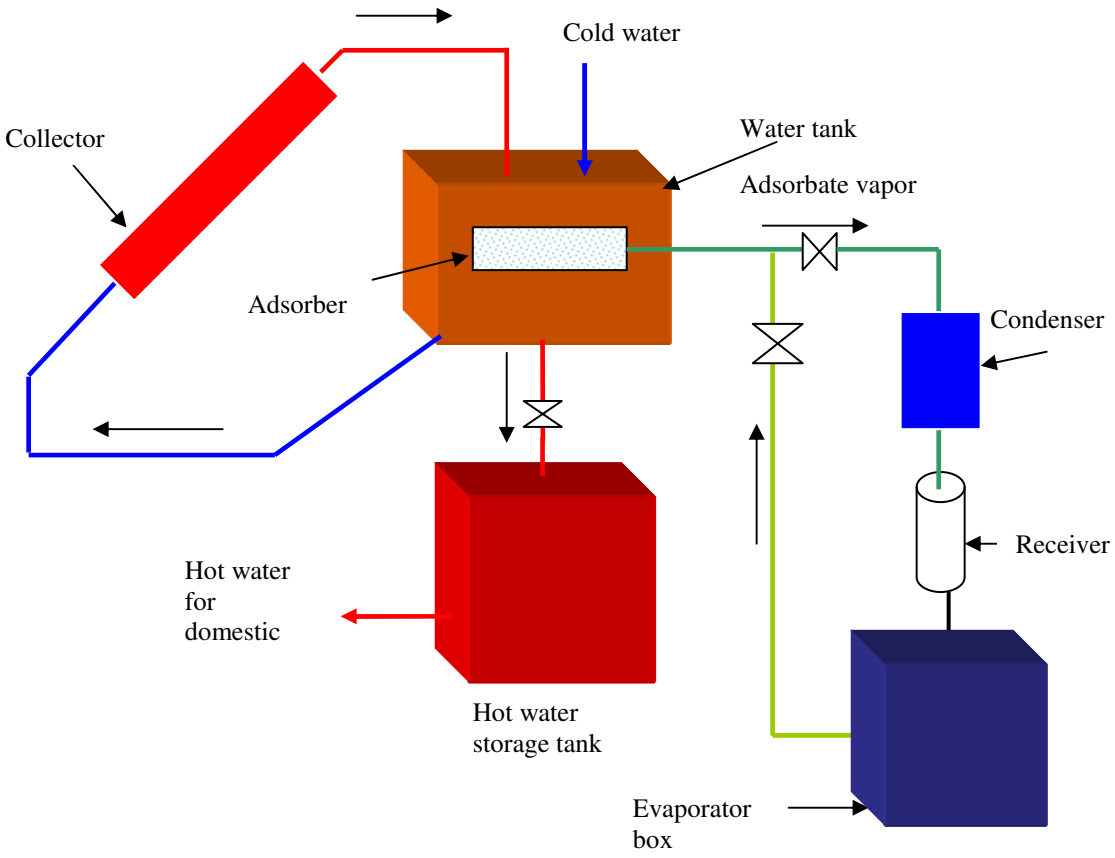


Fig. 4.1: A schematic view of the solar water heating and cooling system

When the temperature of the adsorbent bed reaches the desorption temperature (condenser temperature), desorption of the refrigerant from the adsorption bed is started in the refrigeration subsystem. As the heating of the adsorbent bed progresses, the refrigerant continues to desorb at constant pressure until the adsorbent bed reaches its maximum temperature. The desorption ceases at this temperature and the refrigerant vapor will be

condensed into liquid in the condenser. The liquid adsorbate is then transferred and stored in a liquid receiver from where it is passed to the evaporator.

At the end of desorption, the circulation through the collector is stopped with a gate valve then the hot water in the first water tank is drained and stored in the hot water storage tank for domestic use. The water tank is then filled with cold water which rapidly cools down the adsorber; this initiates the cooling-adsorption-evaporation process. The adsorbent bed temperature drops with a reduction in system pressure to P_e, the evaporator pressure. When the adsorbent bed reaches the evaporating pressure, the bed will begin to adsorb the refrigerant from the evaporator. The liquid refrigerant in the evaporator vaporizes by absorbing heat energy from the water stored in the evaporator, thereby cooling the water and producing ice.

The resulting sensible heat of the adsorber and heat of adsorption preheats the cold water in the tank (heat recovery), thus making more efficient use of the solar energy gained from the collector.

Figure 4.2 shows the Clapeyron (P-T-x) diagram of the working pair. 1-2-3-4-1 represents an ideal combined cycle of both heating and cooling process. The line on the left is the saturated vapor pressure line of methanol; the middle line represents the concentrated isosteric state (1 – 2), and the line on the right is the diluted isosteric state (3 – 4).

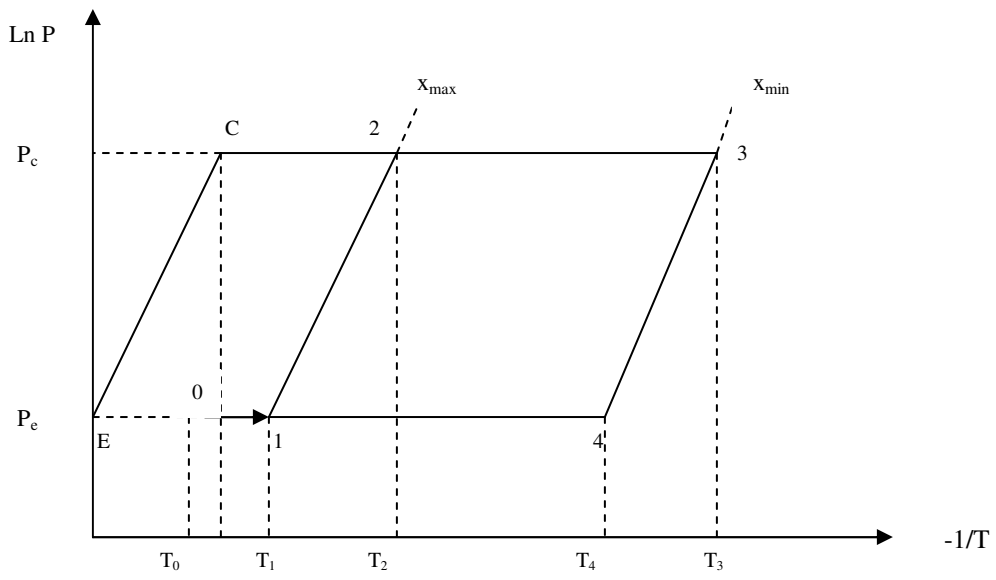


Fig. 4.2: Clapeyron diagram for hybrid solar heating and cooling system with heat recovery.

The cycle begins at the point (1), here the adsorbent is at a low temperature T_1 and low pressure P_e (evaporator pressure); 1- 2 represents the heating of adsorbent and adsorbate with increase in pressure to P_c (condenser pressure). The continuous heating of the adsorbent from 2-3 at constant pressure causes desorption of the adsorbate and the vaporized adsorbate is condensed in the condenser. When the adsorbent reaches the maximum temperature T_3, desorption stops, and the condensed liquid methanol is transferred into the evaporator.

With the draining of the hot water in the water tank and refilling with cold water, the temperature of the adsorbent bed decreases from T_3 to T_4 with an accompanying decrease in pressure from P_c to P_e. As the temperature of the adsorbent drops from T_4 to T_1, evaporation of methanol from the evaporator and adsorption of methanol in the adsorbent

begins. Heat is rejected during this cooling stage to decrease the temperature of the adsorbent and withdraw the adsorption heat; this preheats the water to be circulated to the collector from T_0 to T_1. In the evaporator heat, is extracted from its surroundings providing the cooling effect.

4.2 MODELING OF SYSTEM COMPONENTS

The thermodynamic analysis of the hybrid system is performed on the following components:

- Solar Collector
- Water Tank and Adsorbent bed
- Condenser
- Evaporator

4.2.1 Solar Collector

This is a type of heat exchanger that changes incident solar radiant energy into heat (thermal energy) or directly to electricity (photo voltaic cells). The solar collector is one of the key elements in a solar energy system. There are three major types of thermal solar collectors – Flat plate, Evacuated and Concentrating (optical) solar collectors, these three collector types are modeled in this research.

i) **Flat plate solar collector** – They absorb energy from all directions above the absorber (both beam and diffuse solar irradiance) and as such do not need to track the sun. The flat plate collector is the most economic choice used in applications where energy is required to be delivered at moderate temperatures sometimes up to 100^{o}C above ambient temperature. A typical cross-section of a flat plate collector is shown in Fig. 4.3. The flat plate collector

design is of the sheet and tube type, consisting of a black solar energy absorbing surface (absorber), which can be made of a material like copper, cover transparent to solar radiation (glazing) placed over the absorbing surface to reduce convection and radiation losses to the atmosphere. The collector also has back insulation to reduce losses due to conduction. Solar radiation is absorbed by the absorber plate and transferred to the water that circulates through the collector in tubes.

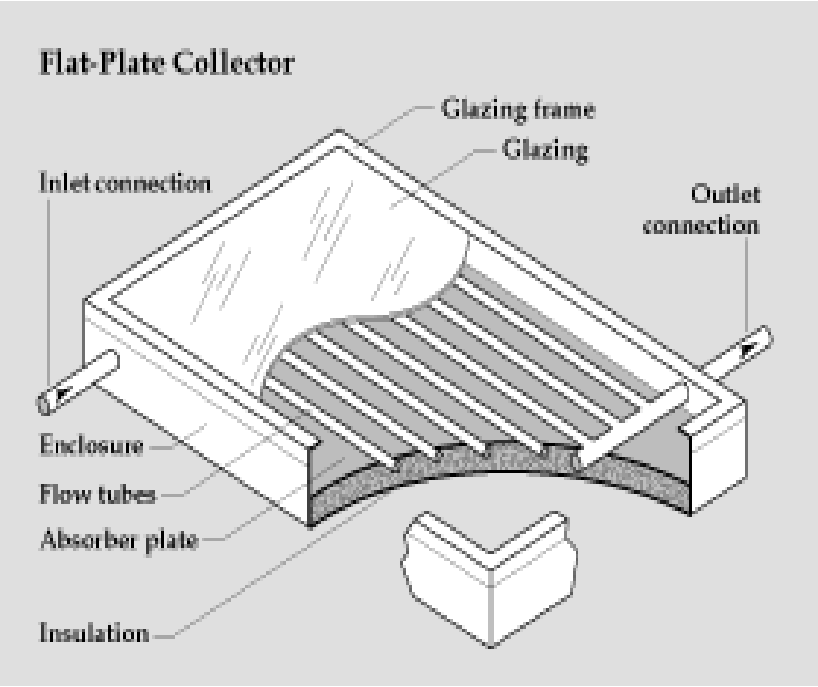


Fig. 4.3: Cross-section of a flat plate solar collector

Since tracking is not required, the flat plate collector can be firmly fixed to a mounting structure, and rigid plumbing used to connect the collector to the other parts of the system.

To model the flat plate collector, the following assumptions are made –

- Performance is steady state
- Headers provide uniform flow to the tubes
- No absorption of solar energy by the cover.

- Heat flow through cover is one-dimensional.
- Negligible temperature drop through the cover.
- Covers are opaque to infrared radiation.
- There is one-dimensional flow through back insulation.
- Temperature gradient around tubes can be neglected.
- Temperature gradients in the direction of flow and between the tubes can be treated independently.
- Properties are independent of temperature.
- Loss through front and back are to the same ambient temperature.
- Specific heat of water at constant pressure is constant.

The actual useful heat gained by the flat plate solar collector Q_u is calculated from the heat balance in the collector by the Hottel-Whillier-Bliss equation (Duffie and Beckman 2006) given as

$$Q_u = \eta Q_s = A_c F_R \left[I_T (\tau\alpha)_n - U_L (T_i - T_a) \right] \quad \text{.....4.1}$$

Where

$$Q_s = A_c I_T \quad \text{4.2}$$

$$\eta = \frac{Q_u}{A_c I_T} = F_R (\tau\alpha)_n - \frac{F_R U_L}{I_T} (T_i - T_a) \quad \text{4.3}$$

The useful energy can also be described in terms of the rate of energy being added to the heat transfer fluid passing through the absorber.

$$Q_u = \dot{m}_w c_{p_w} (T_o - T_i) \quad \text{4.4}$$

Since the loss coefficient is not exactly a constant, a second order efficiency formula is used based on collectors tested according to ASHRAE standards and rated by SRCC (ASHRAE 2003, SRCC 1995).

The second order efficiency is given as

$$\eta_{sc} = \frac{Q_u}{A_c I_T} = F_R(\tau\alpha)_n - \frac{F_R U_L (T_i - T_a)}{I_T} - \frac{F_R U_{L/T} (T_i - T_a)^2}{I_T} \quad \ldots\ldots\ldots\ldots\ldots\ldots 4.5$$

This can be rewritten as

$$\eta = a_0 - a_1 \frac{(\Delta T)}{I_T} - a_2 \frac{(\Delta T)^2}{I_T} \quad \ldots\ldots\ldots\ldots\ldots\ldots\ldots\ldots\ldots\ldots\ldots\ldots\ldots\ldots\ldots 4.6$$

Where

a_0 is the intercept (maximum) of the collector efficiency.

a_1 is the negative of the first-order coefficient.

a_2 is the negative of the second order coefficient.

(ii) **Parabolic Trough collector** – This type of thermal energy collector is constructed as a long parabolic mirror (usually coated silver or polished aluminum) with a Dewar tube running its length at the focal line as shown in Fig. 4.4 below. This allows sunlight to be reflected by the mirror and concentrated on the Dewar tube. The trough is usually aligned on a north-south axis, and rotated to track the sun as it moves across the sky each day. Alternately, the trough can be aligned on an east-west axis; this reduces the overall efficiency of the collector, due to cosine loss, but only requires the trough to be aligned with the change in seasons, avoiding the need for tracking motors. This tracking method works correctly at the equinoxes with errors in the focusing of the light at other times during the year. There is also an error introduced due to the daily motion of the sun across

the sky, this error also reaches a minimum at solar noon. Seasonally adjusted parabolic troughs are generally designed with a lower solar concentration ratio to take care of some of these errors.

Heat transfer fluid (water) runs through the tube to absorb the heat generated by the concentration of the sunlight.

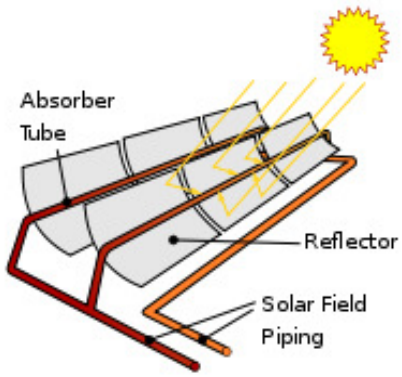


Fig. 4.4: Schematic view of a parabolic trough solar collector (solarpipe-scheme.svg)

The thermal efficiency of a parabolic trough collector is defined as the ratio of the useful energy produced over any time period to the beam radiation incident on the collector aperture over the same period. It can be calculated under steady state conditions using the Hottel-Whillier-Bliss equation

$$\eta = F_R(\tau\alpha)_n - \frac{F_R U_L}{C}\frac{(T_i - T_a)}{I_T} \quad \text{.....4.7}$$

C is the concentration ratio and it is usually defined as the ratio of the collector aperture area A_c to the receiver area A_r.

$$C = \frac{A_c}{A_r} = \frac{W}{\pi d_o} \quad \text{.....4.8}$$

The efficiency can also be expressed in terms of the heat energy added to the heat transfer fluid as

$$\eta = \frac{\dot{m}_w c_{p_w} (T_o - T_i)}{I_T W L_c} \quad \ldots\ldots\ldots\ldots\ldots\ldots\ldots\ldots\ldots\ldots\ldots\ldots\ldots\ldots\ldots\ldots\ldots\ldots 4.9$$

W is the width of aperture and L_c is the length of absorber tube.

Table 4.1: Configurations of typical solar thermal collectors

Motion	Collector type	Absorber type	Concentration ratio	Indicative temperature range (^oC)
Stationary	Flat plate collector (FPC)	Flat	1	30-80
	Evacuated tube collector (ETC)	Flat	1	50-200
	Compound parabolic collector (CPC)	Tubular	1-5	60-240
Single-axis tracking	Linear Fresnel reflector (LFR)	Tubular	10-40	60-250
	Parabolic trough collector (PTC)	Tubular	15-45	60-300
	Cylindrical trough collector (CTC)	Tubular	10-50	60-300
Two-axes tracking	Parabolic dish reflector (PDR)	Point	100-1000	100-500
	Heliostat field collector (HFC)	Point	100-1500	150-2000



Fig. 4.5: Evacuated tube collector (RaBoe/Wikipedia)

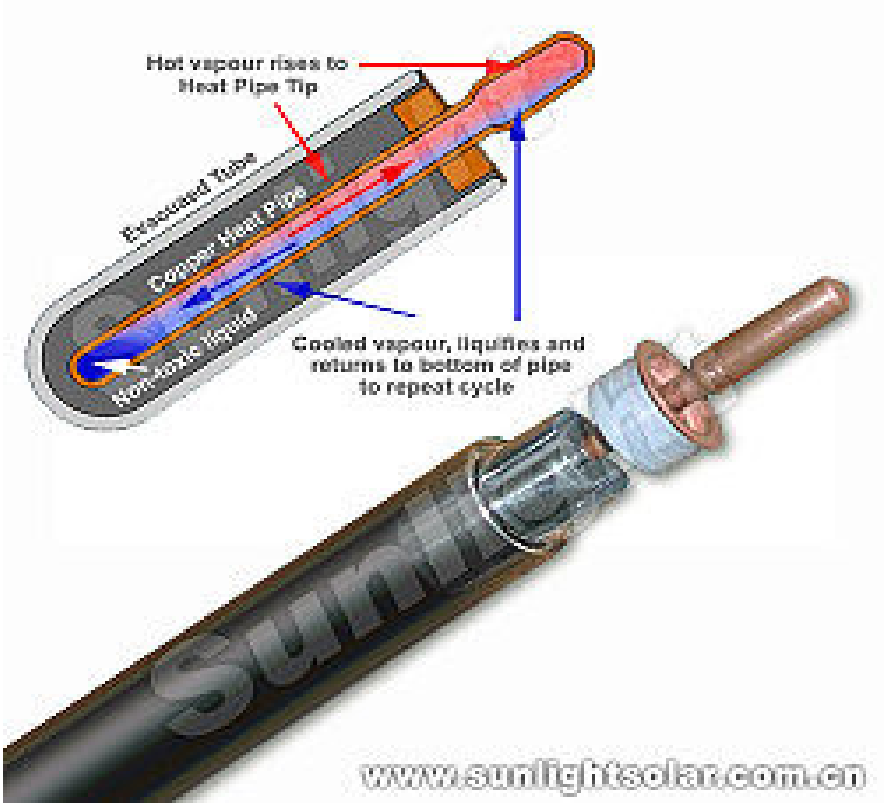


Fig. 4.6: View of a Glass-glass evacuated tube (www.sunlightsolar.com.cn)

(iii) **Evacuated Tube collector**

The evacuated tube solar collector works by absorbing solar energy in the form of UV rays and converting it into thermal energy. An evacuated tube solar collector contains a number of evacuated tubes; each tube is responsible for independently absorbing the sun's radiation that reaches it. An evacuated tube is made up of two layers of strong borosilicate glass that are joined together. There is a vacuum in between the layers of glass; this layer of vacuum allows the tube to retain its heat once it is gathered. The UV rays are absorbed by an absorbing film which lies in between the two layers of glass on the inside layer. The heat absorbed is subsequently transferred by conduction to a copper fin inside the inner layer of glass as shown in fig.4.6. A heat pipe that is inserted into the fin absorbs this heat and transfers it to the copper header at the top of the collector. The heat pipe is a thin copper tube which contains a small amount of acetone which vaporizes once subjected to heat and turns to steam. The steam rises to the top of the heat pipe where it reaches a condenser. The heat is then removed from the condenser by the heating fluid (water), the acetone reverts to liquid and returns to the bottom of the heat pipe to start the cycle again.

Equations (4.3) through (4.4) are also applicable for the thermal efficiency analysis of the evacuated tube solar collector with the constants a_0, a_1, a_2 however having different values. The details of equations used in determining the efficiencies for the three types of collectors are presented in Appendix E.

4.2.2 Water Storage Tank and Adsorbent Bed

The water storage tank is to be of cylindrical cross-section, suitably lagged to reduce heat loss to ambient. In this setup, the material of construction of the water tank is galvanized sheet with fiberglass insulation.

The adsorbent bed is the heart of the adsorption cooling system and thus, its characteristics are the most influential factors in the efficient operation of such systems. An efficient adsorption system requires that the adsorber have good heat collecting and heat releasing properties. The arrangement of the adsorbers in the adsorbent bed is in the manifold arrangement as shown in Fig.4.7. This arrangement increases the contact area between adsorbent bed and water as well as obtaining uniform heating. Activated carbon is packed in the annular space between the two co-axial pipes of the bed shown Fig.4.8. The inner pipe is perforated to allow for the flow of desorbed methanol. The vapor is collected from the individual inner pipes into a header pipe on one end which leads to the condenser with the outer pipe sealed. At the other end, the inner pipe ends are sealed while the outer pipe ends are connected to a header pipe which supplies methanol vapor from the evaporator to the adsorbent bed.

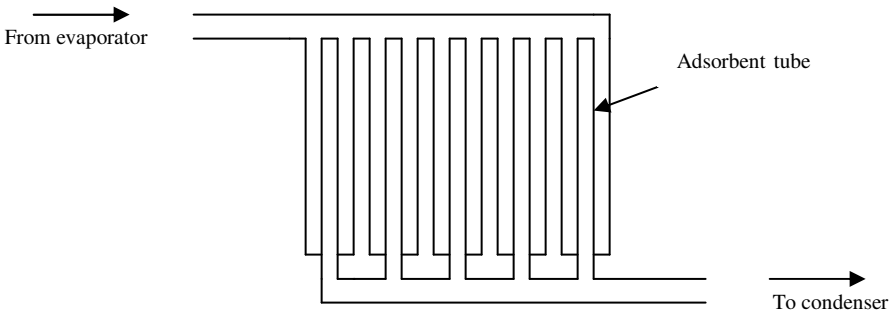


Fig. 4.7: Schematic of the manifold arrangement adsorbent bed.

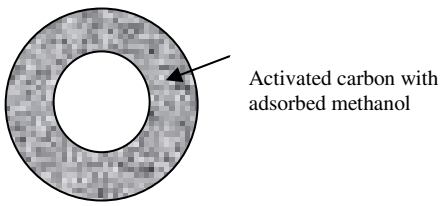


Fig. 4.8: Cross-section of each of the co-axial adsorbent tubes.

The useful energy collected by the three types of collectors, $Q_{u,}$ is transferred to heat the water in the tubes and the hot water subsequently transferred to the water tank in which the adsorbent bed made of stainless steel is immersed. The rise in the temperatures of water and metallic tank, account for the change in internal energy of water and heat transfer to the adsorbers inside the water tank.

The following assumptions are made in the development of the model:

(i) The pressure is uniform in the adsorbent bed.

(ii) The adsorbent bed is considered as a continuous medium whose conduction heat transfer can be characterized by an equivalent thermal conductivity.

(iii) Headers provide uniform flow to and from the adsorber tubes.

(iv) The adsorption/desorption process is an isobaric process.

(v) All phases are continuously in thermal and chemical equilibrium.

(vi) The thermophysical properties of the adsorbate are those of the bulk liquid and the gaseous phase behaves as an ideal gas.

(vii) The condenser and evaporator processes are ideal processes; T_{con} and T_{ev} are constant during the isobaric phases.

(viii) The heat transfer in the adsorbent is radial and the convection heat transfer due to radial mass transfer is neglected.

Assuming negligible heat losses from the tank due to insulation, the useful heat from the collector Qu is supplied as input heat required to heat up (i) the water in the tank (Q_1), (ii) the metallic storage tank (Q_2), (iii) adsorber tubes and adsorbent mass (Q_3), (iv) the adsorbate mass before desorption (Q_4) i.e. sensible heat of adsorbate, (v) desorb a differential amount of adsorbate (Q_5), (vi) the adsorbate mass as desorption starts (Q_6), i.e. sensible heat of the adsorbate left in the adsorbent.

$$Q_u = Q_1 + Q_2 + Q_3 + Q_4 + Q_5 + Q_6 \quad \text{…….4.10}$$

But

$$Q_1 = \int_{T_1}^{T_3} m_w c_{p_w}\, dT \quad \text{……4.11}$$

m_w is mass of water in tank (kg), c_{pw} is the specific heat capacity of water (kJ/kgK)

$$Q_2 = \int_{T_1}^{T_3} m_{wt} c_{p_{wt}} dT \quad \text{……...4.12}$$

m_{wt} is mass of water tank (kg), c_{pwt} is the specific heat capacity of water tank (kJ/kgK)

$$Q_3 = \int_{T_1}^{T_3} \left(m_{ad} c_{p_{ad}} + m_{ac} c_{p_{ac}} \right) dT \quad \text{……...4.13}$$

m_{ad} is the mass of adsorber tube (kg), m_{ac} is the mass of activated carbon in adsorber tube (kg), c_{pad} is the specific heat of adsorber tube (kJ/kgK),and c_{pac} is the specific heat capacity of activated carbon (kg).

$$Q_4 = \int_{T_1}^{T_2} x_{\max} m_{ac}\, c_{v_m}\, dT \quad \text{…….4.14}$$

x_{max} is maximum quantity of methanol adsorbed (kg) per kg of activated carbon and c_{vm} is the specific heat at constant volume of methanol (kJ/kgK).

$$Q_5 = \int_{T_2}^{T_3} m_{ac} h_d \frac{dx}{dT} dT \quad \text{…….4.15}$$

h_d is heat of sorption (kJ/kgK) as evaluated with equation 3.17.

$$Q_6 = \int_{T_2}^{T_3} x\left(T, P_c\right) m_{ac} c_{p_{mv}}\, dT \quad \text{……..4.16}$$

c_{pmv} is the specific heat of methanol vapor (kJ/kgK).

$$\Rightarrow Q_u = \int_{T_1}^{T_3} m_w c_{p_w} dT + \int_{T_1}^{T_3} m_{wt} c_{p_{wt}} dT + \int_{T_1}^{T_3} \left(m_{ad} c_{p_{ad}} + m_{ac} c_{p_{ac}} \right) dT + \int_{T_1}^{T_2} x_{\max} m_{ac} c_{v_m} dT + \int_{T_2}^{T_3} m_{ac} h_d \frac{dx}{dT} dT + \int_{T_2}^{T_3} x(T, P_c) m_{ac} c_{p_{mv}} dT \quad \text{……..4.17}$$

The adsorption equation of activated carbon-methanol is calculated from the Dubnin-Astakhov equation (Wang, 2006)

$$x = x_o \exp\left[-k\left(\frac{T}{T_s}-1\right)^n\right] \quad \text{.....4.18}$$

The useful energy in equation (4.10) can also be expressed as

$$\left(m_w c_{p_w} + m_{wt} c_{p_{wt}}\right)\frac{dT}{dt} = Q_u - h_{c_{w-ad}}\left(T_w - T_{ad}\right)A_{ad} \quad \text{.....4.19}$$

where $h_{c_{w-ad}}$ is the heat transfer coefficient between water and adsorber tubes of diameter d, and can be evaluated using the following correlation given by Deaver et al (1970) as

$$h_{c_{w-ad}} = Nu_d \frac{k_1}{d} \quad \text{.....4.20}$$

and $Nu_d = 0.48 Ra_d^{0.23} \quad for \;\; 10^4 \langle Ra_d \langle 10^7$ .....4..21

The Raleigh number $Ra_d = \dfrac{g\beta' d^3\left(T_w - T_{ad}\right)\mu c_p}{\nu^2 k_1}$ 4.22

Then the energy balance between the hot water in the tank, adsorber tubes and content is

$$\left(m_{ad} c_{p_{ad}} + m_{ac} c_{p_{ac}} + x_{\max} m_{ac} c_{v_m}\right)\frac{dT_{ad}}{dt} = h_{c_{w-ad}}\left(T_w - T_{ad}\right)A_{ad} - m_{ac} h_d \frac{dx}{dt} \quad \text{.....4.23}$$

In the evening, the hot water is drained and replaced with cold which cools the adsorber. The sensible heat of the adsorber and heat of adsorption rejected from the adsorbent bed will cause the temperature of the water in the tank to rise by a few degrees.

Heat rejected from the adsorbent bed into the water tank and heat recovered by the water can be expressed with the following heat balance equation:

$$Q_{ct} = \int_{T_0}^{T_1} m_w c_{p_w}$$
$$= \int_{T_1}^{T_3}\left(m_{ad} c_{p_{ad}} + m_{ac} c_{p_{ac}}\right)dT + \int_{T_4}^{T_3} x_{\min} m_{ac} c_{v_m} dT + \int_{T_1}^{T_4} m_{ac} h_a \frac{dx}{dT} dT + \int_{T_1}^{T_4} x\left(T, P_e\right) m_{ac} c_{p_m} dT \quad 4.24$$

x_{min} is the adsorption capacity after desorption(kg/kg)

h_a the heat of sorption is evaluated using equation 3.17, but $T_s = T_e$ (evaporator pressure).

The cold water to fill the tank in the evening enters at a temperature T_0, which can be expressed as

$$T_1 = T_0 + \frac{Q_{ct}}{\dot{m}_w c_{p_w}} \quad \text{.....4.25}$$

The mass of water is however dependent on the volume of the storage tank.

$$\dot{m}_w = \rho_w \times V_{wt} \quad \text{.....4.26}$$

The volume of the outer adsorber tube of diameter d_o and length L_{ad} is

$$V_o = \frac{\pi d_o^{\,2} L_{ad}}{4} \quad \text{.....4.27}$$

while the volume of the inner adsorber tube of diameter d_i and length L_{ad} is

$$V_i = \frac{\pi d_i^{\,2} L_{ad}}{4} \quad \text{.....4.28}$$

But the activated carbon is packed between the concentric outer and inner tubes, which in turn gives the total volume of activated carbon in N tubes as

$$V_{ac} = (V_o - V_i)N \quad \text{.....4.29}$$

Therefore, for a given density of activated carbon ρ_{ac}, the mass of activated carbon used m_{ac} is

$$m_{ac} = \rho_{ac} V_{ac} \quad \text{.....4.30}$$

4.2.3 Condenser

The condenser is a heat exchanger that rejects heat from the refrigerant (adsorbate) to the air outside. Though there are many configurations available, the bare coil horizontal tube design is used in the refrigerant subsystem. The tube is to be immersed in a stagnant pool of water for efficient cooling of the adsorbate as depicted in Fig. 4.9 below. Fig. 3.8 through 3.10 show that the lower the condenser temperature, the higher the COP achievable by the system. Assuming all the heat released by the condensing adsorbate is transferred to the cooling water across the tube wall, the amount of heat rejected from the condenser can be expressed as

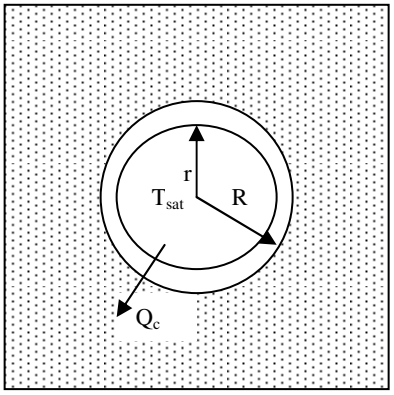


Fig. 4.9: Condenser tube in stagnant pool of water

$$Q_{co} = \dot{m}_m h_{fg}^* = 2\pi r L_{co} h_{cw_i} \left(T_{sat} - T_{cw_i}\right) = \frac{2\pi L_{co}\left(T_{cw_i} - T_{cw_o}\right)}{\frac{1}{R_{co} h_{cw_o}} + \frac{\ln R_{co} / r_{co}}{k_{co}}} \quad \ldots\ldots\ldots\ldots\ldots\ldots\ldots\ldots 4.31$$

The refrigerant is usually cooled below the saturation temperature T_{sat} to an average value between the inside tube temperature T_{cw_i} and T_{sat}, thus, releasing more heat. The actual heat

is larger and is shown by Rohsenow (1956) as being accounted for by replacing h_{fg} with h_{fg}^{*}, the modified latent heat of vaporization.

$$h_{fg}^{*} = h_{fg} + 0.68 c_{p_{ml}} \left(T_{sat} - T_{cw_i} \right) \quad \text{.....4.32}$$

c_{pml} is the specific heat of methanol liquid at the average film temperature. The temperature of the liquid film varies from T_{sat} on the liquid-vapor interface to T_{cwi} at the internal wall surface. Therefore, the properties of the liquid are evaluated at the film temperature

$$T_{f_l} = \frac{T_{sat} + T_{cw_i}}{2} \quad \text{.....4.33}$$

which is approximately the average temperature of the liquid. The latent heat of vaporization, h_{fg}, is however determined at T_{sat} since it is not affected by the subcooling of the liquid.

(a) Heat transfer coefficient for condensation inside horizontal tubes (h_{cwi})

Most condensation processes encountered in refrigeration and airconditioning applications involve condensation on the inner surfaces of horizontal or vertical tubes. The heat transfer analysis of condensation inside tubes is complicated by the fact that it is strongly influenced by the vapor velocity and the rate of liquid accumulation on the walls of the tubes.

For low vapor velocities, Chato (1962) recommended this expression for condensation

$$h_{cw_i} = 0.555 \left[\frac{\rho_l (\rho_l - \rho_v) g h_{fg}^{*} k_l^3}{\mu_l d_c \left(T_{sat} - T_{cw_i} \right)} \right]^{1/4} \quad \text{..... 4.34}$$

The liquid properties ρ_l, k_l and μ_l are determined at the film temperature for

$$\mathrm{Re}_v = \left(\frac{\rho_v v_v d}{\mu_v} \right)_{inlet} \prec 35{,}000 \quad \text{……..4.35}$$

v_v is the average velocity of the condensate (per condenser tube) at the inlet of the flow, ρ_v and μ_v are density and viscosity of the vapor at inlet, while d is the inside diameter of condenser tube. The Reynolds number of the vapor Re_v is thus evaluated at the tube inlet conditions using the internal tube diameter as the characteristic length.

Note that the total rate of condensation of the adsorbate is

$$\dot{m}_m = \frac{h_{cw_i} 2\pi r L_{co} \left(T_{sat} - T_{cw_i} \right)}{h_{fg}^*} \quad \text{……4.36}$$

(b) Convective heat transfer coefficient on the outside of tube (h_{cwo})

$$h_{cw_o} = \frac{Nu_{co} k_w}{D_{co}} \quad \text{……4.37}$$

But for natural convection, the Nusselt number is given by Churchill and Chu (1975) as

$$Nu_c = \left\{ 0.6 + \frac{0.387 Ra_D}{\left[1 + \left(\frac{0.559}{\mathrm{Pr}_w} \right)^{9/16} \right]^{8/27}} \right\} \quad \text{……4.38}$$

For $10^{-5} \prec Ra_D \prec 10^{12}$, $Ra_D = \dfrac{g \beta_{co} \left(T_{cw_i} - T_{cw_o} \right) D_{co}^3 \mathrm{Pr}_w}{\nu_w^2}$ ……..4.39

and $\beta_{co} = \dfrac{1}{T_{f2}}$ ……4.40

k_w, Pr_w and υ_w are evaluated at $T_{f2} = \dfrac{T_{cw_i} + T_{cw_o}}{2}$ at a pressure of 1atm.

4.2.4 Evaporator

The evaporator design is also to be bare coil-in-air type. The model for the evaporator is developed assuming that the rate of adsorption of adsorbate (by adsorption bed) equals the rate of evaporation.

$$Q_{ref} = Q_{ev} = \Delta x\, m_{ad} \left(L_e - c_{p_{ml}} \left(T_{co} - T_{ev}\right)\right) \quad \text{.....4.41}$$

$$\Delta x = x_{\max} - x_{\min}$$

L_e is the latent heat of vaporization of adsorbate (refrigerant), x_{max} is the adsorbent capacity before desorption and x_{min} is the adsorption capacity after desorption. The heat transfer across the evaporator tube wall

$$Q_{ev} = \Delta x m_{ac} \left(L_e - c_{p_{ml}} \left(T_{co} - T_{ev}\right)\right) = 2\pi r_{ev} L_{ev} h_{ev_i} \left(T_{ev_i} - T_{sat}\right)$$

$$= \frac{2\pi L_{ev} \left(T_{cr} - T_{ev_i}\right)}{\frac{\ln R_{ev} / r_{ev}}{k_{ev}} + \frac{1}{R_{ev} h_{ev_o}} + \frac{1}{r_{ev} h_{ev_i}}} \quad \text{..... 4.42}$$

(a) Boiling coefficient inside tube

The boiling coefficient on the evaporating methanol side can be determined using the Chato (1975) equation for boiling inside a tube given as

$$h_{ev_i} = 0.555 \left[\frac{g\, \rho_v \left(\rho_l - \rho_v\right) h_{fg}\, k_v^{\,3}}{\mu_v\, d_{ev} \left(T_{ev_i} - T_{sat}\right)} \right]^{1/4} \quad \text{.....4.43}$$

(b) Heat transfer coefficient on the outside of evaporator tubes

For natural convection, the Nusselt number equation given by Churchill and Chu (1975) and stated in equation 4.38, but the Rayleigh number is determined by

$$Ra_{D_e} = \frac{g\beta_{ev}\left(T_{ev_o} - T_{ev_i}\right)D_{ev}^3 \Pr_a}{\nu^2} \quad \text{……4.44}$$

and $$Nu_{ev} = \frac{h_{ev_o} D_{ev}}{k_{ev}} \quad \text{……4.45}$$

$$\beta_{ev} = \frac{1}{T_{f3}} \quad \text{……4.46}$$

k, Pr, ν are evaluated at average film temperature $T_{f3} = \frac{T_{ev_i} + T_{ev_o}}{2}$ ……..4.47

4.3 REFRIGERATION EFFECT AND SYSTEM EFFICIENCY

The desorbed refrigerant collects and is condensed in the condenser from where it flows into the evaporator. At night, with the introduction of cold water into the water tank, the temperature and subsequently the pressure of the adsorbent bed drops to below the evaporation pressure, causing the refrigerant liquid in the evaporator to vaporize resulting in the refrigeration effect. The refrigeration effect is measured by the system performance efficiency. It is described by the coefficient of performance (COP) as

$$COP = \frac{Q_{ref} - Q_{cc}}{Q_g} \quad \text{……. 4.48}$$

The amount of refrigeration is calculated as

$$Q_{ref} = \Delta x\, m_{ac}\, L_e \quad \text{…… ..4.49}$$

L_e is the latent heat of vaporization of adsorbate.

Q_{cc} is the amount of energy assumed to be utilized in cooling the refrigerant liquid from the condensing temperature T_c to the evaporation temperature T_e. Q_{cc} is estimated as

$$Q_{cc} = m_{ac}\, \Delta x\, c_{p_m}\left(T_{co} - T_{ev}\right) \quad \text{…… ..4.50}$$

Q_g is the heat required for the regeneration of the adsorption bed and it is calculated the equation below. From equation 4.10

$$Q_g = Q_u - (Q_1 + Q_2) \quad \ldots\ldots\ldots\ldots\ldots\ldots\ldots\ldots\ldots\ldots\ldots\ldots\ldots\ldots\ldots\ldots\ldots\ldots 4.51$$

$$\Rightarrow Q_g = Q_3 + Q_4 + Q_5 + Q_6$$

$$Q_g = \int_{T_1}^{T_3} \left(m_{ad}\, c_{p_{ad}} + m_{ac}\, c_{p_{ac}} \right) dT + \int_{T_1}^{T_2} x_{\max}\, m_{ac}\, c_{v_m}\, dT + \int_{T_2}^{T_3} m_{ac}\, h_d \frac{dx}{dT} dT + \int_{T_2}^{T_3} x(T, P_c)\, m_{ac}\, c_{p_{mv}}\, dT$$

The specific cooling power

$$SCP = \frac{Q_{ref} - Q_{cc}}{t_{cycle}.m_{ac}} \quad \ldots\ldots\ldots\ldots\ldots\ldots\ldots\ldots\ldots\ldots\ldots\ldots\ldots\ldots\ldots\ldots\ldots\ldots \quad 4.52$$

The gross solar coefficient of performance is

$$COP_s = \frac{Q_{ref} - Q_{cc}}{\int A_c\, I(t) \partial t} \quad \ldots\ldots\ldots\ldots\ldots\ldots\ldots\ldots\ldots\ldots\ldots\ldots\ldots\ldots\ldots\ldots\ldots\ldots 4.53$$

CHAPTER FIVE

SOLAR THERMAL COOLING SYSTEM MODEL AND OPTIMIZATION

The modeling of the solar thermal cooling system is to be carried out using very versatile software called TRNSYS. TRNSYS which is an acronym for "Transient System Simulation" which is a quasi-steady simulation model developed by the members of the Solar Energy Lab of the University of Wisconsin. The program consists of many subroutines that model subsystem components. The mathematical models for the components are given in terms of their ordinary differential or algebraic equations. The program has the capability of interconnecting system components in any desired manner, solving differential equations and facilitating information output. In using the TRNSYS program, all components of the system have to be identified and a mathematical description of each component made, after which a flow of information diagram is constructed to facilitate the identification of components and the flow of information between them. Each component is represented as a box, which requires a number of constant PARAMETERS and time dependent INPUTS and produces time dependent OUTPUTS. A given OUPUT can however be used as an INPUT to any number of other components. When a flow diagram is drawn in TRNSYS, a deck file is created containing information on all the components of the system, weather data file and the output format.

Subsystem components available in TRNSYS can be seen in the TRNSYS Manual. The program also includes subroutines for processing radiation data, performing integrations, and handling of input and output. Time steps of as small as 1/1000 hr (3.6s) can be used for

reading weather data, which makes the program very flexible with respect to using measured data in simulations.

5.1 THERMAL SYSTEM MODELING

The solar thermal system consists of a solar collector, storage tank and weather data.

5.1.1 Solar Thermal Collectors

Three types of collectors are modeled in this study with their respective performance parameters obtained from commercially available solar thermal collectors. The manufacturers of these collectors are not provided here so as not to commercialize the present study.

(a) Flat plate solar collectors

The flat plate collector is modeled in TRNSYS using built-in component Type 1b. The component is based on the second order efficiency equation given in (4.6). The performance coefficients used in the model are given in Table 5.1.

Table 5.1: Parameters for the flat plate single glazing collector

Parameter	Value
Gross Area	$2m^2$
Frame	Anodized Aluminum
Outer cover	Low iron tempered glass
Absorber plate	Copper fin
Absorber tube	Copper
Absorber coating	Moderately selective black paint

Insulation	Polyisocyanurate
Intercept Efficiency	0.80
First order loss coefficient	5 $W/m^2 K^{-1}$
Second order loss coefficient	0.014 $W/m^2 K^{-2}$
Tested Flow rate	0.0111 $kg/m^2 s$
Specific heat of working fluid	4.190 kJ/kg K

(b) Parabolic trough collector

The parabolic trough collector is modeled using built-in component Type 536 in TRNSYS. The performance coefficients and other necessary parameters for a commercially available parabolic trough collector are shown in Table 5.2.

Table 5.2: Parameters for the parabolic trough collector

Parameter	Value
Collector rim angle	70^o
Reflective surface	Silvered acrylic
Receiver material	Steel
Collector aperture	2.3 m
Receiver surface treatment	Highly selective blackened nickel
Absorptance	0.97
Emmittance (80^oC)	0.18
Glass envelope transmittance	0.96
Absorber outside diameter	50.8 mm

Intercept Efficiency	0.762
First order loss coefficient	0.2125 W/m^2 K^{-1}
Second order loss coefficient	0.001672 W/m^2 K^{-2}
Tested Flow rate	0.015 kg/m^2 s
Specific heat of working fluid	4.190 kJ/kg K
b_0: first order coefficient incidence angle modifier	0.958
b1: second order coefficient incidence angle modifier	-0.298

(c) Evacuated tube solar collector

This collector is modeled with the Type 71 built-in component in TRNSYS. Similarly, the performance coefficients and other parameters are given in Table 5.3.

Table 5.3: Parameters for the evacuated tube solar collector

Parameter	Value
Glass tube diameter	65 mm
Glass thickness	1.6 mm
Collector length	1965 mm
Absorber plate	Copper
Coating	Selective
Absorber area	0.1 m^2
Intercept Efficiency	0.8
First order loss coefficient	1.5 W/m^2 K^{-1}
Second order loss coefficient	0.008 W/m^2 K^{-2}

Tested Flow rate	0.0111 kg/m^2 s
Specific heat of working fluid	4.190 kJ/kg K

5.1.2 Storage Tank

The storage tank is modeled using component Type 4c in TRNSYS. This is a stratified tank with variable inlets and uniform losses with mild steel as the material of construction with fiber glass insulation. The dimensions of the tank are obtained from the optimized tank volume. The hot water from the collectors is stored in this tank which also houses the adsorption bed.

5.1.3 Weather Data

TRNSYS built-in component Type 109-TMY2 is used to model the weather data. This component serves the main purpose of reading weather data at regular intervals from a data file, converting it to a desired system of unit and processing the solar radiation data to obtain tilted surface radiation and angle of incidence for any arbitrary number of surfaces. This component reads the weather data in the standard Typical Meteorological Year format (TMY) which can be generated using a number of programs e.g. Meteonom.

Figs 5.1 and 5.2 below present the ambient temperature and solar radiation data for a typical meteorological year for Kano, Nigeria (latitude 12.05^{o}N, longitude 8.31^{o}E, Elevation 481m) generated by the Type 109 component. These climatic data are used in subsequent simulations.

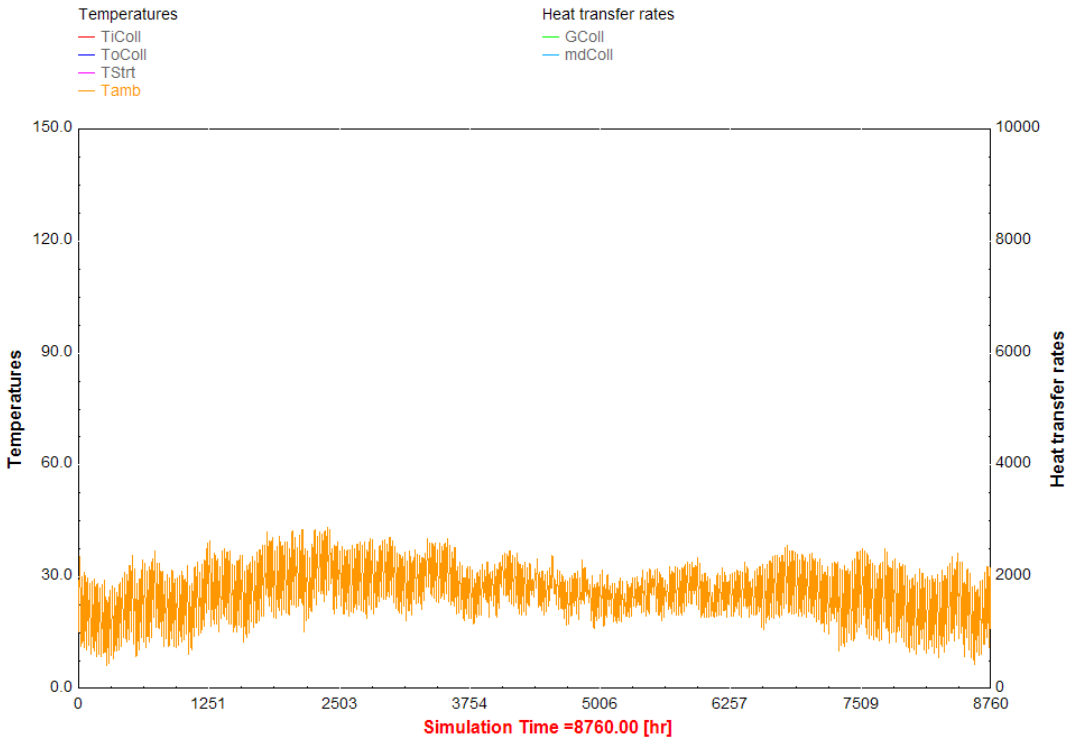


Fig 5.1: Year round Ambient Temperature for Kano, Nigeria.

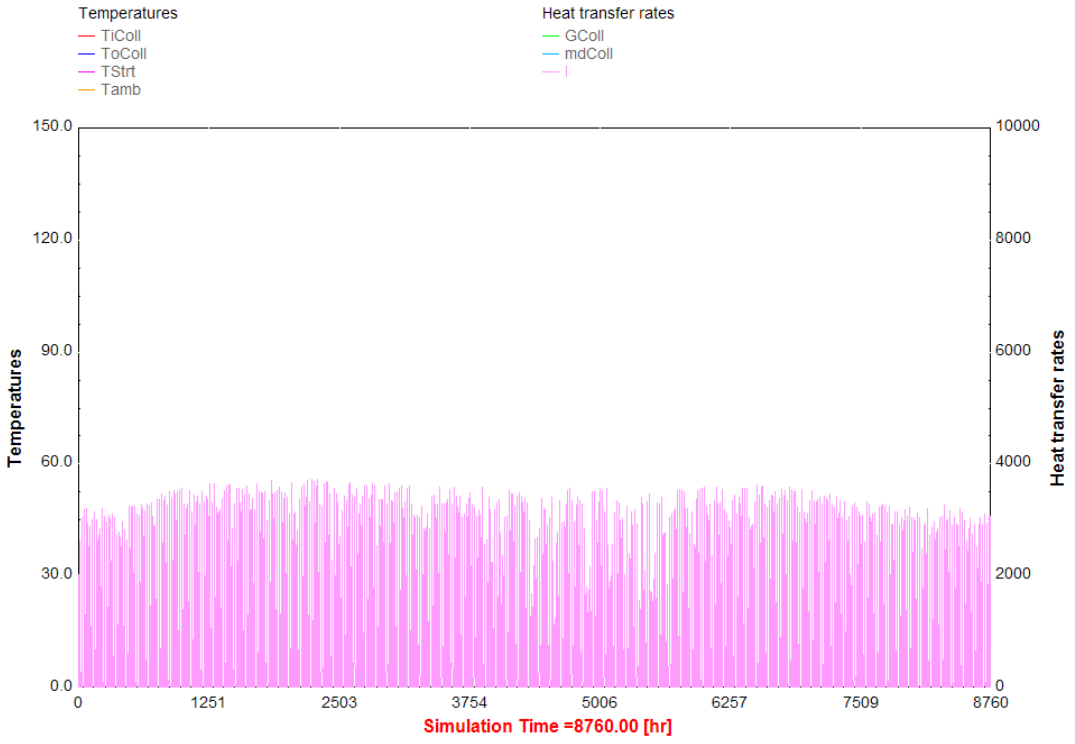


Fig 5.2: Year round Solar Radiation Data for Kano, Nigeria.

5.2 SYSTEM OPTIMIZATION

The system optimization is carried out using weather data for location described in Section 5.1.3 based on the required generation temperature of at least 80^{o}C needed for the desorption of an appreciable amount of methanol from activated-carbon as shown in fig 3.5 for an evaporator and condenser temperature of 0^{o}C and 25^{o}C respectively. The subsequent sizing of collector area and water storage tank volume is such that a temperature of 80^{o}C can be supplied to the adsorption bed. Fig. 5.3 below shows the flow chart of the solar thermal optimization process.

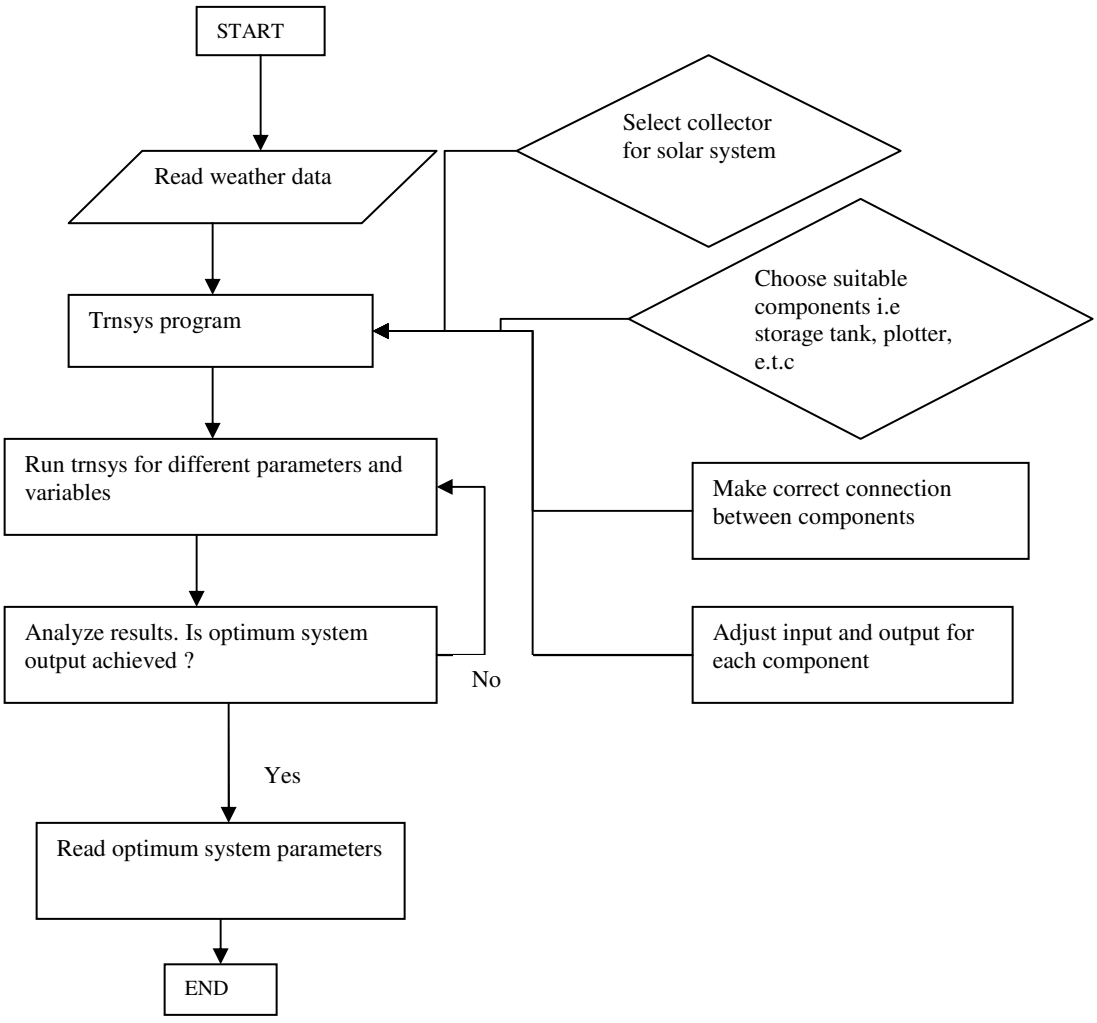


Fig. 5.3: Flow chart of solar thermal system optimization process

5.2.1 Flat Plate Collector (FPC)

The solar thermal system modeled in TRNSYS using the flat plate collector is shown in Fig. 5.4 below. The simulation allows the collector slope, collector area and storage tank volume to be analyzed as functions of useful energy gain and collector efficiency.

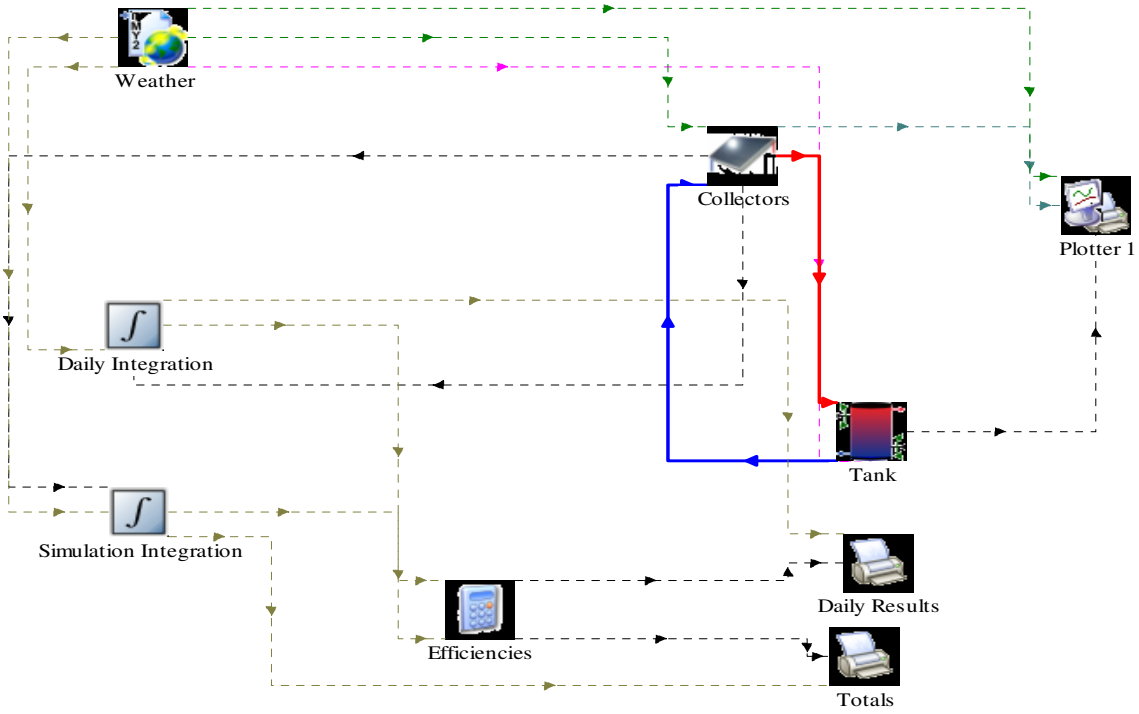


Fig. 5.4: Solar thermal system modeled in TRNSYS with a Flat plate Collector

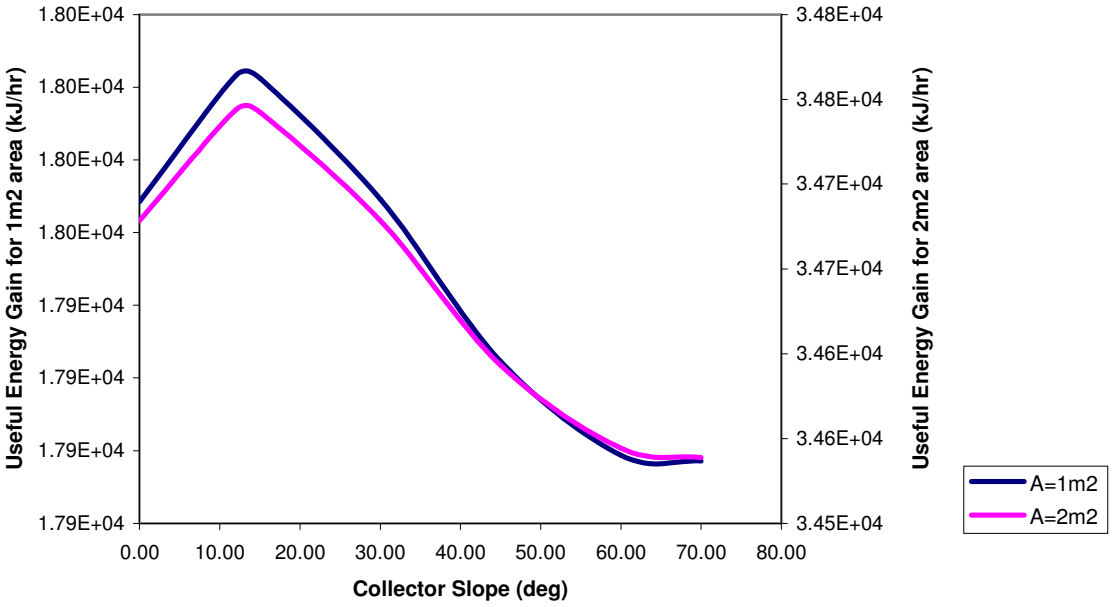


Fig. 5.5: FPC Useful Energy Gain vs Collector Slope

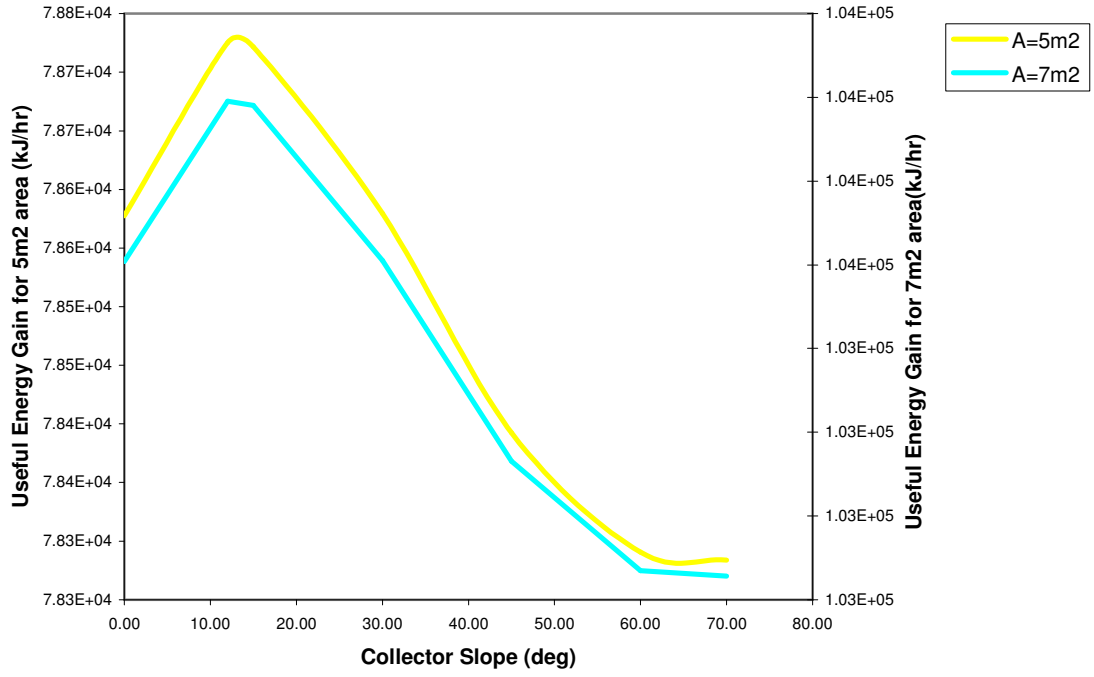


Fig. 5.6: FPC Useful Energy Gain vs Collector Slope

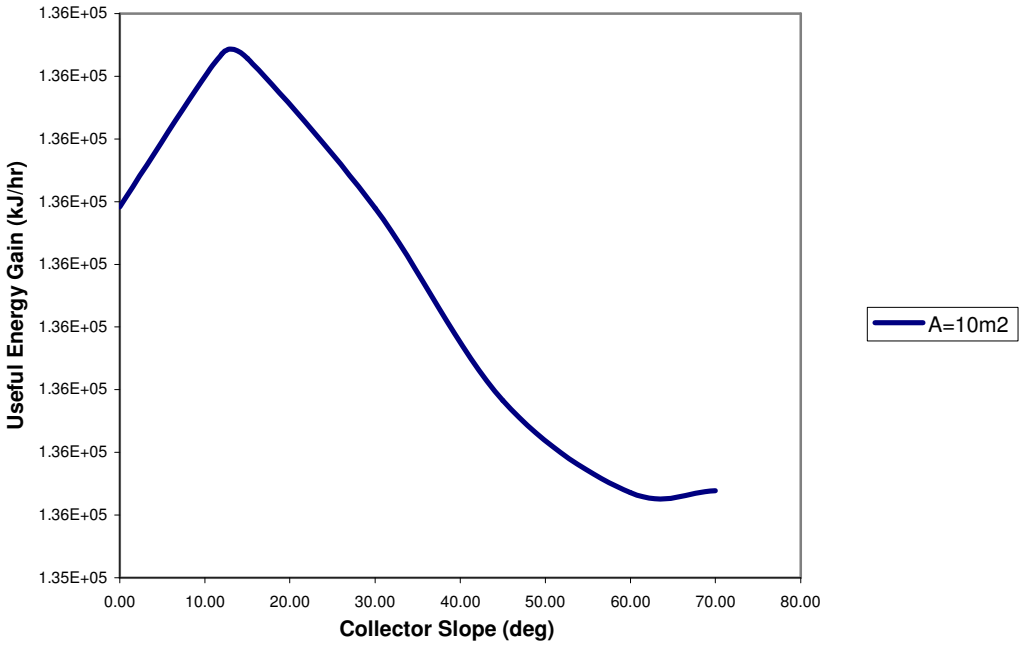


Fig. 5.7: FPC Useful Energy Gain vs Collector Slope

Fig 5.5 to Fig 5.7 show the change in useful energy gain as a function of collector slope, for different collector areas ($1m^2$, $2m^2$, $5m^2$, $7m^2$ and $10m^2$) respectively for a Flat plate collector. It is observed from the figures that the useful energy gain has an optimum value at a collector slope of 12^o, which is independent of the collector area i.e. irrespective of the collector area the maximum useful energy gain for the location occurs at same collector slope value of 12^o which is the latitude of the location (Kano).

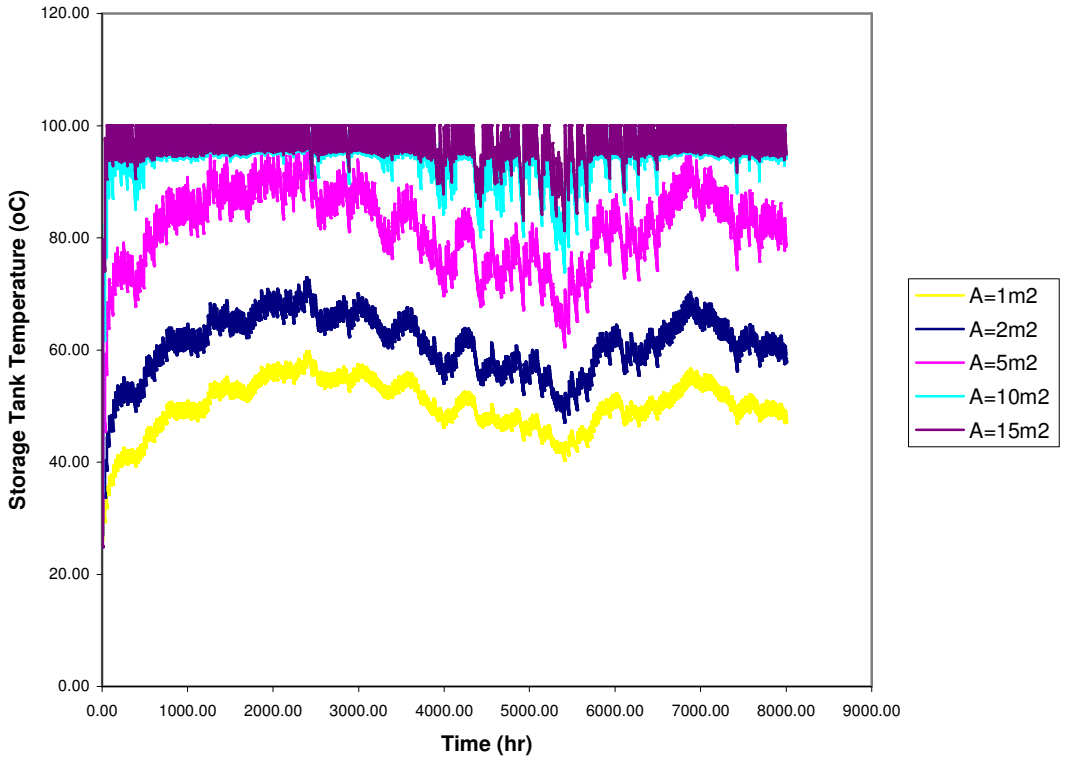


Fig 5.8: Effect of Collector Area on Storage Tank Temperature (FPC)

Fig. 5.8 shows the change in storage tank temperature for different collector areas for a typical meteorological year at the research location. The figure shows that the $1m^2$ collector achieves its highest daily storage tank temperature of 59.75^oC at 2414.75hr (2.45pm on the 11^{th} of April) and a lowest tank temperature of 40.02^oC at 5410.25hr (10.15am on the 14^{th} of August). A highest daily tank temperature of 72.49^oC is achieved at 2414.75hr (2.45pm on the 11^{th} of April) by a $2m^2$ flat plate collector with the lowest temperature of 47.04^oC occurring on the 14^{th} of August at 10.45am (5410.75hr). The storage tank is shown to have attained a maximum temperature of 95.88^oC at 2414.5hr (2.30pm, 11^{th} of April) and a minimum of 60.46^oC at 5410.75hr with a $5m^2$ collector. A $10m^2$ flat plate collector of the same configuration however achieves a storage tank temperature of 100.03^oC at 1.00pm on

the 11th of April (2413hr) and 73.79°C at 5410.5hr (10.30am, 14th of August). The 15m^2 collector however achieves a storage tank temperature of 100.05°C at 2412.75hr (12.45am, 11th of April) with the storage tank temperature achievable on an overcast day being 81.18°C.

This makes a 15m^2 flat plate collector the minimum area collector recommended if any desorption is to take place on an overcast day given the conditions in Fig.3.3.

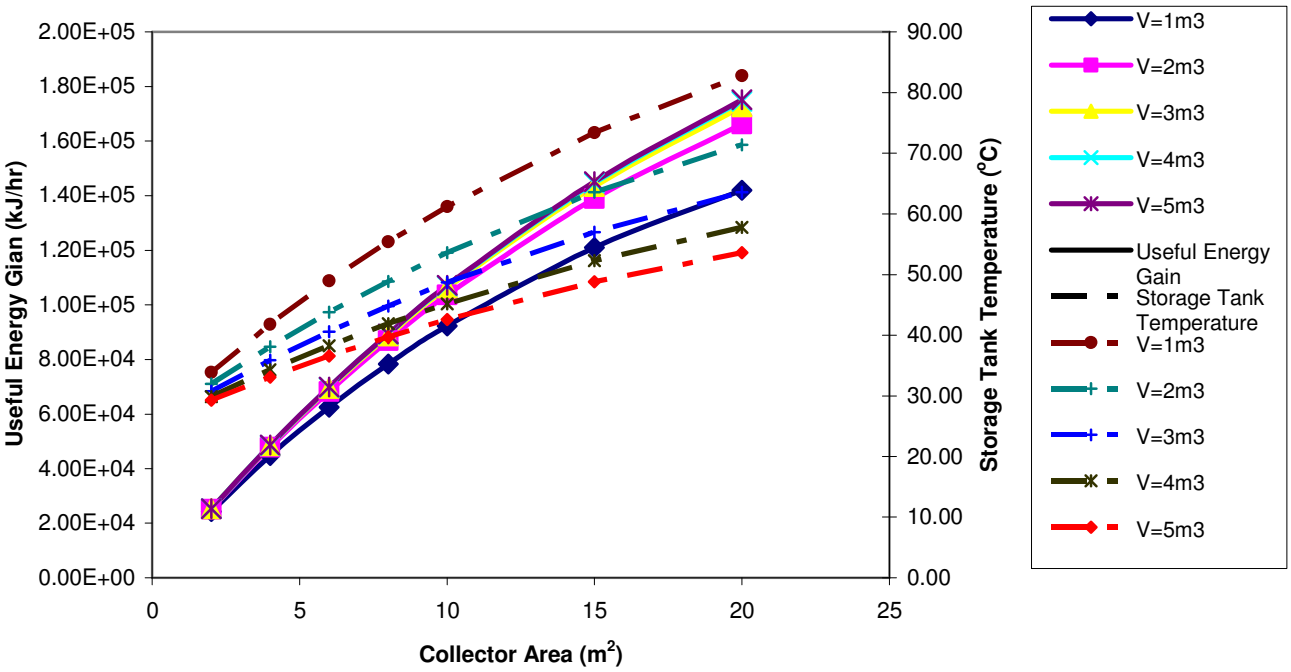


Fig.5.9: Effect of Storage Volume on FPC Useful Energy Gain and Tank Temperature (April)

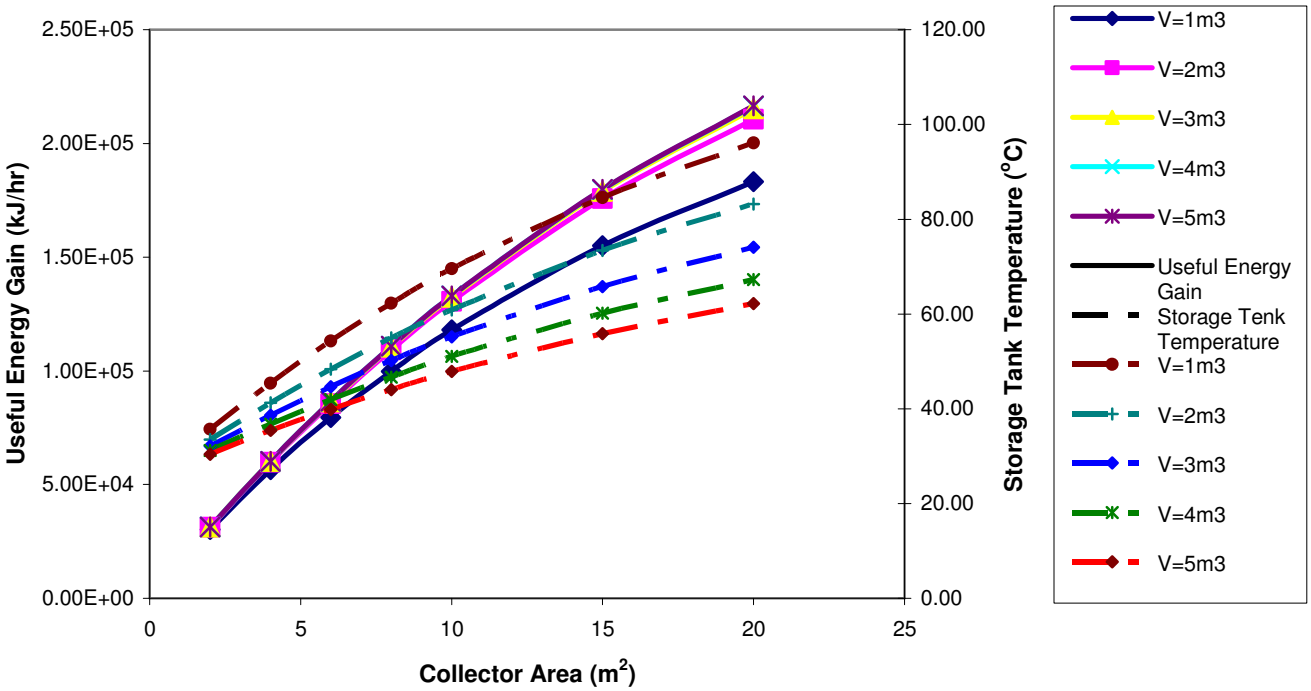


Fig.5.10: Effect of Storage Volume on FPC Useful Energy Gain and Tank Temperature (August)

Fig.5.9, 5.10 and 5.11 show the variation in useful energy gain with collector area for different storage tank volumes for three different months of the year. These figures show that for very small collector areas, the useful energy gain is small for different storage tank sizes. As the collector area increases however, the useful energy gained increases with increase in storage tank volume. For the chosen collector area of $15m^2$ however, there is no appreciable increase in useful energy gain beyond a storage tank volume of $2m^3$. The storage tank temperature however increases with a reduction in tank size.

This research therefore adopts for a flat plate collector, a collector slope of 12^o, an area of not less than $15m^2$ with a storage tank volume of $1m^3$ since a high storage tank temperature is required for the desorption process.

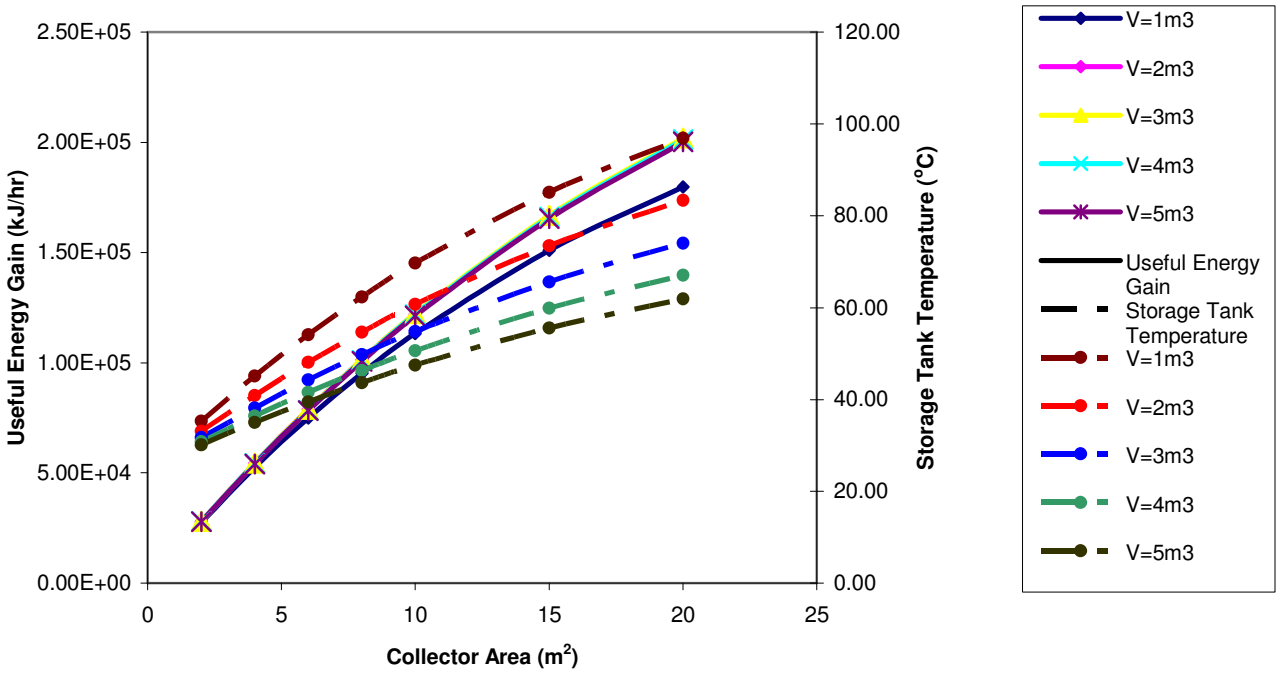


Fig.5.11: Effect of Storage Volume on FPC Useful Energy Gain and Tank Temperature (December)

5.2.2 Parabolic Trough Collector (PTC)

The solar thermal system using a non-tracking parabolic trough collector with N-S orientation as the solar energy collecting surface is modeled in TRNSYS as shown in Fig. 5.12 below. The effects of collector area and storage tank volume are studied to find the best possible combination for optimum performance at the research location.

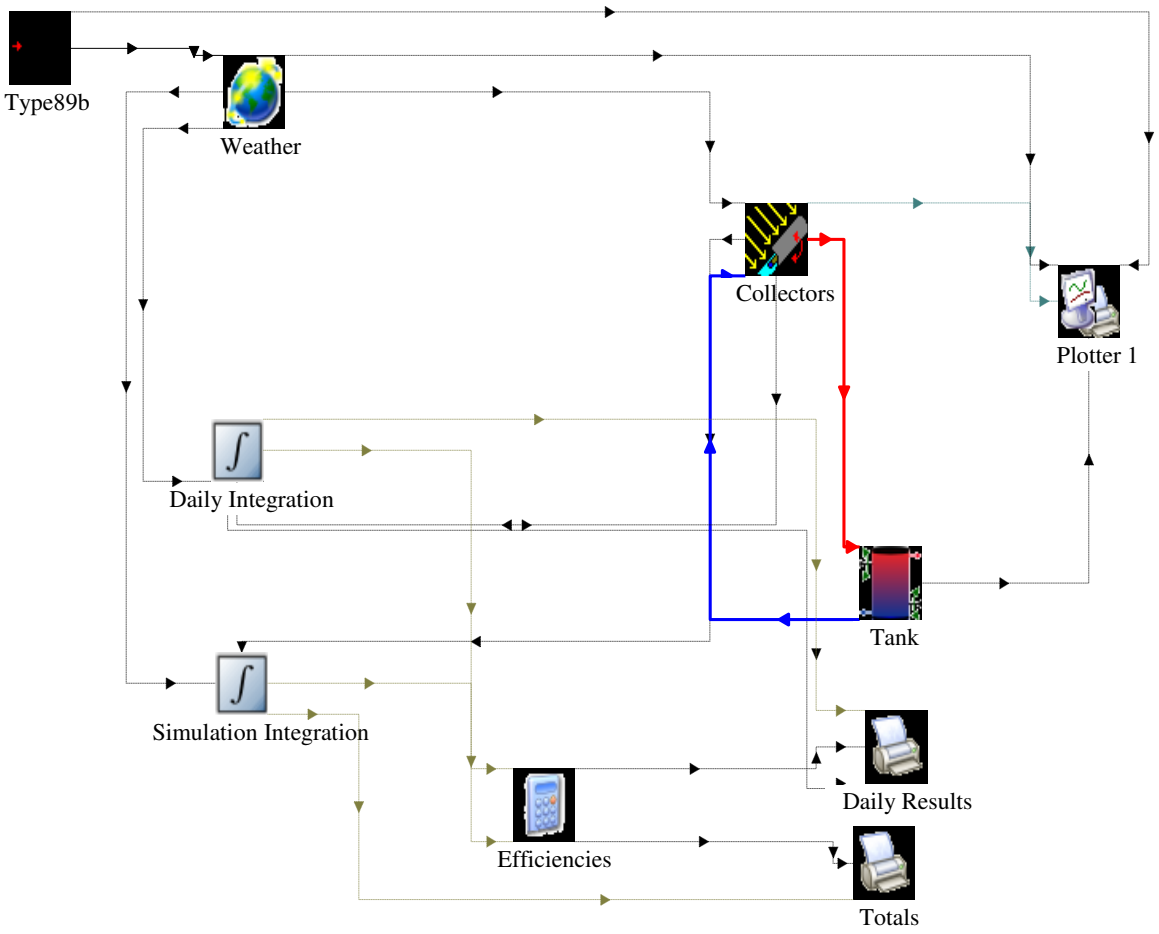


Fig. 5.12: Solar thermal system modeled in TRNSYS with a parabolic trough collector

Figure 5.13 below shows that with the parabolic trough collector, considerable heating of heat transfer fluid is achieved for collector areas greater than 4.6m^2. A storage tank temperature of 69.5^{o}C at 5409hr is achieved for a 4.6m^2 collector area, with 78.4^{o}C for a 6.9m^2 collector area and 81.20^{o}C for a 9.6m^2 collector area on an overcast day. On most days of the year however, the achievable storage tank temperature is enough to cause reasonable desorption of methanol from activated carbon. The 2.3m^2 parabolic trough collector is not recommended for the solar thermal system because of the low temperatures achieved in the storage tank through the year with 41.5^{o}C at 5671.5hr.

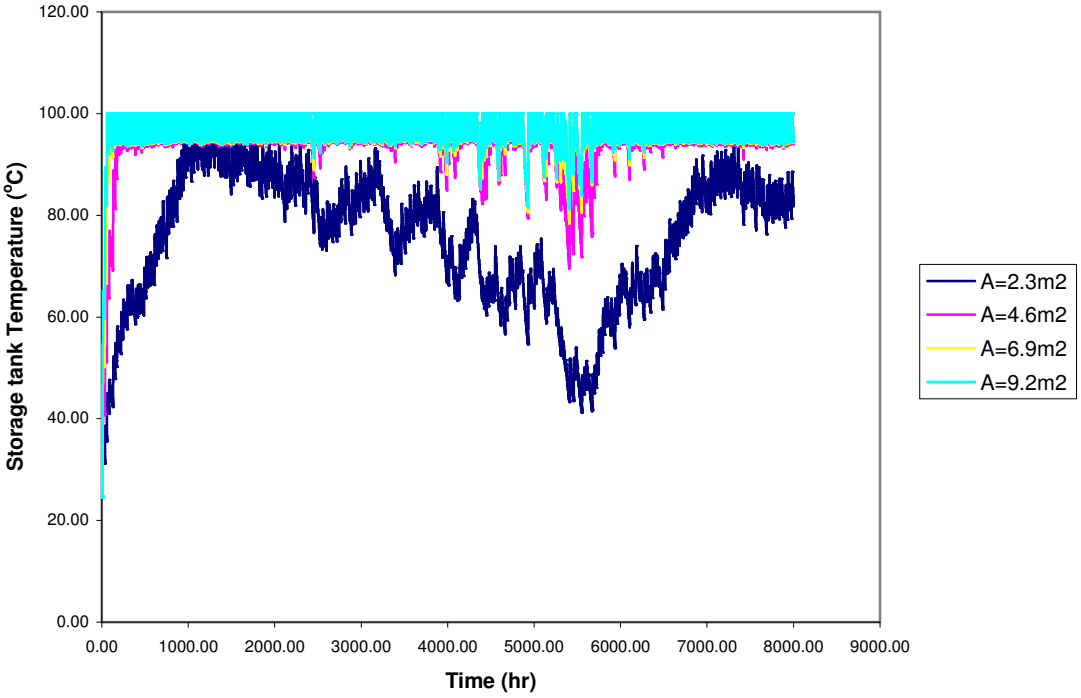


Fig. 5.13: Effect of Collector Area on Storage Tank Temperature (PTC)

Figures 5.14, 5.15 and 5.16 below give the useful energy gained by a parabolic trough collector as a function of collector area with varying storage tank volumes, also shown is the amount of dumped energy in each case. The dumped energy is the energy gained by the collector above that required to raise the temperature of the heat transfer fluid to its predetermined level. This indicates an over sizing of the collector or under sizing of the storage tank volume for the given application. It is observed from the figures the useful energy gained increases as the collector area increases, with the storage tank volume having no effect until a collector area of 13.8m^2 is reached for the months of April and August, which represents days with low solar radiation for the research location. At 13.8m^2 collector area, dumped energy is noticed for a storage tank volume of 1m^3.

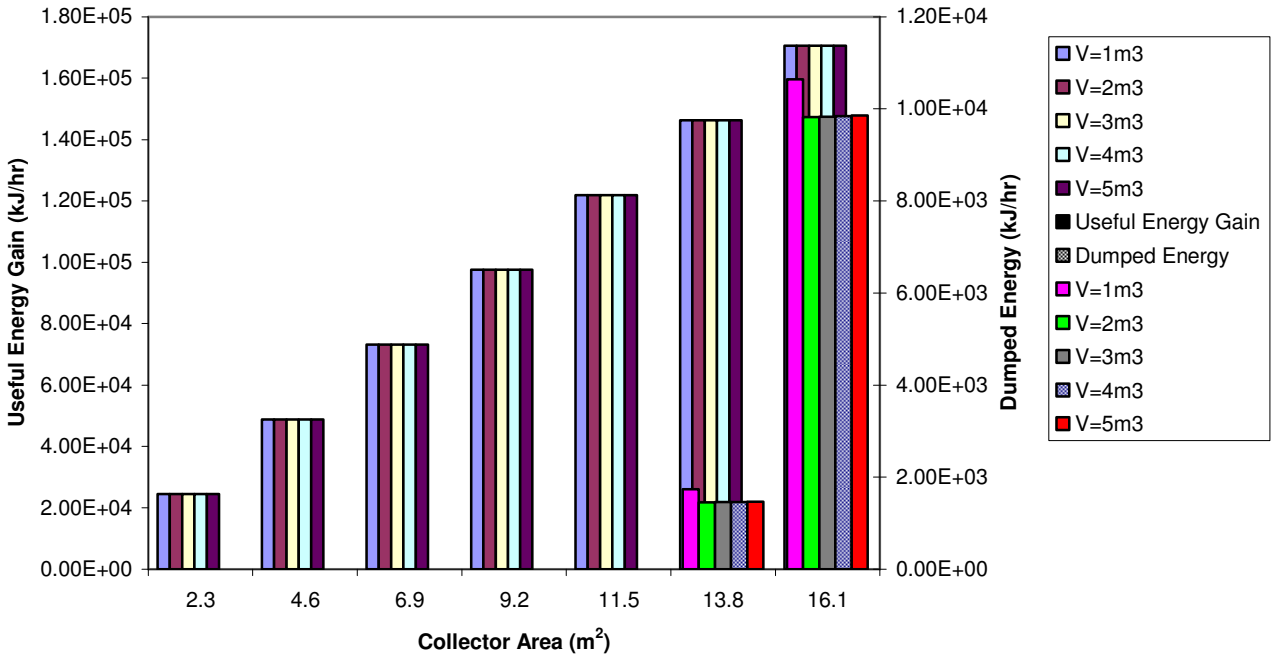


Fig. 5.14: Effect of Storage Volume on PTC Useful Energy Gain (April)

Figs. 5.14 and 5.15 show that a collector area above 11.5m^2 results in dumped energy for the months of April and August, this value can not be used for year round design of the solar thermal system since it is required to work even on overcast days. Fig. 5.16 however shows that for the month of December, dumped energy occurs for collector area larger than 13.8m^2.

A collector area of 13.8m^2 and storage tank volume of 1m^3 is therefore chosen for the thermal system to be heated by a parabolic trough collector. A storage tank volume of 1m^3 has been chosen because from fig. 5.17, it is observed that the larger the storage tank volume, the lower the temperature attainable by the storage tank.

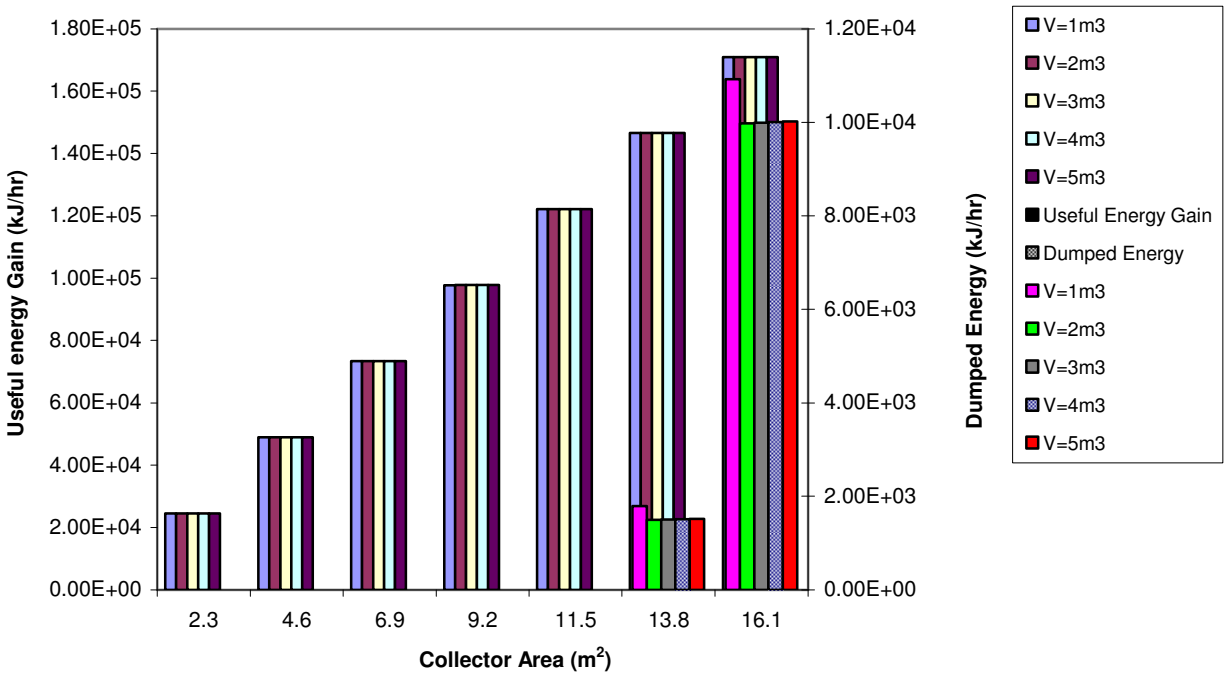


Fig. 5.15: Effect of Storage Volume on PTC Useful Energy Gain (August)

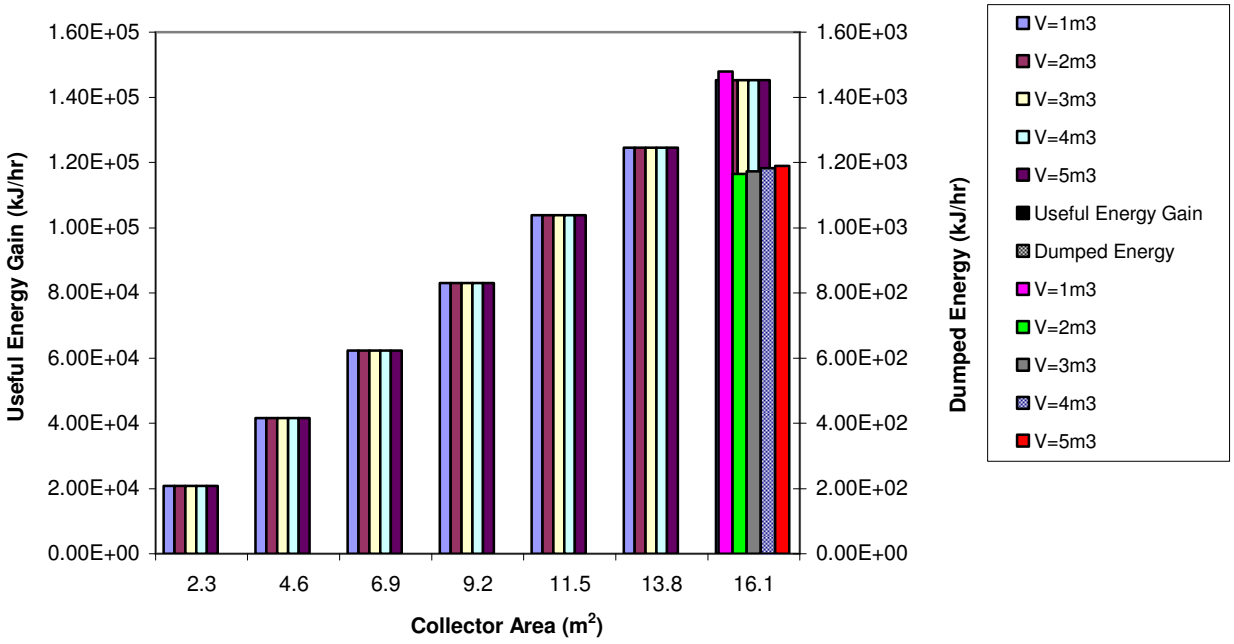


Fig. 5.16: Effect of Storage Volume on PTC Useful Energy Gain (December)

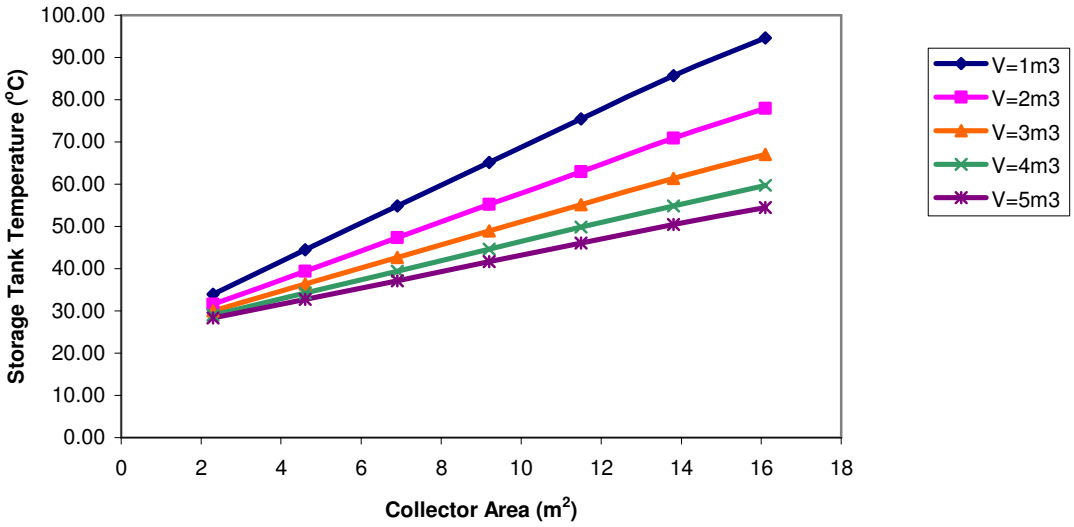


Fig.5.17 : Effect of Tank Volume on Storage Tank Temperature (PTC)

5.2.3 Evacuated Tube Collector (ETC)

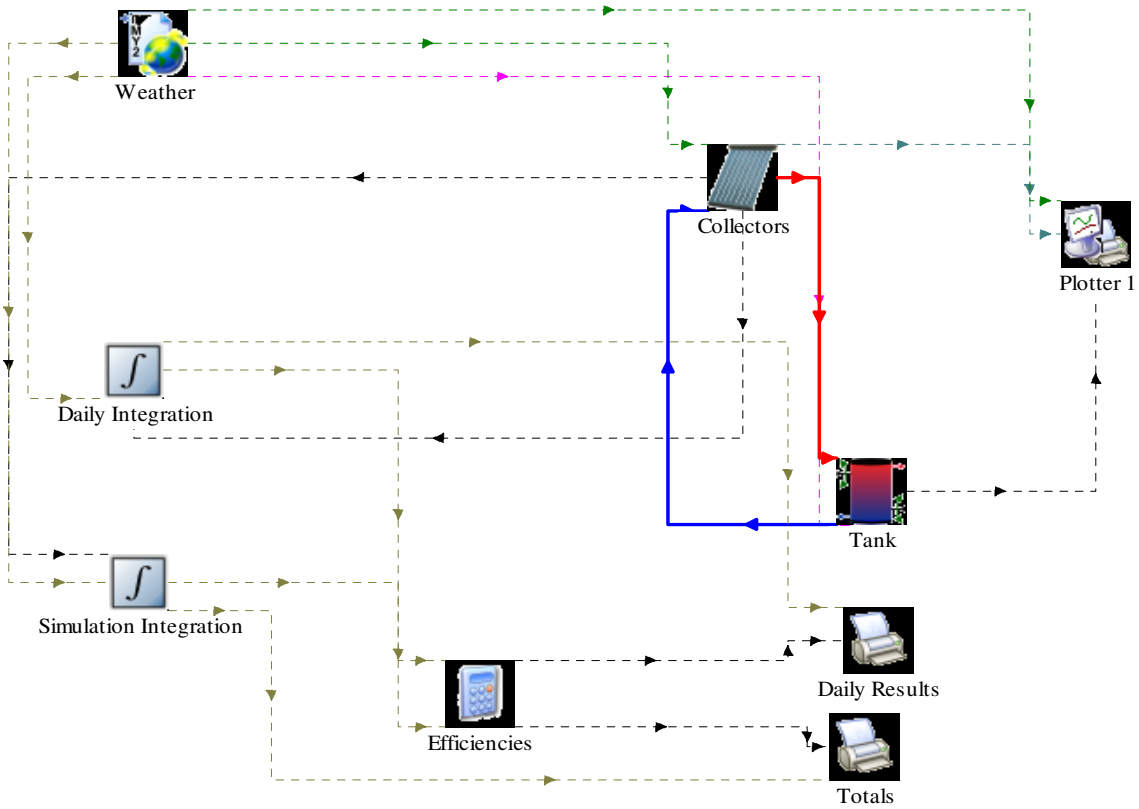


Fig. 5.18: Solar thermal system modeled with an Evacuated tube collector

Fig. 5.18 above shows the solar thermal system modeled in TRNSYS with an evacuated tube collector. The analysis of the system, allows the appropriate evacuated tube solar collector size and storage tank volume to be determined for the research location. This combination would give a good all year round performance for the solar thermal system in terms of temperatures achievable and the time taken for these temperatures to be achieved.

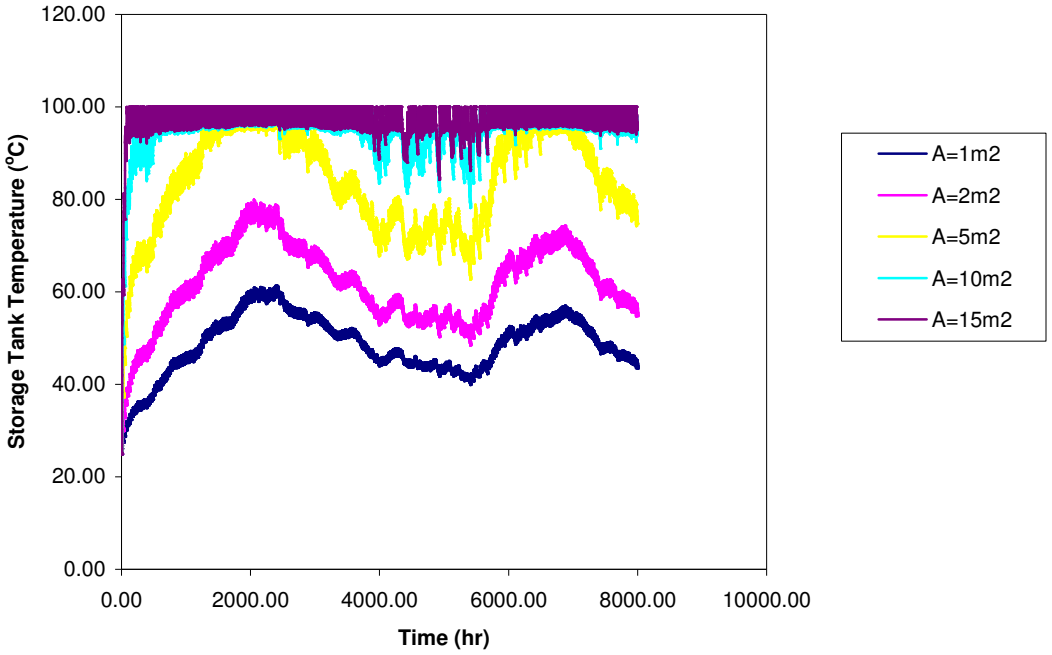


Fig. 5.19: Effect of CollectorArea on ETC Storage Tank Temperature

The storage tank temperature as a function of time for the evacuated tube collector is shown in Fig. 5.19 above. The performances of five different collector areas were studied as shown in the figure. For a $1m^2$ collector area, a temperature of 61.4^oC at 2414.25hr (2.15pm on the 11^{th} of April) is achieved with the storage tank temperature being less than 60^oC for most days of the year. A maximum temperature of 78.9^oC at 2414.25hr is attained with a $2m^2$ collector; the attainable storage tank temperature is less than 65^oC for most days of the year. The solar thermal system with a $5m^2$ collector area achieves a storage tank

temperature of 100°C at 2414.25hr, but during overcast days of the year the attainable temperature is less than 75°C. A $10m^2$ collector also achieves 100°C at 2414.25hr with the tank temperature for most days of the year being above 85°C. The lowest temperature for the $10m^2$ collector is 78.1°C at 5410.75hr. A $15m^2$ collector however achieves 100°C for most days with a low of 86.2°C at 5410.75hr.

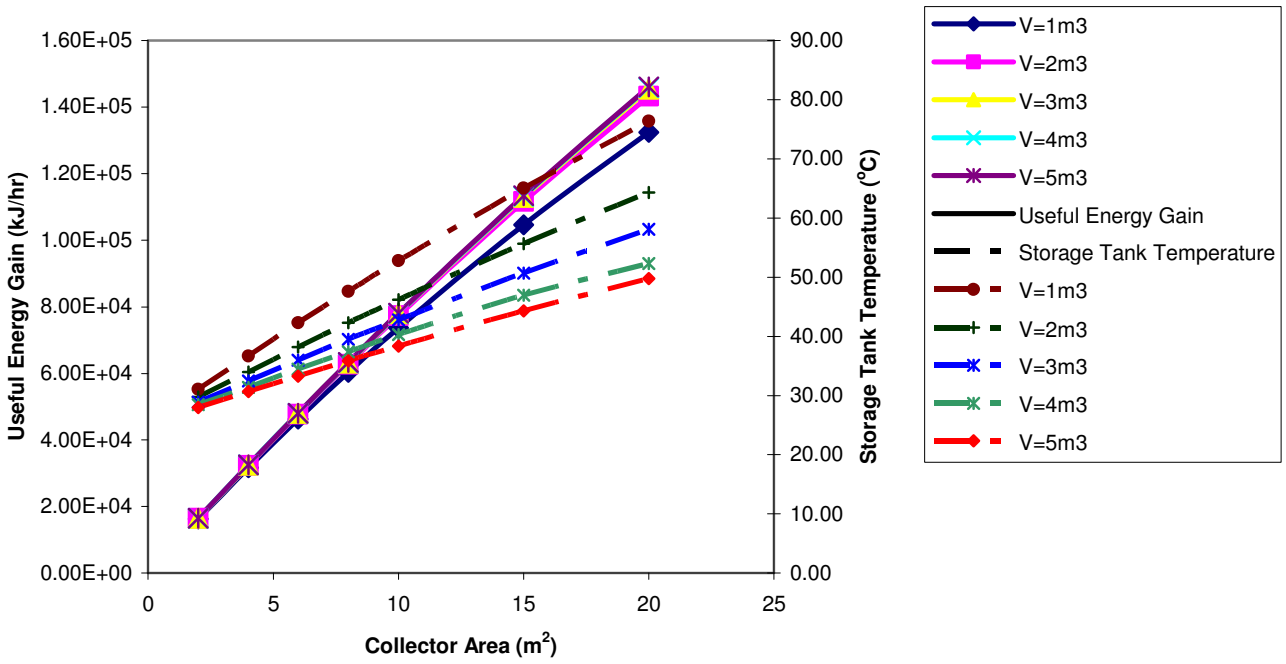


Fig.5.20: Effect of Storage Volume on ETC Useful Energy Gain and Tank Temperature (April)

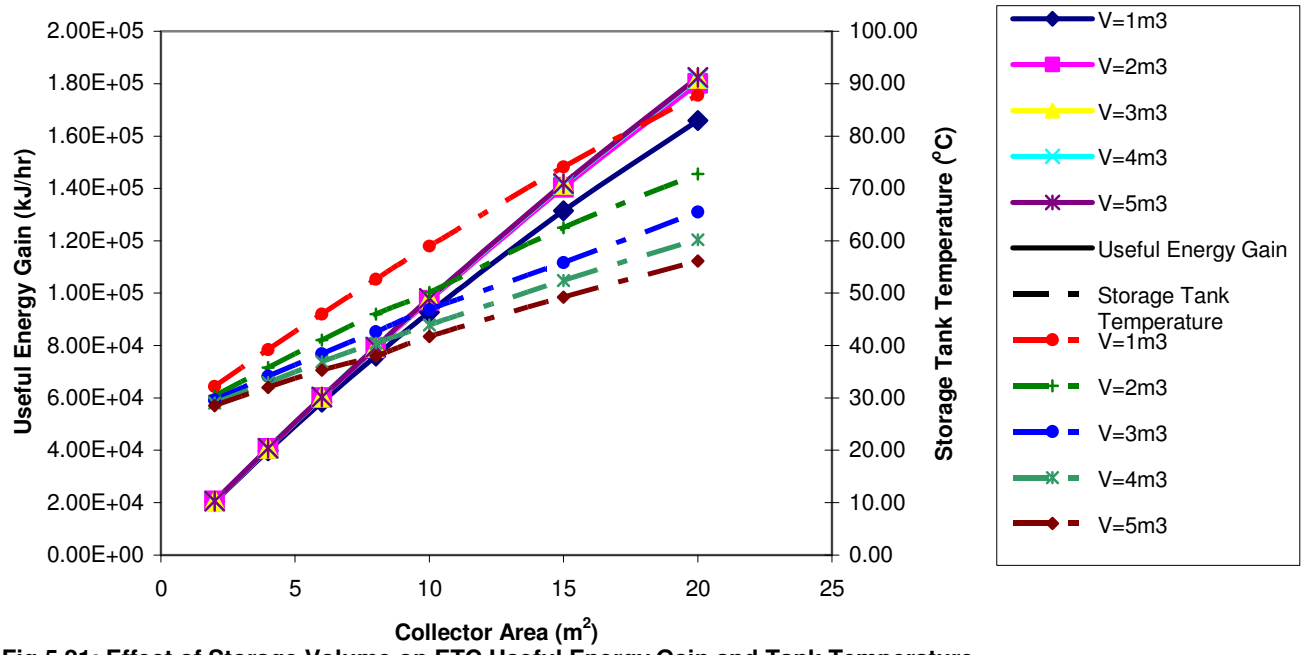


Fig.5.21: Effect of Storage Volume on ETC Useful Energy Gain and Tank Temperature (August)

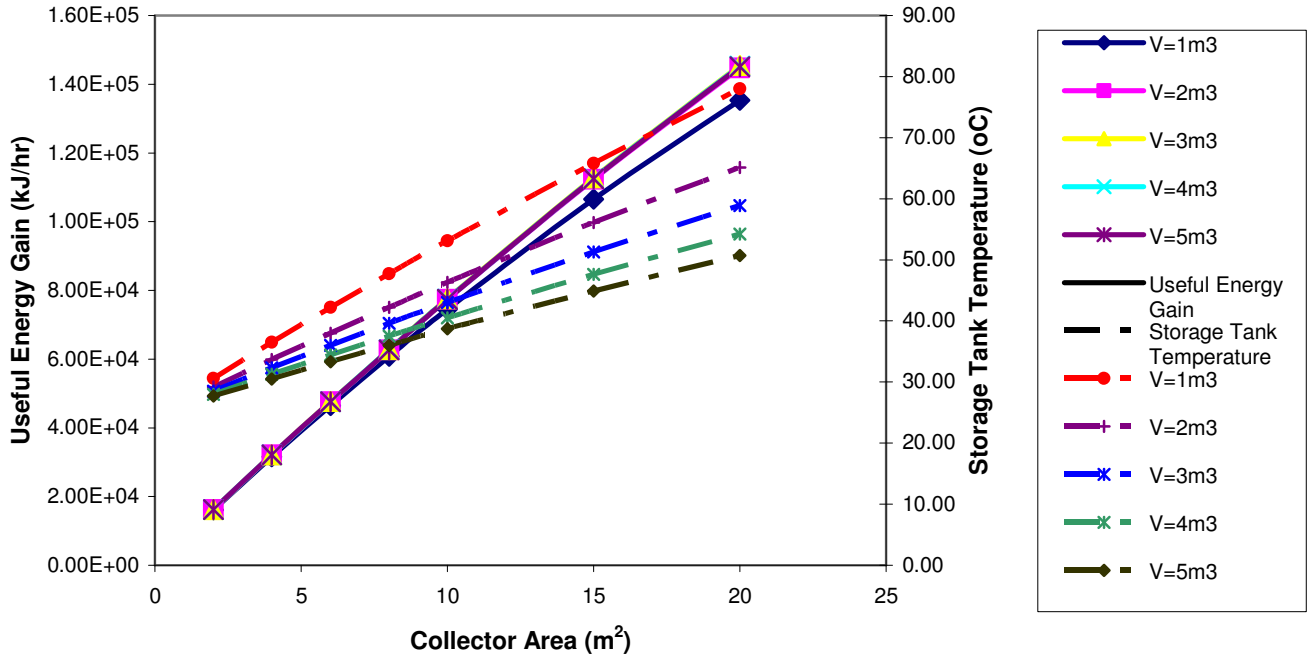


Fig.5.22: Effect of Storage Volume on ETC Useful Energy Gain and Tank Temperature (December)

Figures 5.20, 5.21, 5.22 present the useful energy gained by the evacuated tube collector for three months of the year (April, August and December) as a function of the collector area

for five different storage tank volumes. The figures show that though useful energy gain increases with collector area, it does not increase appreciably with storage tank volume beyond $2m^3$. Also the storage tank temperature though increases with collector area, it reduces with increase in tank volume size.

The solar thermal system with the evacuated tube collector is to use a minimum of $15m^2$ collector area and not more than $1m^3$ storage tank volume.

CHAPTER SIX

ADSORPTION REFRIGERATION SYSTEM SIMULATION

The simulation of the adsorption refrigeration system was carried out in TRNSYS, with the TYPE 155 component used to model the adsorption unit. This TRNSYS type implements a link with Matlab. The modeling equations for the adsorption unit developed in chapter four are written in Matlab code that can be read by the TRNSYS software. The connection with the Matlab engine using Type 155 is launched as a separate process, the FORTRAN routine communicates with the Matlab engine through a Component Object Model (COM) interface.

The three types of collectors studied in chapter five are used separately in the simulation of the refrigeration system as the thermal energy source. Table 6.1 below shows some of the parameters used in the simulation of the adsorption unit. The thermodynamic properties of methanol are as obtained from Methanex Corporation information guide (Methanex Corporation, 2006).

Table 6.1: Parameters Used in the Simulation of Adsorption Unit

Symbol	Parameter	Value	Unit
Activated Carbon			
c_{pac}	Specific heat of activated carbon	0.711	kJ/kgK
ρ_{ac}	Density of activated carbon	2000	kg/m^3
m_{ac}	Mass of activated carbon	26.07	kg
Methanol			
c_{pml}	Specific heat of liquid methanol	2.534	kJ/kgK
c_{pm}	Specific heat of methanol vapor at constant pressure	1.820	kJ/kgK
c_{vm}	Specific heat of methanol vapor at constant pressure	1.560	kJ/kgK
Stainless Steel			
Adsorber tubes			
c_{pad}	Specific heat of adsorber tube material	0.480	kJ/kgK
ρ_{ad}	Density of adsorber tube material	8055	kg/m^3
m_{ad}	Mass of adsorber tubes	12.4	kg
D_o	Diameter of each of the outer co-axial Adsorber tubes	0.0508	m
D_i	Diameter of each of the inner co-axial Adsorber tubes	0.0254	m
l_{ad}	Length of Adsorber tubes	1	m
N	Number of Adsorber tubes	10	-
Evaporator Temperature	0^oC		
Condenser Temperature	25^oC		

The adsorber tubes are to be of stainless steel material, though this material has a low thermal conductivity, its long term performance in solar adsorption refrigeration system is better than the obvious choices of copper or aluminum. This is because methanol though not supposed to decompose at temperatures less than 150^{o}C tends to decompose in the presence of these alloys and carbon within the operating temperature range of the adsorption system (Hu, 1998). This decomposition produces unwanted gas which is adsorbed by the carbon thereby reducing the surface area available for the subsequent adsorption of methanol and thus reducing system performance. The mass of activated carbon used is determined with its density and the volume between the two concentric tubes which it occupies and the number of tubes that make up the adsorbent bed (Equations 4.27 to 4.30).

The simulation of the performance of the adsorption refrigeration system is investigated for each month of the year using the recommended average days for months (Duffie, 2006).

Table 6.2: Recommended Average Days for months and Values of n_1 (Day of the Year) by months

	For Average Day of Month		
Month	Date	n_1	Hours
January	17	17	384 – 408
February	16	47	1104 – 1128
March	16	75	1824 – 1848
April	15	105	2496 – 2520
May	15	135	3216 – 3240
June	11	162	3864 – 3888
July	17	198	4728 – 4752
August	16	228	5448 – 5472
September	15	258	6168 – 6192
October	15	288	6888 – 6912
November	14	318	7608 – 7632
December	10	344	8256 – 8280

6.1 ADSORPTION REFRIGERATION SYSTEM WITH FPC

The adsorption refrigeration system powered by a flat plate collector simulated in TRNSYS is shown in Fig. 6.1 below and the deck file generated by TRNSYS for this simulation is shown in Appendix B.

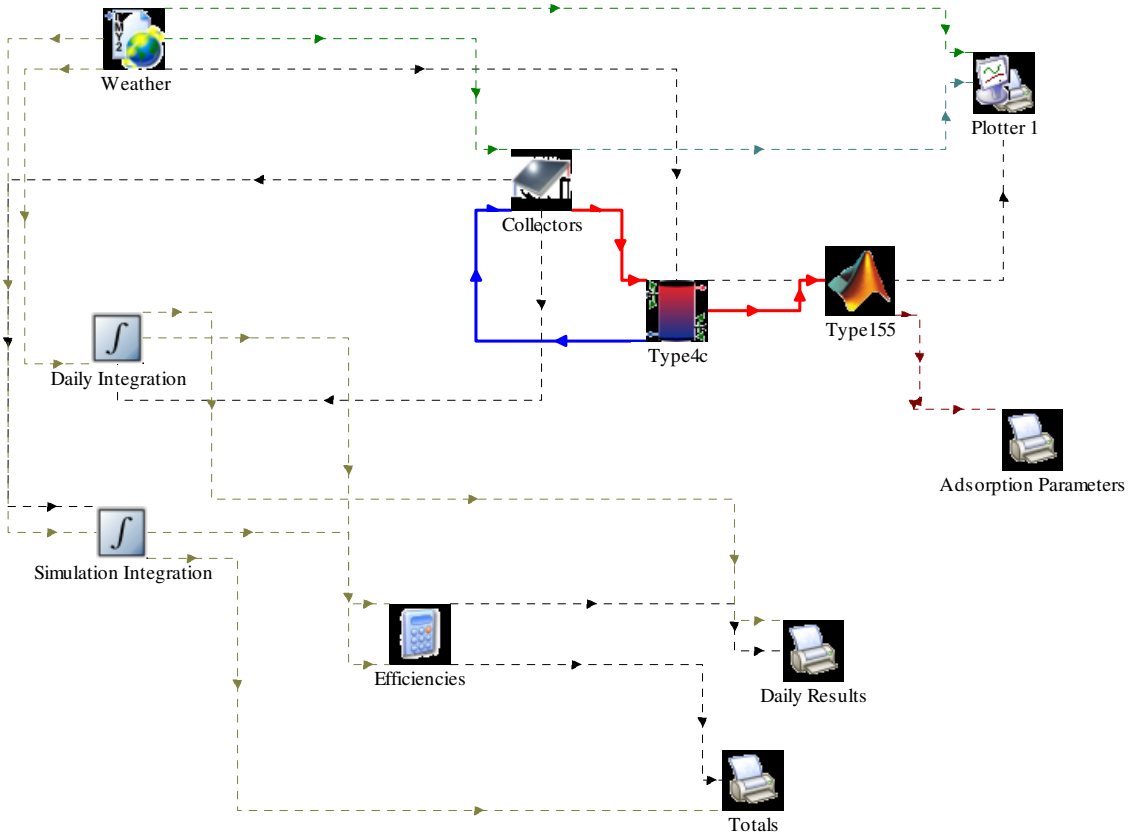


Fig.6.1: Adsorption Refrigeration system simulation with a Flat plate collector

The adsorbent maximum quantity of methanol adsorbed by the activated carbon at 25^{o}C (starting temperature) using equation 3.19 is 0.311kg/kg; X_{min} gives the quantity of methanol left in the adsorbent as the generation temperature increases. The change in X_{min} and generation temperature as well as the COP_{solar} and COP attained by the system throughout the year are presented in Figures 6.2 to 6.25.

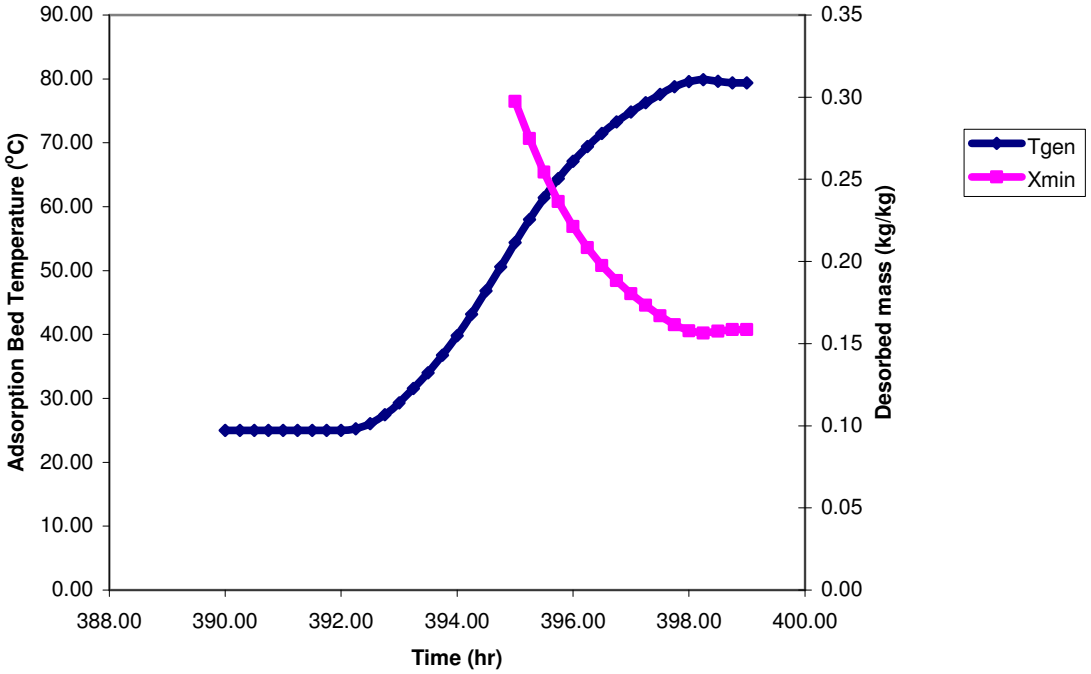


Fig.6.2: Variation of Adsorption bed Temperature and Desorbed mass with Time (FPC Jan)

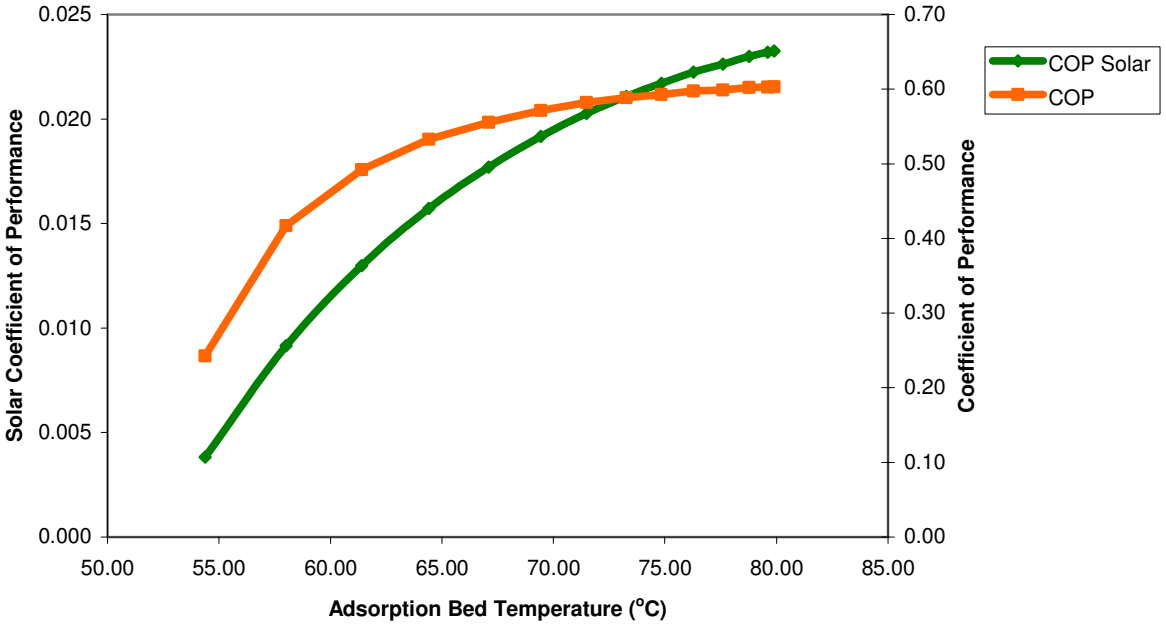


Fig. 6.3: Effect of Adsorption Bed Temperature on Coefficient of Performance (FPC Jan)

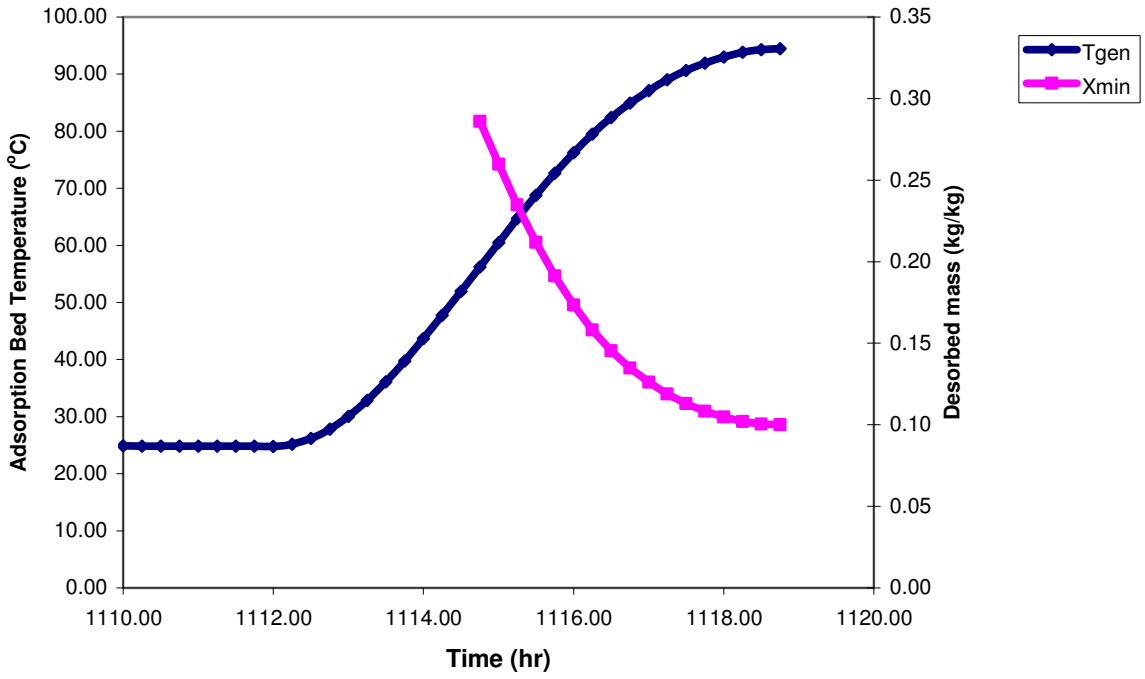


Fig.6.4: Variation of Adsorption Bed Temeperature and Desorbed mass with Time (FPC Feb)

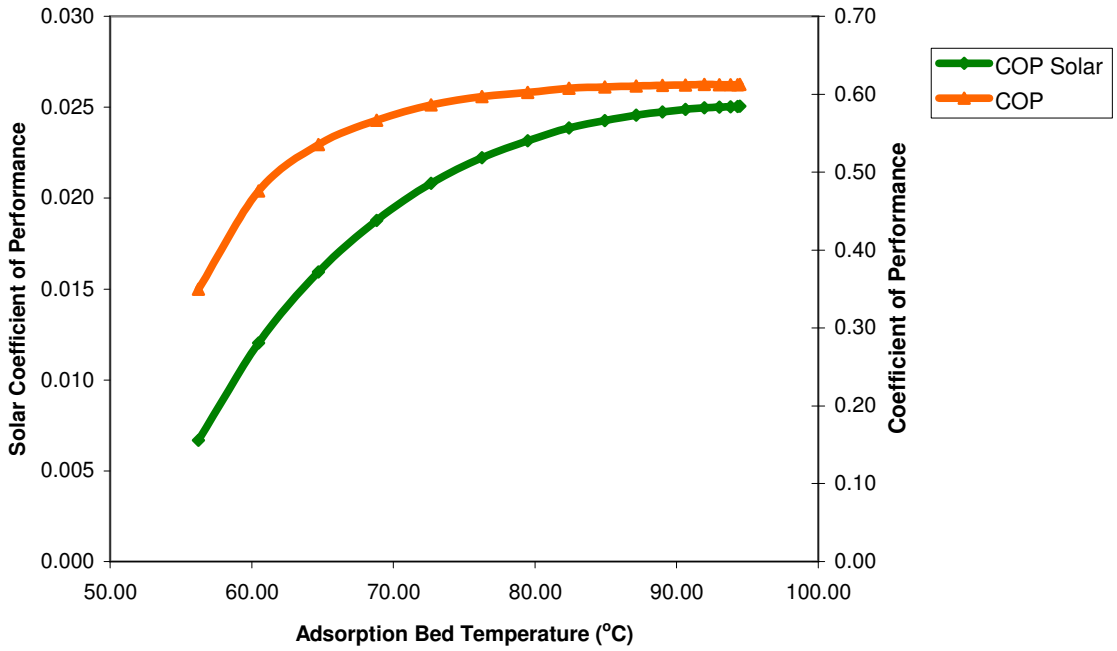


Fig.6.5: Effect of Adsorption Bed Temperature on Coefficient of performance (FPC Feb)

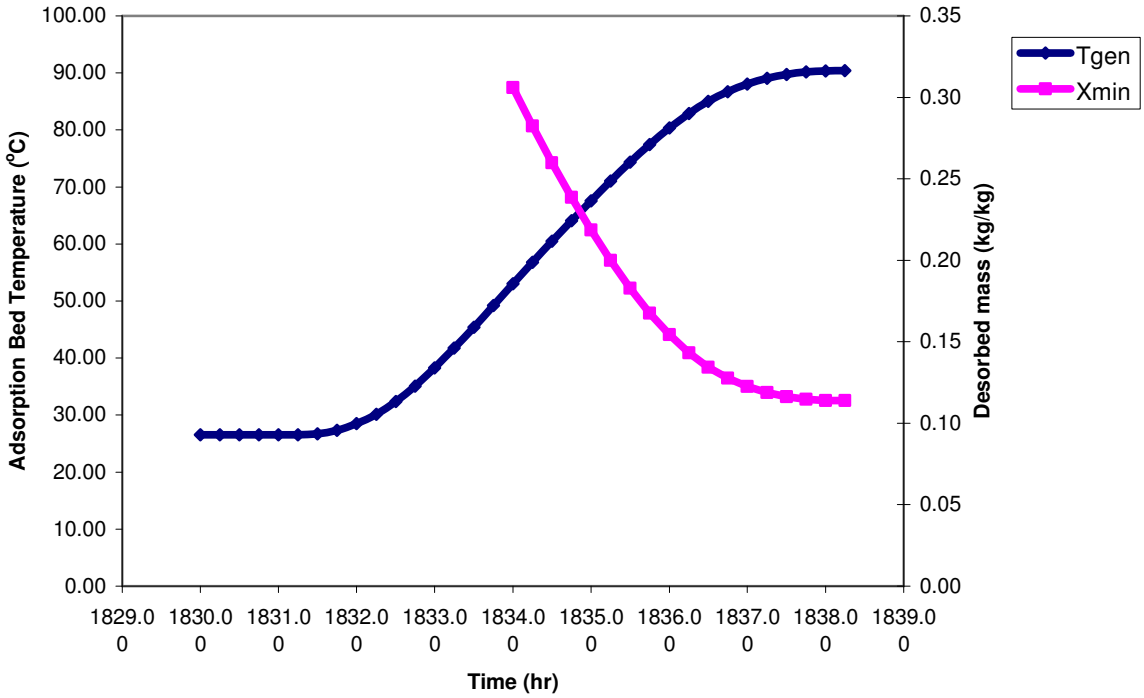


Fig.6.6: Variation of Adsorption Bed Temperature and Desorbed mass with Time (FPC Mar)

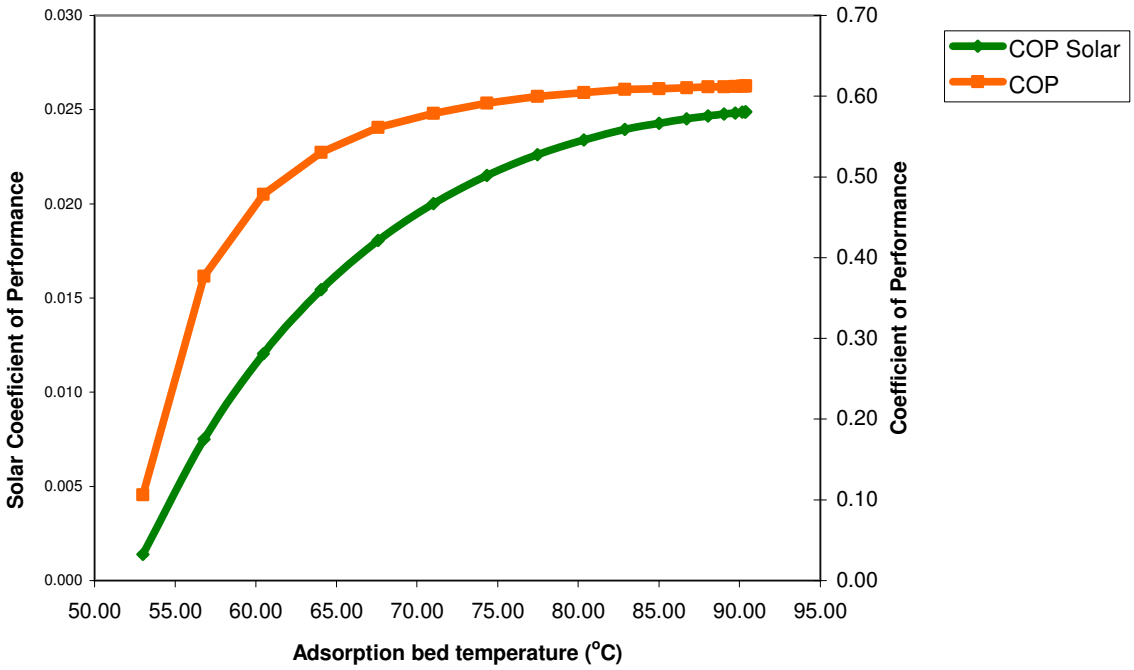


Fig.6.7: Effect of Adsorption Bed Temperature on Coefficient of Performance (FPC Mar)

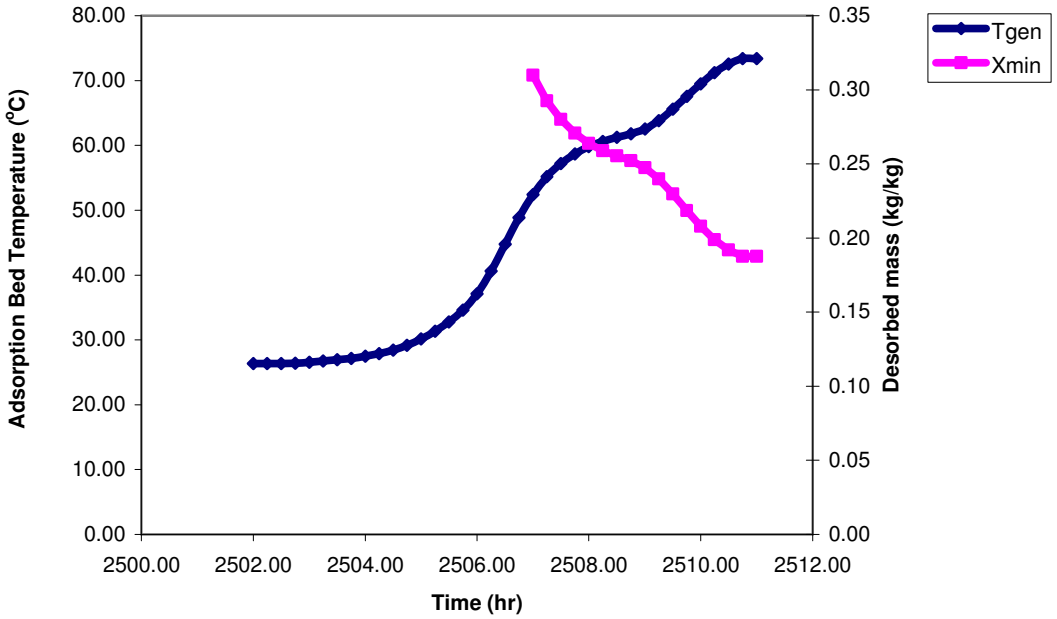


Fig.6.8: Variation of Adsorption Bed Temperature and Desorbed Mass with Time (FPC Apr)

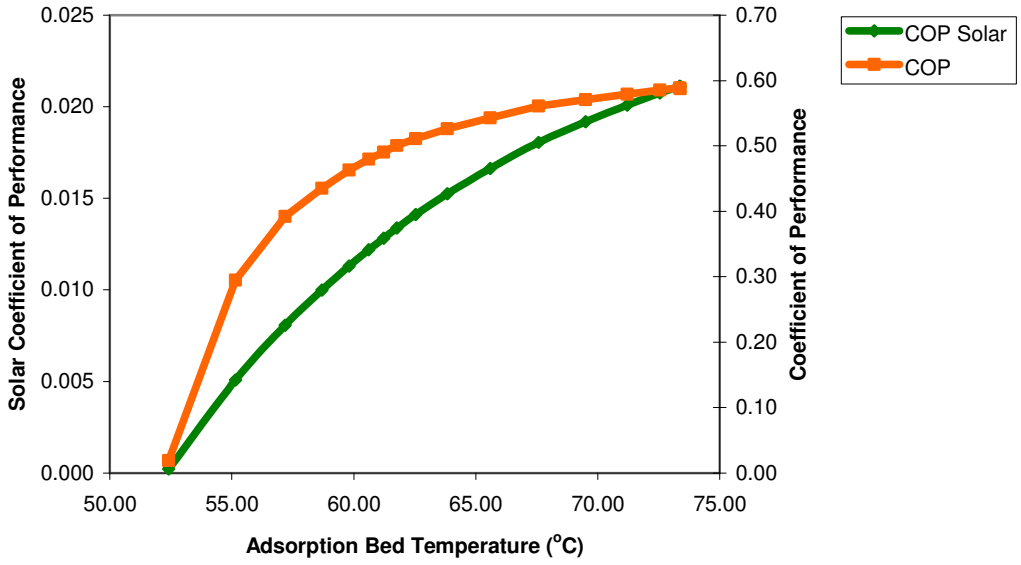


Fig.6.9: Effect of Adsorption Bed Temperature on Coefficient of Performance (FPC Apr)

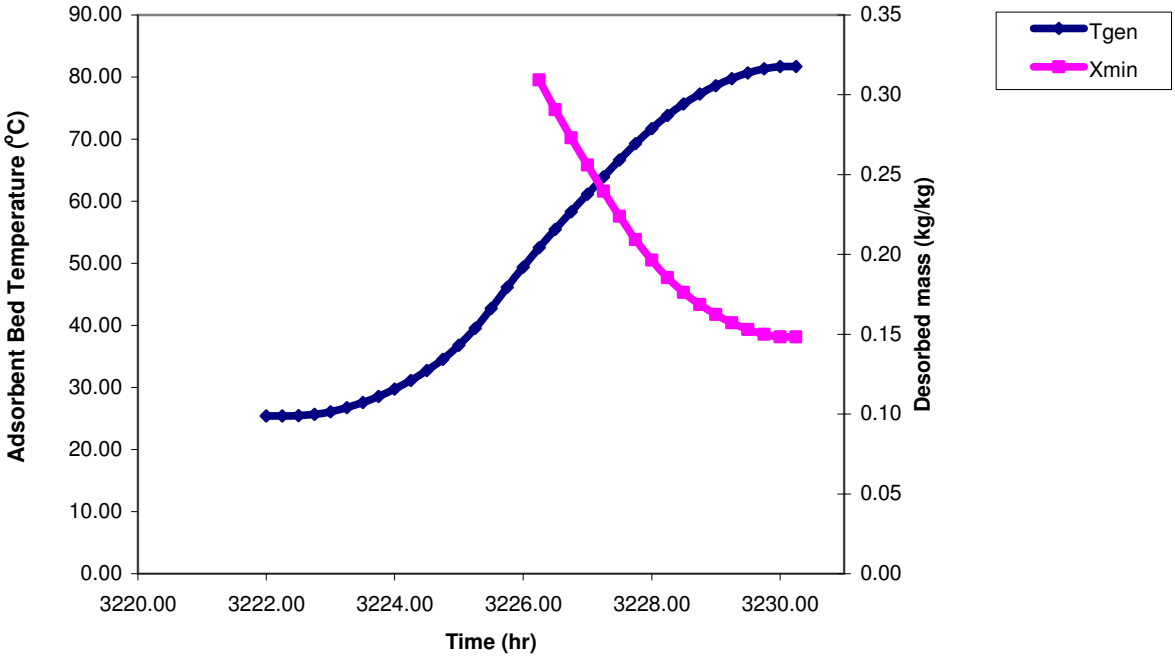


Fig.6.10: Variation of Adsorption Bed Temperature and Desorbed mass with Time (FPC May)

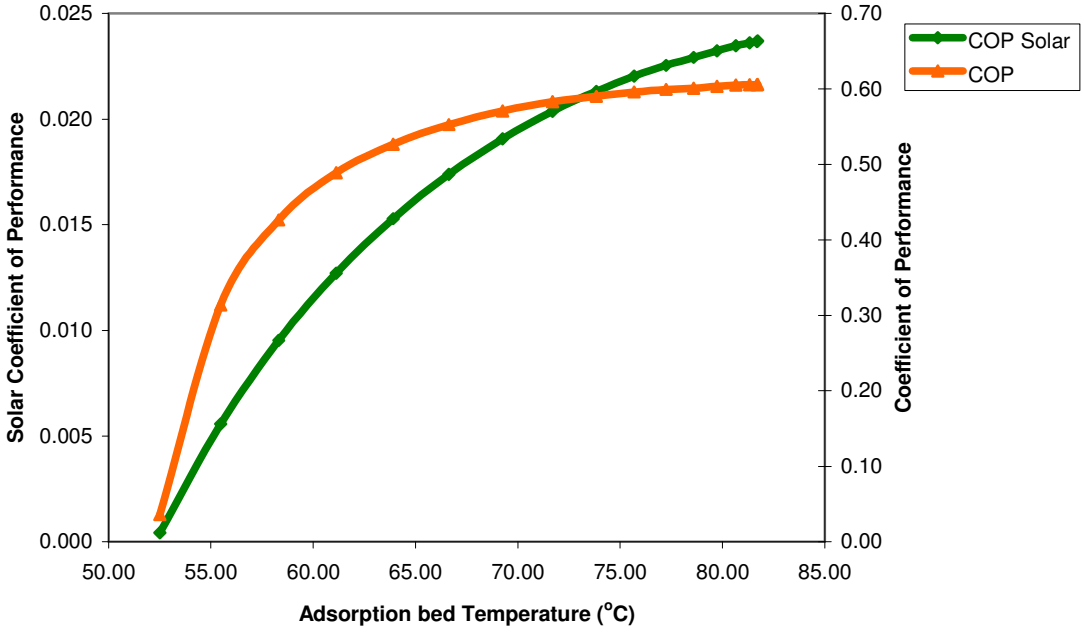


Fig.6.11: Effect of Adsorption Bed Temperature on Coefficient of Performance (FPC May)

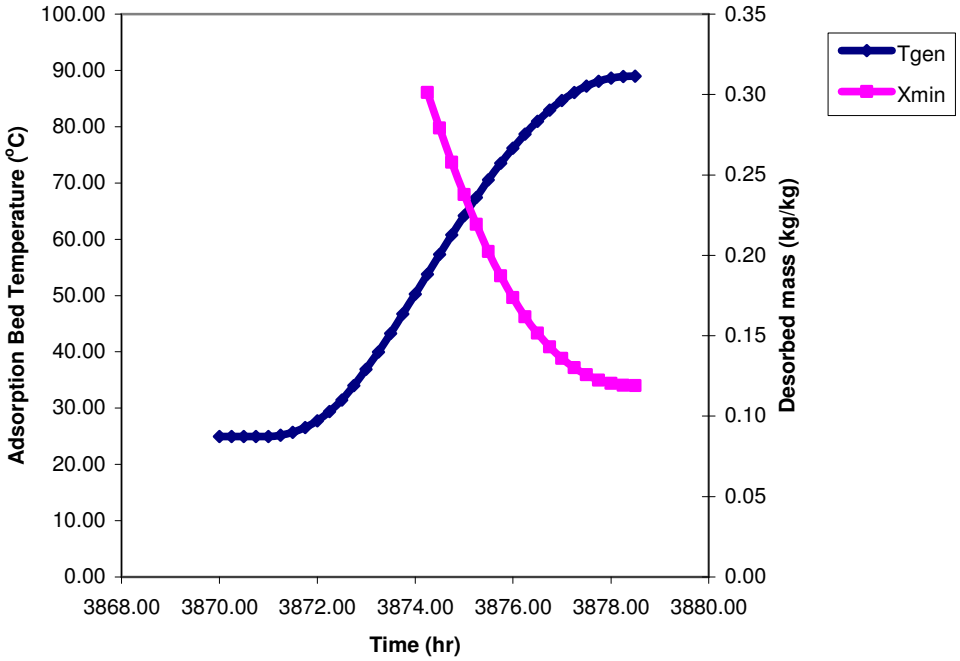


Fig.6.12: Variation of adsorption Bed Temperature and Desorbed mass with Time (FPC Jun)

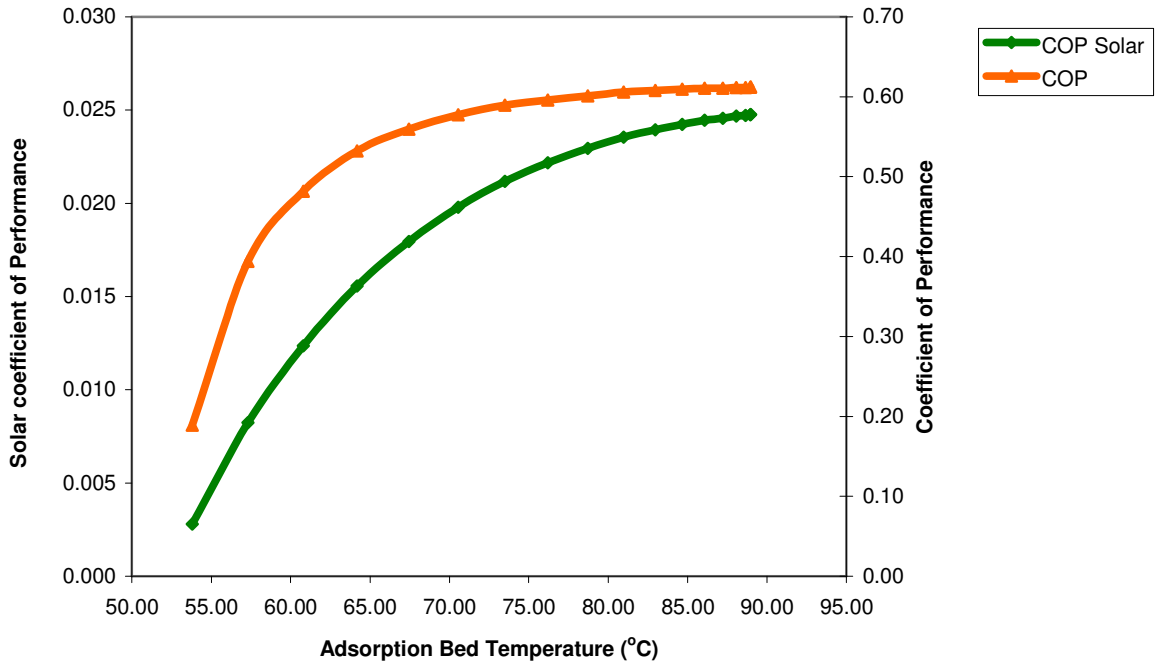


Fig.6.13: Effect of Adsorption Bed Temperature on Coefficient of Performance (FPC Jun)

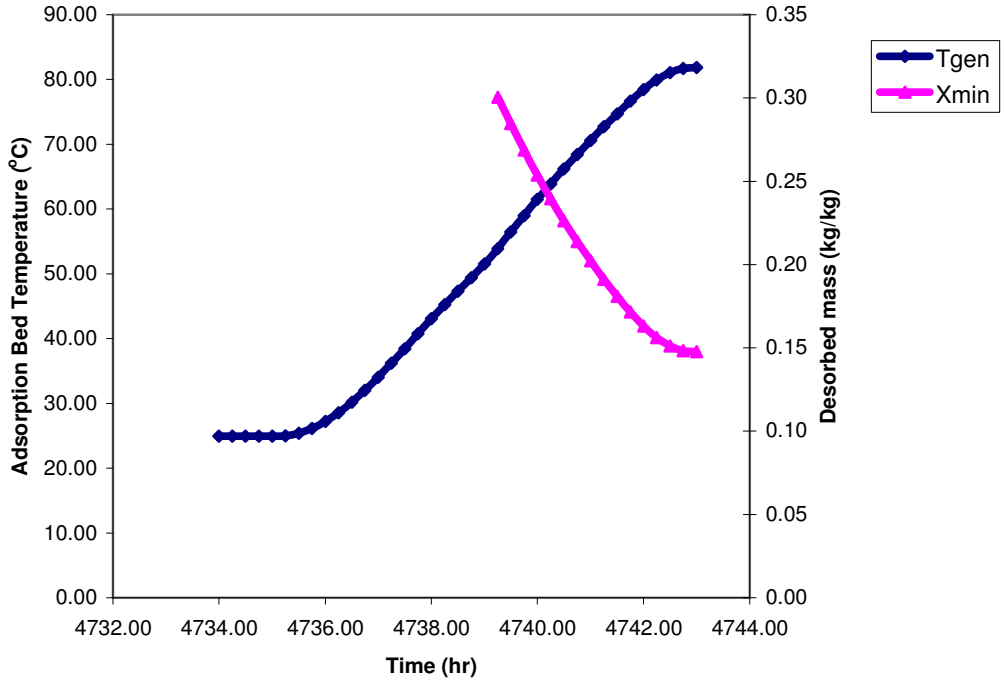


Fig.6.14: Variation of Adsorption Bed Temperature and Desorbed mass with Time (FPC Jul)

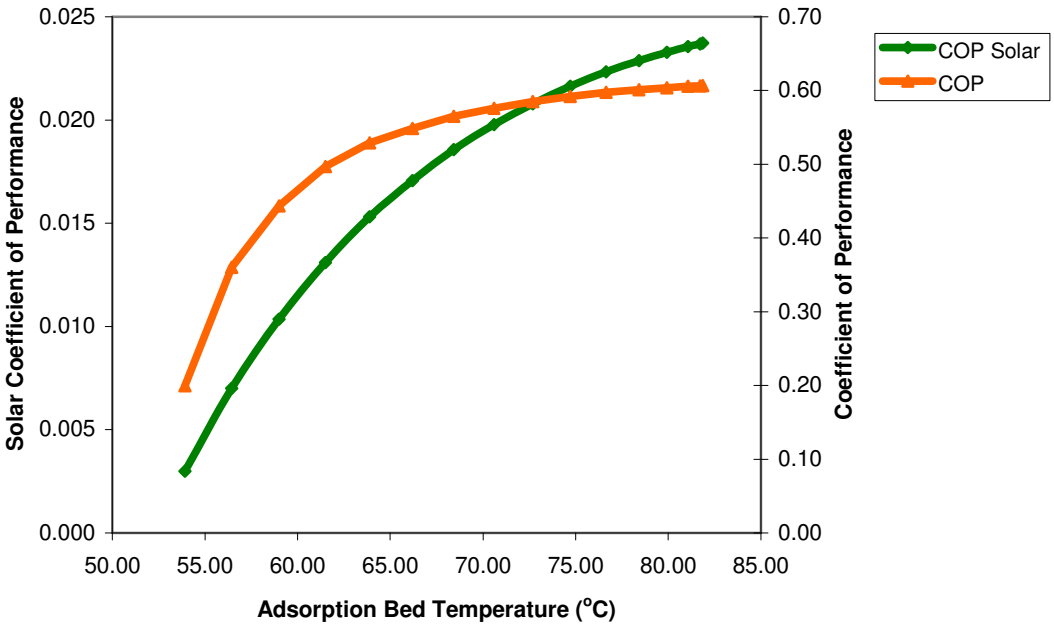


Fig.6.15: Effect of Adsorption Bed Temperature on Coefficient of Performance (FPC Jul)

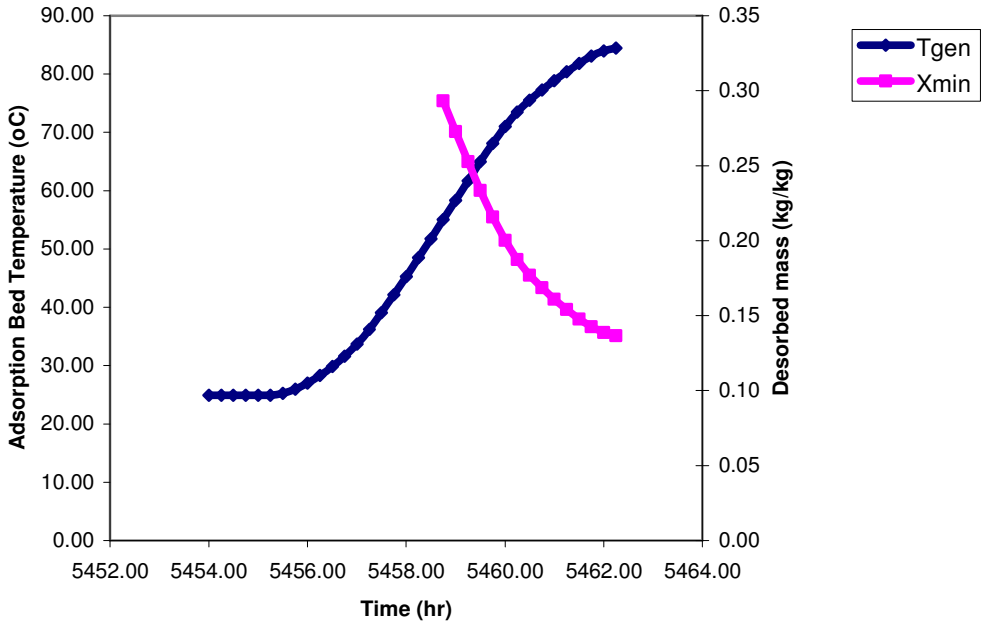


Fig.6.16: Variation of Adsorption Bed Temperature and Desorbed mass with Time (FPC Aug)

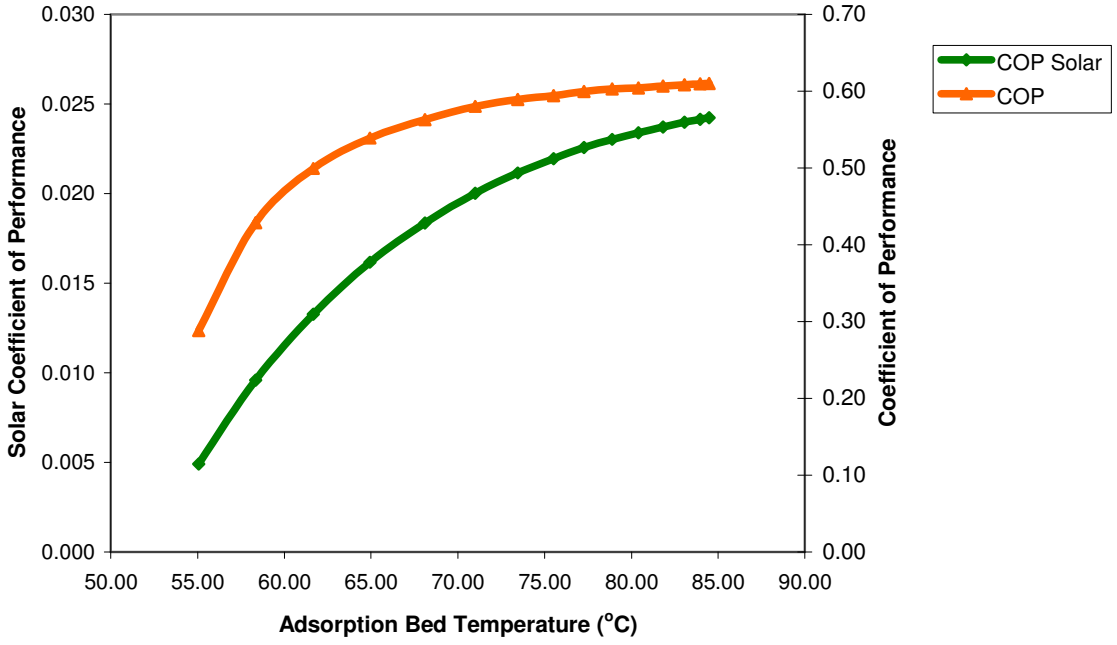


Fig.6.17: Effect of Adsorption Bed Temperature on Coefficient of Performance (FPC Aug)

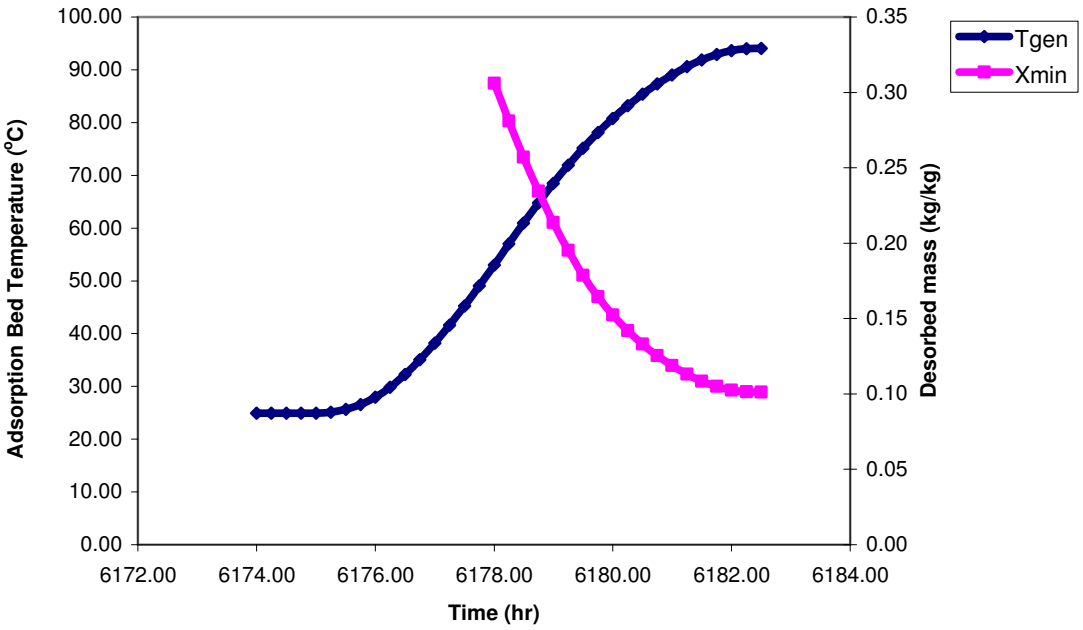


Fig.6.18: Variation of Adsorption Bed Temperature and Desorbed mass with Time (FPC Sep)

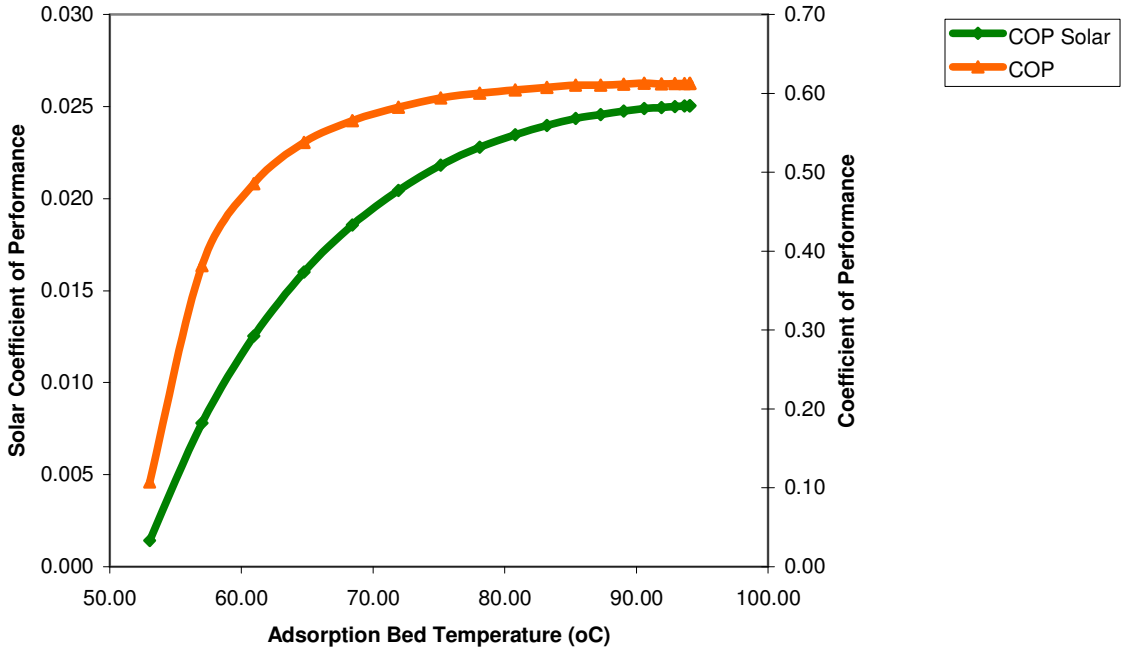


Fig.6.19: Effect of Adsorption Bed Temperature on Coefficient of Performance (FPC Sep)

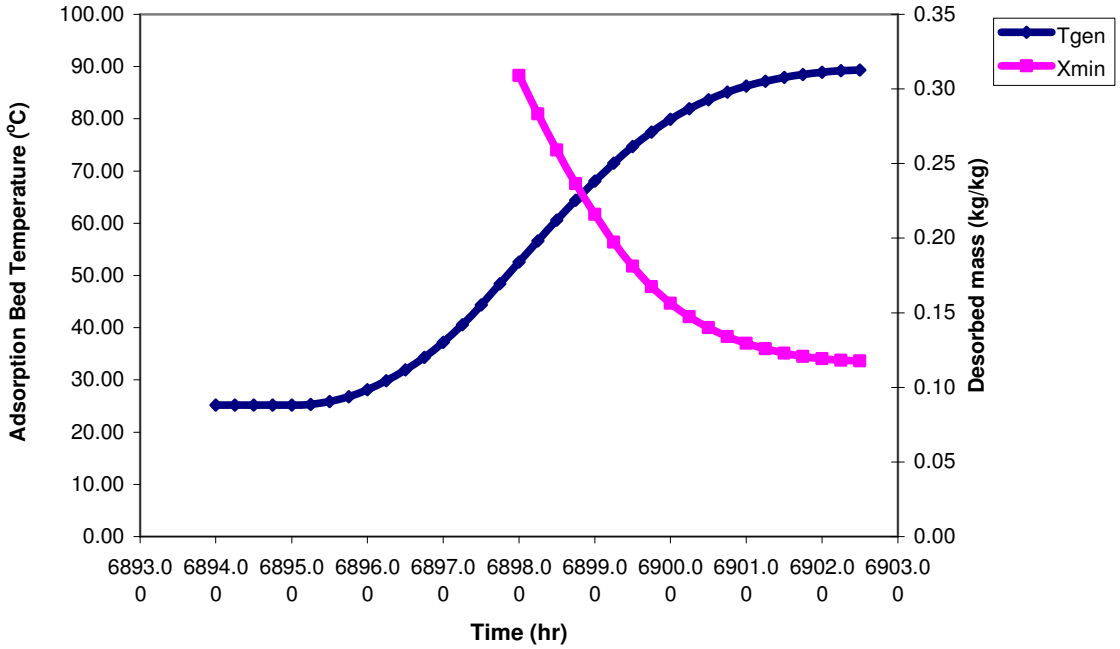


Fig.6.20: Variation of Adsorption Bed Temperature and Desorbed mass with Time (FPC Oct)

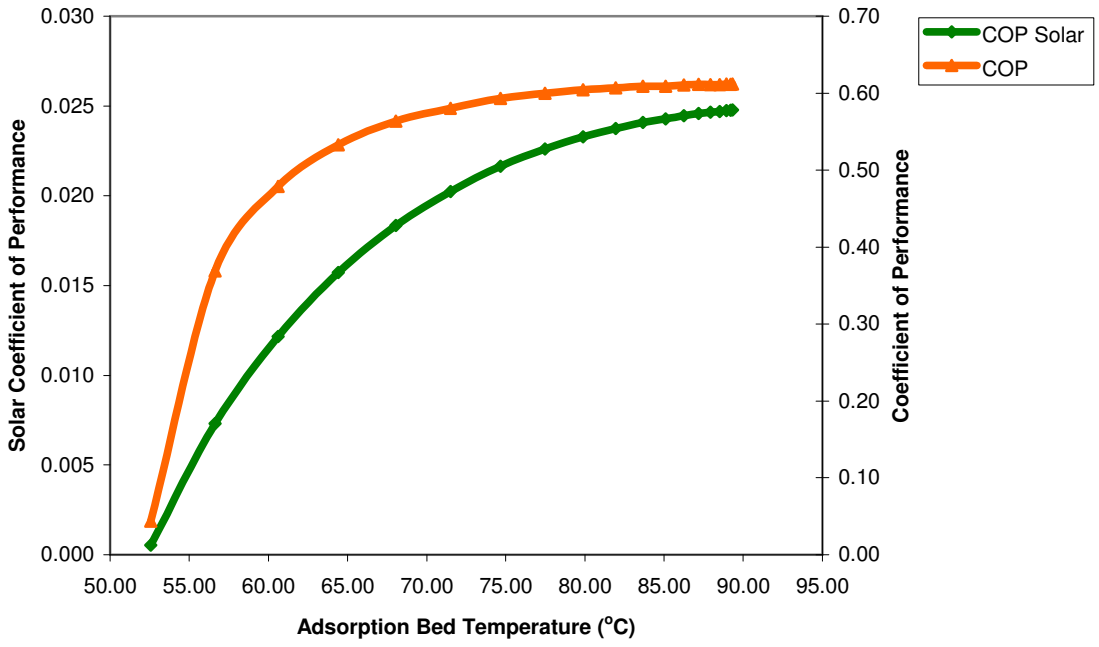


Fig.6.21: Effect of Adsorption Bed Temperature on Coefficient of Performance (FPC Oct)

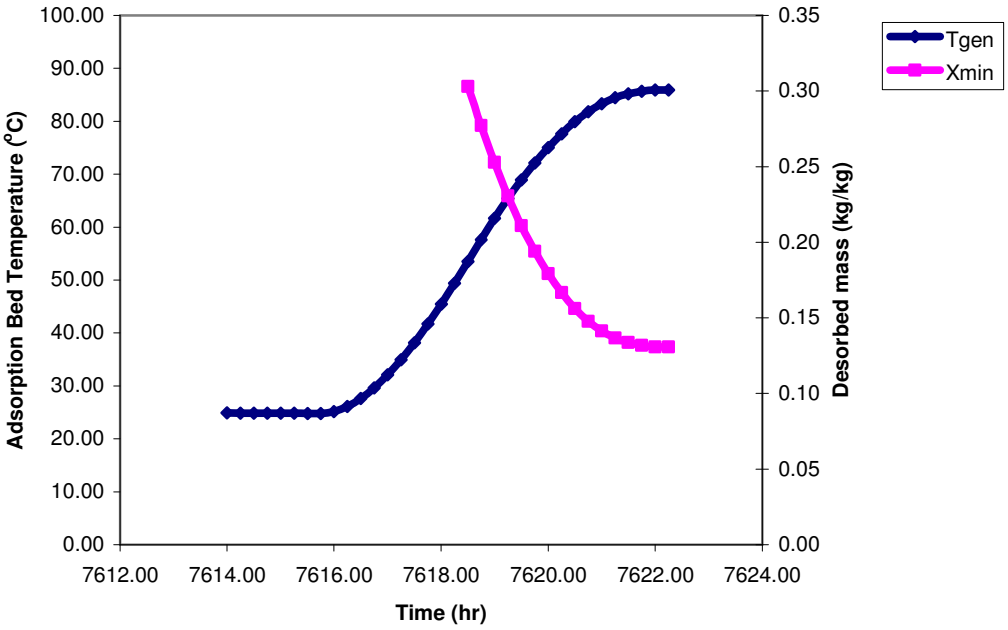


Fig.6.22: Variation of Adsorption Bed Temperature and Desorbed mass with Time (FPC Nov)

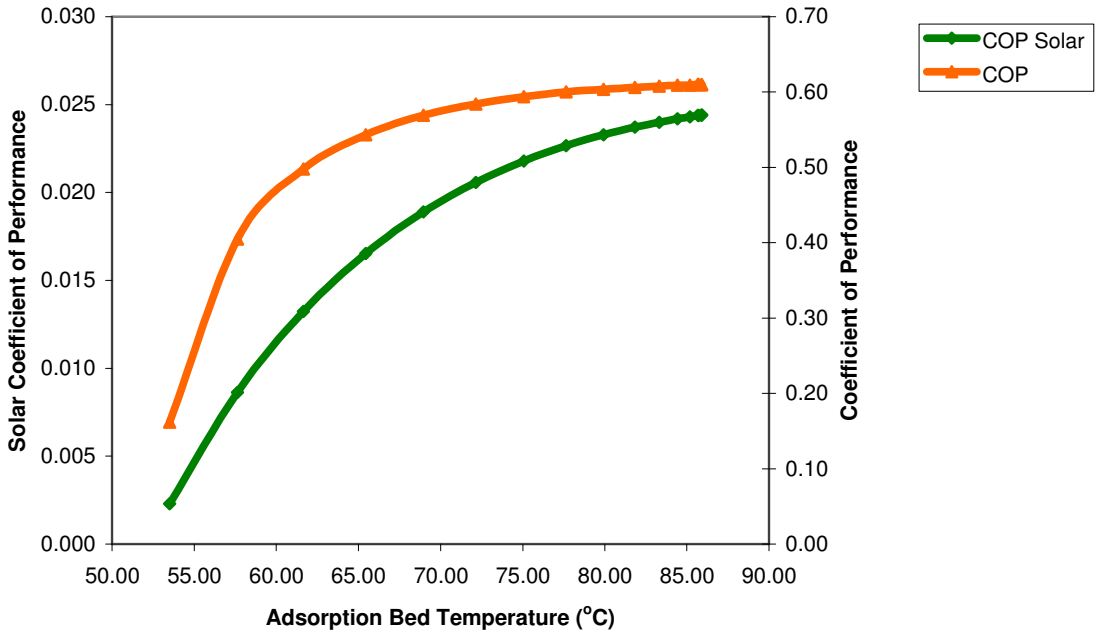


Fig.6.23: Effect of Adsorption Bed Temperature on Coefficient of Performance (FPC Nov)

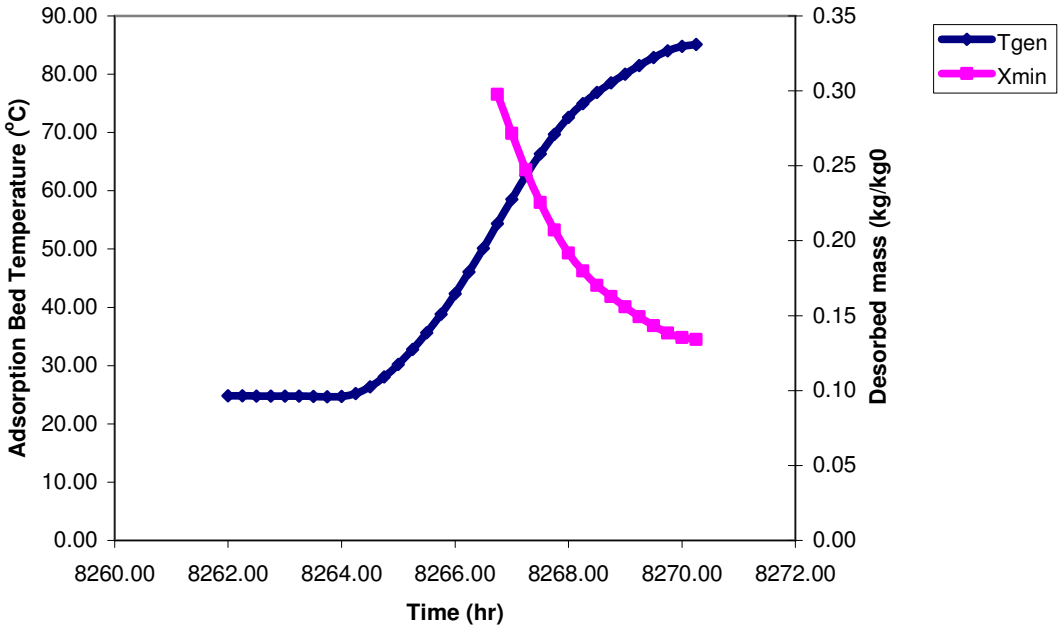


Fig.6.24: Variation of Adsorption Bed temperature and desorbed mass with Time (FPC Dec)

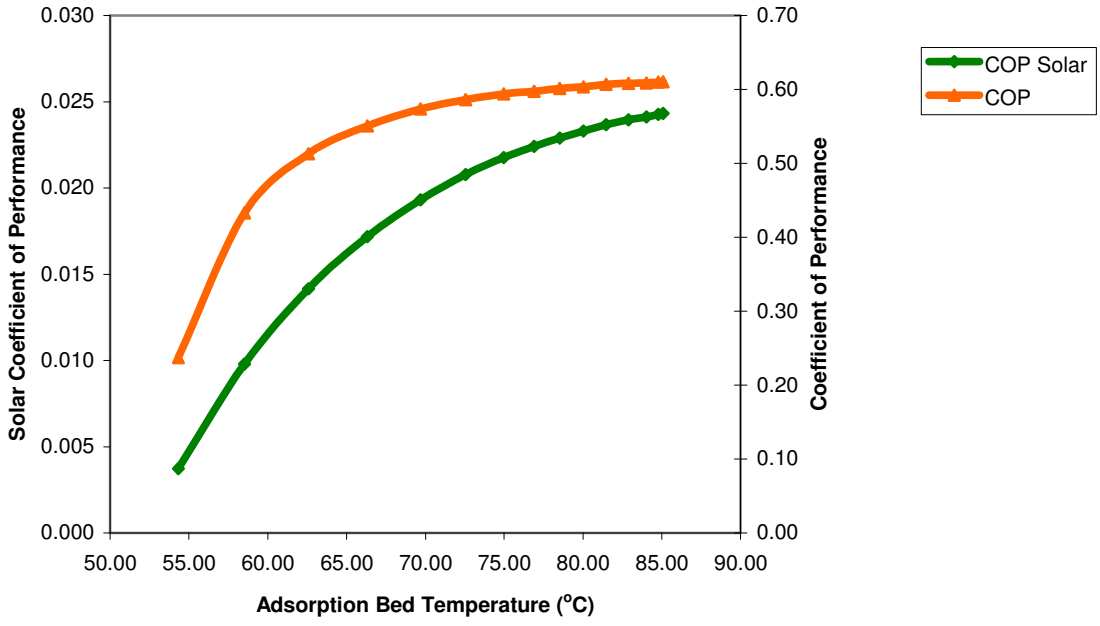


Fig.6.25: Effect of Adsorption Bed Temperature on Coefficient of Performance (FPC Dec)

6.2 ADSORPTION REFRIGERATION SYSTEM WITH ETC

Figure 6.26 below shows the schematics of an ETC powered adsorption refrigeration system modeled in TRNSYS.

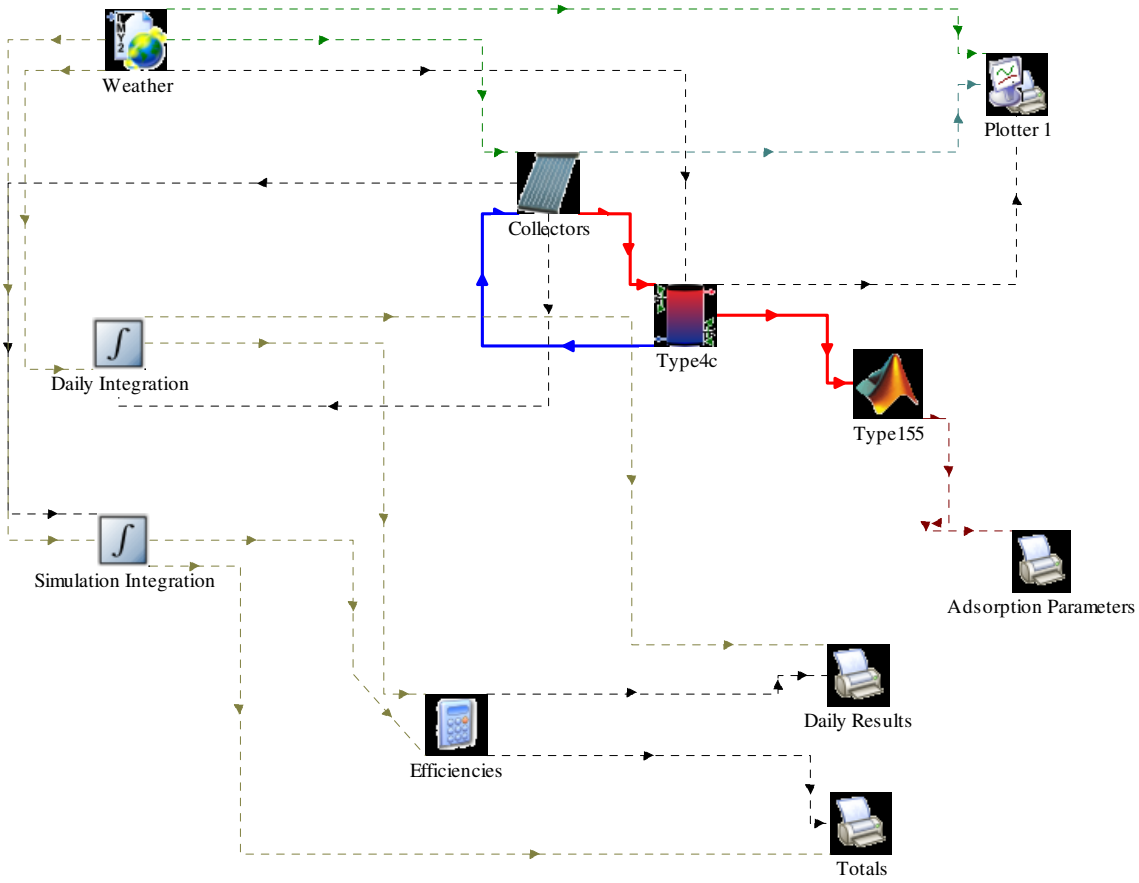


Fig. 6.26: Adsorption Refrigeration system simulation with Evacuated tube collector

The parameters in Tables 6.1 and 6.2 are also used for the simulation of the ETC powered system with the results presented in the figures below. The typical deck file for this simulation is presented in Appendix C.

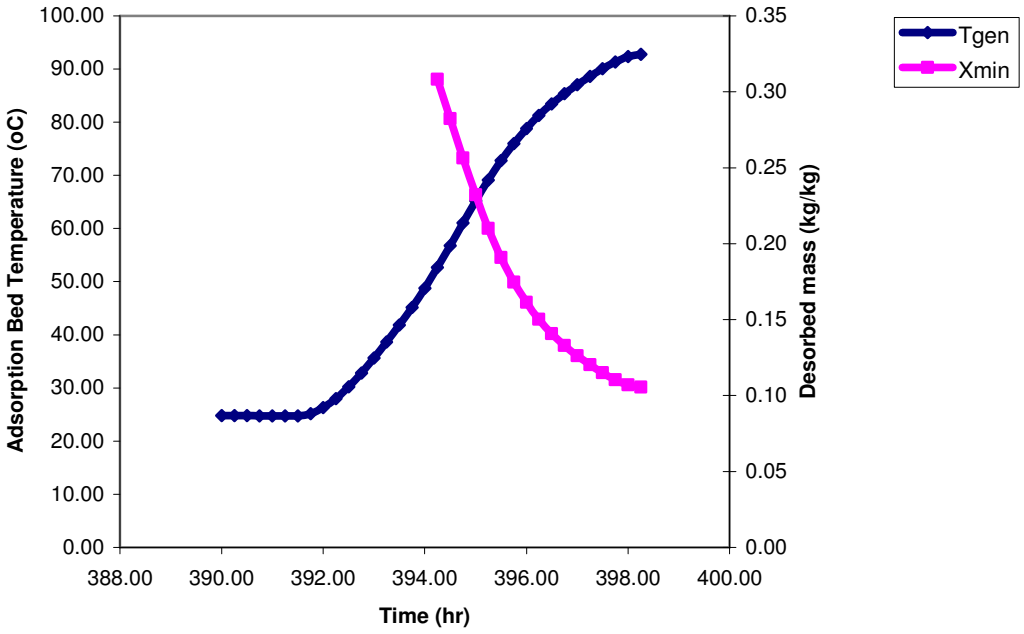


Fig.6.27: Variation of Adsorption Bed Temperature and Desorbed mass with Time (ETC Jan)

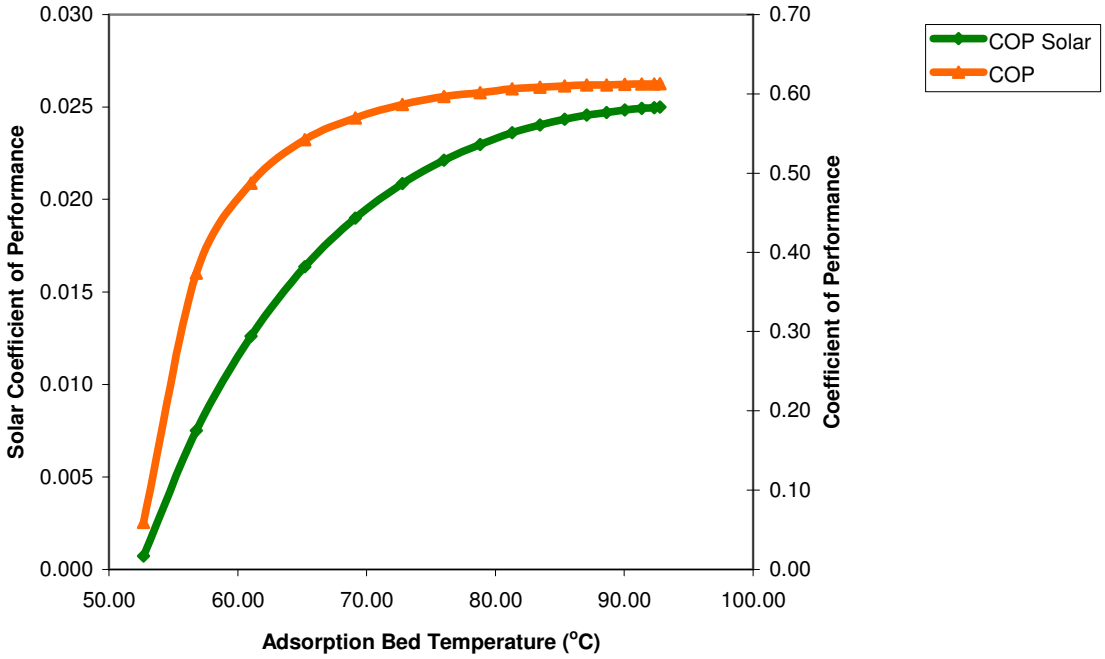


Fig.6.28: Effect of Adsorption Bed Temperature on Coefficient of Performance (ETC Jan)

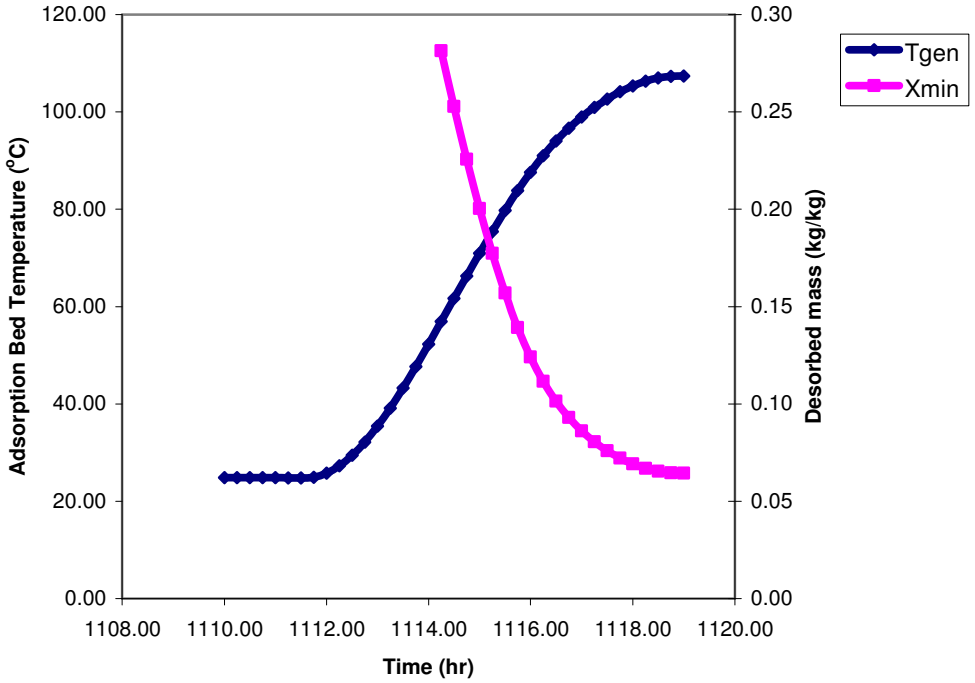


Fig.6.29: Variation of Adsorption Bed Temperature and Desorbed mass with Time (ETC Feb)

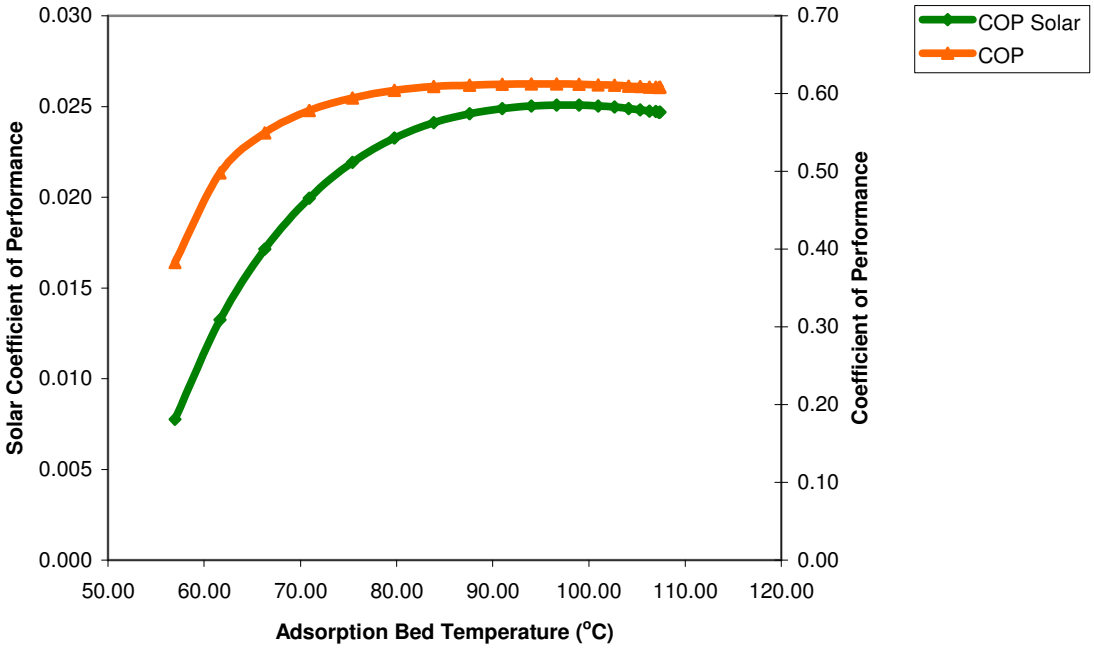


Fig.6.30: Effect of Adsorption Bed Temperature on Coefficient of Performance (ETC Feb)

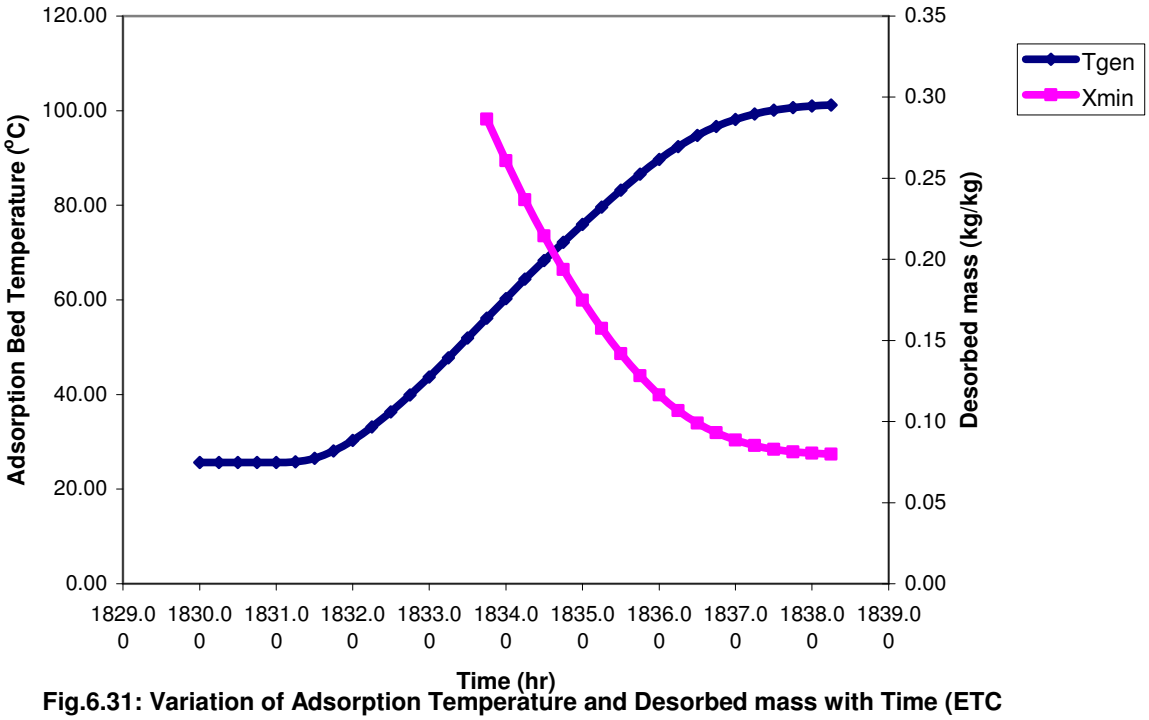


Fig.6.31: Variation of Adsorption Temperature and Desorbed mass with Time (ETC Mar)

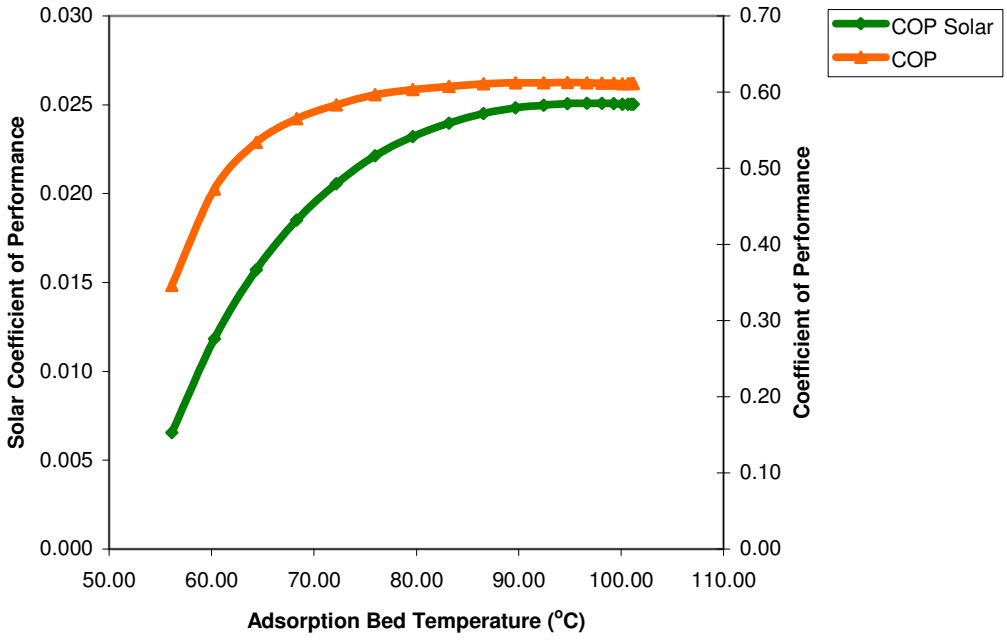


Fig.6.32: Effect of Adsorption Bed Temperature on Coefficient of Performance (ETC Mar)

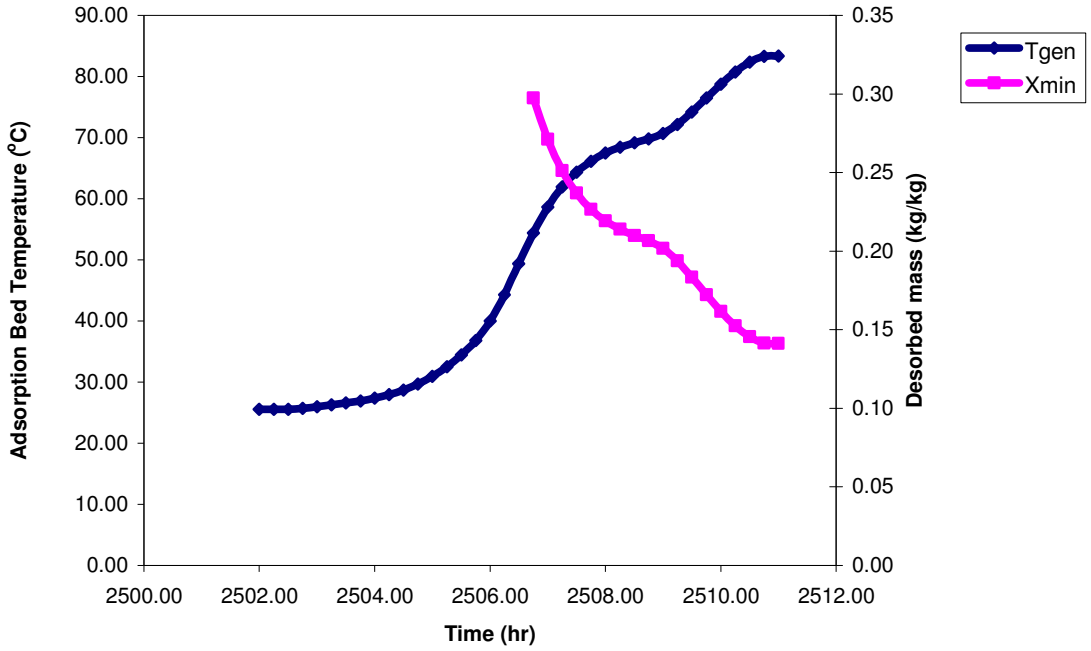


Fig.6.33: Variation of Adsorption Bed Temperature and Desorbed mass with Time (ETC Apr)

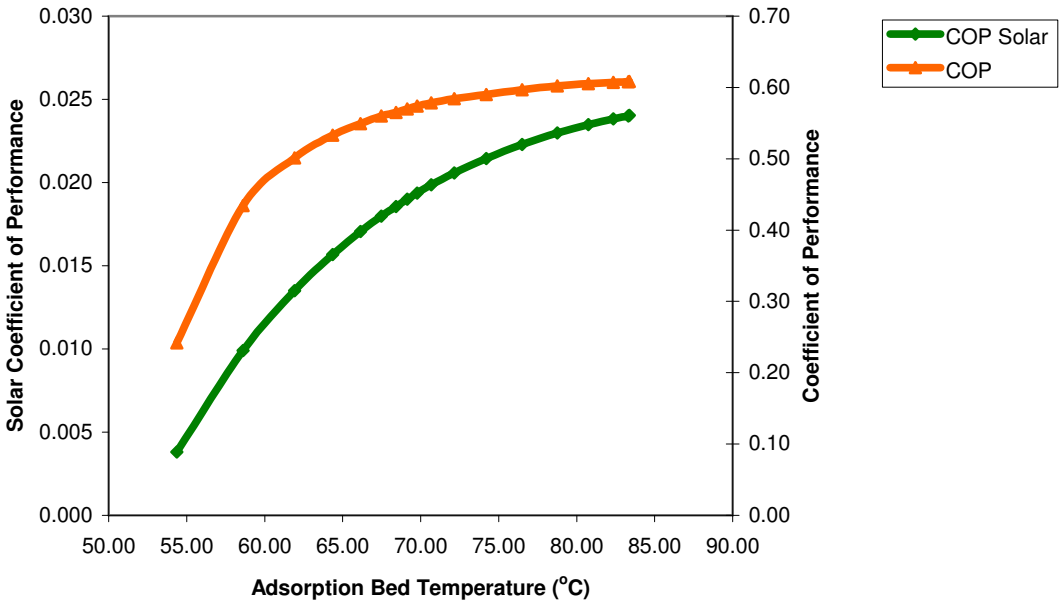


Fig.6.34: Effect of Adsorption Bed Temperature on Coefficient of Performance (ETC Apr)

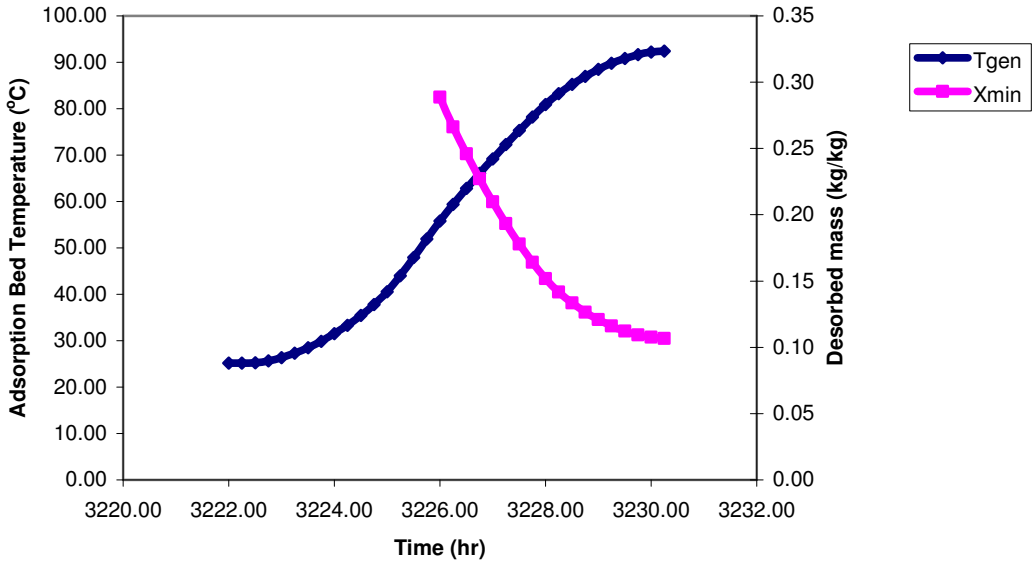


Fig.6.35: Variation of Adsorption Bed Temperature and Desorbed mass with Time (ETC May)

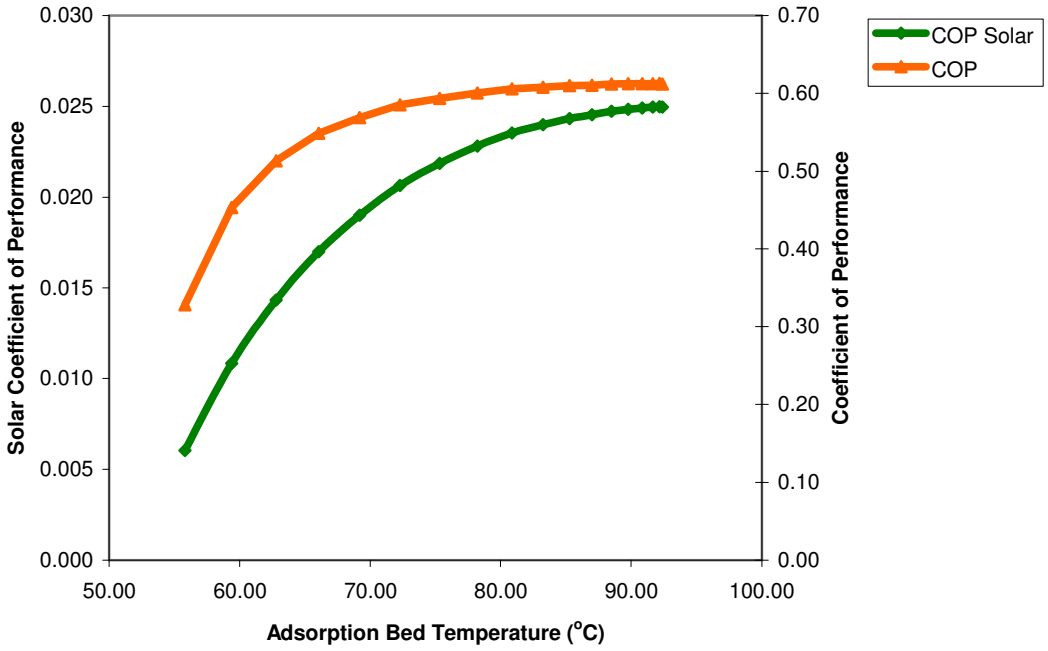


Fig.6.36: Effect of Adsorption Bed Temperature on Coefficient of Performance (ETC May)

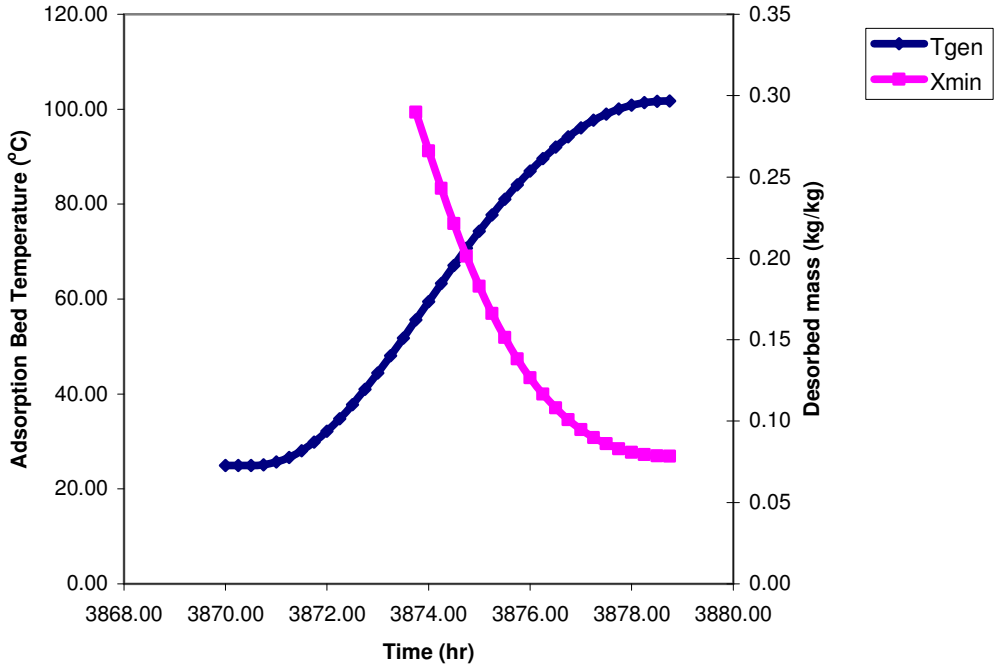


Fig.6.37: Variation of Adsorption Bed Temperature and Desorbed mass with Time (ETC Jun)

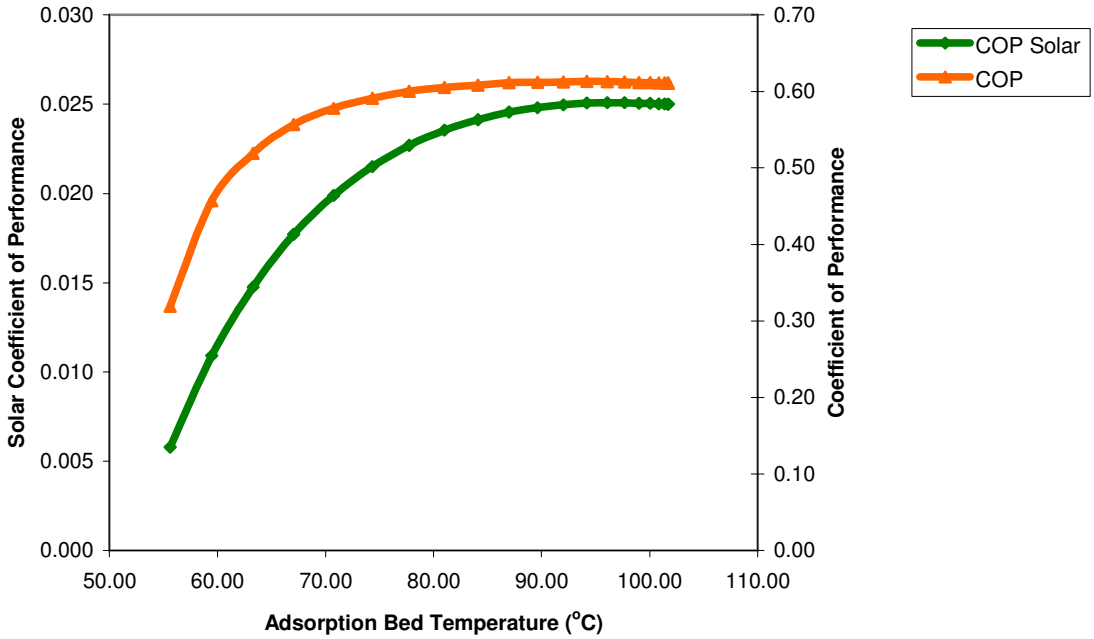


Fig.6.38: Effect of Adsorption Bed Temperature on Coefficient of Performance (ETC Jun)

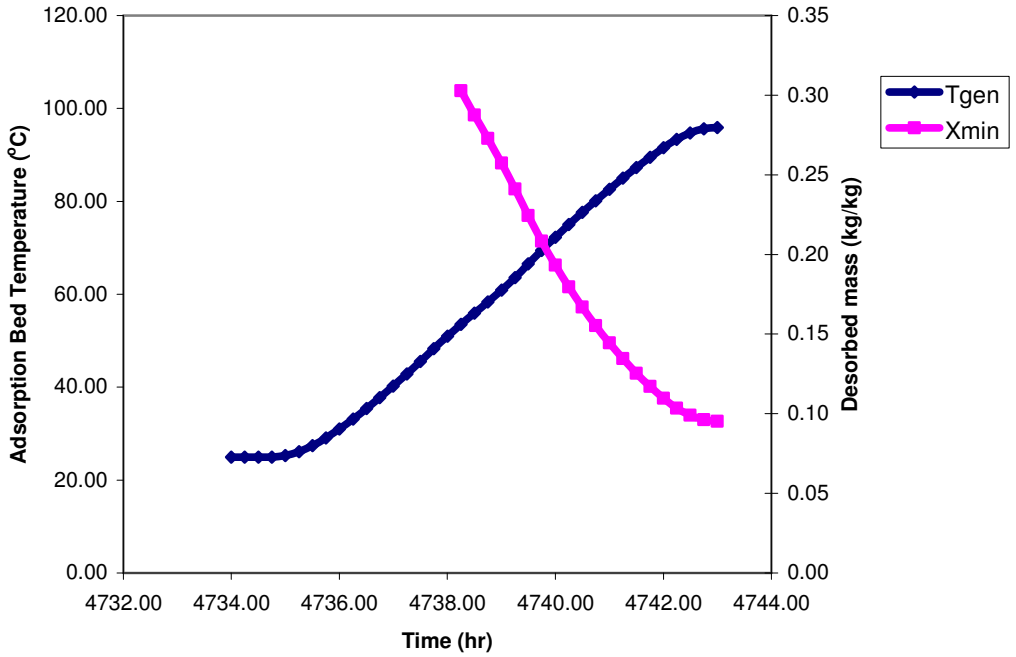


Fig.6.39: Variation of Adsorption Bed Temperature and Desorbed mass with Time (ETC Jul)

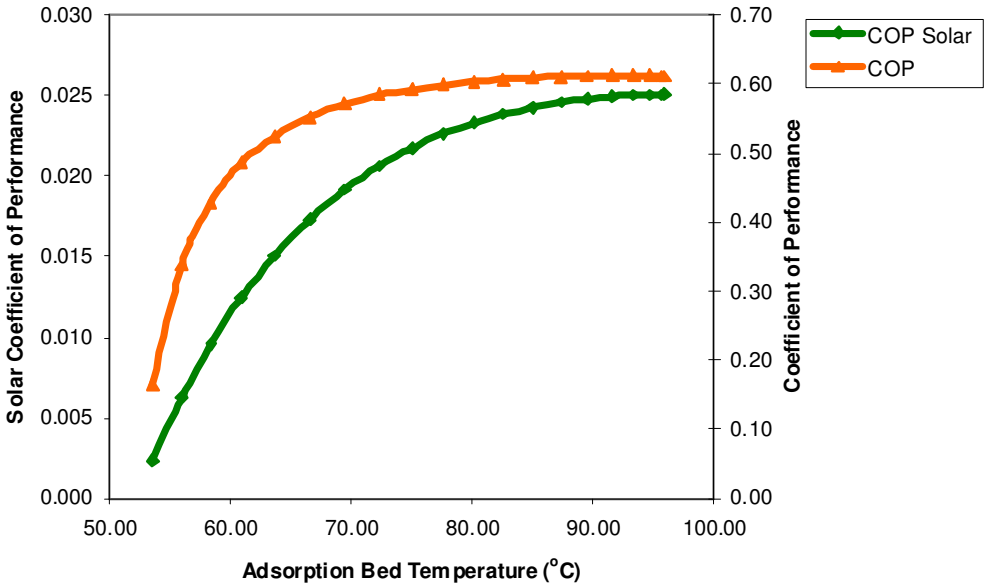


Fig.6.40: Effect of Adsorption Bed Temperature on Coefficient of Performance (ETC Jul)

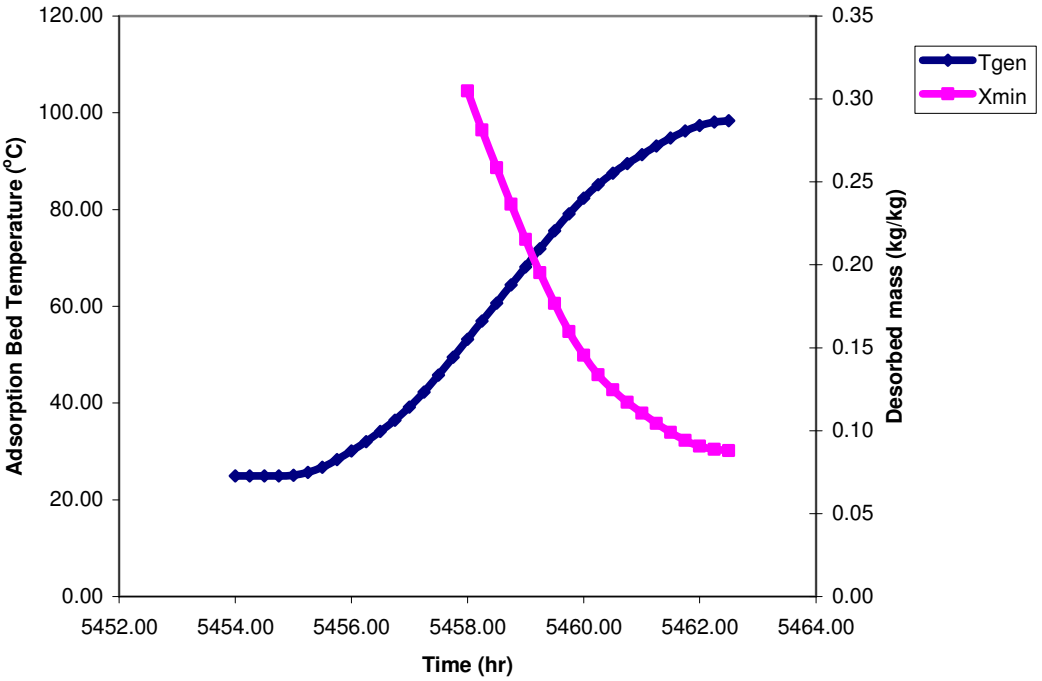


Fig.6.41: Variation of Adsorption Bed Temperature and Desobed mass with Time (ETC Aug)

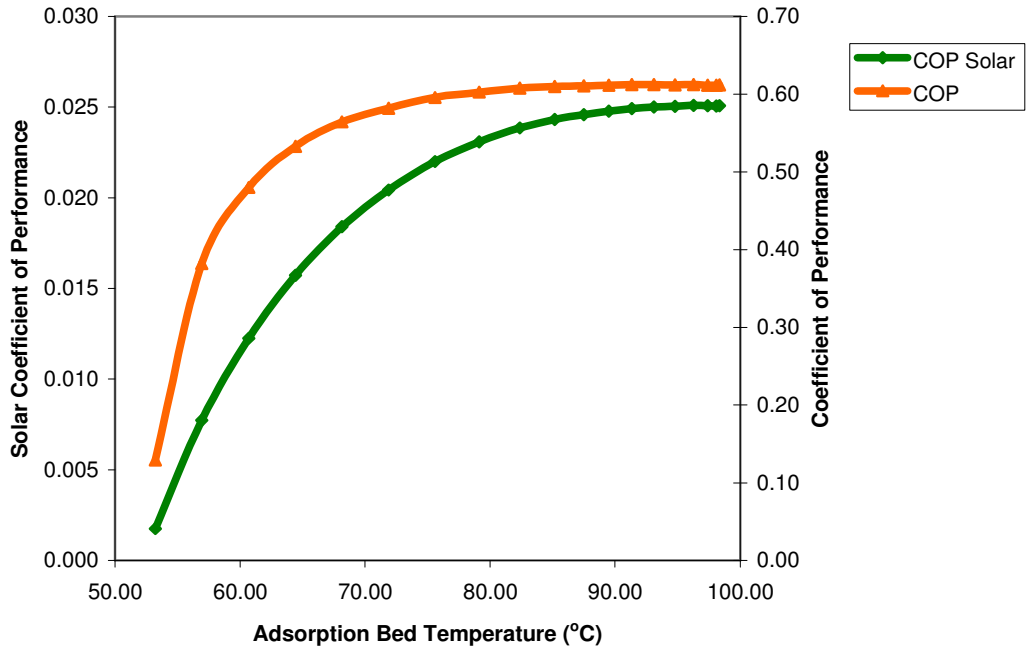


Fig.6.42: Effect of Adsorption Bed Temperature on Coefficient of Performance (ETC Aug)

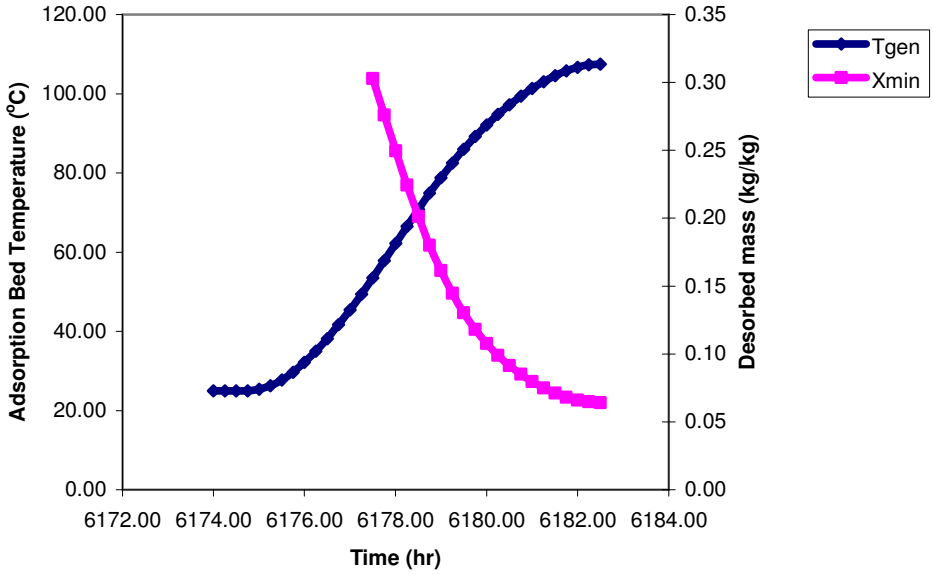


Fig.6.43: Variation of Adsorption Bed Temperature and Desorbed mass with Time (ETC Sep)

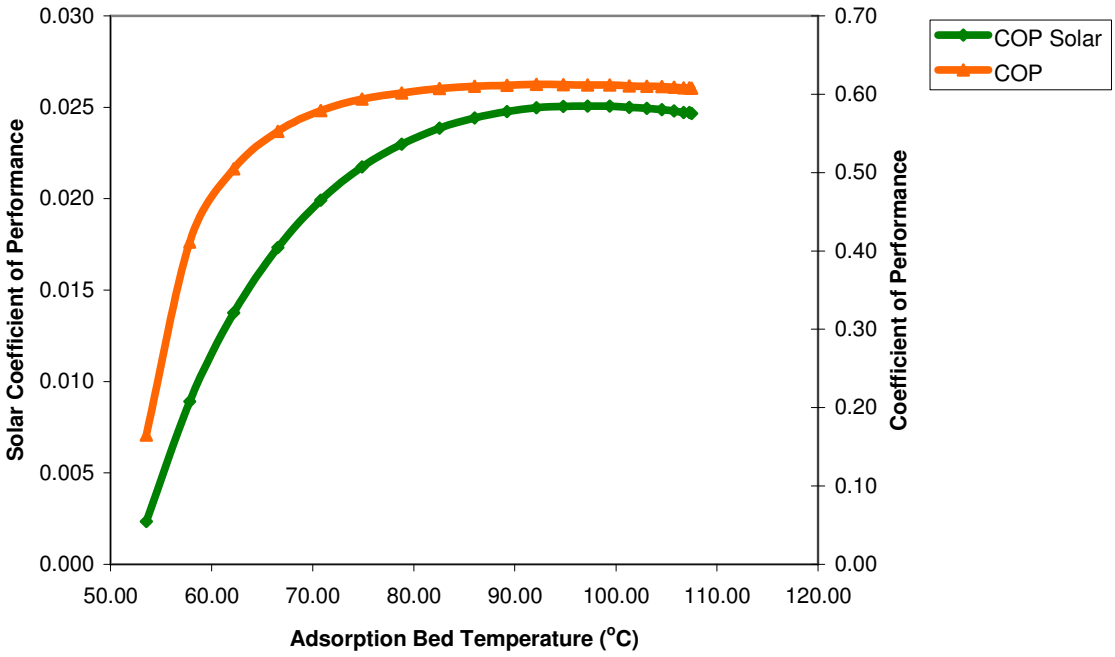


Fig.6.44: Effect of Adsorption Bed Temperature on Coefficient of Performance (ETC Sep)

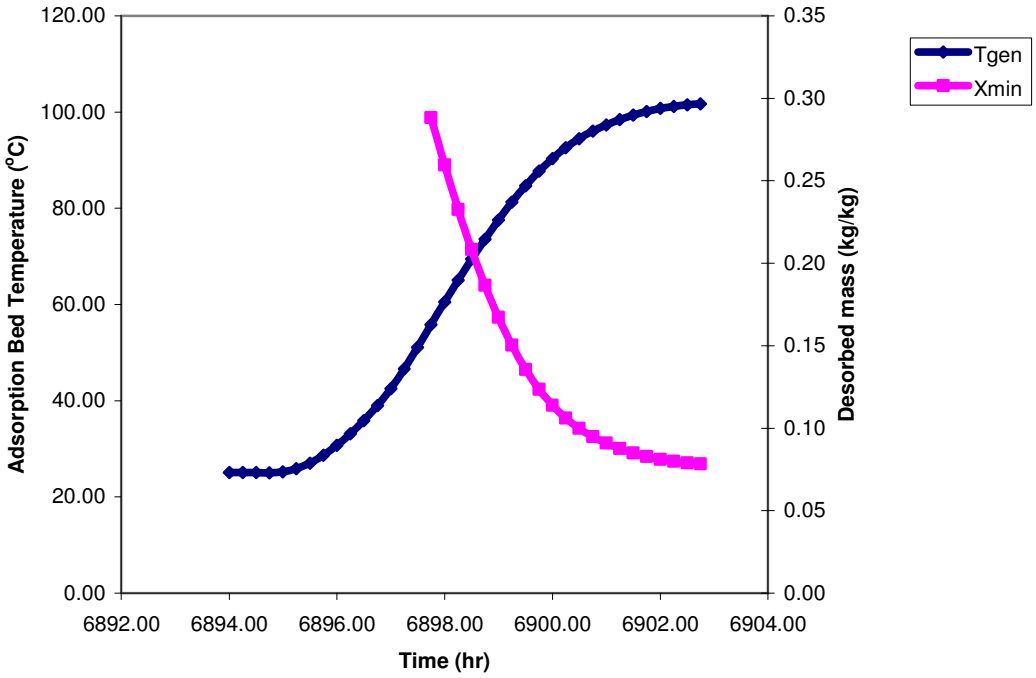


Fig.6.45: Variation of Adsorption Bed Temperature and Desorbed mass with Time (ETC Oct)

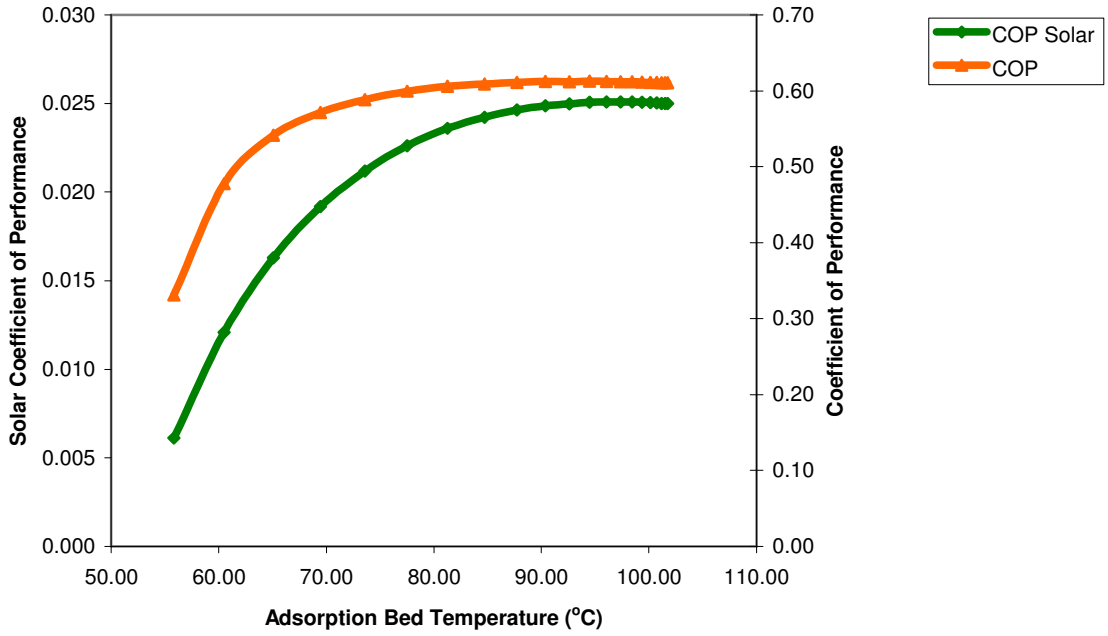


Fig.6.46: Effect of Adsorption Bed Temperature on Coefficient of Performance (ETC Oct)

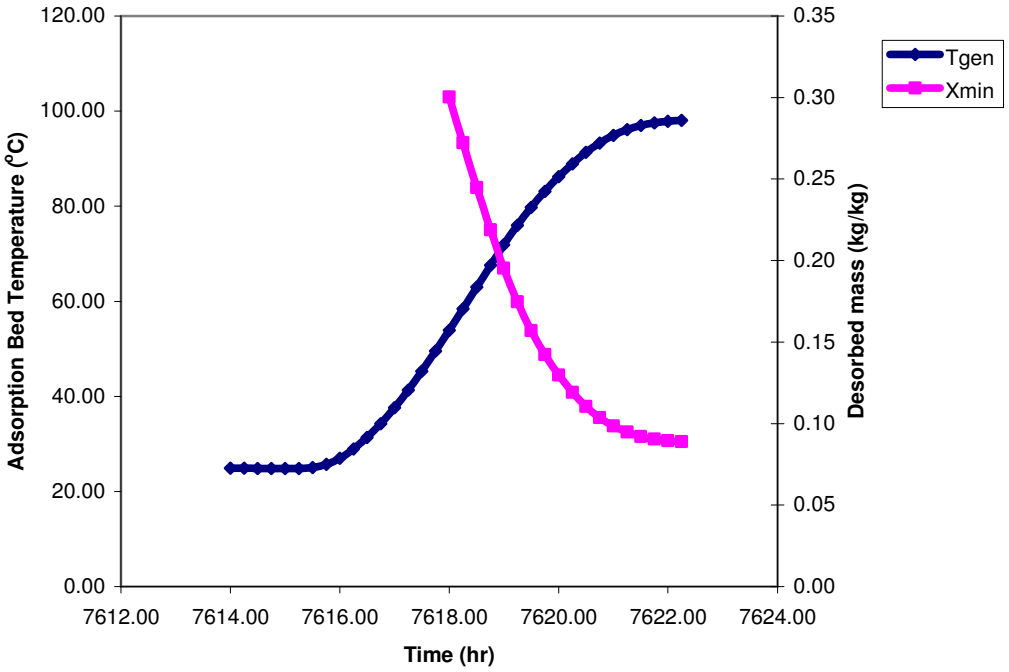


Fig.6.47: Variation of Adsorption Bed Temperature and Desorbed mass with Time (ETC Nov)

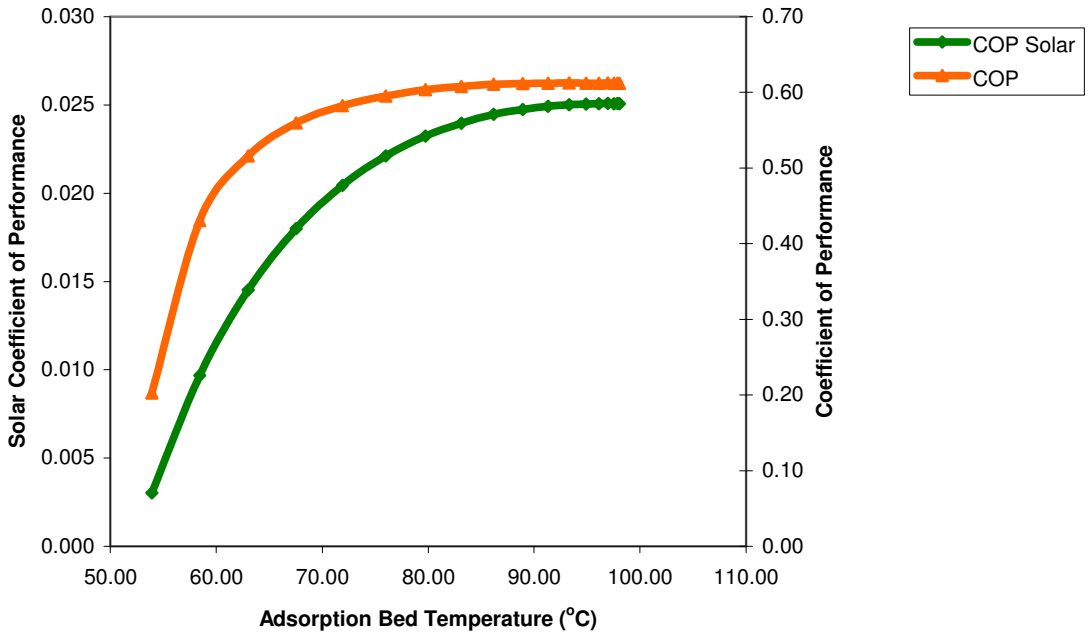


Fig.6.48: Effect of Adsorption Bed Temperature on Coefficient of Performance (ETC Nov)

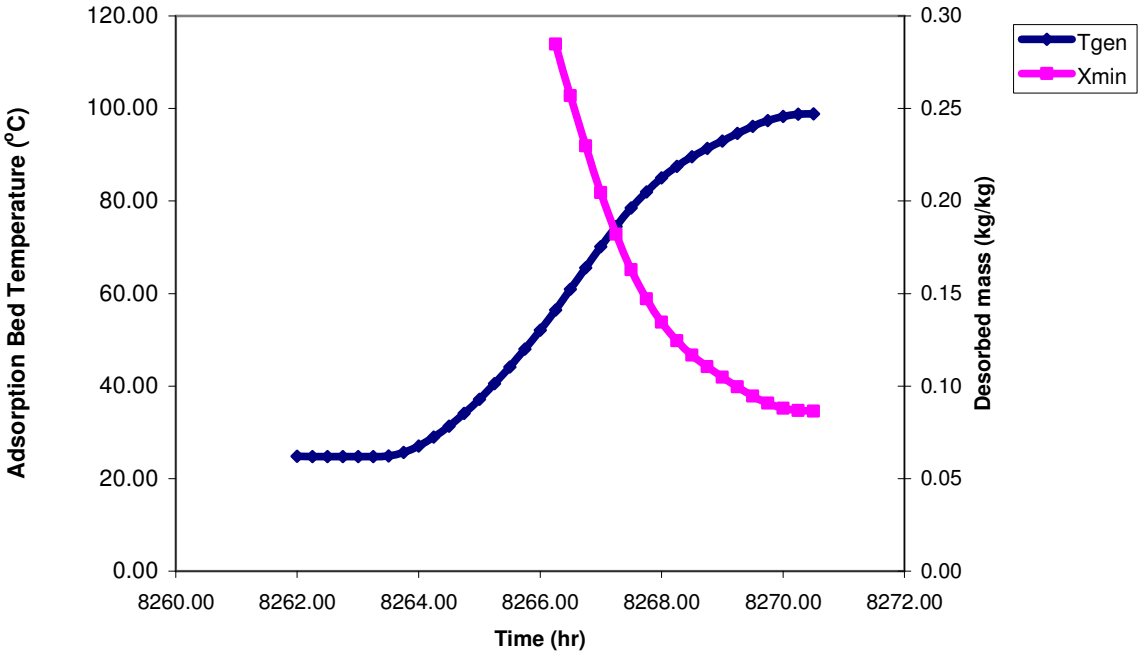


Fig.6.49: Variation of Adsorption Bed Temperature and Desorbed mass with Time (ETC Dec)

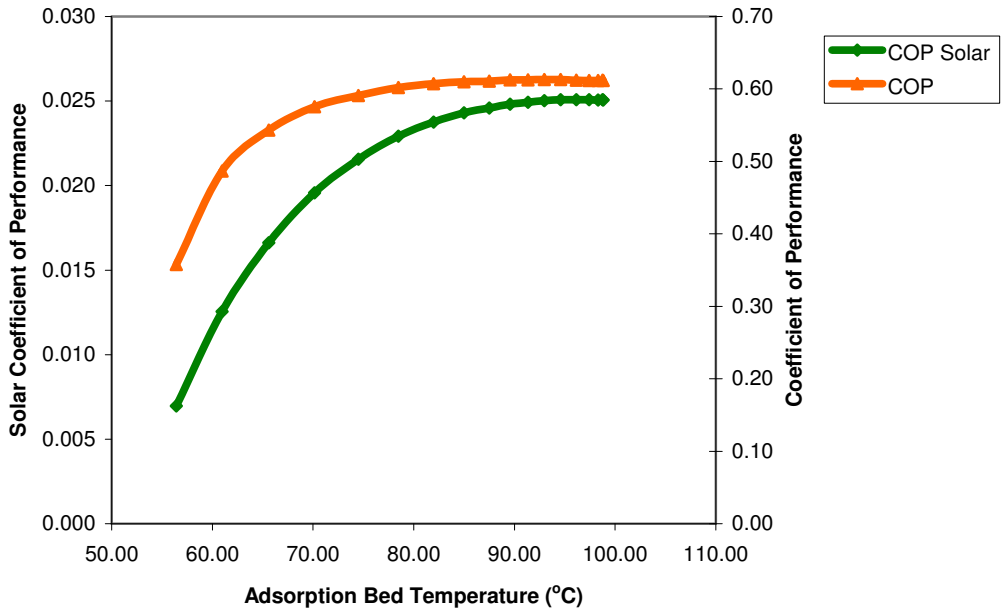


Fig.6.50: Effect of Adsorption Bed Temperature on Coefficient of Performance (ETC Dec)

6.3 ADSORPTION REFRIGERATION SYSTEM WITH PTC

The PTC powered adsorption refrigeration system simulated in TRNSYS is shown in Fig.6.51 below. The simulation parameters listed in Tables 6.1 and 6.2 are utilized in the simulation of the system with the main performance evaluation parameters presented in the figures 6.52 to 6.75 and the deck file generated shown in Appendix D.

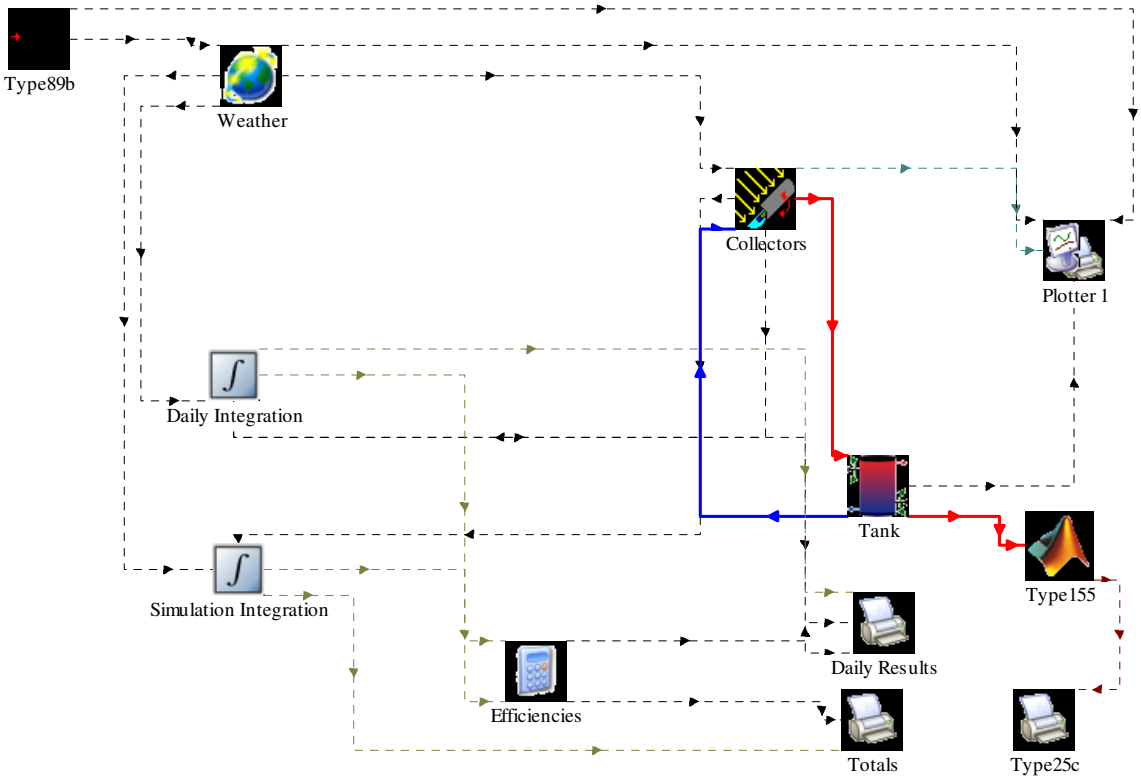


Fig. 6.51: Adsorption Refrigeration system simulation with Parabolic Trough collector

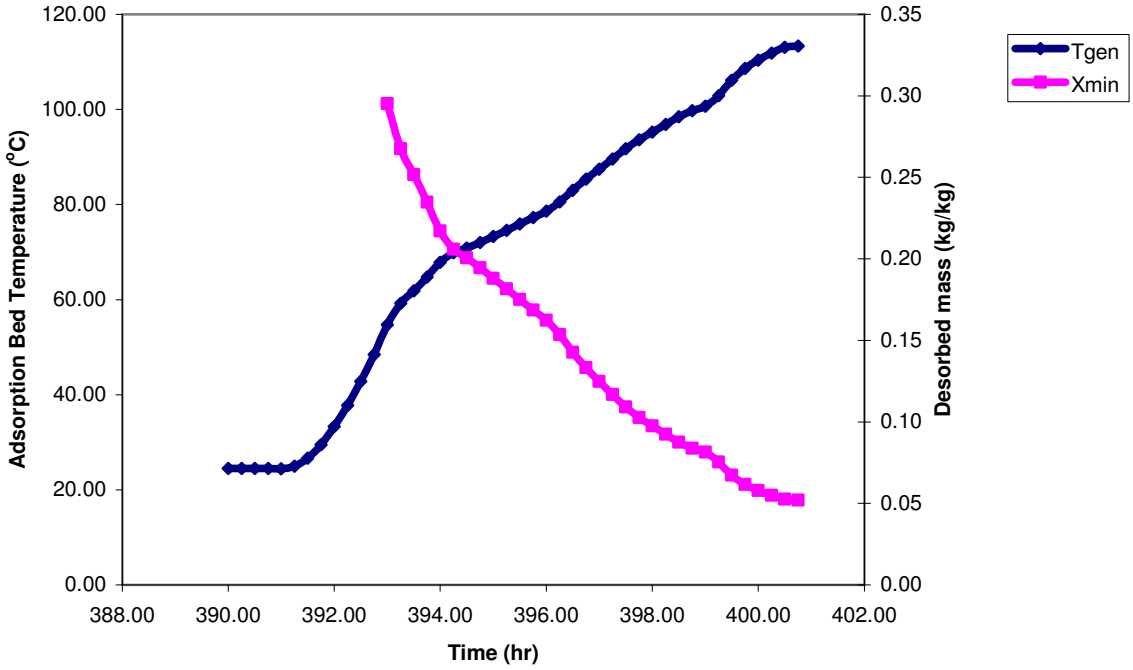


Fig.6.52: Variation of adsorption Bed Temperature and desorbed mass with Time (PTC Jan)

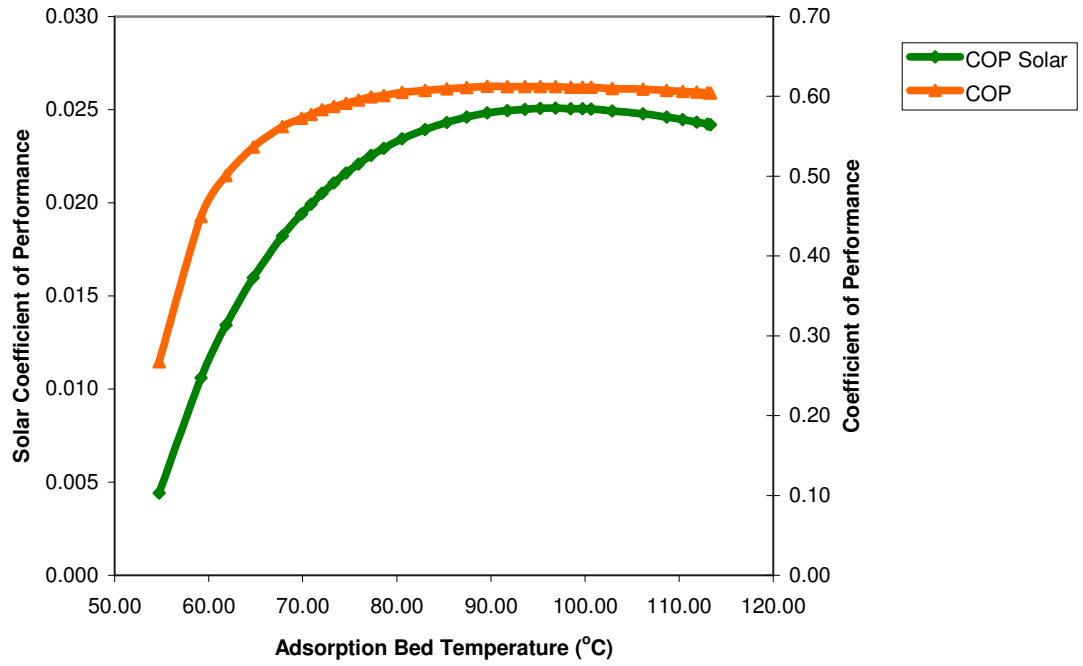


Fig.6.53: Effect of Adsorption Bed Temperature on Coefficient of Performance (PTC Jan)

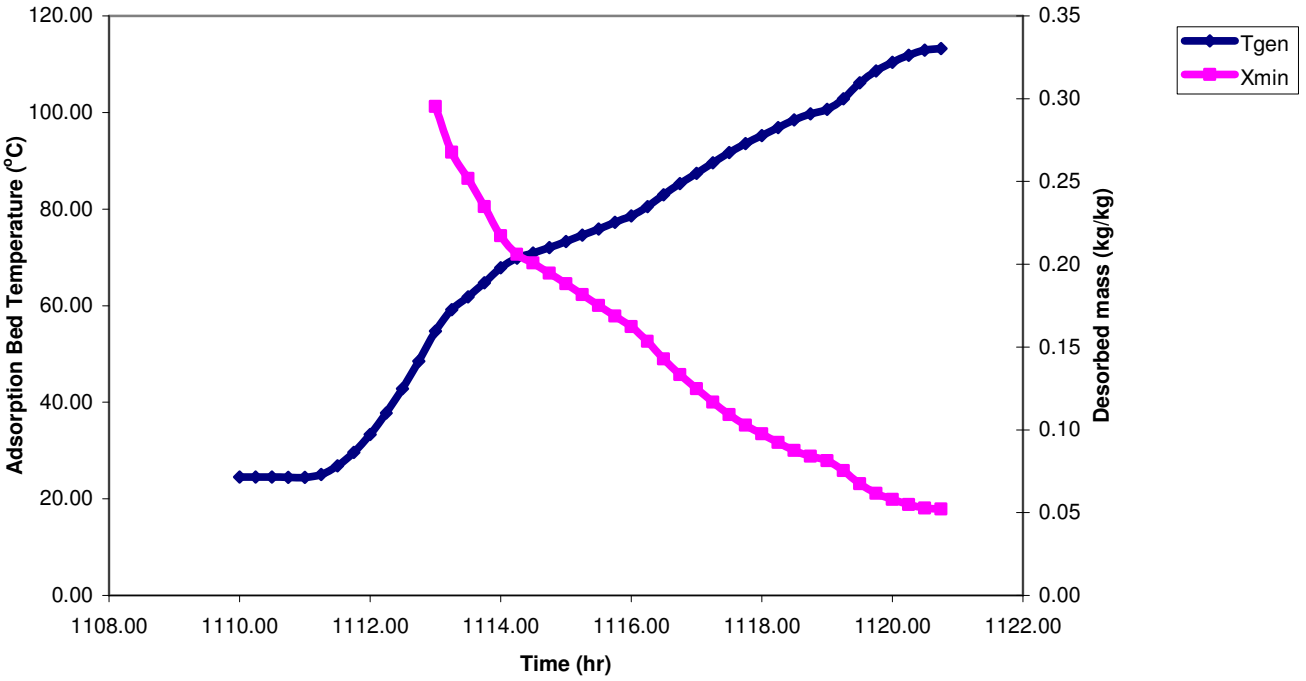


Fig.6.54: Variation of adsorption Bed Temperature and Desorbed mass with Time (PTC Feb)

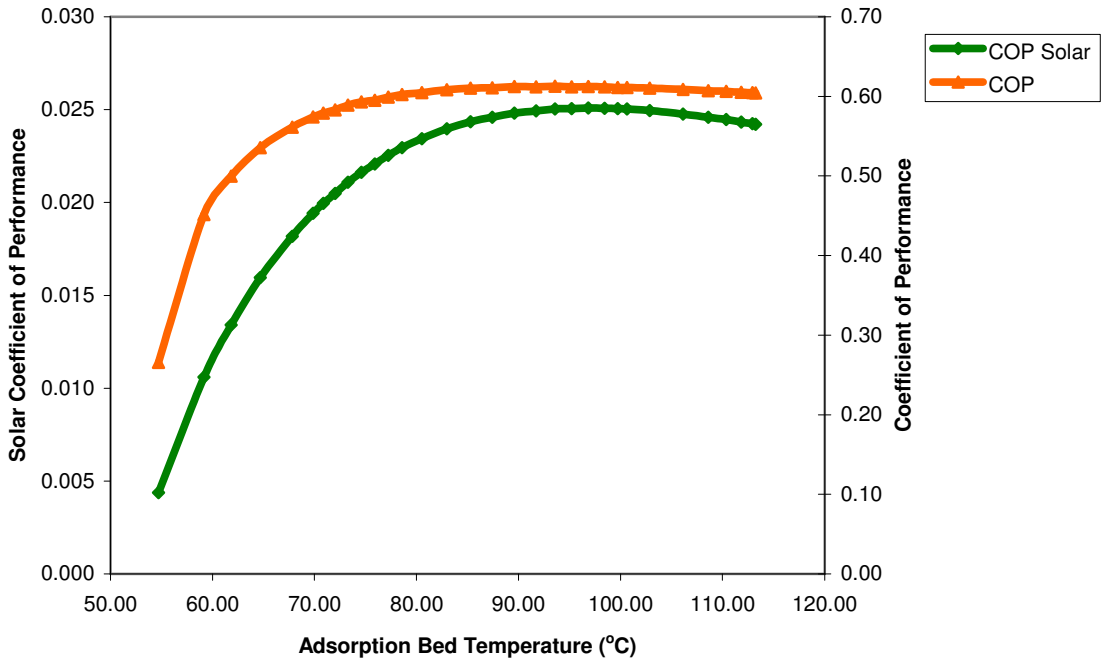


Fig.6.55: Effect of Adsorption Bed Temperature on Coefficient of Performance (PTC Feb)

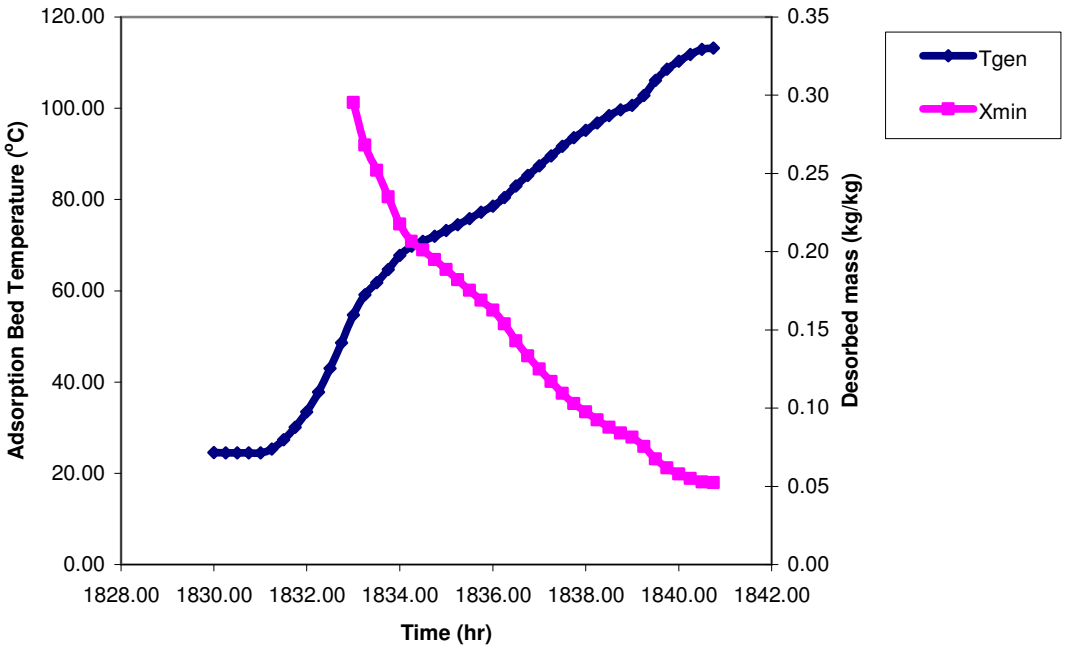


Fig.6.56: Variation of Adsorption Bed Temperature and Desorbed mass with Time (PTC Mar)

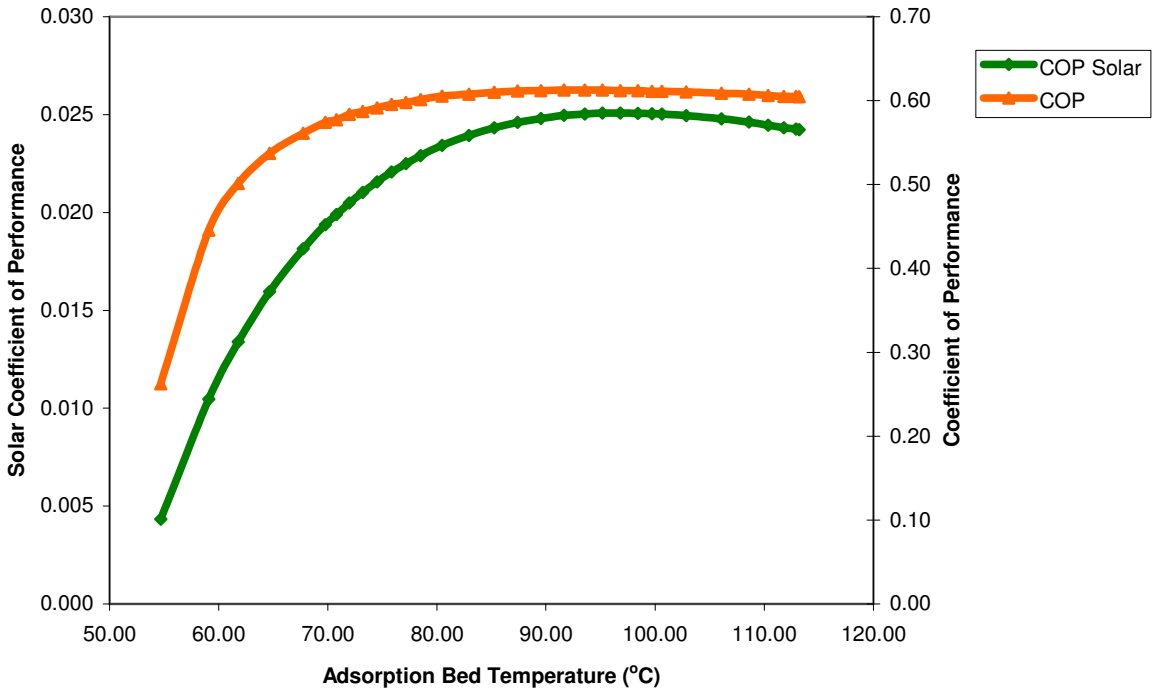


Fig.6.57: Effect of Adsorption Bed Temperature on Coefficient of Performance (PTC Mar)

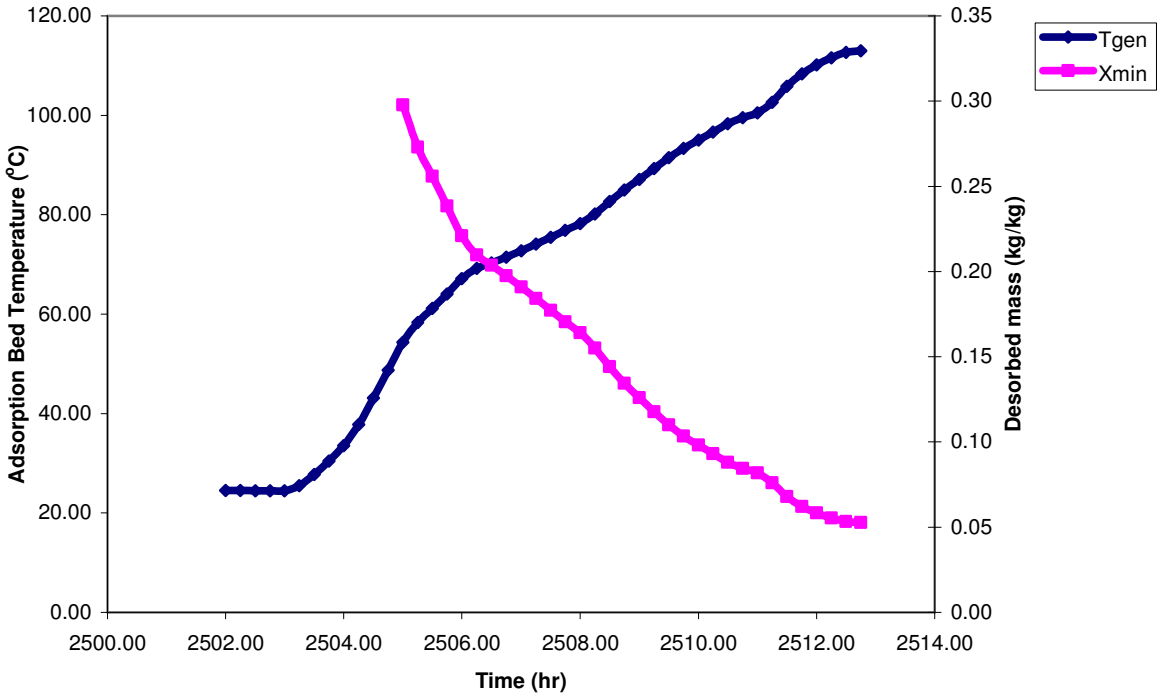


Fig.6.58: Variation of Adsorption Bed Temperature and Desorbed mass with Time (PTC Apr)

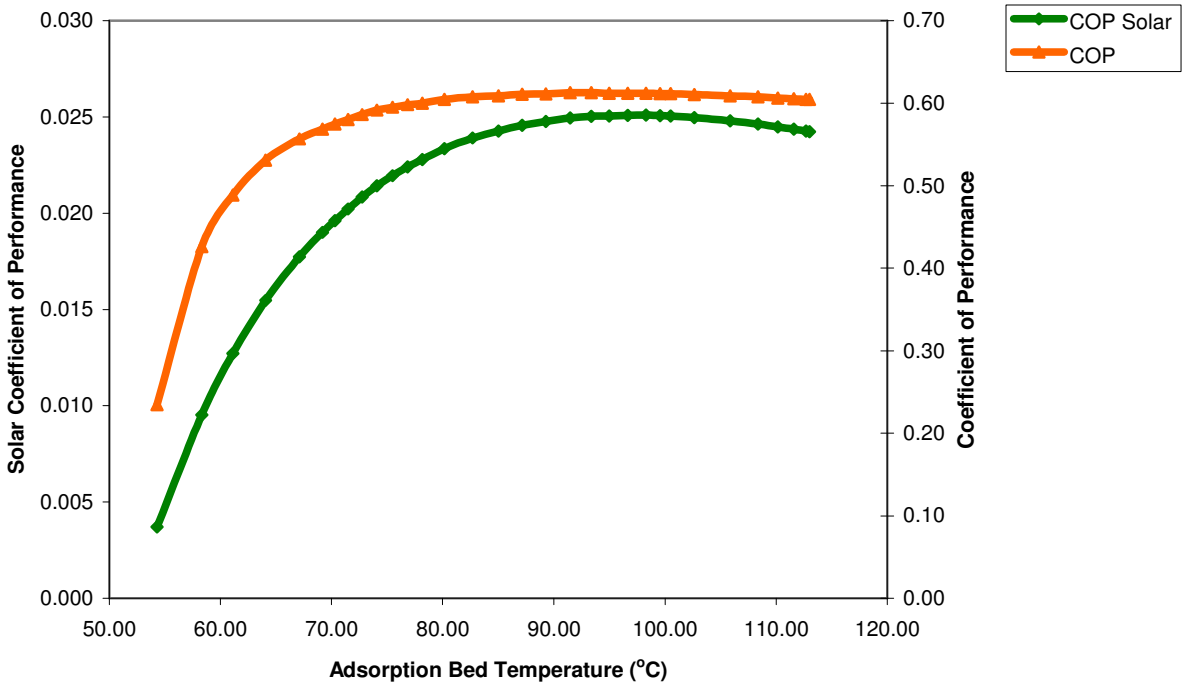


Fig.6.59: Effect of Adsorption Bed Temperature on Coefficient of Performance (PTC Apr)

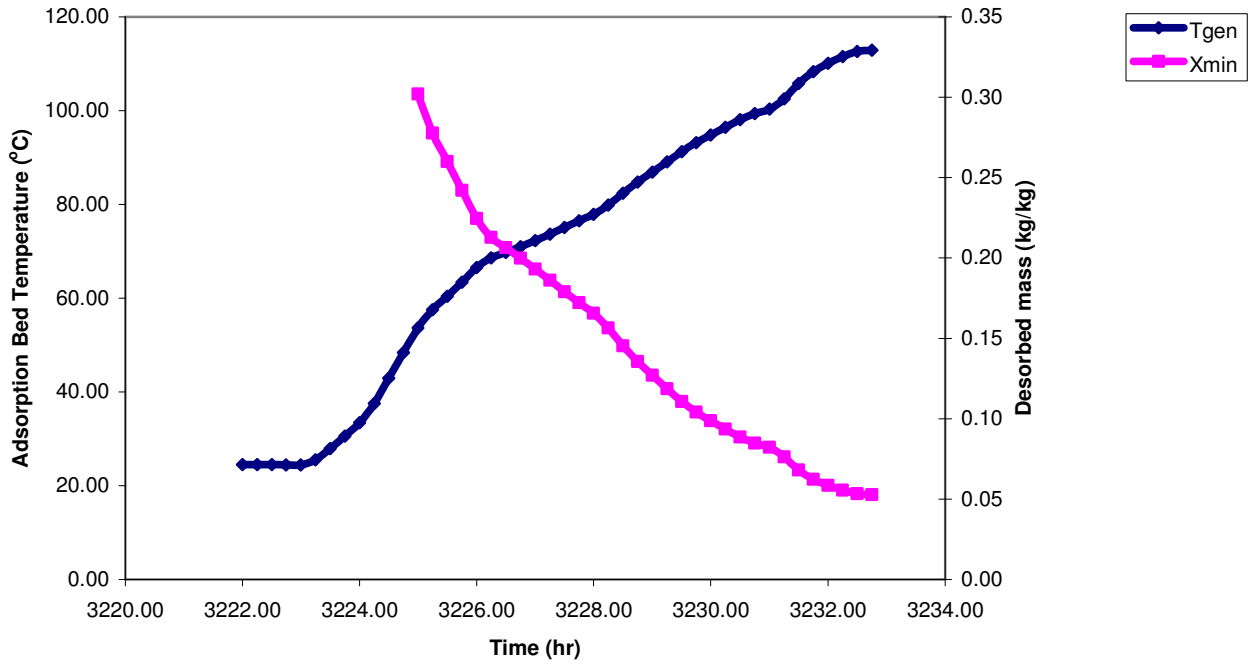


Fig.6.60: Variation of Adsorption Bed Temperature and Desorbed mass with Time (PTC May)

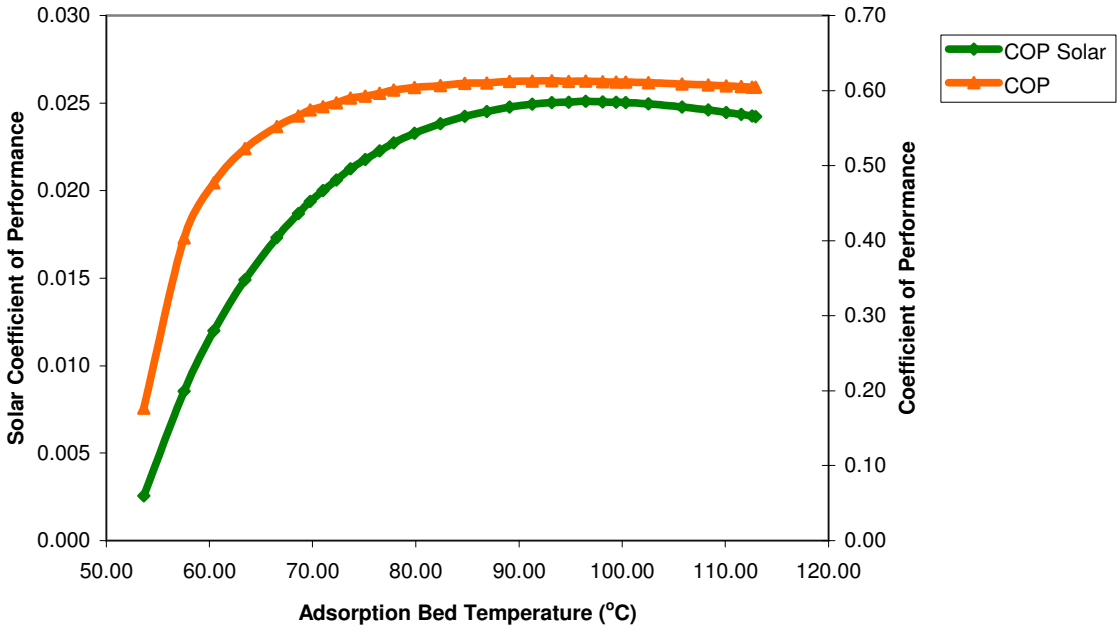


Fig.6.61: Effect of Adsorption Bed Temperature on Coefficient of Performance (PTC May)

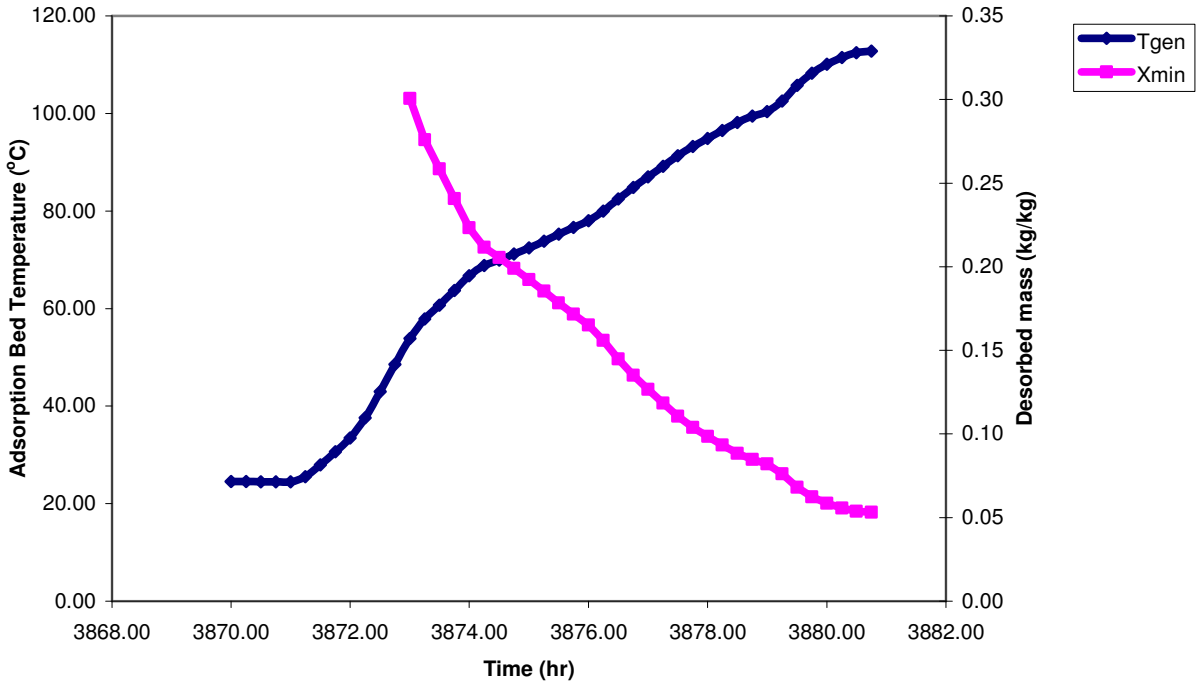


Fig.6.62: Variation of Adsorption Bed Temperature and Desorbed mass with Time (PTC Jun)

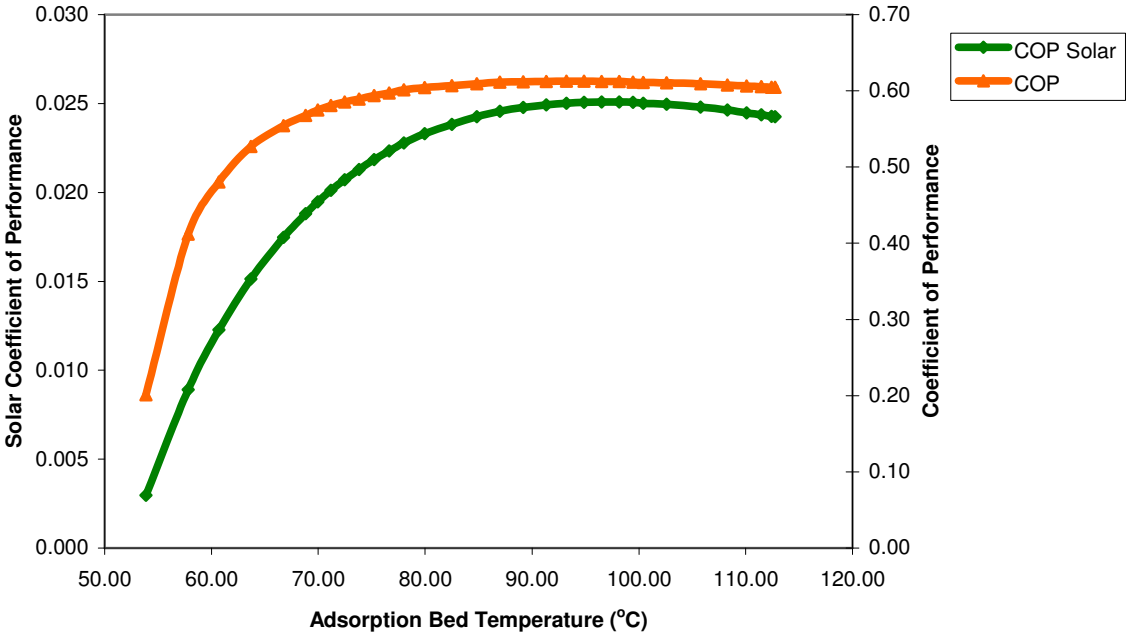


Fig.6.63: Effect of Adsorption Bed Temperature on Coefficient of Performance (PTC Jun)

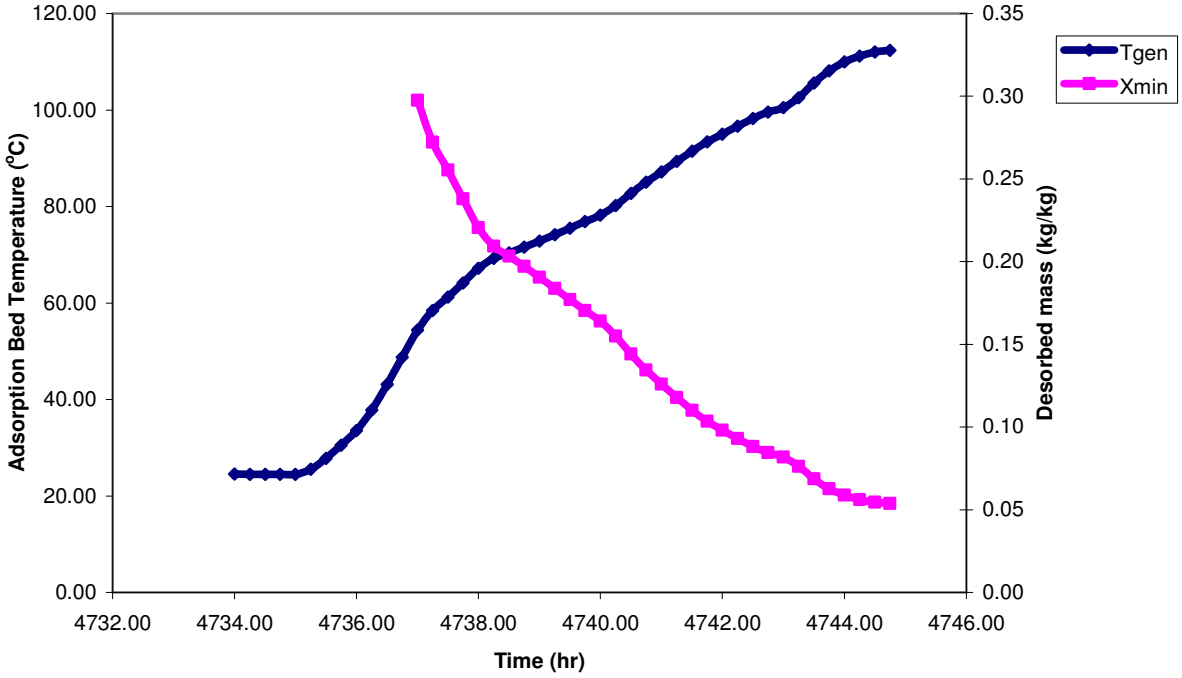


Fig.6.64: Variation of Adsorption Bed Temperature and Desorbed mass with Time (PTC Jul)

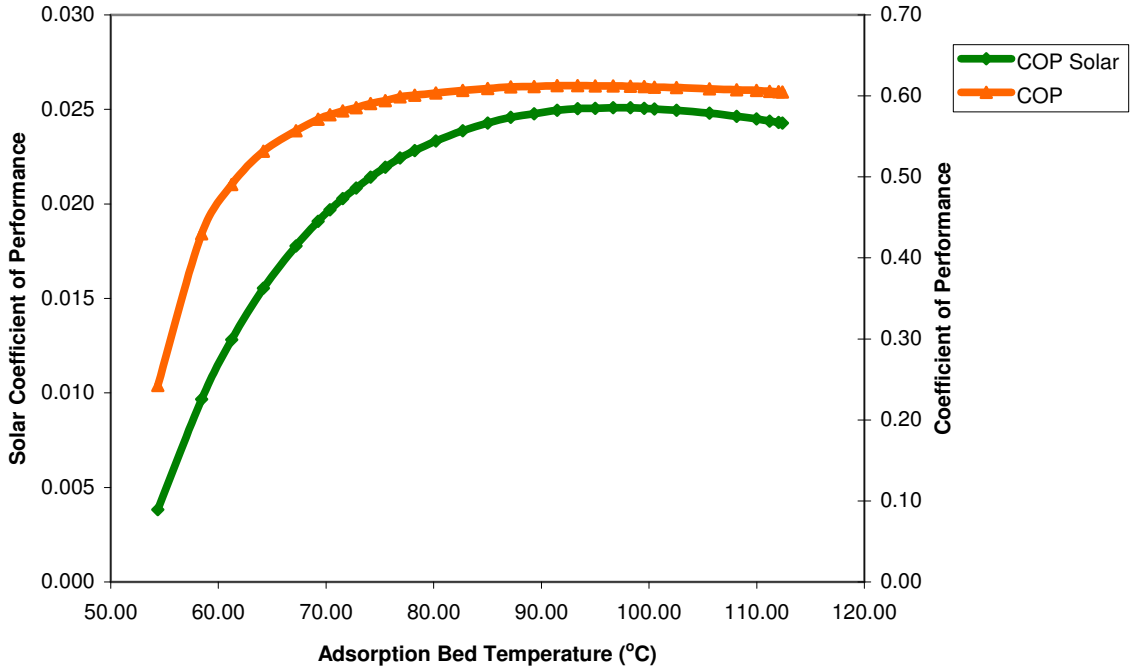


Fig.6.65: Effect of Adsorption Bed Temperature on Coefficient of Performance (PTC Jul)

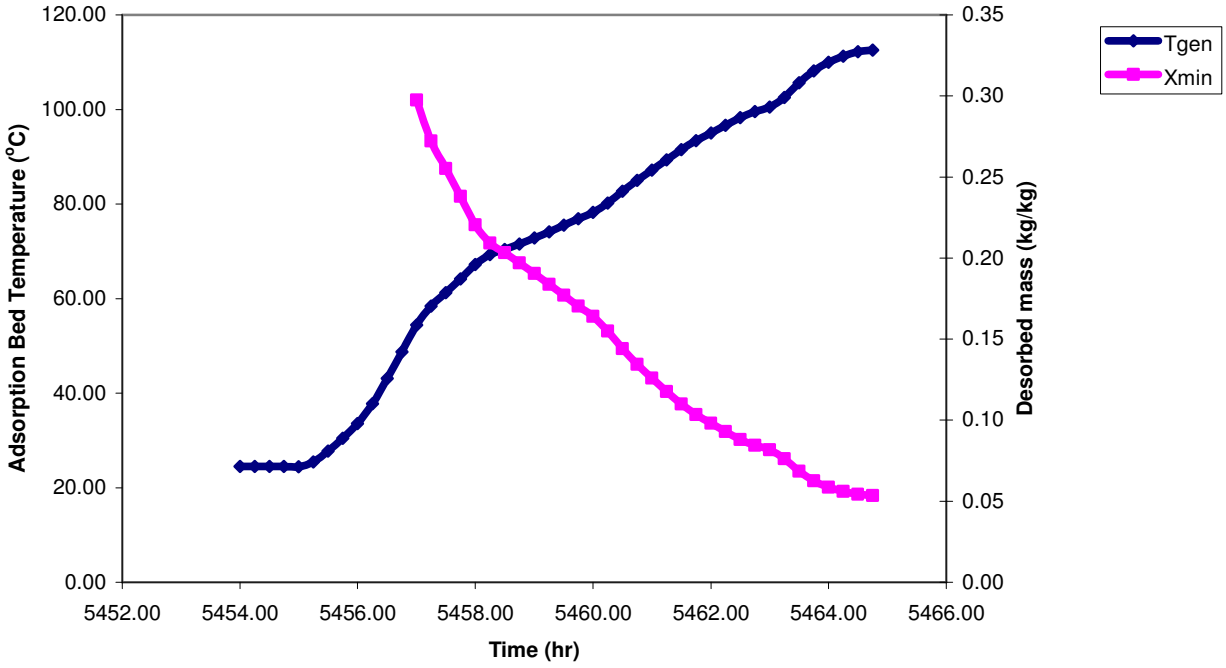


Fig.6.66: Variation of Adsorption Bed Temperature and Desorbed mass with Time (PTC Aug)

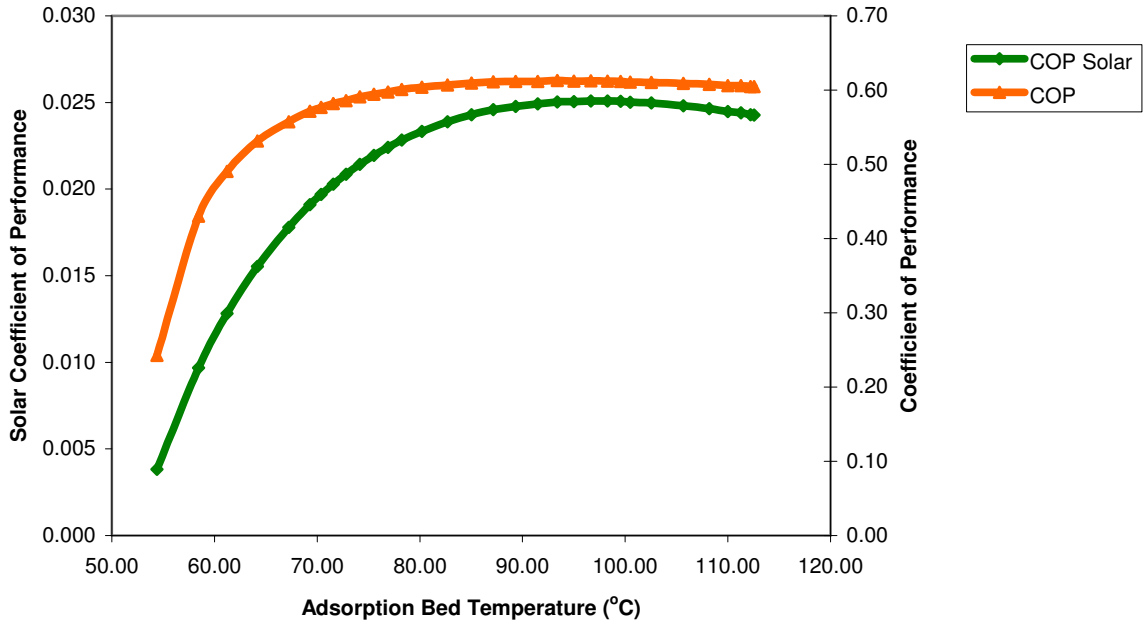


Fig.6.67: Effect of Adsorption Bed Temperature on Coefficient of Performance (PTC Aug)

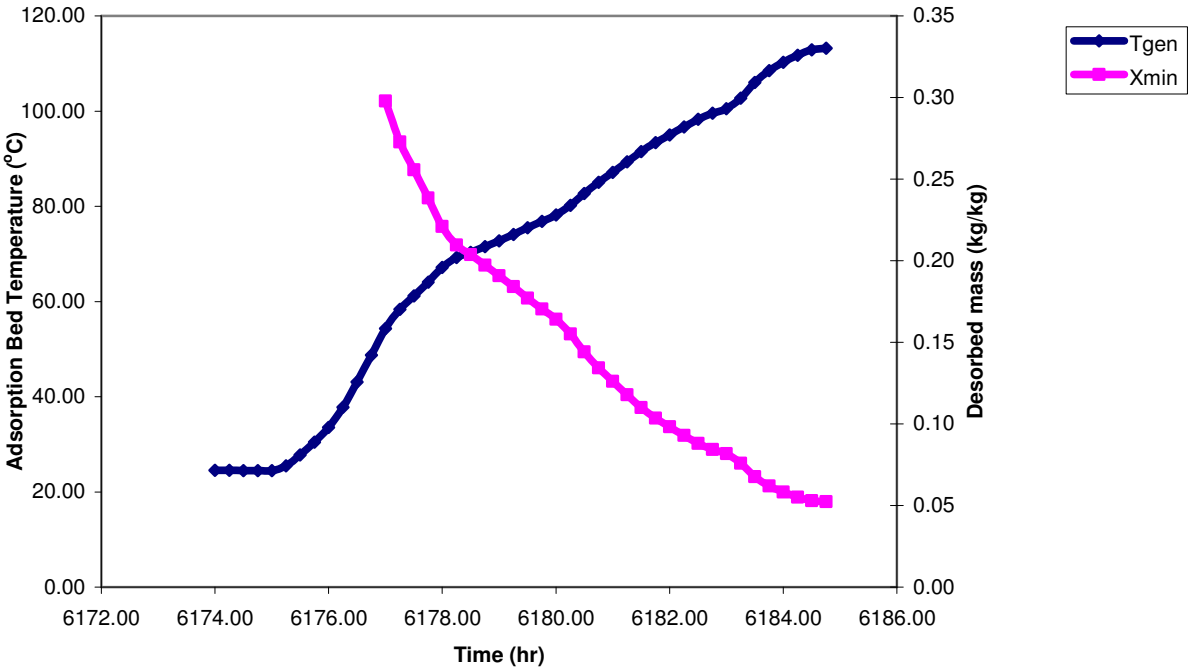


Fig.6.68: Variation of Adsorption Bed Temperature and Desorbed mass with Time (PTC Sep)

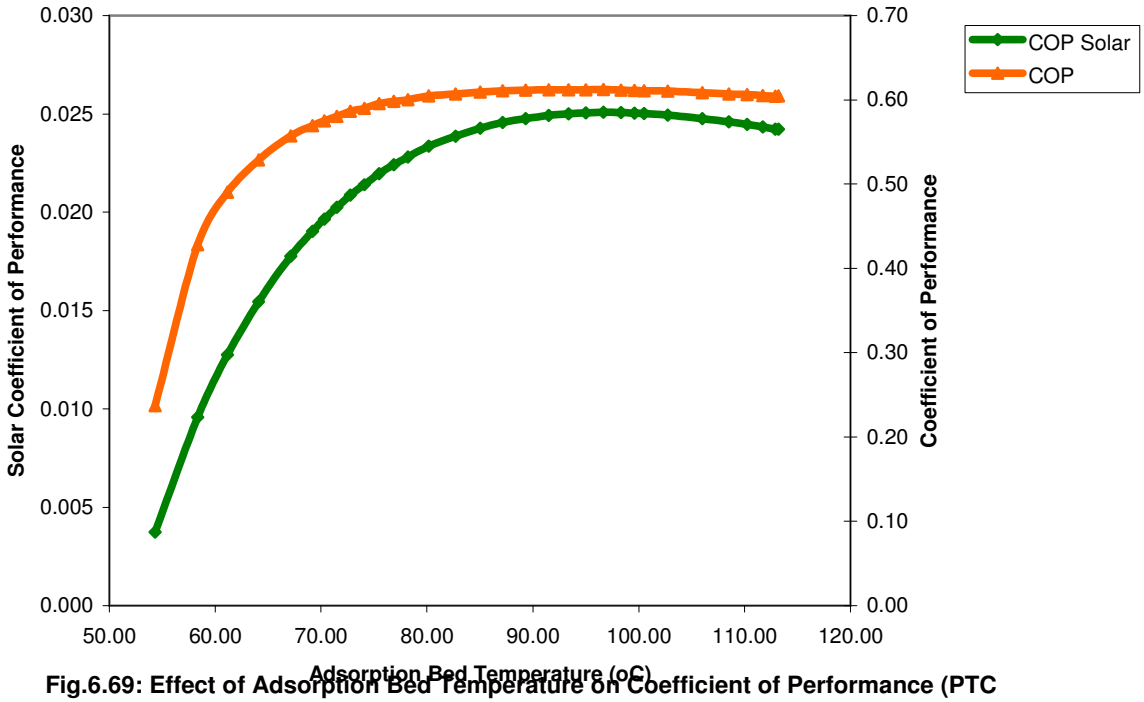


Fig.6.69: Effect of Adsorption Bed Temperature on Coefficient of Performance (PTC Sep)

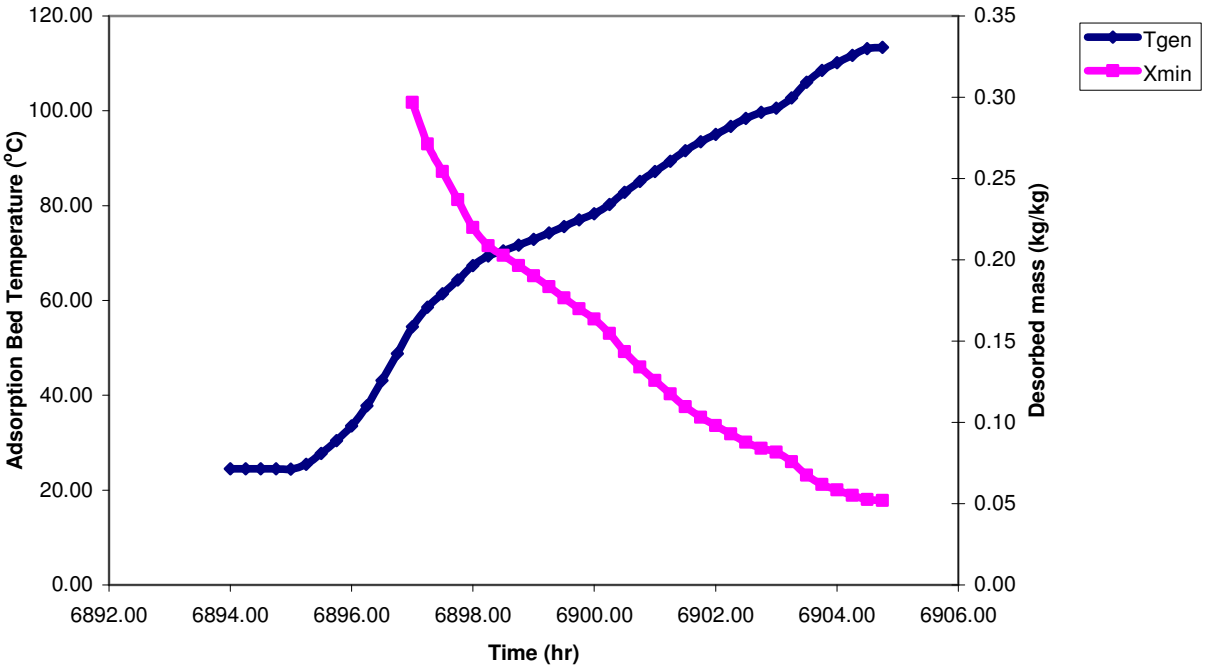


Fig.6.70: Variation of Adsorption Bed Temperature and Desorbed mass with Time (PTC Oct)

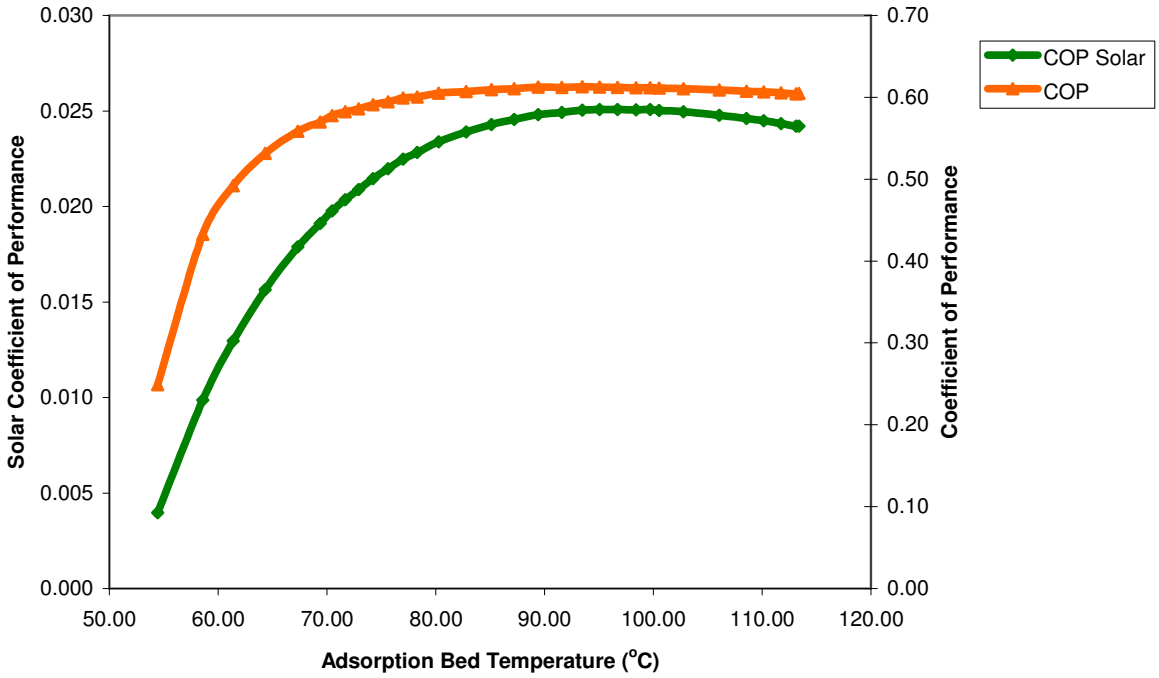


Fig.6.71: Effect of Adsorption Bed Temperature on Coefficient of Performance (PTC Oct)

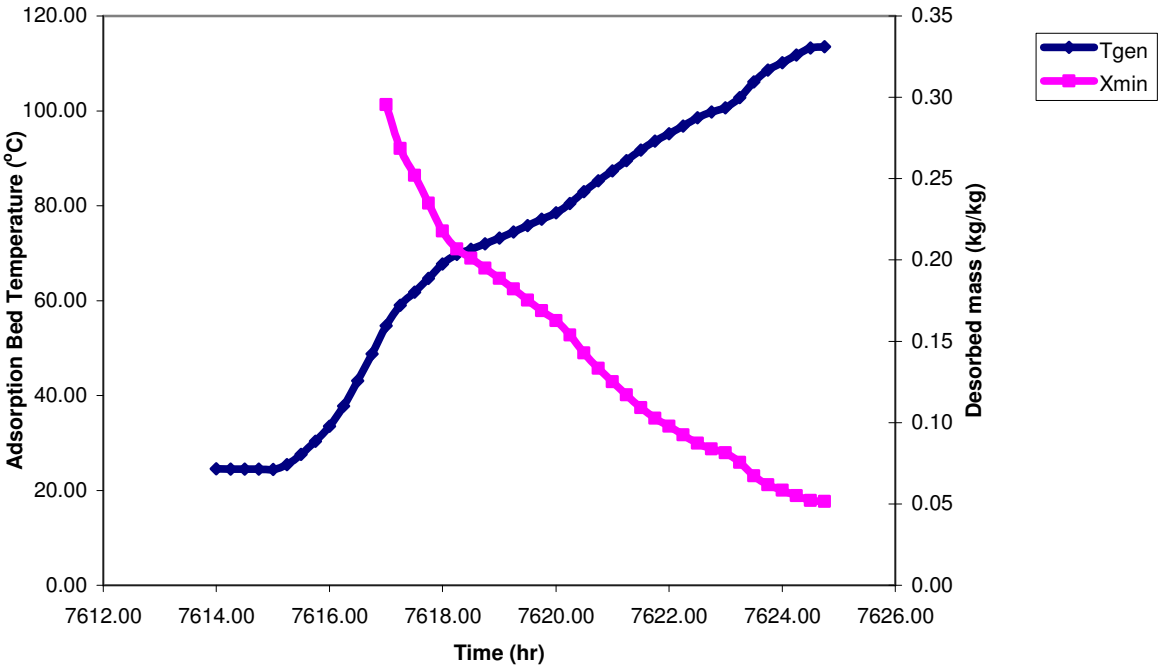


Fig.6.72: Variation of Adsorption Bed Temperature and Desorbed mass with Time (PTC Nov)

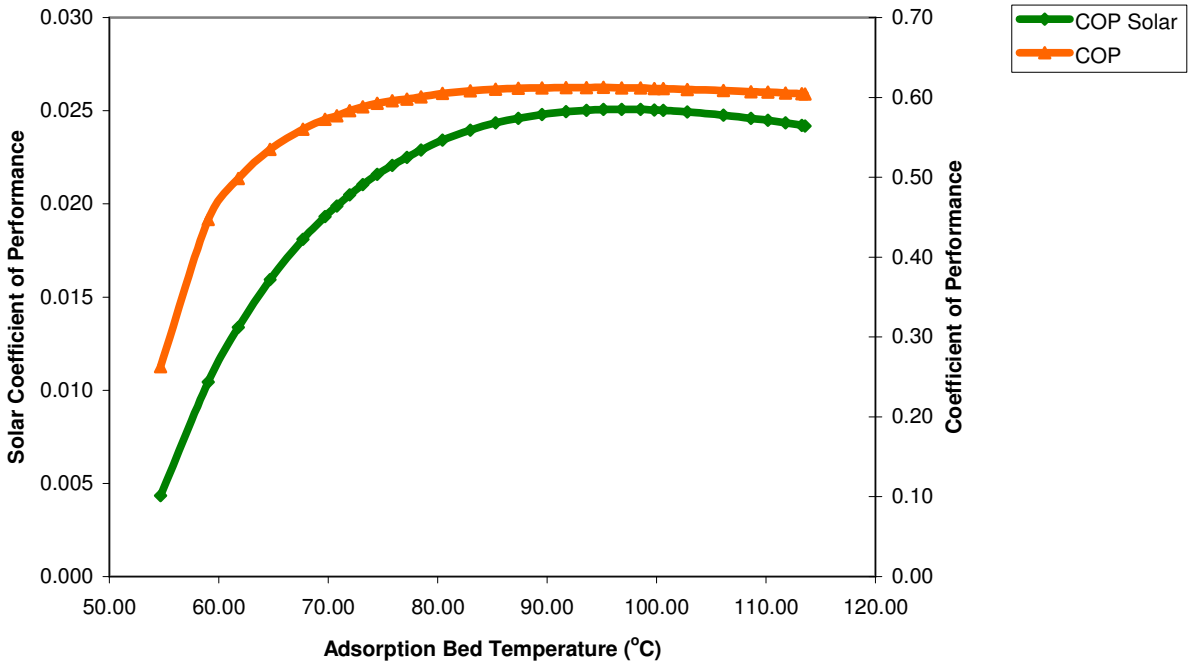


Fig.6.73: Effect of Adsorption Bed Temperature on Coefficient of Performance (PTC Nov)

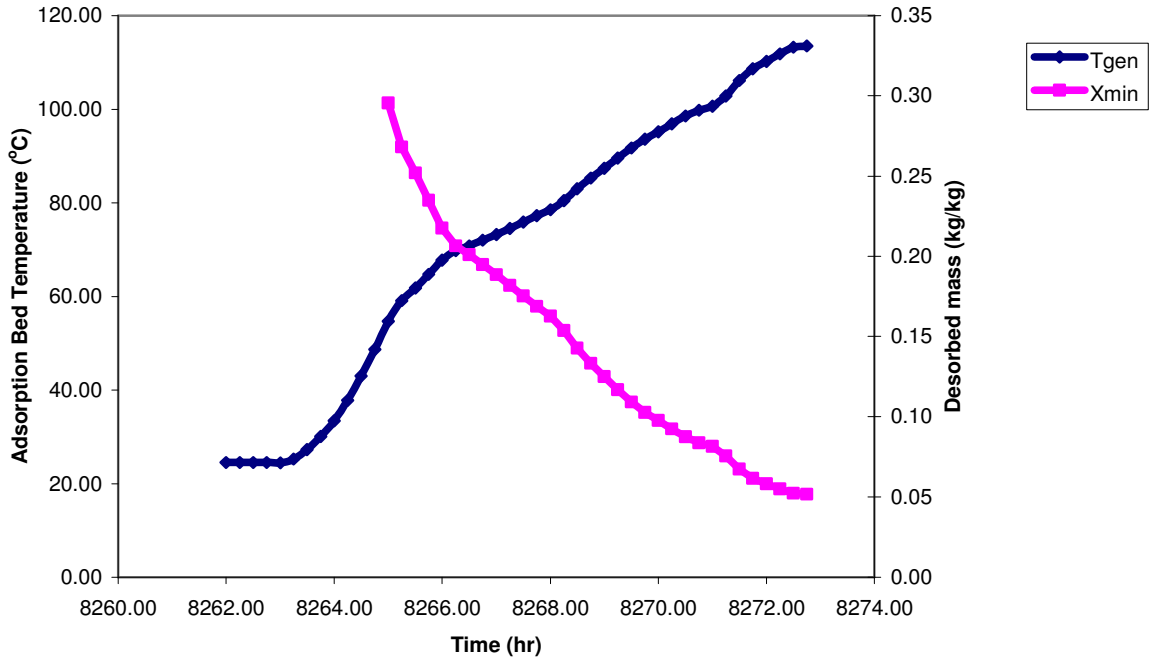


Fig.6.74: Variation of Asorption Bed Temperature and Desorbed mass with Time (PTC Dec)

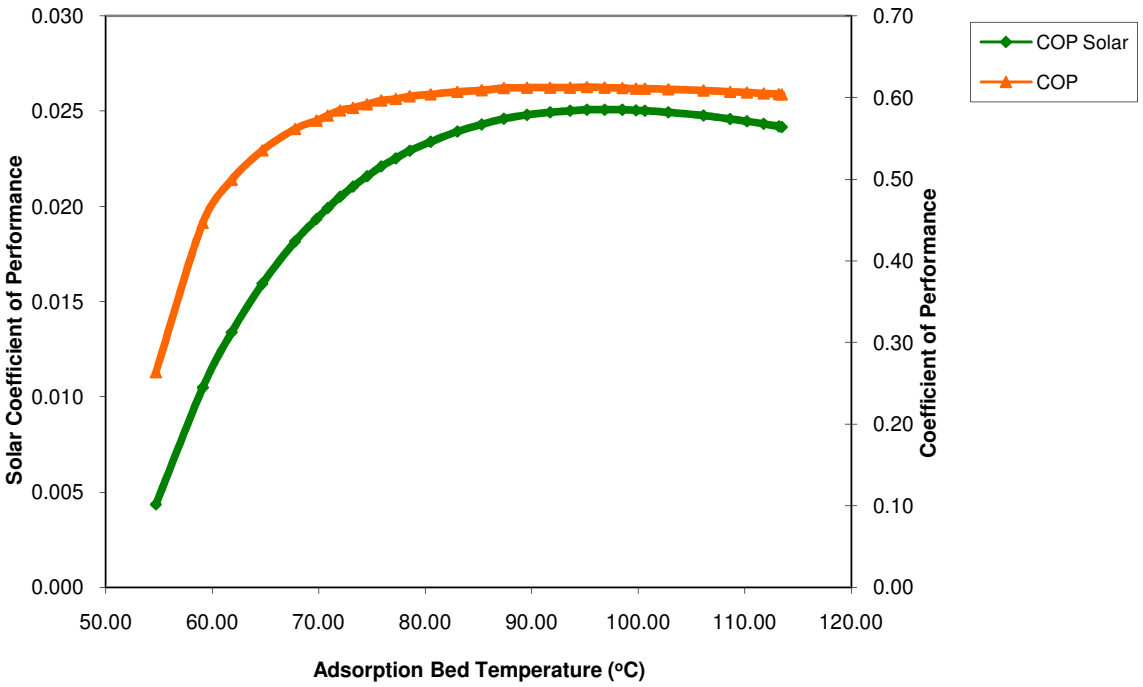


Fig.6.75: Effect of Adsorption Bed Temperature on Coefficient of Performance (PTC Dec)

Table 6.3: Simulation Parameters of the Adsorption Refrigeration System

Month	T_{gen} (^{o}C)			Δx (kg/kg)			DesorptionTime (min)		
	FPC	ETC	PTC	FPC	ETC	PTC	FPC	ETC	PTC
January	79.89	92.78	89.59	0.155	0.205	0.194	195	240	255
February	94.4	96.65	93.58	0.211	0.218	0.208	240	150	285
March	90.38	94.75	95.17	0.197	0.211	0.213	255	165	300
April	73.37	83.37	93.37	0.123	0.170	0.207	225	255	285
May	81.72	92.17	93.18	0.163	0.203	0.207	240	240	285
June	88.97	94.19	94.87	0.192	0.210	0.212	255	180	300
July	81.86	91.58	93.37	0.163	0.201	0.207	210	225	285
August	84.48	91.33	93.39	0.174	0.201	0.208	210	180	285
September	94.06	92.14	96.65	0.210	0.203	0.218	270	150	315
October	89.34	94.48	93.49	0.193	0.211	0.208	270	165	285
November	85.67	93.31	95.16	0.179	0.207	0.213	225	165	300
December	85.09	94.59	95.17	0.177	0.211	0.213	210	180	300
Average	85.77	92.61	93.58	0.178	0.204	0.209	234	191	290
Design values				0.211	0.218	0.218			

Table 6.4: Simulated Performance Parameters of the Adsorption Refrigeration System

Month	Q_e (kJ)			COP			COP_s			η		
	FPC	ETC	PTC	FPC	ETC	PTC	FPC	ETC	PTC	FPC	ETC	PTC
Jan	4177.96	5553.04	5250.68	0.603	0.613	0.612	0.023	0.025	0.025	0.42	0.58	0.76
Feb	5704.82	5893.11	5627.93	0.613	0.612	0.613	0.025	0.025	0.025	0.47	0.60	0.76
Mar	5328.60	5732.06	5768.01	0.613	0.613	0.613	0.025	0.025	0.025	0.50	0.62	0.76
Apr	3329.27	4588.91	5608.87	0.589	0.609	0.613	0.021	0.024	0.025	0.51	0.64	0.76
May	4398.02	5499.35	5591.77	0.606	0.613	0.613	0.024	0.025	0.025	0.49	0.62	0.76
Jun	5189.30	5681.83	5742.05	0.612	0.613	0.613	0.025	0.025	0.025	0.46	0.60	0.76
Jul	4413.64	5443.61	5608.92	0.607	0.613	0.613	0.024	0.025	0.025	0.44	0.60	0.76
Aug	4713.57	5420.52	5610.22	0.610	0.612	0.613	0.024	0.025	0.025	0.45	0.60	0.76
Sep	5670.69	5495.88	5893.57	0.613	0.612	0.612	0.025	0.025	0.025	0.47	0.60	0.76
Oct	5226.20	5707.36	5619.23	0.612	0.613	0.613	0.025	0.025	0.025	0.49	0.62	0.76
Nov	4844.88	5603.77	5766.80	0.611	0.612	0.613	0.024	0.025	0.025	0.47	0.60	0.76
Dec	4780.96	5717.18	5768.72	0.610	0.613	0.613	0.024	0.025	0.025	0.43	0.58	0.76
Average	4814.83	5528.05	5654.73	0.608	0.612	0.613	0.024	0.025	0.025	0.46	0.61	0.76

6.4 CALCULATIONS

The average values of the refrigeration effects (Table 6.4) and maximum desorption (Table 6.3) achievable by the three different systems is utilized in the design of the evaporator and condenser to be used by the cooling unit. The design is carried out using the Engineering Equation Solver (EES) software since some level of iteration is required to obtain some of the parameters. A typical calculation procedure for the FPC powered system evaporator and condenser design is presented below. The equations used are stated in chapter 4 of this work, a 12-hr evaporation period (adsorption time) is assumed (Anyanwu,2003), while copper is chosen as the material of construction for the condenser and evaporator tubes. The choice of copper tubes is to take advantage of its high thermal conductivity, to ensure rapid cooling of refrigerant vapor in the condenser and good heat transfer from the cold room to the evaporator during vaporization. The length of the evaporator tubes has been designed to hold the entire desorbed liquid methanol.

"Evaporator Design"

Q_e=Q_ev

"Heat transfer across evaporator wall (Q_ev)"

Q_e = 0.1115*10^3; T_sat=273.15; R_e_o=0.006; r_e_i=0.0054; P_atm=1.01325

Q_ev=2*pi*r_e_i*L_ev*n*h_ev_i*(T_ev_i-T_sat)

Q_ev=(2*pi*L_ev*n*(T_ev_o -T_ev_i))/(((LN(R_e_o/r_e_i))/k_et)+(1/(R_e_o*h_ev_o)))

Q_ev=(2*pi*L_ev*n*(T_cr -T_sat))/((1/(R_e_o*h_ev_o)+(LN(R_e_o/r_e_i))/k_et)+(1/(r_e_i*h_ev_i)))

h_ev_i=0.555*((g#*rho_e_v*(rho_e_l-rho_e_v)*h_e_fg*k_e_v^3)/(n*mu_e_v*2*r_e_i*(T_ev_i-T_sat)))^(1/4)

"The length of evaporator tube L_ev is such that the volume contains total volume desorbed methanol liquid"

n=10 "no of tubes"

"Maximum mass of methanol desorbed is 0.211 kg/kg of activated carbon"

L_ev=m_m/(pi*r_e_i^2*rho_e_l)

m_ac = 26.07 "mass of activated carbon"

m_m= 0.211*m_ac "maximum mass of desorbed methanol"

rho_e_v=0.0565 "density of methanol vapor"

rho_e_l=809 "density of liquid methanol"

k_e_v=0.01407 "thermal conductivity of methanol vapor"

mu_e_v=(9.68*10^(-6)) [Pa-s] "dynamic viscosity of methanol vapor"

h_e_fg=1200.2*10^3 "latent heat of vaporization of methanol"

k_et=385 “Thermal conductivity of copper"

Nus_ev=(0.6+(0.387*(Ra_D)^(1/6))/(1+(.559/Pr_a)^(9/16))^(8/27)) "Nusselt number"

Ra_D=(g#*beta_ev*(T_ev_o - T_ev_i)*D_ev_o^3*Pr_a)/nu_a^2 "Rayleigh number"

T_f_3=(T_ev_o + T_ev_i)/2

Pr_a=Prandtl(air_ha,T=T_f_3,P=P_atm)

D_ev_o=2*R_e_o

nu_a=mu_a/rho_a "kinematic viscosity of air"

mu_a=viscosity(air_ha,T=T_f_3,P=P_atm)

rho_a=density(air_ha,T=T_f_3,P=P_atm)

Nus_ev=(h_ev_o*D_ev_o)/k_a

k_a=conductivity(air_ha,T=T_f_3,P=P_atm)

beta_ev=1/T_f_3

Solution

Variables in Main

beta_ev=0.003652 [1/K]

D_ev_o=0.012 [m]

h_ev_i=313.2 [W/m^2-K]

h_ev_o=2.942 [W/m^2-K]

h_e_fg=1.200E+06 [J/kg]

k_a=0.02441 [W/m-K]

k_et=385 [W/m-K]

k_e_v=0.01407 [W/m-K]

L_ev=74.22 [m]

mu_a=0.00001725 [kg/m-s]

mu_e_v=0.00000968 [kg/m-s]

m_ac=26.07 [kg]

m_m=5.501 [kg]

n=10

Nus_ev=1.446

nu_a=0.00001338 [m^2/s]

Pr_a=0.711

P_atm=1.013 [bar]

Q_e=111.5 [W]

Q_ev=111.5 [W]

Ra_D=333

rho_a=1.29 [kg/m^3]

rho_e_l=809 [kg/m^3]

rho_e_v=0.0565 [kg/m^3]

r_e_i=0.0054 [m]

R_e_o=0.006 [m]

T_cr=274.5 [K]

T_ev_i=273.2 [K]

T_ev_o=274.5 [K]

T_f_3=273.8 [K]

T_sat=273.1 [K]

"Condenser Design"

T_w=293.15; k_ct=385; R_o_c=0.006; r_i_c=0.0054; P_atm=1.01325; m_dot_sb=3.918*10^(-4);

h_fg=1168.69*10^3; n_o=5

"Heat Transfer across Condenser wall (Q_con)"

Q_con=2*pi*r_i_c*L_con*n_o*h_cw_i*(T_sat-T_cw_i)

Q_con=2*pi*R_o_c*L_con*n_o*h_cw_o*(T_cw_o-T_w)

Q_con=m_dot_sb*h`_fg

Q_con=(2*pi*L_con*n_o*(T_sat-

T_w))/((1/(R_o_c*h_cw_o))+((LN(R_o_c/r_i_c))/k_ct)+(1/(r_i_c*h_cw_i)))

h`_fg=h_fg+0.68*c_p_l*(T_sat-T_cw_i) "Latent heat of vaporization"

c_p_l=specheat(methanol,T=T_f_1,P=0.16905)

T_f_1=(T_sat+T_cw_i)/2

T_sat=298.15

h_cw_i=0.555*((g#*rho_l*E*k_l^3*h`_fg)/(n_o*mu_l*d_i_c*G))^(1/4)

E=rho_l-rho_v

G=T_sat-T_cw_i

rho_l=786.6 "density of liquid methanol"

mu_l=0.544*10^(-3) "dynamic viscosity of liquid methanol"

k_l=0.2 "Thermal conductivity of liquid methanol"

d_i_c=2*r_i_c "internal diameter of condenser pipe"

D_o_c=2*R_o_c "outer diameter of condensr pipe"

rho_v=0.0565 "density of methanol vapor"

Nus_c=(0.6+(0.387*Ra_D)/(1+(.559/Pr_cw)^(9/16))^(8/27)) "Nusselt number"

Ra_D=(g#*beta_c*(T_cw_i-T_cw_o)*D_o_c^3*Pr_cw)/nu_cw^2 "Rayleigh number"

Pr_cw=(mu_cw*c_p_cw)/k_cw "Prandtl number"

c_p_cw=4.18*10^3 "Specific heat of water"

nu_cw=mu_cw/rho_cw "Kinematic viscosity of water"

mu_cw=950*10^(-6) "Dynamic viscosity of water"

rho_cw=1000 "Density of water"

Nus_c=(h_cw_o*D_o_c)/k_cw

k_cw=0.607 "Thermal conductivity of water"

T_f_2=(T_cw_i+T_cw_o)/2

beta_c=1/T_f_2

Solution

beta_c=0.00341 [1/K]

c_p_cw=4180 [J/kg-K]

c_p_l=2520 [J/kg-K]

d_i_c=0.0108 [m]

D_o_c=0.012 [m]

E=786.5 [kg/m^3]

G=4.903 [K]

h_cw_i=2477 [W/m^2-K]

h_cw_o=137758 [W/m^2-K]

h_fg=1.169E+06 [J/kg]

h`_fg=1.177E+06 [J/kg]

k_ct=385 [W/m-K]

k_cw=0.607 [W/m-K]

k_l=0.2 [W/m-K]

L_con=0.2239 [m]

mu_cw=0.00095 [kg/m-s]

mu_l=0.000544 [kg/m-s]

m_dot_sb=0.0003918 [kg/s]

Nus_c=2723

nu_cw=9.500E-07 [m^2/s]

n_o=5

Pr_cw=6.542

P_atm=1.013 [bar]

Q_con=461.2 [W]

Ra_D=7518

rho_cw=1000 [kg/m^3]

rho_l=786.6 [kg/m^3]

rho_v=0.0565 [kg/m^3]

r_i_c=0.0054 [m]

R_o_c=0.006 [m]

T_cw_i=293.2 [K]

T_cw_o=293.2 [K]

T_f_1=295.7 [K]

T_f_2=293.2 [K]

T_sat=298.1 [K]

T_w=293.2 [K]

Table 6.5: Evaporator and Condenser Parameters

Collector Type	Refrigeration Effect Q_{ev} (W)	Cold Room Temp. T_{cr} (K)	Length of Evaporator Tubes (m)	Heat Released in Condenser (W)	Length of Condenser Tubes (m)
FPC	111.45	274.5	74.22	461.2	0.2239
ETC	127.96	274.7	76.69	583.7	0.2833
PTC	130.9	274.7	76.69	384.4	0.1866

6.5 DISCUSSION OF RESULTS

Figures 6.2 through 6.75 show the simulated results of the adsorption refrigeration system powered by three different collectors; these results have also been summarized in Tables 6.3 and 6.4. The figures show that desorption does not start before a generation temperature of 50^{o}C is attained by any of the collectors though the time taken for desorption to reach the maximum attainable for the individual collectors differed.

In the flat plate collector powered system (figs. 6.2- 6.25), heating of the adsorbent bed started on the average at about 8am with desorption starting about 11am and reaching a maximum generation temperature between the hours of 2-3pm. The period between 8 – 11am represents the isosteric heating phase, where the adsorbent bed continuously absorbs heat from the hot water tank. This results in a rapid increase in the adsorption bed temperature (as shown in the figures for the FPC) from about 25^{o}C to about 55^{o}C in a time period of about 3 hours after which methanol starts to desorb from the activated carbon and flows to the condenser. The rate of heating and its associated adsorbent bed temperature rise is however lower for the isobaric desorption phase. The highest generation temperature recorded for this system is 94.4^{o}C in the month of February (high insolation month) with the lowest peak temperature of 73.37^{o}C recorded in the month of April (low insolation month). This system also recorded appreciable desorption of methanol (0.123 – 0.211 kg/kg of activated carbon) resulting in a refrigeration effect ranging from 3329.27 kJ to 5704 kJ within an average desorption time of 234mins (3hr 54mins). The system achieved an average cooling process COP of 0.608, COP_{solar} of 0.024 and efficiency for the heating process of 0.47.

The Evacuated tube collector powered refrigeration system (figs. 6.27- 6.50) attained higher generation temperatures than the flat plate collector powered system. The time taken for the initial pressurization of the system from evaporator pressure to condenser pressure is lower than that for the FPC system. Desorption for this system also started earlier (about 10.30am) at a temperature ranging between 52 – 56^{o}C. A peak desorption temperature of 96.65^{o}C was recorded in the month of February and the lowest peak of 83.37^{o}C in the month of April. The quantity of methanol desorbed was also more, with values ranging from 0.170 – 0.218 kg/kg of activated carbon; this gave a refrigeration effect of 4588.91 – 5893.11 kJ. The average heating time for the system to attain optimum generation temperature is 191mins (3hr 11mins) after which if heating continues, the system COP was observed to drop. This implies that further heating does not cause appreciable desorption, it rather increases the sensible heat of the adsorbent bed thereby increasing the cooling time of the bed. This means that for this system the heating period must not exceed this time for it to be switched to the cooling mode where the tank is emptied of hot water and cold water introduced. The average COP for this system is 0.612, COP_{solar} of 0.025 and heating efficiency of 0.61, these values are higher than those achieved with the flat plate collector.

The last system to be evaluated is the parabolic trough collector powered system (figs. 6.52-6.75). The system recorded an earlier time for the start of desorption (9.00am), at which time it had attained an average temperature of 54^{o}C. A peak desorption temperature of 96.65^{o}C was recorded for the month of September, while the lowest peak temperature of 89.59^{o}C occurred in January. The change in the months for peak temperatures is due to the north-south orientation of the trough which allows for more energy to be collected in the summer months (months with high cooling loads requirements) than the winter months. The quantity of desorbed methanol ranged from 0.194 – 0.218 kg/kg activated carbon

resulting in a refrigeration effect of between 5250.68 – 5893.57 kJ. The refrigeration effect achieved while being higher than those for the FPC and ETC, it is observed that the average heating time of 290mins (4hr 50mins) is more than those for the FPC and ETC systems. The PTC powered system also achieved optimum generation temperatures for most of the year beyond which the COP of the system drops. The average performance parameters for this system are COP of 0.613, COP_{solar} of 0.025 and a heating efficiency of 0.76.

The evaporator and condenser design parameters for the three systems studied in this work are presented in Table 6.5. The three systems gave cold room temperatures of about 274 K ($1^{o}C$), though from the refrigeration effects presented, the PTC powered system has the ability to carry a larger product load closely followed by the ETC powered system. The quantity of methanol desorbed by the individual systems is reflected in the length of evaporator tube required, the ETC and PTC system have the same evaporator tube lengths since they desorbed on the average equal quantities of methanol. The heat released by methanol vapor in the condenser is also presented in Table 6.5; the highest value of 583.7 W is recorded for the ETC system. This is because of the smaller heating time taken to desorb the quantity of methanol recorded. The lengths of the condenser tubes required are also presented in Table 6.5.

6.6 VALIDATION OF SIMULATION WITH SOME EXPERIMENTAL RESULTS

In order to validate the simulation results of the solar powered adsorption refrigeration system, the parameters for experimentation of a similarly developed system were used as simulation parameters. This was to determine the level of correlation between the simulation results and the results obtained by experiments. The system for the validation of the simulation results is that developed by Wang et al (2002) at the Institute of

Refrigeration and Cryogenics, Shanghai Jiao Tong University, China. Wang et al experimented with a hybrid heating and cooling system using Shanghai "YK" (coconut shell type) activated carbon-methanol pair powered by an evacuated tube collector. The experiments showed that a 120kg water bath can be heated up from 22^{o}C to 92^{o}C achieving a COP_{cycle} of 0.41. The experimental data from this system used in the validation of the simulation procedure are as stated below.

Mass of Activated Carbon = 28 kg; Specific heat of carbon = 900 J/kgK

Mass of Adsorber Stainless Steel = 5 kg; Specific heat of Stainless steel =902 J/kgK

Adsorption Temperature = 20^{o}C

Condensing Temperature = 30^{o}C

Evaporator Temperature = -1^{o}C

The parameters of the Dubinin-Astakhov equation for the activated carbon-methanol pair used are xo = 0.284 kg/kg; k = 12.21; n=1.39; A=4413 in the heat of desorption equation and the latent heat of vaporization of methanol is taken as 1102 kJ/kg in the study. Table 6.6 below shows the comparison of the values of COP obtained by experiments and those obtained by simulations.

Table 6.6: Comparison of Wang's Experimental Results with Simulated values

	Hot Water Temp. ^{o}C	Experimental COP_{cycle}	Simulated COP_{cycle}	% Difference
April 10-11, 1999	92	0.41	0.53	29.2
April 15-16, 1999	81	0.39	0.51	30.7
April 20-21, 1999	72	0.37	0.48	29.7

Table 6.6 shows an overestimation by the simulation model of an average of 29.9% which is about consistent for the days evaluated. The overestimation is to be expected as numerical experiments (simulations) assume ideal conditions of operation without taking into account unavoidable loss that naturally occur during operation. The simulations also gave desorption start temperature of about 69^{o}C which is within the range recorded during experimentation as shown in Fig 6.76 below.

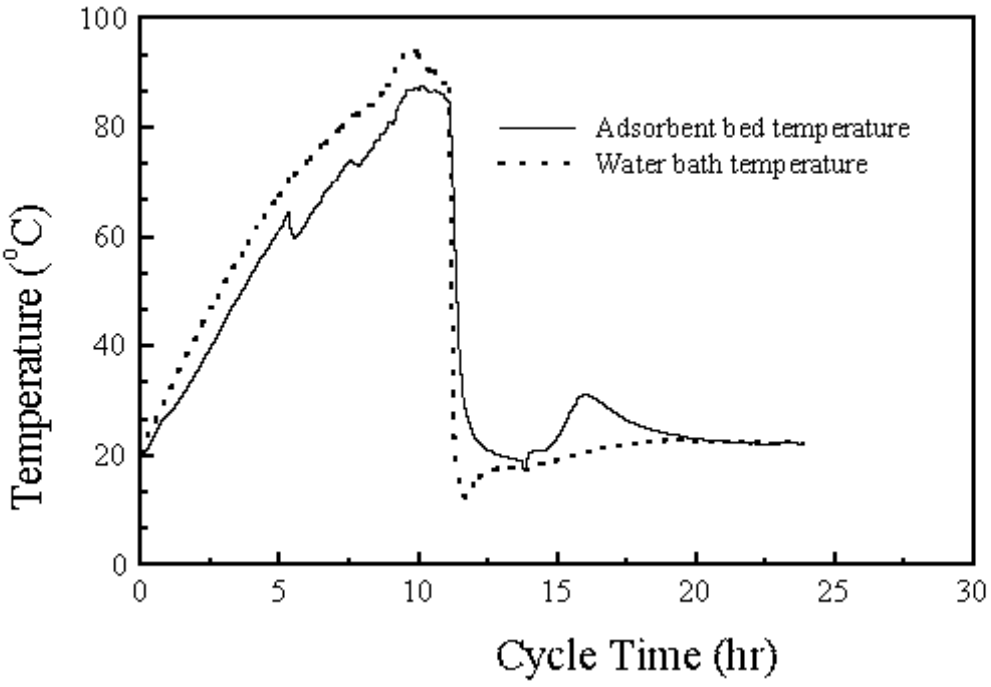


Fig. 6.76: Adsorbent Bed Temperature and Water Bath Temperature versus Cycle Time (Wang et al, 2002)

The point of first temperature drop down in the figure above represents the start of desorption. Another reason for the difference between the experimental results and those of

simulations lies in the fact that, during numerical experiments, the water bed temperature is assumed to be equal to the adsorbent bed temperature. Fig. 6.76 above however shows that there is a slight difference between the temperatures attained by the water bath and the adsorbent, and this result in a break down of this assumption. The implication is that in simulations, a higher desorption rate is assumed to calculate the refrigerating effect leading to a higher COP.

El Fadar (2009) carried out the modeling and performance study of a continuous adsorption refrigeration system driven by a parabolic trough solar collector.

Some of the results of El Fadar's work are represented in Figs. 6.77 and 6.78 showing a refrigeration cycle COP of 0.43. El Fadar's design utilized activated carbon-ammonia pair with two adsorbent beds operated out of phase (i.e. while one was undergoing heating, the other was being cooled). These results were obtained for a July day in Tetouan, Morrocco.

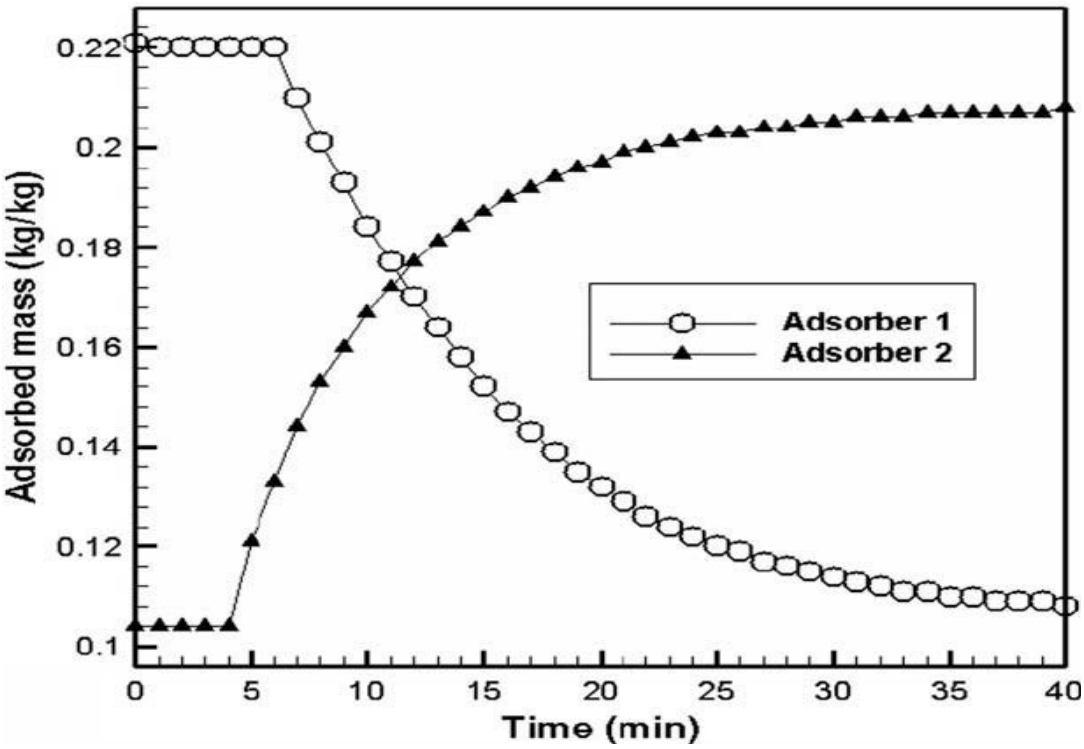


Fig. 6.77: Adsorbed mass variation during isosteric heating-desorption process for adsorber 1 and isosteric cooling-adsorption process for adsorber 2 (El Fadar, 2009b)

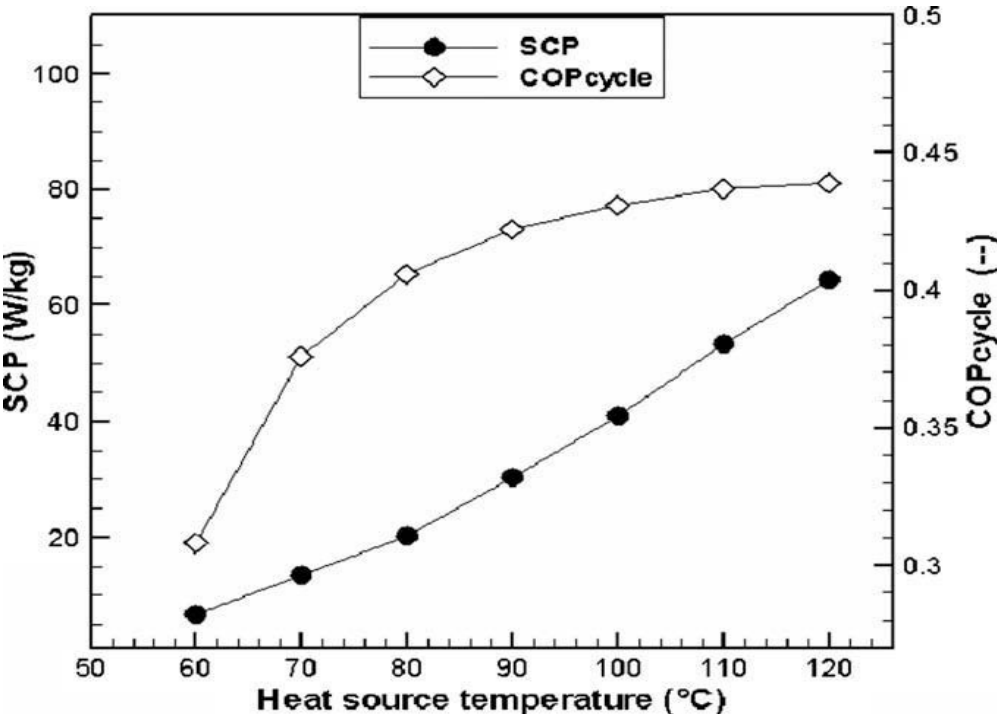


Fig. 6.78: Effect of the heat source temperature on SCP and on COP_{cycle} (El Fadar, 2009b)

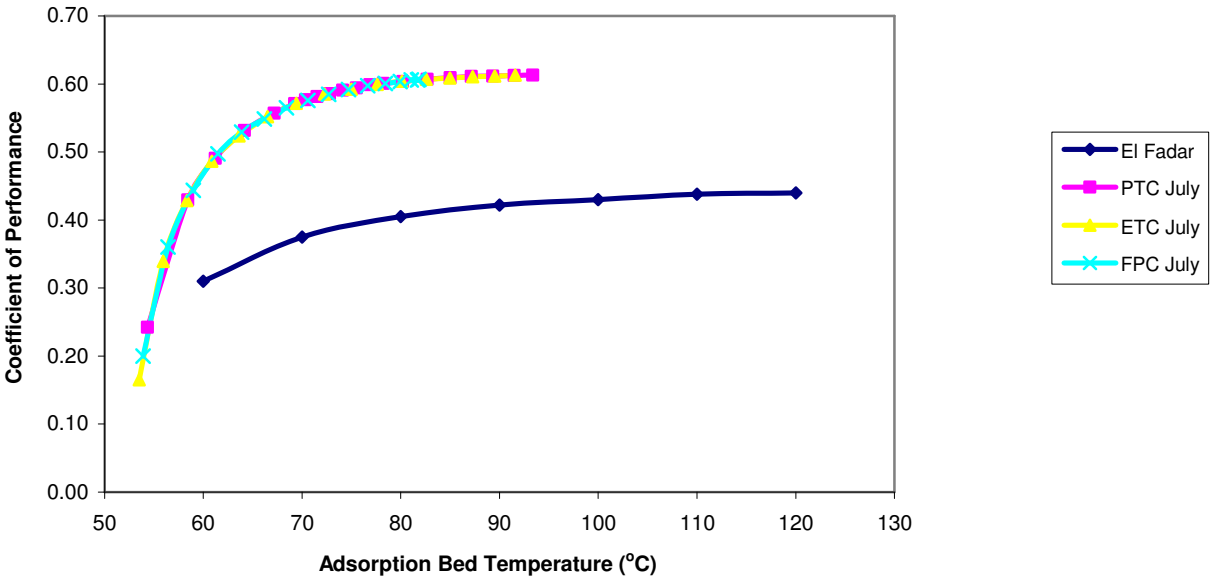


Fig.6.79: Comparison between El Fadar's result and Present Study Simulated values

Fig.6.79 above shows a comparison between El Fadar's activated carbon-ammonia system and the simulated activated carbon-methanol of this study for the month of July. The figure shows that the activated carbon- methanol gave higher COP values for a given adsorption bed temperature and that desorption of methanol also started at a much lower temperature than ammonia. The higher values of COP for the activated carbon-methanol simulated system are better understood with the research work of Wang et al (2006). Wang (2006) studied the adsorption quantity of methanol and ammonia in activated carbon over a range of temperatures.

The study showed that adsorption performance of activated carbon-methanol was better than that of activated carbon-ammonia as reflected in fig. 6.80 below with the difference being as large as 59% (Wang, 2006) at some instant.

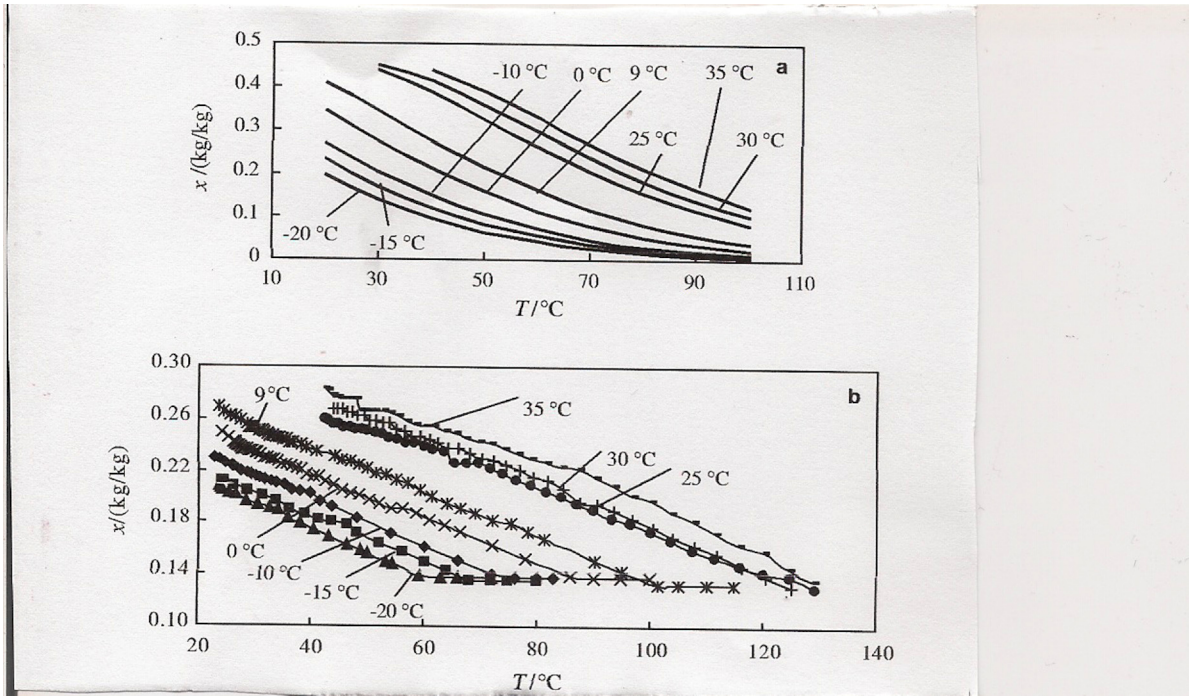


Fig. 6.80: Isobaric adsorption properties of activated carbon (a) methanol, (b) ammonia. (Wang, 2006)

This observation further justifies the choice of methanol as the refrigerant for the present study as it performs better than ammonia under the same adsorption bed temperatures.

6.7 RELATIVE COST COMPARISON OF SIMULATED SYSTEM

The relative costs of the FPC, ETC and PTC system is calculated to determine which of the systems is most viable economically. The costs compared are limited to the cost of the collector only as the other components of the system are assumed to be the same. In comparing the cost of the collector, the collector area and maximum refrigeration effect achievable are employed. This is achieved by determining the cost of producing 1kJ of refrigeration effect.

First the FPC system, the flat plate collector costs $325 for a collector area of 2.02m^2 (www.siliconsolar.com). Therefore the cost of producing 1kJ of refrigeration effect is determined as follows:

$$Cost / m^2 = \frac{\$325}{2.02m^2} = \$160.89 / m^2$$

The maximum refrigeration effect produced with the FPC is 5704.82kJ using a collector area of 15m^2. This implies that the refrigeration effect produced per m^2 of collector is

$$Q_e / m^2 = \frac{5704.82kJ}{15m^2} = 380.32kJ / m^2$$

Therefore the cost of producing 1kJ of cooling is

$$Cost / kJ = \frac{160.89}{380.2} = \$0.42 / kJ$$

Similarly, ETC cost of $800 for a collector area of 4.41m^2 (www.siliconsolar.com) and refrigeration effect of 5893.11kJ produced using a collector area of 15m^2. The cost of producing 1kJ of refrigeration effect is $0.46/kJ.

Lastly, the PTC costs $750 for an area of 1.44m^2 (WWW.GAIA-SOLAR.COM) and refrigeration effect of 5893.57kJ produced using a collector area of 13.8m^2. The cost, therefore of producing 1kJ of cooling is $1.22/kJ

This makes the FPC system the most viable economically, this is because the solar powered adsorption system is basically a low energy input system and the application of very high efficiency (costly) collector like the PTC results in a waste of resources.

CHAPTER SEVEN

CONCLUSIONS AND RECOMMENDATIONS

7.1 CONCLUSIONS

The modeling and transient simulation of a solar powered adsorption refrigeration system using activated carbon-methanol adsorbent/adsorbate pair has been successfully undertaken. The performances of three types of collectors for powering this system, the flat plate collector, evacuated tube collector and parabolic trough collector were studied.

The study showed that for appreciable desorption of methanol from activated carbon in a cooling system with 0^oC and 25^oC evaporator and condenser temperatures respectively, a temperature of at least 80^oC is required by the adsorbent bed. Based on this temperature requirement, the optimization of solar thermal system was undertaken to determine the size of collector and hot water tank needed. The optimization results gave the minimum values for collector areas as $15m^2$ for the FPC and ETC with the PTC having a value of $13.8m^2$. The maximum tank size however for the three systems is $1m^3$.

These parameters were then used in the transient simulation of the cooling system over a period of a typical year.

The FPC system gave average values of refrigeration effect of 4814.83 kJ, solar coefficient of performance (COP_s) of 0.024, a cooling COP of 0.608 and a heating efficiency of 0.46. The ETC powered system gave average values of refrigeration effect of 5528.05 kJ, solar coefficient of performance (COP_s) of 0.025, a cooling COP of 0.612 and a heating efficiency of 0.61. The PTC powered system however gave average values of refrigeration

effect of 5654.73 kJ, solar coefficient of performance (COP_s) of 0.025, a cooling COP of 0.613 and a heating efficiency of 0.76.

A cost comparison of the three types of collectors used in this research was made. The flat plate solar collector was however found to be the most economically viable.

This study shows that solar powered adsorption refrigeration can be effective, economic, practicable and eco-friendly option for Kano in the northern region of Nigeria with abundant sunshine, the choice of the type of collector to be used for powering the system would however depend on the product load (cold room) requirements.

7.2 RECOMMENDATIONS

It is recommended that the construction of the modeled systems be undertaken so that physical experiments can be conducted and the results further compared with the simulations to determine the level of agreement between them. This would help in adjusting the simulation parameters to further improve its performance.

REFERENCES

Anyanwu, E.E., Oteh, U.U. and Ogueke, N.V. (2001). Simulation of a solid adsorption solar refrigerator using activated carbon/methanol adsorbent/refrigerant. *Energy Conversion and Management*, 42(7): 899-915.

Anyanwu, E.E. and Ezekwe, C.I. (2003). Design, Construction and test run of solid adsorption solar refrigerator using activated carbon/methanol as adsorbent/adsorbate pair. *Energy Conversion and Management*, 44(18): 2879-2892.

Anyanwu, E.E. and Ogueke, N.V. (2005). Thermodynamic design procedure for solid adsorption solar refrigerator. *Renewable Energy*, 30(1): 81-96.

Awoniyi, J.A. (1980). The design and construction of a solar-powered, vapor-absorption refrigeration system. Unpublished M.Sc Thesis. Ahmadu Bello University, Zaria.

Bula, A.J., Navarro, L.F., Herrera, D.L. and Corredor, L.A. (2000). Thermodynamic simulation of a Solar Absorption Refrigeration System Generator – Heat Exchanger. iies.faces.ula.ve/AMSE 2000/papers/simulation/MSN 2000_Bula.pdf

Boubakri, A., Arsalene, M., Yous, B., Ali-Moussa, L., Pons, M., Meunier, F. and Guillemiot, J.J. (1992b). Experimental study of adsorptive solar-powered ice-makers in Agadir (Morocco)-2. Influences of Meteorological parameters. *Renewable Energy*, 2(1): 15-21.

Chang, W.-S., Wang, C.-C. and Shieh, C.-C. (2007). Experimental study of a solid adsorption cooling system using flat-tube heat exchangers as adsorption bed. *Applied Thermal Engineering*, 27: 2195-2199.

Daou, K., Wang, R.Z. and Xia, Z.Z. (2006). Desiccant cooling air conditioning: a review. *Renewable and Sustainable Energy Reviews*, 10: 55-77.

Deaver, F.K. and Eckert, E.R.G. (1970). An interferometric investigation of convective heat transfer in a horizontal fluid cylinder with wall temperature increasing at a uniform rate. Proceedings of 4th International Heat Transfer Conference Paper N.C. 1.1

Demirocak, E.D. (2008). Thermodynamic and Economic Analysis of a Solar Thermal Powered Adsorption Cooling System. Unpublished M.Sc. Thesis. Middle East Technical University, Turkey.

Duffie, J.A. and Beckman, W.A. (2006). Solar Engineering of Thermal Processes. 3rd Ed, John Wiley and Sons Inc. New Jersey.

Eduardo, D. and Sagredo, P.E. (2004). Design and construction of a solar energy refrigeration system using vacuum concentric tubes with adsorption. Second LACCEI International Latin American and Caribbean Conference for Engineering and Technology (LACCEI' 2004). "Challenges and opportunities for engineering education, research and development". 2-4 June 2004, Miami, Florida, USA.

Enibe, S.O. and Ileoje, O.C. (1997). Design optimization of the flat plate collector for a solid adsorption solar refrigerator. *Solar Energy*, 60(2): 77-87.

Erhard, P., Spindler, K. and Ehahne, P. (1998). Test and simulation of a solar powered solid sorption cooling machine. *International Journal of Refrigeration*, 21(2): 133-141.

El Fadar, A., Mimet, A. and Perez-Garcia, M. (2009[a]). Study of an adsorption refrigeration system powered by parabolic trough collector coupled with a heat pipe. *Renewable Energy*, 34: 2271-2279.

El Fadar, A., Mimet, A. and Perez-Garcia, M. (2009b). Modeling and Performance study of a continous adsorption refrigeration system driven by parabolic trough solar collector. *Solar Energy*, 83: 850-861.

Florides, G.A., Kalogirou, S.A., Tassou, S.A. and Wrobel, L.C. (2002). Modeling and Simulation of an absorption solar cooling system for Cyprus. *Solar Energy*, 72: 43-51.

Gordon, J.N. and Ng, K.C. (2000). High-Efficiency solar cooling. *Solar Energy*, 68(1): 23-31.

Habib, K., Saha, B.B., Chakraborty, A., Koyama, S. and Srinivasan, K. (2011). Performance evaluation of combined adsorption refrigeration cycles. *International Journal of Refrigeration*, 34: 129-137.

Hamamoto, Y., Alam, K.C.A., Saha, B.B., Koyama, S., Akisawa, A. and Kasiwagi, T. (2006). Study on adsorption refrigeration cycle utilizing activated carbon fibers. Part 2. Cycle performance evaluation. *International Journal of Refrigeration*, 29: 315-327.

Hamdih, N.H.A. and Al-Muhtaseb, M.A. (2009). Optimization of Solar Adsorption Refrigeration System Using Experimental and Statistical Techniques. GCREEDER 2009, Amman-Jordan, 31 March – 2 April 2009.

Hassan, H.Z., Mohamad, A.A. and Bennacer, R. (2011). Simulation of an adsorption solar cooling system. *Energy*, 36: 530-537.

Headley, O.S., Kothdiwal, A.F. and McDoom, I.A. (1994). Charcoal-methanol adsorption refrigeration powered by a compound parabolic concentrating solar collector. *Solar Energy*, 53: 191-198.

Hildebrand, C., Dind, Ph., Pons, M. and Buchter, F. (2004). A new solar powered adsorption refrigerator with high performance. *Solar Energy*, 77: 311-318.

Hollands, K.G.T., Unny, T.E., Raithby, G.D. and Konicek, L. (1976). Free convection heat transfer across inclined air layers. *Trans. ASME J. Heat Transfer*, 98: 189.

Holman, J.P. (1997). Heat Transfer, 8th Ed., McGraw-Hill. New York.

Ibitoye, F.I. and Adenikinju, A. (2007). Future demand for electricity in Nigeria. *Applied Energy*, 84(5): 492-504.

Iloeje, O.C. (1983). Design, construction and test run of a solar powered solid absorption refrigerator. National Annual Solar Energy Forum (NASEF), April 1983, Bida. Niger State, Nigeria.

International Energy Agency: World Energy Outlook 2004.

International Energy Agency: World Energy Outlook Executive Summary 2010.

Khattab, N.M. (2004). A novel solar powered adsorption refrigeration module. *Applied Thermal Engineering*, 24: 2747-2760.

Khattab, N.M. (2006). Simulation and optimization of a novel solar-powered adsorption refrigeration module. *Solar Energy*, 80: 823-833.

Klein, S.A. and Beckman, W.A. (1979). A general design method for closed-loop solar energy system. *Solar Energy*, 22(3): 269-282.

Lemmini F. and Errougani A. (2005). Building and experimentation of a solar powered adsorption refrigerator. *Renewable Energy*, 30: 1989-2003.

Leite, A.P.F., Grilo, M.B., Andrade, R.R.D., Belo, F.A. and Meunier, F. (2004). Experimental data on a Solar-Powered Adsorption Refrigerator for Ice Production using Activated Carbon-Methanol Pair. ECOS 2004 – 17th International Conference on Efficiency, Costs, Optimization, Simulation and Environment Impact of Energy and Process Systems. July 7-9, 2004 – Guanajuato, Mexico.

Li, Z.F. and Sumathy, K. (1999). A solar-powered ice-maker with solid adsorption pair of activated carbon and methanol. *International Journal of Energy Research*, 23(6): 517-527.

Li, M. and Wang, R, Z. (2002). A study of the effects of collector and environment parameters on the performance of a solar powered solid adsorption refrigerator. *Renewable Energy*, 27(3): 369-382.

Li, X.R. (2003). Experimental study on the adsorption performance of consolidated activated carbon-methanol pair. Unpublished M.Sc Thesis, Shanghai Jiao Tong University, Shanghai, China.

Lucas, L. (1998). IIR News, *International Journal of Refrigeration*, 21(2): 87-88.

Lundqvist, P. (1993). Stirling Cycle Heat Pumps and Refrigerators. Unpublished Thesis, Royal Institute of Technology, KTH. Stockholm, Sweden.

Mande, S., Ghosh, P., Kisire, V.V.N., Oertel, K. and Sprengel, U. (1996). Development of an Advanced Solar-hybrid Adsorption Cooling System for Decentralized Storage of Agricultural Products in India. DLR-TERI Joint project Report submitted to The Commission of the European Communities, DG-XII, 1996.

McAdams, W.H. (1954). Heat Transmission, 3rd Ed. McGraw-Hill. New York.

Methanex Corporation (2006). Technical Information and Safe Handling Guide for Methanol. Version 3.0, September, 2006

Mittal, V., Kasana, K.S., and Thakur, N.S. (2006). Modeling and Simulation of a Solar Absorption cooling system for India. *Journal of Energy in Southern Africa*, 17(3).

Oertal, K. and Fischer, M. (1998). Adsorption cooling system for cold storage using methanol/silicagel. *Applied Thermal Engineering,* 18(9):773-786

Ogueke, N.V. and Anyanwu, E.E. (2008). Design Inprovements for a collector/generator/adsorber of a solid adsorption solar refrigerator. *Renewable Energy*, 33(11): 2428 – 2440.

Onochie, E.U. (1987). Design and construction of a 100% solar powered vapor absorption refrigerator. National Solar Energy Forum. 22-25th April 1987, Akoka, Lagos.

Pridasawas, W. and Nemeriam, T. (2003). Solar Cooling. Assignment for Ph.D. Course: Solar Heating. Technical University of Denmark (DTU). June 27.

Pridasawas, W. (2006). Solar Driven Refrigeration Systems with Focus on the Ejector Cycle. Unpublished Doctoral Thesis, Royal Institute of Technology, KTH. Stockholm, Sweden.

Pridasawas, W. and Lundqvist, P. (2007). A year-round dynamic simulation of a solar-driven ejector refrigeration system with iso-butane as a refrigerant. *International Journal of Refrigeration,* 30(5): 840-850.

Rahman, M.H., Akhanda, A.R. and Sadrul Islam, A.K.M. (2006). Study, Design and Fabrication of a Solar Powered Adsorption Refrigeration System. *ISESCO Science and Technology Vision*, 2(1): 10-13.

Saha, B.B., El-Sharkawy, I.I., Chakraborty, A. and Koyama, S. (2007). Study on an activated carbon fiber-ethanol adsorption chiller: Part I – system description and modeling. *International Journal Refrigeration*, 30: 86-95.

Saha, B.B., El-Sharkawy, I.I., Chakraborty, A. and Koyama, S. (2007). Study on an activated carbon fiber-ethanol adsorption chiller: Part II – system description and modeling. *International Journal Refrigeration*, 30: 96-102.

Srivastava, N.C. and Eames, I.W. (1998). A review of adsobents and adsorbates in solid – vapor adsorption heat pump systems. *Applied Thermal Engineering*, 18: 707-714.

Thome, J.R. (2005). Condensation in Plain Horizontal Tubes: Recent Advances in Modeling of Heat Transfer to Pure Fluids and Mixtures. *Journal of the Brazilian Society of Mech. Sci. and Eng.,* Vol. XXVII, No1: 23-30.

Valizadeh, H. and Ashrafi, N. (1996). A continuous cycle solar thermal refrigeration system. *Renewable Energy,* 9(1-4):632-640.

Wang, L.W., Wu, J.Y., Wang, R.Z., Xu, Y.X., Wang, S.G. and Li, X.R. (2003). Study of the performance of activated carbon-methanol adsorption systems concerning heat and mass transfer. *Applied Thermal Engineering*, 23(13): 1605-1617.

Wang, L.W., Wang, R.Z., Lu, Z.S., Chen, C.J., Wang, K. and Wu, J.Y. (2006). The performance of two adsorption ice making test units using activated carbon and a carbon composite as adsorbents. *Carbon*, 44: 2671-2680.

Waszkiewicz, S., Saidani-Scott, H. and Tierney, M. (2001). Analysis of adsorption Refrigeration System using Zeolite and Methanol. Heat Powered Cycles Conference, conservatoire national des arts et métiers, Paris. 5-7th September, 2001.

Webb, R.L. and Na, B. (2003). A fundamental understanding of factors affecting frost nucleation. *International Journal of Heat and Mass Transfer*, 46(20): 3797-3808.

Wu, W-D., Zhang, H. and Sun, D-W. (2009). Mathematical Simulation and Experimental Study of a Modified Zeolite 13X-Water adsorption refrigeration module. *Applied Thermal Engineering*, 29: 645-651.

Yeung K.H. and Sumathy K. (2003). Thermodynamic analysis and optimization of a combined adsorption heating and cooling system. *International Journal of Energy Research*, 27: 1299-1315.

Zhang, X.J. and Wang, R.Z. (2002). Design and performance simulation of new solar continuous solid adsorption refrigerating and heating hybrid system. *Renewable Energy*, 27: 401-415.

APPENDIX A: Matlab Code for Adsorption Cycle Simulation

```
CLC
CLEAR ALL
CLOSE
TIC
K = 273.15;  %CONVERSION CONSTANT CELCIUS TO KELVIN
TEV = 5+K;
TCOND = 30+K;
%TGEN = 140+K;
DELT = 0.1;
%DT = DELT*2;
MAC = 1;   %MASS OF ACTIVATED CARBON IN KG
CPAC = 0.711; %SPECIFIC HEAT OF ACTIVATED CARBON [KJ/KG K]
CPML = 2.534;  %SPECIFIC HEAT OF LIQUID METHANOL [KJ/KG K]
CPM = 1.820; %SPECIFIC HEAT AT CONSTANT PRESSURE FOR METHANOL [KJ/KG K]
CVM = 1.560; %SPECIFIC HEAT AT CONSTANT VOLUME FOR METHANOL [KJ/KG K]
PCOND = T2P(TCOND);
PEV = T2P(TEV);
RUN = 83;
QE = ZEROS(RUN,1);
QTOT = ZEROS(RUN,1);
COP = ZEROS(RUN,2);
TA1 = ZEROS(RUN,1);
T1NEW = ZEROS(RUN,1);
TINT = ZEROS(RUN,1);
THRESHOLD = 0.01;
REGTEMP = 57;  %INITIAL REGENERATION TEMPERATURE
FOR I = 1:RUN
TGEN = REGTEMP+K+I;
XMIN = ADSX3_TX(TGEN);
%ASSUMING ADSORPTION TEMP (TA2) IS EQUAL TO TCOND
XMAX = ADSX1_TX(TCOND);
TG1 = ADSX2_TX(XMAX);
TA2 = ADSX4_TX(XMAX);
TA1(I) = ADSX4_TX(XMIN);
TG2 = ADSX2_TX(XMIN);
T1NEW(I) = TA2;
TINT(I) = T1NEW(I);

X1 = XMIN;
X2 = XMAX;
QIH = 0;
QDES = 0;
QSD = 0;
%HEAT REQUIRED FOR ISOSTERIC HEATING PROCESS (1->2)
QIH = QIH + MAC*(CPAC + CVM*X2)*(TG1 - TINT(I));
FOR T=TG1:DELT:(TG2 - DELT);
XB = ADSX3_TX(T);
XA = ADSX3_TX((T+DELT));
%AVERAGE HEAT OF DESORPTION FOR EACH STEP
```

```
HA = (ADSH1(T) + ADSH1(T+DELT))/2;
%HEAT OF DESORPTION PROCESS (2->3)
QDES = QDES + MAC*HA*(XB-XA);
QSD = QSD + MAC*(CPAC + CPM*(XB-XA))*DELT;
END
%THE EVAPORATION PROCESS
LEV = 1102;  %LATENT HEAT OF EVAPORATION OF METHANOL [KJ/KG]
QE(I) = MAC*(X2-X1)*(LEV - CPML*(TCOND - TEV));
QD = QDES + QSD;
QTOT(I) = QD + QIH;
COP(I,1) = TGEN-K;
COP(I,2) = QE(I)/QTOT(I);
QD = 0;
END
TOC
T = TOC/60 %#OK<NOPTS>
I = 1:RUN;
G = PLOT(COP(I,1),COP(I,2),'-R');
XLABEL('REGENERATION TEMPERATURE (\CIRCC)')
YLABEL('COP')
TITLE('ACTIVATED       CARBON-METHANOL       PAIR,       T_{EV}=5\CIRCC,
T_{COND}=30\CIRCC')
```

APPENDIX B: TRNSYS Deck File for FPC Powered Adsorption Refrigeration System

```
VERSION 16.1
*** TRNSYS INPUT FILE (DECK) GENERATED BY TRNSYSSTUDIO
*** ON TUESDAY, MARCH 29, 2011 AT 23:13
***         FROM         TRNSYSSTUDIO         PROJECT:         C:\PROGRAM
FILES\TRNSYS16_1\MYPROJECTS\PHDMJAN.TPF
***
*** IF YOU EDIT THIS FILE, USE THE FILE/IMPORT TRNSYS INPUT FILE FUNCTION
IN
*** TRNSYSSTUDIO TO UPDATE THE PROJECT.
***
*** IF YOU HAVE PROBLEMS, QUESTIONS OR SUGGESTIONS PLEASE CONTACT YOUR
LOCAL
*** TRNSYS DISTRIBUTOR OR MAILTO:SOFTWARE@CSTB.FR
***


*** UNITS

*** CONTROL CARDS
   • START, STOP AND STEP
CONSTANTS 3
START=384
STOP=408
STEP=0.25
* USER DEFINED CONSTANTS

*                              SIMULATION START TIME   END TIME    TIME
STEP
SIMULATION   START       STOP  STEP
*                              INTEGRATION  CONVERGENCE
TOLERANCES 0.001 0.001
*                              MAX ITERATIONS     MAX WARNINGS      TRACE
LIMIT
LIMITS 30 30 30
*                              TRNSYS NUMERICAL INTEGRATION SOLVER METHOD
DFQ 1
*                              TRNSYS   OUTPUT   FILE   WIDTH,   NUMBER   OF
CHARACTERS
WIDTH 80
*                              NOLIST STATEMENT
LIST
*                              MAP STATEMENT
MAP
*                              SOLVER STATEMENT  MINIMUM RELAXATION FACTOR
      MAXIMUM RELAXATION FACTOR
SOLVER 0 1 1
   • DEBUG STATEMENT
NAN_CHECK 0
```

```
OVERWRITE_CHECK 0
TIME_REPORT 0
   • EQUATION SOLVER STATEMENT
EQSOLVER 1

* MODEL “WEATHER” (TYPE 109)
*

UNIT 2 TYPE 109    WEATHER
*$UNIT_NAME WEATHER
*$MODEL     .\WEATHER     DATA     READING     AND     PROCESSING\STANDARD
FORMAT\TMY2\TYPE109-TMY2.TMF
*$POSITION 181 85
*$LAYER WEATHER / DATA FILES # WEATHER - DATA FILES #
PARAMETERS 4
* 1 DATA READER MODE
2
* 2 LOGICAL UNIT
41
* 3 SKY MODEL FOR DIFFUSE RADIATION
4
   • 4 TRACKING MODE
1
INPUTS 3
* [UNCONNECTED] GROUND REFLECTANCE
0,0
* [UNCONNECTED] SLOPE OF SURFACE
0,0
* [UNCONNECTED] AZIMUTH OF SURFACE
0,0
*** INITIAL INPUT VALUES
0.2 12 0
*** EXTERNAL FILES
ASSIGN   “C:\PROGRAM   FILES\TRNSYS16_1\WEATHER\METEONORM\AFRICA\NG-KANO-
650460.TM2” 41
*|? WEATHER DATA FILE |1000
*-------------------------------------------------------------------------

* MODEL “COLLECTORS” (TYPE 1)
*

UNIT 3 TYPE 1      COLLECTORS
*$UNIT_NAME COLLECTORS
*$MODEL  .\SOLAR  THERMAL  COLLECTORS\QUADRATIC  EFFICIENCY  COLLECTOR\2ND-
ORDER INCIDENCE ANGLE MODIFIERS\TYPE1B.TMF
*$POSITION 449 178
*$LAYER MAIN #
PARAMETERS 11
* 1 NUMBER IN SERIES
1
* 2 COLLECTOR AREA
15
* 3 FLUID SPECIFIC HEAT
4.19
* 4 EFFICIENCY MODE
2
* 5 TESTED FLOW RATE
```

```
40
* 6 INTERCEPT EFFICIENCY
0.8
* 7 EFFICIENCY SLOPE
18
* 8 EFFICIENCY CURVATURE
0.054
* 9 OPTICAL MODE 2
2
* 10 1ST-ORDER IAM
0.2
* 11 2ND-ORDER IAM
0.0
INPUTS 9
* TYPE4C:TEMPERATURE TO HEAT SOURCE ->INLET TEMPERATURE
16,1
* TYPE4C:FLOWRATE TO HEAT SOURCE ->INLET FLOWRATE
16,2
* WEATHER:AMBIENT TEMPERATURE ->AMBIENT TEMPERATURE
2,1
* WEATHER:TOTAL RADIATION ON TILTED SURFACE ->INCIDENT RADIATION
2,18
* WEATHER:TOTAL RADIATION ON HORIZONTAL ->TOTAL HORIZONTAL RADIATION
2,12
*  WEATHER:SKY  DIFFUSE  RADIATION  ON  HORIZONTAL  ->HORIZONTAL  DIFFUSE
RADIATION
2,14
* [UNCONNECTED] GROUND REFLECTANCE
0,0
* WEATHER:ANGLE OF INCIDENCE FOR TILTED SURFACE  ->INCIDENCE ANGLE
2,22
* WEATHER:SLOPE OF TILTED SURFACE ->COLLECTOR SLOPE
2,23
*** INITIAL INPUT VALUES
20 100 25 0 0 0 0.2 90 12.00
*------------------------------------------------------------------------

* MODEL “SIMULATION INTEGRATION” (TYPE 24)
*

UNIT 14 TYPE 24    SIMULATION INTEGRATION
*$UNIT_NAME SIMULATION INTEGRATION
*$MODEL .\UTILITY\INTEGRATORS\QUANTITY INTEGRATOR\TYPE24.TMF
*$POSITION 173 410
*$LAYER TOTALS #
PARAMETERS 2
* 1 INTEGRATION PERIOD
STOP
   •  2 RELATIVE OR ABSOLUTE START TIME
0
INPUTS 2
* WEATHER:TOTAL RADIATION ON TILTED SURFACE ->INPUT TO BE INTEGRATED-1
2,18
* COLLECTORS:USEFUL ENERGY GAIN ->INPUT TO BE INTEGRATED-2
3,3
*** INITIAL INPUT VALUES
0 0
```

```
*--------------------------------------------------------------------

* MODEL “PLOTTER 1” (TYPE 65)
*

UNIT 5 TYPE 65     PLOTTER 1
*$UNIT_NAME PLOTTER 1
*$MODEL    .\OUTPUT\ONLINE    PLOTTER\ONLINE    PLOTTER    WITH    FILE\NO
UNITS\TYPE65C.TMF
*$POSITION 753 114
*$LAYER OUTPUTS #
PARAMETERS 12
* 1 NB. OF LEFT-AXIS VARIABLES
4
* 2 NB. OF RIGHT-AXIS VARIABLES
2
* 3 LEFT AXIS MINIMUM
0
* 4 LEFT AXIS MAXIMUM
150
* 5 RIGHT AXIS MINIMUM
0
* 6 RIGHT AXIS MAXIMUM
10000
* 7 NUMBER OF PLOTS PER SIMULATION
1
* 8 X-AXIS GRIDPOINTS
7
* 9 SHUT OFF ONLINE W/O REMOVING
0
* 10 LOGICAL UNIT FOR OUTPUT FILE
40
* 11 OUTPUT FILE UNITS
0
   •  12 OUTPUT FILE DELIMITER
0
INPUTS 6
* TYPE4C:TEMPERATURE TO HEAT SOURCE ->LEFT AXIS VARIABLE-1
16,1
* COLLECTORS:OUTLET TEMPERATURE ->LEFT AXIS VARIABLE-2
3,1
* TYPE4C:TEMPERATURE TO LOAD ->LEFT AXIS VARIABLE-3
16,3
* WEATHER:AMBIENT TEMPERATURE ->LEFT AXIS VARIABLE-4
2,1
* WEATHER:TOTAL RADIATION ON TILTED SURFACE ->RIGHT AXIS VARIABLE-1
2,18
* COLLECTORS:OUTLET FLOWRATE ->RIGHT AXIS VARIABLE-2
3,2
*** INITIAL INPUT VALUES
TICOLL TOCOLL TSTRT TAMB GCOLL MDCOLL
LABELS  3
“TEMPERATURES”
“HEAT TRANSFER RATES”
“WEATHER - SOLAR LOOP”
*** EXTERNAL FILES
ASSIGN “***.PLT” 40
```

```
*|? WHAT FILE SHOULD THE ONLINE PRINT TO? |1000
*------------------------------------------------------------------------

* MODEL “DAILY INTEGRATION” (TYPE 24)
*

UNIT 13 TYPE 24    DAILY INTEGRATION
*$UNIT_NAME DAILY INTEGRATION
*$MODEL .\UTILITY\INTEGRATORS\QUANTITY INTEGRATOR\TYPE24.TMF
*$POSITION 170 282
*$LAYER TOTALS #
PARAMETERS 2
* 1 INTEGRATION PERIOD
24
   •  2 RELATIVE OR ABSOLUTE START TIME
0
INPUTS 2
* WEATHER:TOTAL RADIATION ON TILTED SURFACE ->INPUT TO BE INTEGRATED-1
2,18
* COLLECTORS:USEFUL ENERGY GAIN ->INPUT TO BE INTEGRATED-2
3,3
*** INITIAL INPUT VALUES
0 0
*------------------------------------------------------------------------

* MODEL “TOTALS” (TYPE 25)
*

UNIT 18 TYPE 25    TOTALS
*$UNIT_NAME TOTALS
*$MODEL .\OUTPUT\PRINTER\UNFORMATTED\NO UNITS\TYPE25C.TMF
*$POSITION 590 573
*$LAYER OUTPUTS #
PARAMETERS 10
* 1 PRINTING INTERVAL
STOP
* 2 START TIME
STOP
* 3 STOP TIME
STOP
* 4 LOGICAL UNIT
43
* 5 UNITS PRINTING MODE
0
* 6 RELATIVE OR ABSOLUTE START TIME
0
* 7 OVERWRITE OR APPEND
-1
* 8 PRINT HEADER
-1
* 9 DELIMITER
0
   •  10 PRINT LABELS
1
INPUTS 3
* SIMULATION INTEGRATION:RESULT OF INTEGRATION-1 ->INPUT TO BE PRINTED-1
14,1
```

```
* SIMULATION INTEGRATION:RESULT OF INTEGRATION-2 ->INPUT TO BE PRINTED-2
14,2
* EFFICIENCIES:ETACOLL ->INPUT TO BE PRINTED-3
ETACOLL
*** INITIAL INPUT VALUES
ICOLL QUCOLL ETACOLL
*** EXTERNAL FILES
ASSIGN "TOTALS.TXT" 43
*|? OUTPUT FILE FOR PRINTED RESULTS |1000
*------------------------------------------------------------------------

* EQUATIONS "EFFICIENCIES"
*
EQUATIONS 3
ETACOLL_D = [13,2]/(15*[13,1]+1E-6)
ETACOLL = [14,2]/(15*[14,1]+1E-6)
NEW = TIME/(TIME-START-8765)
*$UNIT_NAME EFFICIENCIES
*$LAYER MAIN
*$POSITION 369 477

*------------------------------------------------------------------------


* MODEL "DAILY RESULTS" (TYPE 25)
*

UNIT 15 TYPE 25    DAILY RESULTS
*$UNIT_NAME DAILY RESULTS
*$MODEL .\OUTPUT\PRINTER\UNFORMATTED\NO UNITS\TYPE25C.TMF
*$POSITION 628 488
*$LAYER OUTPUTS #
PARAMETERS 10
* 1 PRINTING INTERVAL
24
* 2 START TIME
START
* 3 STOP TIME
STOP
* 4 LOGICAL UNIT
42
* 5 UNITS PRINTING MODE
0
* 6 RELATIVE OR ABSOLUTE START TIME
0
* 7 OVERWRITE OR APPEND
-1
* 8 PRINT HEADER
-1
* 9 DELIMITER
0
   • 10 PRINT LABELS
1
INPUTS 3
* DAILY INTEGRATION:RESULT OF INTEGRATION-1 ->INPUT TO BE PRINTED-1
13,1
* DAILY INTEGRATION:RESULT OF INTEGRATION-2 ->INPUT TO BE PRINTED-2
```

```
13,2
* EFFICIENCIES:ETACOLL_D ->INPUT TO BE PRINTED-3
ETACOLL_D
*** INITIAL INPUT VALUES
ICOLL QUCOLL ETACOLL_D
*** EXTERNAL FILES
ASSIGN “DAILY.TXT” 42
*|? OUTPUT FILE FOR PRINTED RESULTS |1000
*-----------------------------------------------------------------------

* MODEL “ADSORPTION PARAMETERS” (TYPE 25)
*

UNIT 11 TYPE 25    ADSORPTION PARAMETERS
*$UNIT_NAME ADSORPTION PARAMETERS
*$MODEL .\OUTPUT\PRINTER\UNFORMATTED\NO UNITS\TYPE25C.TMF
*$POSITION 772 349
*$LAYER OUTPUTS #
PARAMETERS 10
* 1 PRINTING INTERVAL
STEP
* 2 START TIME
START
* 3 STOP TIME
STOP
* 4 LOGICAL UNIT
45
* 5 UNITS PRINTING MODE
0
* 6 RELATIVE OR ABSOLUTE START TIME
0
* 7 OVERWRITE OR APPEND
-1
* 8 PRINT HEADER
-1
* 9 DELIMITER
0
   • 10 PRINT LABELS
1
INPUTS 12
* TYPE155:OUTPUT-1 ->INPUT TO BE PRINTED-1
12,1
* TYPE155:OUTPUT-2 ->INPUT TO BE PRINTED-2
12,2
* TYPE155:OUTPUT-3 ->INPUT TO BE PRINTED-3
12,3
* TYPE155:OUTPUT-4 ->INPUT TO BE PRINTED-4
12,4
* TYPE155:OUTPUT-5 ->INPUT TO BE PRINTED-5
12,5
* TYPE155:OUTPUT-6 ->INPUT TO BE PRINTED-6
12,6
* TYPE155:OUTPUT-7 ->INPUT TO BE PRINTED-7
12,7
* TYPE155:OUTPUT-8 ->INPUT TO BE PRINTED-8
12,8
* TYPE155:OUTPUT-9 ->INPUT TO BE PRINTED-9
```

```
12,9
* TYPE155:OUTPUT-10 ->INPUT TO BE PRINTED-10
12,10
* TYPE155:OUTPUT-11 ->INPUT TO BE PRINTED-11
12,11
* TYPE155:OUTPUT-12 ->INPUT TO BE PRINTED-12
12,12
*** INITIAL INPUT VALUES
TGEN TG1 TG2 TA1 TA2 XMAX XMIN QE QTOT COP1 QTOT1 COP
*** EXTERNAL FILES
ASSIGN "***.TXT" 45
*|? OUTPUT FILE FOR PRINTED RESULTS |1000
*------------------------------------------------------------------------

* MODEL "TYPE155" (TYPE 155)
*

UNIT 12 TYPE 155   TYPE155
*$UNIT_NAME TYPE155
*$MODEL .\UTILITY\CALLING EXTERNAL PROGRAMS\MATLAB\TYPE155.TMF
*$POSITION 658 244
*$LAYER MAIN #
PARAMETERS 5
* 1 MODE
0
* 2 NUMBER OF INPUTS
3
* 3 NUMBER OF OUTPUTS
12
* 4 CALLING MODE
0
   • 5 KEEP MATLAB OPEN AFTER SIMULATION
1
INPUTS 3
* TYPE4C:TEMPERATURE TO LOAD ->INPUT-1
16,3
* [UNCONNECTED] INPUT-2
0,0
* TYPE4C:FLOWRATE TO LOAD ->INPUT-3
16,4
*** INITIAL INPUT VALUES
0 0 0
LABELS 1
"ADSORPTIONUNIT.M"
*------------------------------------------------------------------------

* MODEL "TYPE4C" (TYPE 4)
*

UNIT 16 TYPE 4     TYPE4C
*$UNIT_NAME TYPE4C
*$MODEL .\THERMAL STORAGE\STRATIFIED STORAGE TANK\VARIABLE INLETS\UNIFORM
LOSSES\TYPE4C.TMF
*$POSITION 538 264
*$LAYER WATER LOOP #
PARAMETERS 25
* 1 VARIABLE INLET POSITIONS
```

```
2
* 2 TANK VOLUME
1
* 3 FLUID SPECIFIC HEAT
4.190
* 4 FLUID DENSITY
1000.0
* 5 TANK LOSS COEFFICIENT
0
* 6 HEIGHT OF NODE-1
0.3
* 7 HEIGHT OF NODE-2
0.3
* 8 HEIGHT OF NODE-3
0.3
* 9 HEIGHT OF NODE-4
0.3
* 10 HEIGHT OF NODE-5
0.3
* 11 HEIGHT OF NODE-6
0.3
* 12 AUXILIARY HEATER MODE
1
* 13 NODE CONTAINING HEATING ELEMENT -1
1
* 14 NODE CONTAINING THERMOSTAT -1
1
* 15 SET POINT TEMPERATURE FOR ELEMENT-1
60.0
* 16 DEADBAND FOR HEATING ELEMENT-1
5.0
* 17 MAXIMUM HEATING RATE OF ELEMENT -1
0
* 18 NODE CONTAINING HEATING ELEMENT -2
1
* 19 NODE CONTAINING THERMOSTAT -2
1
* 20 SET POINT TEMPERATURE FOR ELEMENT-2
60.0
* 21 DEADBAND FOR HEATING ELEMENT-2
5.0
* 22 MAXIMUM HEATING RATE OF ELEMENT -2
0
* 23 NOT USED (FLUE UA)
0.0
* 24 NOT USED (TFLUE)
20.0
* 25 BOILING POINT
150.0
INPUTS 7
* COLLECTORS:OUTLET TEMPERATURE ->HOT-SIDE TEMPERATURE
3,1
* COLLECTORS:OUTLET FLOWRATE ->HOT-SIDE FLOWRATE
3,2
* [UNCONNECTED] COLD-SIDE TEMPERATURE
0,0
* [UNCONNECTED] COLD-SIDE FLOWRATE
```

```
0,0
* WEATHER:AMBIENT TEMPERATURE ->ENVIRONMENT TEMPERATURE
2,1
* [UNCONNECTED] CONTROL SIGNAL FOR ELEMENT-1
0,0
* [UNCONNECTED] CONTROL SIGNAL FOR ELEMENT-2
0,0
*** INITIAL INPUT VALUES
0 0 25.0 0 0 0.0 0.0
DERIVATIVES 6
* 1 INITIAL TEMPERATURE OF NODE-1
25
* 2 INITIAL TEMPERATURE OF NODE-2
25
* 3 INITIAL TEMPERATURE OF NODE-3
25
* 4 INITIAL TEMPERATURE OF NODE-4
25
* 5 INITIAL TEMPERATURE OF NODE-5
25
* 6 INITIAL TEMPERATURE OF NODE-6
25
*-------------------------------------------------------------------

END
```

APPENDIX C: TRNSYS Deck File for ETC Powered Adsorption Refrigeration System

```
VERSION 16.1
**********************************************************************
******
*** TRNSYS INPUT FILE (DECK) GENERATED BY TRNSYSSTUDIO
*** ON WEDNESDAY, MARCH 30, 2011 AT 18:46
***         FROM         TRNSYSSTUDIO         PROJECT:         C:\PROGRAM
FILES\TRNSYS16_1\MYPROJECTS\PHDM1JAN.TPF
***
*** IF YOU EDIT THIS FILE, USE THE FILE/IMPORT TRNSYS INPUT FILE FUNCTION
IN
*** TRNSYSSTUDIO TO UPDATE THE PROJECT.
***
*** IF YOU HAVE PROBLEMS, QUESTIONS OR SUGGESTIONS PLEASE CONTACT YOUR
LOCAL
*** TRNSYS DISTRIBUTOR OR MAILTO:SOFTWARE@CSTB.FR
***
**********************************************************************
******


**********************************************************************
******
*** UNITS
**********************************************************************
******

**********************************************************************
******
*** CONTROL CARDS
**********************************************************************
******
* START, STOP AND STEP
CONSTANTS 3
START=384
STOP=408
STEP=0.25
* USER DEFINED CONSTANTS

*                            SIMULATION START TIME   END TIME    TIME
STEP
SIMULATION   START       STOP  STEP
*                                 INTEGRATION  CONVERGENCE
TOLERANCES 0.001 0.001
*                            MAX ITERATIONS     MAX WARNINGS      TRACE
LIMIT
LIMITS 30 30 30
*                            TRNSYS NUMERICAL INTEGRATION SOLVER METHOD
DFQ 1
*                            TRNSYS   OUTPUT   FILE   WIDTH,   NUMBER   OF
CHARACTERS
```

```
WIDTH 80
*                               NOLIST STATEMENT
LIST
*                               MAP STATEMENT
MAP
*                               SOLVER STATEMENT  MINIMUM  RELAXATION  FACTOR
      MAXIMUM RELAXATION FACTOR
SOLVER 0 1 1
*                               DEBUG STATEMENT
NAN_CHECK 0
OVERWRITE_CHECK 0
TIME_REPORT 0
*                               EQUATION SOLVER STATEMENT
EQSOLVER 1

* MODEL "WEATHER" (TYPE 109)
*

UNIT 2 TYPE 109    WEATHER
*$UNIT_NAME WEATHER
*$MODEL     .\WEATHER     DATA     READING     AND     PROCESSING\STANDARD
FORMAT\TMY2\TYPE109-TMY2.TMF
*$POSITION 181 85
*$LAYER WEATHER / DATA FILES # WEATHER - DATA FILES #
PARAMETERS 4
* 1 DATA READER MODE
2
* 2 LOGICAL UNIT
41
* 3 SKY MODEL FOR DIFFUSE RADIATION
4
* 4 TRACKING MODE
1
INPUTS 3
* [UNCONNECTED] GROUND REFLECTANCE
0,0
* [UNCONNECTED] SLOPE OF SURFACE
0,0
* [UNCONNECTED] AZIMUTH OF SURFACE
0,0
*** INITIAL INPUT VALUES
0.2 12 0
*** EXTERNAL FILES
ASSIGN    "C:\PROGRAM    FILES\TRNSYS16_1\WEATHER\METEONORM\AFRICA\NG-KANO-
650460.TM2" 41
*|? WEATHER DATA FILE |1000
*------------------------------------------------------------------------

* MODEL "COLLECTORS" (TYPE 71)
*

UNIT 3 TYPE 71     COLLECTORS
*$UNIT_NAME COLLECTORS
*$MODEL .\SOLAR THERMAL COLLECTORS\EVACUATED TUBE COLLECTOR\TYPE71.TMF
*$POSITION 449 178
*$LAYER MAIN #
PARAMETERS 11
```

```
* 1 NUMBER IN SERIES
1
* 2 COLLECTOR AREA
15
* 3 FLUID SPECIFIC HEAT
4.19
* 4 EFFICIENCY MODE
1
* 5 FLOW RATE AT TEST CONDITIONS
39.96
* 6 INTERCEPT EFFICIENCY
0.8
* 7 NEGATIVE OF FIRST ORDER EFFICIENCY COEFICIENT
5.4
* 8 NEGATIVE OF SECOND ORDER EFFICIENCY COEFICIENT
0.0288
* 9 LOGICAL UNIT OF FILE CONTAINING BIAXIAL IAM DATA
45
* 10 NUMBER OF LONGITUDINAL ANGLES FOR WHICH IAMS ARE PROVIDED
5
* 11 NUMBER OF TRANSVERSE ANGLES FOR WHICH IAMS ARE PROVIDED
5
INPUTS 10
* TYPE4C:TEMPERATURE TO HEAT SOURCE ->INLET TEMPERATURE
16,1
* TYPE4C:FLOWRATE TO HEAT SOURCE ->INLET FLOWRATE
16,2
* WEATHER:AMBIENT TEMPERATURE ->AMBIENT TEMPERATURE
2,1
* WEATHER:TOTAL RADIATION ON TILTED SURFACE ->INCIDENT RADIATION
2,18
* [UNCONNECTED] INCIDENT DIFFUSE RADIATION
0,0
* [UNCONNECTED] SOLAR INCIDENCE ANGLE
0,0
* [UNCONNECTED] SOLAR ZENITH ANGLE
0,0
* [UNCONNECTED] SOLAR AZIMUTH ANGLE
0,0
* WEATHER:SLOPE OF TILTED SURFACE ->COLLECTOR SLOPE
2,23
* [UNCONNECTED] COLLECTOR AZIMUTH
0,0
*** INITIAL INPUT VALUES
20 100 25 0 0.0 0.0 0.0 0.0 30 0.0
*** EXTERNAL FILES
ASSIGN  "C:\PROGRAM  FILES\TRNSYS16_1\TESS  MODELS\SAMPLECATALOGDATA\BI-
AXIAL IAMS\IAM_2D.DAT" 45
*|? WHAT FILE CONTAINS THE 2D IAM DATA? |1000
*-------------------------------------------------------------------------

* MODEL "SIMULATION INTEGRATION" (TYPE 24)
*

UNIT 14 TYPE 24    SIMULATION INTEGRATION
*$UNIT_NAME SIMULATION INTEGRATION
*$MODEL .\UTILITY\INTEGRATORS\QUANTITY INTEGRATOR\TYPE24.TMF
```

```
*$POSITION 173 410
*$LAYER TOTALS #
PARAMETERS 2
* 1 INTEGRATION PERIOD
STOP
* 2 RELATIVE OR ABSOLUTE START TIME
0
INPUTS 2
* WEATHER:TOTAL RADIATION ON TILTED SURFACE ->INPUT TO BE INTEGRATED-1
2,18
* COLLECTORS:USEFUL ENERGY GAIN ->INPUT TO BE INTEGRATED-2
3,3
*** INITIAL INPUT VALUES
0 0
*------------------------------------------------------------------------

* MODEL "PLOTTER 1" (TYPE 65)
*

UNIT 5 TYPE 65     PLOTTER 1
*$UNIT_NAME PLOTTER 1
*$MODEL    .\OUTPUT\ONLINE    PLOTTER\ONLINE    PLOTTER    WITH    FILE\NO
UNITS\TYPE65C.TMF
*$POSITION 753 114
*$LAYER OUTPUTS #
PARAMETERS 12
* 1 NB. OF LEFT-AXIS VARIABLES
4
* 2 NB. OF RIGHT-AXIS VARIABLES
2
* 3 LEFT AXIS MINIMUM
0
* 4 LEFT AXIS MAXIMUM
150
* 5 RIGHT AXIS MINIMUM
0
* 6 RIGHT AXIS MAXIMUM
10000
* 7 NUMBER OF PLOTS PER SIMULATION
1
* 8 X-AXIS GRIDPOINTS
7
* 9 SHUT OFF ONLINE W/O REMOVING
0
* 10 LOGICAL UNIT FOR OUTPUT FILE
40
* 11 OUTPUT FILE UNITS
0
* 12 OUTPUT FILE DELIMITER
0
INPUTS 6
* TYPE4C:TEMPERATURE TO HEAT SOURCE ->LEFT AXIS VARIABLE-1
16,1
* COLLECTORS:OUTLET TEMPERATURE ->LEFT AXIS VARIABLE-2
3,1
* TYPE4C:TEMPERATURE TO LOAD ->LEFT AXIS VARIABLE-3
16,3
```

```
* WEATHER:AMBIENT TEMPERATURE ->LEFT AXIS VARIABLE-4
2,1
* WEATHER:TOTAL RADIATION ON TILTED SURFACE ->RIGHT AXIS VARIABLE-1
2,18
* COLLECTORS:OUTLET FLOWRATE ->RIGHT AXIS VARIABLE-2
3,2
*** INITIAL INPUT VALUES
TICOLL TOCOLL TSTRT TAMB GCOLL MDCOLL
LABELS  3
"TEMPERATURES"
"HEAT TRANSFER RATES"
"WEATHER - SOLAR LOOP"
*** EXTERNAL FILES
ASSIGN "***.PLT" 40
*|? WHAT FILE SHOULD THE ONLINE PRINT TO? |1000
*-------------------------------------------------------------------

* MODEL "DAILY INTEGRATION" (TYPE 24)
*

UNIT 13 TYPE 24    DAILY INTEGRATION
*$UNIT_NAME DAILY INTEGRATION
*$MODEL .\UTILITY\INTEGRATORS\QUANTITY INTEGRATOR\TYPE24.TMF
*$POSITION 170 282
*$LAYER TOTALS #
PARAMETERS 2
* 1 INTEGRATION PERIOD
24
* 2 RELATIVE OR ABSOLUTE START TIME
0
INPUTS 2
* WEATHER:TOTAL RADIATION ON TILTED SURFACE ->INPUT TO BE INTEGRATED-1
2,18
* COLLECTORS:USEFUL ENERGY GAIN ->INPUT TO BE INTEGRATED-2
3,3
*** INITIAL INPUT VALUES
0 0
*-------------------------------------------------------------------

* MODEL "TOTALS" (TYPE 25)
*

UNIT 18 TYPE 25    TOTALS
*$UNIT_NAME TOTALS
*$MODEL .\OUTPUT\PRINTER\UNFORMATTED\NO UNITS\TYPE25C.TMF
*$POSITION 643 626
*$LAYER OUTPUTS #
PARAMETERS 10
* 1 PRINTING INTERVAL
STOP
* 2 START TIME
STOP
* 3 STOP TIME
STOP
* 4 LOGICAL UNIT
43
* 5 UNITS PRINTING MODE
```

```
0
* 6 RELATIVE OR ABSOLUTE START TIME
0
* 7 OVERWRITE OR APPEND
-1
* 8 PRINT HEADER
-1
* 9 DELIMITER
0
* 10 PRINT LABELS
1
INPUTS 3
* SIMULATION INTEGRATION:RESULT OF INTEGRATION-1 ->INPUT TO BE PRINTED-1
14,1
* SIMULATION INTEGRATION:RESULT OF INTEGRATION-2 ->INPUT TO BE PRINTED-2
14,2
* EFFICIENCIES:ETACOLL ->INPUT TO BE PRINTED-3
ETACOLL
*** INITIAL INPUT VALUES
ICOLL QUCOLL ETACOLL
*** EXTERNAL FILES
ASSIGN "TOTALS.TXT" 43
*|? OUTPUT FILE FOR PRINTED RESULTS |1000
*------------------------------------------------------------------------

* EQUATIONS "EFFICIENCIES"
*
EQUATIONS 3
ETACOLL_D = [13,2]/(15*[13,1]+1E-6)
ETACOLL = [14,2]/(15*[14,1]+1E-6)
NEW = TIME/(TIME-START-8765)
*$UNIT_NAME EFFICIENCIES
*$LAYER MAIN
*$POSITION 389 530

*------------------------------------------------------------------------


* MODEL "DAILY RESULTS" (TYPE 25)
*

UNIT 15 TYPE 25    DAILY RESULTS
*$UNIT_NAME DAILY RESULTS
*$MODEL .\OUTPUT\PRINTER\UNFORMATTED\NO UNITS\TYPE25C.TMF
*$POSITION 650 498
*$LAYER OUTPUTS #
PARAMETERS 10
* 1 PRINTING INTERVAL
24
* 2 START TIME
START
* 3 STOP TIME
STOP
* 4 LOGICAL UNIT
42
* 5 UNITS PRINTING MODE
0
```

```
* 6 RELATIVE OR ABSOLUTE START TIME
0
* 7 OVERWRITE OR APPEND
-1
* 8 PRINT HEADER
-1
* 9 DELIMITER
0
* 10 PRINT LABELS
1
INPUTS 3
* DAILY INTEGRATION:RESULT OF INTEGRATION-1 ->INPUT TO BE PRINTED-1
13,1
* DAILY INTEGRATION:RESULT OF INTEGRATION-2 ->INPUT TO BE PRINTED-2
13,2
* EFFICIENCIES:ETACOLL_D ->INPUT TO BE PRINTED-3
ETACOLL_D
*** INITIAL INPUT VALUES
ICOLL QUCOLL ETACOLL_D
*** EXTERNAL FILES
ASSIGN "DAILY.TXT" 42
*|? OUTPUT FILE FOR PRINTED RESULTS |1000
*-------------------------------------------------------------------

* MODEL "ADSORPTION PARAMETERS" (TYPE 25)
*

UNIT 11 TYPE 25    ADSORPTION PARAMETERS
*$UNIT_NAME ADSORPTION PARAMETERS
*$MODEL .\OUTPUT\PRINTER\UNFORMATTED\NO UNITS\TYPE25C.TMF
*$POSITION 814 477
*$LAYER OUTPUTS #
PARAMETERS 10
* 1 PRINTING INTERVAL
STEP
* 2 START TIME
START
* 3 STOP TIME
STOP
* 4 LOGICAL UNIT
46
* 5 UNITS PRINTING MODE
0
* 6 RELATIVE OR ABSOLUTE START TIME
0
* 7 OVERWRITE OR APPEND
-1
* 8 PRINT HEADER
-1
* 9 DELIMITER
0
* 10 PRINT LABELS
1
INPUTS 12
* TYPE155:OUTPUT-1 ->INPUT TO BE PRINTED-1
12,1
* TYPE155:OUTPUT-2 ->INPUT TO BE PRINTED-2
```

```
12,2
* TYPE155:OUTPUT-3 ->INPUT TO BE PRINTED-3
12,3
* TYPE155:OUTPUT-4 ->INPUT TO BE PRINTED-4
12,4
* TYPE155:OUTPUT-5 ->INPUT TO BE PRINTED-5
12,5
* TYPE155:OUTPUT-6 ->INPUT TO BE PRINTED-6
12,6
* TYPE155:OUTPUT-7 ->INPUT TO BE PRINTED-7
12,7
* TYPE155:OUTPUT-8 ->INPUT TO BE PRINTED-8
12,8
* TYPE155:OUTPUT-9 ->INPUT TO BE PRINTED-9
12,9
* TYPE155:OUTPUT-10 ->INPUT TO BE PRINTED-10
12,10
* TYPE155:OUTPUT-11 ->INPUT TO BE PRINTED-11
12,11
* TYPE155:OUTPUT-12 ->INPUT TO BE PRINTED-12
12,12
*** INITIAL INPUT VALUES
TGEN TG1 TG2 TA1 TA2 XMAX XMIN QE QTOT COP1 QTOT1 COP
*** EXTERNAL FILES
ASSIGN "***.TXT" 46
*|? OUTPUT FILE FOR PRINTED RESULTS |1000
*-------------------------------------------------------------------------

* MODEL "TYPE155" (TYPE 155)
*

UNIT 12 TYPE 155   TYPE155
*$UNIT_NAME TYPE155
*$MODEL .\UTILITY\CALLING EXTERNAL PROGRAMS\MATLAB\TYPE155.TMF
*$POSITION 669 308
*$LAYER MAIN #
PARAMETERS 5
* 1 MODE
0
* 2 NUMBER OF INPUTS
3
* 3 NUMBER OF OUTPUTS
12
* 4 CALLING MODE
0
* 5 KEEP MATLAB OPEN AFTER SIMULATION
1
INPUTS 3
* TYPE4C:TEMPERATURE TO LOAD ->INPUT-1
16,3
* TYPE4C:ENERGY RATE TO LOAD ->INPUT-2
16,6
* TYPE4C:FLOWRATE TO LOAD ->INPUT-3
16,4
*** INITIAL INPUT VALUES
0 0 0
LABELS 1
```

```
"ADSORPTIONUNIT.M"
*-------------------------------------------------------------------

* MODEL "TYPE4C" (TYPE 4)
*

UNIT 16 TYPE 4     TYPE4C
*$UNIT_NAME TYPE4C
*$MODEL .\THERMAL STORAGE\STRATIFIED STORAGE TANK\VARIABLE INLETS\UNIFORM
LOSSES\TYPE4C.TMF
*$POSITION 538 264
*$LAYER WATER LOOP #
PARAMETERS 25
* 1 VARIABLE INLET POSITIONS
2
* 2 TANK VOLUME
1
* 3 FLUID SPECIFIC HEAT
4.190
* 4 FLUID DENSITY
1000.0
* 5 TANK LOSS COEFFICIENT
2.5
* 6 HEIGHT OF NODE-1
0.3
* 7 HEIGHT OF NODE-2
0.3
* 8 HEIGHT OF NODE-3
0.3
* 9 HEIGHT OF NODE-4
0.3
* 10 HEIGHT OF NODE-5
0.3
* 11 HEIGHT OF NODE-6
0.3
* 12 AUXILIARY HEATER MODE
1
* 13 NODE CONTAINING HEATING ELEMENT -1
1
* 14 NODE CONTAINING THERMOSTAT -1
1
* 15 SET POINT TEMPERATURE FOR ELEMENT-1
60.0
* 16 DEADBAND FOR HEATING ELEMENT-1
5.0
* 17 MAXIMUM HEATING RATE OF ELEMENT -1
0
* 18 NODE CONTAINING HEATING ELEMENT -2
1
* 19 NODE CONTAINING THERMOSTAT -2
1
* 20 SET POINT TEMPERATURE FOR ELEMENT-2
60.0
* 21 DEADBAND FOR HEATING ELEMENT-2
5.0
* 22 MAXIMUM HEATING RATE OF ELEMENT -2
0
```

```
* 23 NOT USED (FLUE UA)
0.0
* 24 NOT USED (TFLUE)
20.0
* 25 BOILING POINT
150
INPUTS 7
* COLLECTORS:OUTLET TEMPERATURE ->HOT-SIDE TEMPERATURE
3,1
* COLLECTORS:OUTLET FLOWRATE ->HOT-SIDE FLOWRATE
3,2
* [UNCONNECTED] COLD-SIDE TEMPERATURE
0,0
* [UNCONNECTED] COLD-SIDE FLOWRATE
0,0
* WEATHER:AMBIENT TEMPERATURE ->ENVIRONMENT TEMPERATURE
2,1
* [UNCONNECTED] CONTROL SIGNAL FOR ELEMENT-1
0,0
* [UNCONNECTED] CONTROL SIGNAL FOR ELEMENT-2
0,0
*** INITIAL INPUT VALUES
0 0 25.0 0 0 0.0 0.0
DERIVATIVES 6
* 1 INITIAL TEMPERATURE OF NODE-1
25
* 2 INITIAL TEMPERATURE OF NODE-2
25
* 3 INITIAL TEMPERATURE OF NODE-3
25
* 4 INITIAL TEMPERATURE OF NODE-4
25
* 5 INITIAL TEMPERATURE OF NODE-5
25
* 6 INITIAL TEMPERATURE OF NODE-6
25
*-------------------------------------------------------------------------

END
```

APPENDIX D: TRNSYS Deck File for PTC Powered Adsorption Refrigeration System

```
VERSION 16.1
*** TRNSYS INPUT FILE (DECK) GENERATED BY TRNSYSSTUDIO
*** ON MONDAY, APRIL 04, 2011 AT 17:16
***         FROM         TRNSYSSTUDIO         PROJECT:         C:\PROGRAM
FILES\TRNSYS16_1\MYPROJECTS\PHDM2JAN.TPF
***
*** IF YOU EDIT THIS FILE, USE THE FILE/IMPORT TRNSYS INPUT FILE FUNCTION
IN
*** TRNSYSSTUDIO TO UPDATE THE PROJECT.
***
*** IF YOU HAVE PROBLEMS, QUESTIONS OR SUGGESTIONS PLEASE CONTACT YOUR
LOCAL
*** TRNSYS DISTRIBUTOR OR MAILTO:SOFTWARE@CSTB.FR
***


*** UNITS

*** CONTROL CARDS
   • START, STOP AND STEP
CONSTANTS 3
START=384
STOP=408
STEP=0.25
* USER DEFINED CONSTANTS

*                              SIMULATION START TIME   END TIME    TIME
STEP
SIMULATION   START       STOP  STEP
*                              INTEGRATION  CONVERGENCE
TOLERANCES 0.001 0.001
*                              MAX ITERATIONS     MAX WARNINGS      TRACE
LIMIT
LIMITS 30 30 30
*                              TRNSYS NUMERICAL INTEGRATION SOLVER METHOD
DFQ 1
*                              TRNSYS   OUTPUT   FILE   WIDTH,   NUMBER   OF
CHARACTERS
WIDTH 80
*                              NOLIST STATEMENT
LIST
*                              MAP STATEMENT
MAP
*                              SOLVER STATEMENT  MINIMUM RELAXATION FACTOR
      MAXIMUM RELAXATION FACTOR
SOLVER 0 1 1
   • DEBUG STATEMENT
NAN_CHECK 0
OVERWRITE_CHECK 0
```

```
TIME_REPORT 0
   •  EQUATION SOLVER STATEMENT
EQSOLVER 1

* MODEL “WEATHER” (TYPE 16)
*

UNIT 2 TYPE 16     WEATHER
*$UNIT_NAME WEATHER
*$MODEL  .\PHYSICAL  PHENOMENA\RADIATION  PROCESSORS\TOTAL  HORIZ,  DIRECT
NORMAL KNOWN (MODE=4)\TYPE16G.TMF
*$POSITION 181 85
*$LAYER WEATHER / DATA FILES # WEATHER - DATA FILES #
PARAMETERS 9
* 1 HORIZ. RADIATION MODE
4
* 2 TRACKING MODE
2
* 3 TILTED SURFACE MODE
2
* 4 STARTING DAY
384
* 5 LATITUDE
12.05
* 6 SOLAR CONSTANT
4871
* 7 SHIFT IN SOLAR TIME
-6.47
* 8 NOT USED
2
   •  9 SOLAR TIME?
1
INPUTS 7
*  TYPE89B:GLOBAL  HORIZONTAL  RADIATION  ->TOTAL  RADIATION  ON  HORIZONTAL
SURFACE
11,4
* TYPE89B:DIRECT NORMAL RADIATION ->DIRECT NORMAL BEAM RADIATION
11,3
* TYPE89B:TIME OF LAST READ ->TIME OF LAST DATA READ
11,99
* TYPE89B:TIME OF NEXT READ ->TIME OF NEXT DATA READ
11,100
* [UNCONNECTED] GROUND REFLECTANCE
0,0
* [UNCONNECTED] SLOPE OF SURFACE
0,0
* [UNCONNECTED] AZIMUTH OF SURFACE
0,0
*** INITIAL INPUT VALUES
0 0 0 0 0.2 12.05 0
*-------------------------------------------------------------------------

* MODEL “COLLECTORS” (TYPE 536)
*

UNIT 3 TYPE 536    COLLECTORS
*$UNIT_NAME COLLECTORS
```

```
*$MODEL    \PROGRAM    FILES\TRNSYS16_1\STUDIO\PROFORMAS\SOLAR    LIBRARY
(TESS)\LINEAR PARABOLIC CONCENTRATOR\TYPE536.TMF
*$POSITION 520 166
*$LAYER MAIN #
*$# THE LINEAR PARABOLIC CONCENTRATOR MODEL IS BASED ON EQUATIONS TAKEN
FROM DUFFIE AND BECKMAN'S
*$# "SOLAR ENGINEERING OF THERMAL PROCESSES"
*$#
*$#
*$#
*$#
*$#
PARAMETERS 10
* 1 NUMBER OF COLLECTORS IN SERIES
1
* 2 NUMBER OF COLLECTORS IN PARALLEL
6
* 3 APERTURE AREA
2.3
* 4 CONCENTRATION RATIO
14.375
* 5 INTERCEPT EFFICIENCY (FRTAN)
0.762
* 6 EFFICIENCY SLOPE (FRUL)
0.765
* 7 FLUID SPECIFIC HEAT
4.19
* 8 LOGICAL UNIT
44
* 9 NUMBER OF IAM POINTS
2
   • 10 TESTED FLOW RATE
54
INPUTS 6
* TANK:TEMPERATURE TO HEAT SOURCE ->INLET TEMPERATURE
7,1
* TANK:FLOWRATE TO HEAT SOURCE ->INLET FLOW RATE
7,2
* [UNCONNECTED] AMBIENT TEMPERATURE
0,0
* WEATHER:BEAM RADIATION ON SURFACE 1 ->INCIDENT BEAM RADIATION
2,8
* WEATHER:INCIDENCE ANGLE FOR SURFACE 1 ->INCIDENCE ANGLE
2,10
* [UNCONNECTED] MAXIMUM OUTLET TEMPERATURE
0,0
*** INITIAL INPUT VALUES
20 54 25 0. 0 150
*** EXTERNAL FILES
ASSIGN "C:\PROGRAM FILES\TRNSYS16_1\TESS MODELS\SAMPLECATALOGDATA\SINGLE-
AXIS IAM'S\IAM_1D.DAT" 44
*|? WHICH FILE CONTAINS THE INCIDENCE ANGLE MODIFIERS? |1000
*-------------------------------------------------------------------------

* MODEL "SIMULATION INTEGRATION" (TYPE 24)
*
```

```
UNIT 14 TYPE 24    SIMULATION INTEGRATION
*$UNIT_NAME SIMULATION INTEGRATION
*$MODEL .\UTILITY\INTEGRATORS\QUANTITY INTEGRATOR\TYPE24.TMF
*$POSITION 173 410
*$LAYER TOTALS #
PARAMETERS 2
* 1 INTEGRATION PERIOD
STOP
   •  2 RELATIVE OR ABSOLUTE START TIME
0
INPUTS 3
* WEATHER:BEAM RADIATION ON SURFACE 1 ->INPUT TO BE INTEGRATED-1
2,8
* COLLECTORS:USEFUL ENERGY GAIN ->INPUT TO BE INTEGRATED-2
3,3
* COLLECTORS:DUMPED ENERGY ->INPUT TO BE INTEGRATED-3
3,4
*** INITIAL INPUT VALUES
0 0 0
*-------------------------------------------------------------------------

* MODEL “PLOTTER 1” (TYPE 65)
*

UNIT 5 TYPE 65     PLOTTER 1
*$UNIT_NAME PLOTTER 1
*$MODEL    .\OUTPUT\ONLINE    PLOTTER\ONLINE    PLOTTER    WITH    FILE\NO
UNITS\TYPE65C.TMF
*$POSITION 723 200
*$LAYER OUTPUTS #
PARAMETERS 12
* 1 NB. OF LEFT-AXIS VARIABLES
4
* 2 NB. OF RIGHT-AXIS VARIABLES
2
* 3 LEFT AXIS MINIMUM
0
* 4 LEFT AXIS MAXIMUM
150
* 5 RIGHT AXIS MINIMUM
0
* 6 RIGHT AXIS MAXIMUM
10000
* 7 NUMBER OF PLOTS PER SIMULATION
1
* 8 X-AXIS GRIDPOINTS
7
* 9 SHUT OFF ONLINE W/O REMOVING
0
* 10 LOGICAL UNIT FOR OUTPUT FILE
40
* 11 OUTPUT FILE UNITS
0
   •  12 OUTPUT FILE DELIMITER
0
INPUTS 6
* TANK:TEMPERATURE TO HEAT SOURCE ->LEFT AXIS VARIABLE-1
```

```
7,1
* COLLECTORS:OUTLET TEMPERATURE ->LEFT AXIS VARIABLE-2
3,1
* TANK:TEMPERATURE TO LOAD ->LEFT AXIS VARIABLE-3
7,3
* TYPE89B:DRY BULB AT NEXT TIMESTEP ->LEFT AXIS VARIABLE-4
11,105
* WEATHER:BEAM RADIATION ON SURFACE 1 ->RIGHT AXIS VARIABLE-1
2,8
* COLLECTORS:OUTLET FLOW RATE ->RIGHT AXIS VARIABLE-2
3,2
*** INITIAL INPUT VALUES
TICOLL TOCOLL TSTRT TAMB GCOLL MDCOLL
LABELS  3
"TEMPERATURES"
"HEAT TRANSFER RATES"
"WEATHER - SOLAR LOOP"
*** EXTERNAL FILES
ASSIGN "***.PLT" 40
*|? WHAT FILE SHOULD THE ONLINE PRINT TO? |1000
*------------------------------------------------------------------------

* MODEL "DAILY INTEGRATION" (TYPE 24)
*

UNIT 13 TYPE 24    DAILY INTEGRATION
*$UNIT_NAME DAILY INTEGRATION
*$MODEL .\UTILITY\INTEGRATORS\QUANTITY INTEGRATOR\TYPE24.TMF
*$POSITION 170 282
*$LAYER TOTALS #
PARAMETERS 2
* 1 INTEGRATION PERIOD
24
   •  2 RELATIVE OR ABSOLUTE START TIME
0
INPUTS 3
* WEATHER:BEAM RADIATION ON SURFACE 1 ->INPUT TO BE INTEGRATED-1
2,8
* COLLECTORS:USEFUL ENERGY GAIN ->INPUT TO BE INTEGRATED-2
3,3
* COLLECTORS:DUMPED ENERGY ->INPUT TO BE INTEGRATED-3
3,4
*** INITIAL INPUT VALUES
0 0 0
*------------------------------------------------------------------------

* MODEL "TANK" (TYPE 4)
*

UNIT 7 TYPE 4      TANK
*$UNIT_NAME TANK
*$MODEL .\THERMAL STORAGE\STRATIFIED STORAGE TANK\VARIABLE INLETS\UNIFORM
LOSSES\TYPE4C.TMF
*$POSITION 597 355
*$LAYER WATER LOOP #
PARAMETERS 25
* 1 VARIABLE INLET POSITIONS
```

```
2
* 2 TANK VOLUME
1
* 3 FLUID SPECIFIC HEAT
4.19
* 4 FLUID DENSITY
1000
* 5 TANK LOSS COEFFICIENT
2.5
* 6 HEIGHT OF NODE-1
0.3
* 7 HEIGHT OF NODE-2
0.3
* 8 HEIGHT OF NODE-3
0.3
* 9 HEIGHT OF NODE-4
0.3
* 10 HEIGHT OF NODE-5
0.3
* 11 HEIGHT OF NODE-6
0.3
* 12 AUXILIARY HEATER MODE
1
* 13 NODE CONTAINING HEATING ELEMENT -1
1
* 14 NODE CONTAINING THERMOSTAT -1
1
* 15 SET POINT TEMPERATURE FOR ELEMENT-1
60
* 16 DEADBAND FOR HEATING ELEMENT-1
5
* 17 MAXIMUM HEATING RATE OF ELEMENT -1
0
* 18 NODE CONTAINING HEATING ELEMENT -2
1
* 19 NODE CONTAINING THERMOSTAT -2
1
* 20 SET POINT TEMPERATURE FOR ELEMENT-2
60
* 21 DEADBAND FOR HEATING ELEMENT-2
5
* 22 MAXIMUM HEATING RATE OF ELEMENT -2
0
* 23 NOT USED (FLUE UA)
0
* 24 NOT USED (TFLUE)
20
```

- 25 BOILING POINT

```
150
INPUTS 7
* COLLECTORS:OUTLET TEMPERATURE ->HOT-SIDE TEMPERATURE
3,1
* COLLECTORS:OUTLET FLOW RATE ->HOT-SIDE FLOWRATE
3,2
* [UNCONNECTED] COLD-SIDE TEMPERATURE
0,0
* [UNCONNECTED] COLD-SIDE FLOWRATE
```

```
0,0
* [UNCONNECTED] ENVIRONMENT TEMPERATURE
0,0
* [UNCONNECTED] CONTROL SIGNAL FOR ELEMENT-1
0,0
* [UNCONNECTED] CONTROL SIGNAL FOR ELEMENT-2
0,0
*** INITIAL INPUT VALUES
0 0 25 0 0 0 0
DERIVATIVES 6
* 1 INITIAL TEMPERATURE OF NODE-1
25
* 2 INITIAL TEMPERATURE OF NODE-2
25
* 3 INITIAL TEMPERATURE OF NODE-3
25
* 4 INITIAL TEMPERATURE OF NODE-4
25
* 5 INITIAL TEMPERATURE OF NODE-5
25
* 6 INITIAL TEMPERATURE OF NODE-6
25
*-----------------------------------------------------------------------

* MODEL “TOTALS” (TYPE 25)
*

UNIT 18 TYPE 25    TOTALS
*$UNIT_NAME TOTALS
*$MODEL .\OUTPUT\PRINTER\UNFORMATTED\NO UNITS\TYPE25C.TMF
*$POSITION 592 509
*$LAYER OUTPUTS #
PARAMETERS 10
* 1 PRINTING INTERVAL
STOP
* 2 START TIME
STOP
* 3 STOP TIME
STOP
* 4 LOGICAL UNIT
43
* 5 UNITS PRINTING MODE
0
* 6 RELATIVE OR ABSOLUTE START TIME
0
* 7 OVERWRITE OR APPEND
-1
* 8 PRINT HEADER
-1
* 9 DELIMITER
0
   •  10 PRINT LABELS
1
INPUTS 4
* SIMULATION INTEGRATION:RESULT OF INTEGRATION-1 ->INPUT TO BE PRINTED-1
14,1
* SIMULATION INTEGRATION:RESULT OF INTEGRATION-2 ->INPUT TO BE PRINTED-2
```

```
14,2
* EFFICIENCIES:ETACOLL ->INPUT TO BE PRINTED-3
ETACOLL
* SIMULATION INTEGRATION:RESULT OF INTEGRATION-3 ->INPUT TO BE PRINTED-4
14,3
*** INITIAL INPUT VALUES
ICOLL QUCOLL ETACOLL DENERGY
*** EXTERNAL FILES
ASSIGN “TOTALS.TXT” 43
*|? OUTPUT FILE FOR PRINTED RESULTS |1000
*-----------------------------------------------------------------------

* EQUATIONS “EFFICIENCIES”
*
EQUATIONS 3
ETACOLL_D = [13,2]/(13.8*[13,1]+1E-6)
ETACOLL = [14,2]/(13.8*[14,1]+1E-6)
NEW = TIME/(TIME-START-8765)
*$UNIT_NAME EFFICIENCIES
*$LAYER MAIN
*$POSITION 369 477

*-----------------------------------------------------------------------


* MODEL “DAILY RESULTS” (TYPE 25)
*

UNIT 15 TYPE 25    DAILY RESULTS
*$UNIT_NAME DAILY RESULTS
*$MODEL .\OUTPUT\PRINTER\UNFORMATTED\NO UNITS\TYPE25C.TMF
*$POSITION 598 445
*$LAYER OUTPUTS #
PARAMETERS 10
* 1 PRINTING INTERVAL
24
* 2 START TIME
START
* 3 STOP TIME
STOP
* 4 LOGICAL UNIT
42
* 5 UNITS PRINTING MODE
0
* 6 RELATIVE OR ABSOLUTE START TIME
0
* 7 OVERWRITE OR APPEND
-1
* 8 PRINT HEADER
-1
* 9 DELIMITER
0
   • 10 PRINT LABELS
1
INPUTS 4
* DAILY INTEGRATION:RESULT OF INTEGRATION-1 ->INPUT TO BE PRINTED-1
13,1
```

```
* DAILY INTEGRATION:RESULT OF INTEGRATION-2 ->INPUT TO BE PRINTED-2
13,2
* EFFICIENCIES:ETACOLL_D ->INPUT TO BE PRINTED-3
ETACOLL_D
* DAILY INTEGRATION:RESULT OF INTEGRATION-3 ->INPUT TO BE PRINTED-4
13,3
*** INITIAL INPUT VALUES
ICOLL QUCOLL ETACOLL_D DENERGY
*** EXTERNAL FILES
ASSIGN "DAILY.TXT" 42
*|? OUTPUT FILE FOR PRINTED RESULTS |1000
*-------------------------------------------------------------------------

* MODEL "TYPE89B" (TYPE 89)
*

UNIT 11 TYPE 89    TYPE89B
*$UNIT_NAME TYPE89B
*$MODEL  .\UTILITY\DATA  READERS\STANDARD  WEATHER  FILES\TMY2\SIMULATION
START IS FIRST LINE\TYPE89B.TMF
*$POSITION 42 61
*$LAYER MAIN #
PARAMETERS 2
* 1 MODE
2
   •  2 LOGICAL UNIT
45
*** EXTERNAL FILES
ASSIGN   "C:\PROGRAM   FILES\TRNSYS16_1\WEATHER\METEONORM\AFRICA\NG-KANO-
650460.TM2" 45
*|? WHICH FILE CONTAINS THE TMY2 WEATHER INFORMATION? |1000
*-------------------------------------------------------------------------

* MODEL "TYPE155" (TYPE 155)
*

UNIT 12 TYPE 155   TYPE155
*$UNIT_NAME TYPE155
*$MODEL .\UTILITY\CALLING EXTERNAL PROGRAMS\MATLAB\TYPE155.TMF
*$POSITION 713 394
*$LAYER MAIN #
PARAMETERS 5
* 1 MODE
0
* 2 NUMBER OF INPUTS
3
* 3 NUMBER OF OUTPUTS
12
* 4 CALLING MODE
0
   •  5 KEEP MATLAB OPEN AFTER SIMULATION
1
INPUTS 3
* TANK:TEMPERATURE TO LOAD ->INPUT-1
7,3
* TANK:ENERGY RATE TO LOAD ->INPUT-2
7,6
```

```
* TANK:FLOWRATE TO LOAD ->INPUT-3
7,4
*** INITIAL INPUT VALUES
0 0 0
LABELS 1
“ADSORPTIONUNIT.M”
*-------------------------------------------------------------------------

* MODEL “TYPE25C” (TYPE 25)
*

UNIT 16 TYPE 25    TYPE25C
*$UNIT_NAME TYPE25C
*$MODEL .\OUTPUT\PRINTER\UNFORMATTED\NO UNITS\TYPE25C.TMF
*$POSITION 767 466
*$LAYER OUTPUTS #
PARAMETERS 10
* 1 PRINTING INTERVAL
STEP
* 2 START TIME
START
* 3 STOP TIME
STOP
* 4 LOGICAL UNIT
46
* 5 UNITS PRINTING MODE
0
* 6 RELATIVE OR ABSOLUTE START TIME
0
* 7 OVERWRITE OR APPEND
-1
* 8 PRINT HEADER
-1
* 9 DELIMITER
0
   • 10 PRINT LABELS
1
INPUTS 12
* TYPE155:OUTPUT-1 ->INPUT TO BE PRINTED-1
12,1
* TYPE155:OUTPUT-2 ->INPUT TO BE PRINTED-2
12,2
* TYPE155:OUTPUT-3 ->INPUT TO BE PRINTED-3
12,3
* TYPE155:OUTPUT-4 ->INPUT TO BE PRINTED-4
12,4
* TYPE155:OUTPUT-5 ->INPUT TO BE PRINTED-5
12,5
* TYPE155:OUTPUT-6 ->INPUT TO BE PRINTED-6
12,6
* TYPE155:OUTPUT-7 ->INPUT TO BE PRINTED-7
12,7
* TYPE155:OUTPUT-8 ->INPUT TO BE PRINTED-8
12,8
* TYPE155:OUTPUT-9 ->INPUT TO BE PRINTED-9
12,9
* TYPE155:OUTPUT-10 ->INPUT TO BE PRINTED-10
```

```
12,10
* TYPE155:OUTPUT-11 ->INPUT TO BE PRINTED-11
12,11
* TYPE155:OUTPUT-12 ->INPUT TO BE PRINTED-12
12,12
*** INITIAL INPUT VALUES
TGEN TG1 TG2 TA1 TA2 XMAX XMIN QE QTOT COP1 QTOT1 COP
*** EXTERNAL FILES
ASSIGN “***.TXT” 46
*|? OUTPUT FILE FOR PRINTED RESULTS |1000
*-------------------------------------------------------------------------

END
```

APPENDIX E: Equations for Determining the Efficiencies of the FPC, ETC, and PTC Collectors.

The actual useful heat gained by the solar collector Q_u is calculated from the heat balance in the collector by the Hottel-Whillier-Bliss equation (Duffie and Beckman 2006) given as

$$Q_u = \eta_{sc} Q_s = A_c F_R \left[G(\tau\alpha)_p - U_L(T_i - T_a)\right] \quad \text{(1)}$$

U_L the collector overall heat loss coefficient is

$$U_L = U_t + U_b + U_e \quad \text{(2)}$$

$$U_t = \left(\frac{1}{h_{c_{p-c}} + h_{r_{p-c}}} + \frac{1}{h_w + h_{r_{c-a}}} \right)^{-1} \quad \text{(3)}$$

Where the radiation coefficient from the collector plate to the glass cover is

$$h_{r_{p-c}} = \frac{\sigma\left(T_p^2 + T_c^2\right)\left(T_p + T_c\right)}{\frac{1}{\varepsilon_p} + \frac{1}{\varepsilon_c} - 1} \quad \text{(4)}$$

The convection coefficient between collector plate and glass cover is

$$h_{c_{p-c}} = Nu \frac{k}{L_1} \quad \text{(5)}$$

Nu – Nusselt number

k – thermal conductivity of air at mean plate temperature

L_1 – plate spacing

Hollands et al (1976) give the relationship between Nusselt number and Rayleigh number for tilt angles from 0- 75^o as

$$Nu = 1.44\left[1 - \frac{1708(\sin 1.8\beta)^{1.6}}{Ra\cos\beta}\right]\left[1 - \frac{1708}{Ra\cos\beta}\right]^{+} + \left[\left(\frac{Ra\cos\beta}{5830}\right)^{1/3} - 1\right]^{+} \quad \text{(6)}$$

and

$$Ra = \frac{g\beta'\Delta T L^3}{\upsilon\alpha} \quad \text{..... (7)}$$

$$\beta' = \frac{1}{T_m} \quad \text{..... (8)}$$

$$T_{pm} = \frac{T_p + T_c}{2} \quad \text{..... (9)}$$

g – gravitational constant

ΔT – temperature difference between plates

υ – kinematic viscosity

α – thermal diffusivity

$$h_{r_{c-a}} = \frac{\sigma\varepsilon_c\left(T_c + T_s\right)\left(T_c^2 + T_s^2\right)\left(T_c - T_s\right)}{T_c - T_a} \quad \text{..... (10)}$$

The wind heat transfer coefficient as given by McAdams (1954) is

$$h_w = 5.7 + 3.8v \quad \text{..... (11)}$$

v is the wind velocity

The cover glass temperature is given by Duffie and Beckman (2006) as

$$T_c = T_p - \frac{U_t\left(T_p - T_a\right)}{h_{c_{p-c}} + h_{r_{p-c}}} \quad \text{..... (12)}$$

However, Klein (1979) developed an empirical equation for U_t as

$$U_t = \left(\frac{N}{\frac{c}{T_{pm}}\left[\frac{\left(T_{pm} - T_a\right)}{\left(N + f\right)}\right]^e} + \frac{1}{h_w} \right)^{-1} + \frac{\sigma\left(T_{pm} + T_a\right)\left(T_{pm}^2 + T_a^2\right)}{\frac{1}{\varepsilon_p + 0.00591 N h_w} + \frac{2N + f - 1 + 0.133\varepsilon_p}{\varepsilon_g} - N} \quad \text{.... (13)}$$

$$f = (1 + 0.089 h_w - 0.1166 h_w \varepsilon_p)(1 + 0.07866 N) \quad \text{..... (14)}$$

$$c = 520(1 - 0.000051 \beta^2) \text{ for } 0^o < \beta < 70^o \quad \text{..... (15)}$$

$$e = 0.430\left(1 - 100 / T_{pm}\right) \quad \text{..... (16)}$$

where

N – number of glass covers

β - collector tilt angle

ε_g – emittance of glass

ε_p – emittance of plate

T_a – ambient temperature

The back loss coefficient U_b is given by Duffie and Beckman (2006) is

$$U_b = \frac{k_i}{L_i} \quad \text{..... (17)}$$

k_i – insulation thermal conductivity

L_i - insulation thickness

The edge loss coefficient U_e is

$$U_e = \frac{(UA)_{edge}}{A_c} \quad \text{..... (18)}$$

The energy balance on collector plate is evaluated as

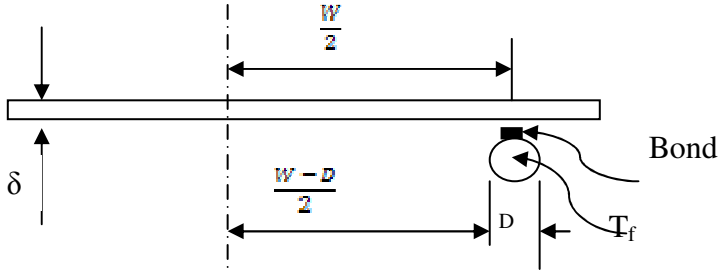
$$(mc)_e \frac{dT_p}{dt} = A_c\left[G(\tau\alpha)_e - U_L(T_p - T_a)\right] \quad \text{..... (19)}$$

For a one cover system, the effective transmittance-absorptance product

$$(\tau\alpha)_e = (\tau\alpha) + (1-\tau_a)\left[\frac{U_t}{U_{c-a}}\right] \quad \text{..... (20)}$$

The effective heat capacity of the collector with double cover is

$$(mc)_e = (mc)_p + \frac{U_L}{U_{c-a}}(mc)_c \quad \text{..... (21)}$$



The useful energy gain transferred to the water in tube is however given as

$$q_u' = W F'\left[G(\tau\alpha)_e - U_l(T_f - T_a)\right] \quad \text{..... (22)}$$

where F' is the collector efficiency factor given as

$$F' = \frac{1/U_L}{W\left[\frac{1}{U_L(D+(W-D)F)} + \frac{1}{c_b} + \frac{1}{\pi D_i h_{fi}}\right]} \quad \text{..... (23)}$$

W – tube spacing

D – tube diameter

D_i – inner tube diameter

h_{fi} – heat transfer coefficient between fluid and wall tube

c_b – bond conductance

$$c_b = \frac{k_b b}{\gamma} \quad \text{..... (24)}$$

k_b – bond thermal conductivity

γ – average bond thickness

b – bond width

F is standard fin efficiency for straight fins with rectangular profile given by Duffie et al (2006) as

$$F = \frac{\tanh\left(m\left(W-D\right)/2\right)}{m\left(W-D\right)/2} \quad \text{..... (25)}$$

$$m = \sqrt{\frac{U_L}{k_p \delta}} \quad \text{..... (26)}$$

δ – collector sheet thickness

For the evacuated tube collector the overall heat loss from the outer glass cover q_{loss} is

$$q_{loss} = \left(h_{cg1-} + h_{r_{g1-a}}\right)\left(T_{g_1} - T_a\right) \quad \text{..... (27)}$$

The radiation and convective heat transfer coefficient are

$$h_{r_{g1-a}} = \sigma \varepsilon_g \left(T_{g_1}^2 + T_a^2\right)\left(T_{g_1} + T_a\right) \quad \text{..... (28)}$$

$$h_{c_{g1-a}} = Nu_d \frac{k}{d} \quad \text{..... (29)}$$

According to Deaver et al (1970) $Nu_d = 0.386\mathrm{Re}^{0.592}\mathrm{Pr}^{1/3}$

The energy balance on the outer glass cover of the collector is evaluated as

$$m_{g_1} c_{p_g} \frac{dT_{g1}}{dt} = \frac{A_{g1}}{2}\left[G(\tau\alpha)_{g1} + h_{r_{g1-g2}}\left(T_{g2} - T_{g1}\right) - U_{g1}\left(T_{g1} - T_a\right)\right] \quad \text{..... (30)}$$

where the radiative heat transfer coefficient between the inner and outer glass is

$$h_{r_{g1-g2}} = \frac{\sigma\left(T_{g1}^2 + T_{g2}^2\right)\left(T_{g1} + T_{g2}\right)}{\frac{1}{\varepsilon_{g1}} + \frac{d_{g1}}{d_{g2}}\left[\left(\frac{1}{\varepsilon_{g2}}\right) - 1\right]} \quad \text{..... (31)}$$

The energy balance on the inner glass cover is given by

$$m_{g2} c_{p_g} \frac{dT_{g2}}{dt} = \frac{A_{g2}}{2}\left[G(\tau\alpha)_{g2} - h_{r_{g1-g2}}\left(T_{g2} - T_{g1}\right) - 2h_{c_{g2-w}}\left(T_{g2} - T_{g_1}\right)\right] \text{..... (32)}$$

For natural convection of heat form glass to water, the convective heat transfer coefficient for a horizontal tube with the wall temperature increasing at uniform rate given by Holman (1997) is

$$h_{c_{g2-w}} = Nu\frac{k}{d} = \left[1.181\left(Gr\,\mathrm{Pr}\right)^{0.214}\right]\frac{k}{d} \quad \text{..... (33)}$$